Analysis of the FGF signalling pathway during embryogenesis of the red flour beetle *Tribolium castaneum*

Dissertation

zur

Erlangung des akademischen Grades

doctor rerum naturalium (Dr. rer. nat.)

der Mathematisch-Naturwissenschaftlichen Fakultät

der Universität Rostock

Universität Rostock

Traditio et Innovatio

vorgelegt von

M.Sc. Rahul Sharma

01.12.1983

Aligarh, India

Rostock, February 2014

Analysis of the FGF signalling pathway during embryogenesis of the red flour beetle *Tribolium castaneum*

Dissertation

to obtain the academic degree

Doctor rerum naturalium (Dr. rer.nat.)

[Doctor of Philosophy (Ph.D.)]

at the

Faculty of Mathematics and Natural Sciences (MNF),

University of Rostock

Universität Rostock

Traditio et Innovatio

Submitted by

M.Sc. Rahul Sharma

01.12.1983

Aligarh, India

Rostock, February 2014

This work has been conducted under the supervision of **Prof. Dr. Reinhard Schröder** at the Department of Genetics, Institute for Biological Sciences, University of Rostock, Rostock, Germany.

Parts of this dissertation have been published:

Sharma R., Beermann. A., Schröder R.; 2013. FGF signalling controls anterior extraembryonic and embryonic fate in the beetle *Tribolium*; *Developmental Biol*ogy *381: 121-133*

Sharma R., Beermann A., Schröder R.; 2013. The dynamic expression of extraembryonic marker genes in the beetle *Tribolium castaneum* reveals the complexity of serosa and amnion formation in a short germ insect; *Gene Expression Patterns 13: 362–371*

मेरे संपूर्ण परिवार को समर्पित

(Dedicated to my entire family)

Table of Contents

Abbreviations

α	anti-
%	percentage
Ab	Antibody
AP	Alkaline Phosphatase
ATP	Adenosine triphosphate
BBR	Boehringer- Blocking-Reagent
BCIP	5-bromo-4-chloro-3-indolyphosphate
BF	Bright Field
BLAST	Basic Local Alignment Search Too
bp	Base pair
byn	*brachyenteron* gene
CDS	coding sequences
CE	Convergent Extension
cDNA	complementary DNA
°C	Degree Celsius
DAPI	4', 6-diamidino-2-phenylindole
Dll	*Distalless* gene
DIC	Differential interference contrast
DIG	Digioxigenine
DNA	Deoxyribonucleic acid
DNase I	Deoxyribonuclease I
dNTP	deoxyribonucleotide
dsRNA	Double stranded - RNA
DTT	Dithiothreitol
eve	even - skipped
FGF	Fibroblast growth factor
FGFR	Fibroblast growth factor receptor
GDP	Guanosine diphosphate
GTP	Guanosine triphosphate
h	Hour
INT	2-(4-Iodophenyl)-3-(4-nitrophenyl)-5-phenyltetrazolium chloride
IVT	*in vitro* - transcription
mg	Milligram
min	Minute

ml	Millilitre
µg	Microgram
µl	Millilitre
NBT	Nitro-blue tetrazolium chloride
NCBI	National Centre for Biotechnology Information
PBS	Phosphate Buffer Saline
PBT	Phosphate Buffer Saline -Tween
PCR	Polymerase Chain Reaction
pDNA	Plasmid - DNA
RNA	Ribonucleic acid
RNAi	RNA – Interference
RACE	Rapid Amplification of cDNA Ends
siRNA	small interfering RNA
TdT	Terminal deoxynucleotidyl transferase
Tris	Tris(hydroxymethyl)aminomethane
TUNEL	TdT mediated dUTP nick end labeling
U	Unit
dUTP	deoxyUridine-5'-triphosphate
UTP	Uridine-5'-triphosphate
WT	Wildtype

Zusammenfassung

In vielzelligen Organismen steuern eine große Zahl von Signalübertragungswegen die Kommunikation zwischen Zellen. Die präzise Regulation dieser Signalwege ist für den Ablauf vieler Prozesse während der Embryonalentwicklung und der Adultphase von enormer Bedeutung. Einer dieser Signalwege, der Fibroblasten Wachstumsfaktor-(FGF)-Signalweg, ist in der Evolution stark konserviert und kontrolliert bei Vertebraten und bei Nichtvertebraten das Wanderungsverhalten von Zellen, die Spezifizierung der Körperachse und die Differenzierung des Mesoderms.

Während in Vertebraten 22 verschiedene FGF-Liganden und 4 FGF-Rezeptoren vorhanden sind, ist dieser Signalweg in Insekten wie der Fliege *Drosophila* mit 3 Liganden und nur 2 FGF-Rezeptoren wesentlich weniger komplex.

Ich habe in dieser Arbeit die Funktion des FGF-Signalweges unter evolutionären Aspekten während der Embryonalentwicklung eines Kurzkeim-Insekts, dem Mehlkäfer *Tribolium* untersucht. Das Genom von *Tribolium* enthält vier Gene, die für einen FGF-Liganden kodieren (*Tc-fgf1a*, *Tc-fgf1b*, *Tc-fgf8* and *Tc-branchless*) und nur ein Gen für einen FGF-Rezeptor (*Tc-fgfr*). Die Herrunterregulierung der Genfunktion mittels RNA-Interferenz von *fgf1*, das im Fliegengenom nicht enthalten ist, zeigte zum ersten Mal in einem Insektenmodellorganismus, dass dieser Ligand für die Festlegung von extra-embryonalem und embryonalem Gewebe im frühen Embryo eine kritische Rolle spielt. Dies konnte ich mit der exakten Analyse der Expressionsmuster von Markergenen in Wildtyp- und in FGF-RNAi-Embryonen belegen. Weiterhin konnte ich zeigen, dass Fgf8 das Signal für den einzigen Fgf-Rezeptor darstellt und für die Mesodermdifferenzierung benötigt wird. Im Gegensatz zu *Drosophila* fungiert derselbe Rezeptor auch bei der Bildung des Tracheensystems.

Im Forschungsgebiet „Evolution & Entwicklung ("Evo-Devo") belegen meine Ergebnisse die evolutionäre Vielseitigkeit des FGF-Signalwegs während der Embryogenese von Tieren.

Summary

The precise regulation of cell-cell communication by numerous signal-transduction pathways is fundamental for many different processes during embryonic development and morphogenesis in multicellular organisms. One important signalling pathway is the fibroblast-growth-factor (FGF)-pathway that is evolutionary conserved and controls processes like cell migration, axis specification and mesoderm formation in vertebrate and invertebrate animals. In comparison to vertebrates with their 22 different FGF ligands (FGFs) and 4 FGF receptors (FGFRs), FGF signalling in invertebrates is far less complex as illustrated by the presence of only three Fgf ligands and two Fgf receptors in the fly *Drosophila*.

To understand FGF signalling from an evolutionary perspective, I studied the function of this pathway during embryogenesis of the short germband beetle *Tribolium*. The *Tribolium* genome contains four Fgf ligand genes (*Tc-fgf1a*, *Tc-fgf1b*, *Tc-fgf8* and *Tc-branchless*) and only a single Fgf receptor gene (*Tc-fgfr*). The knockdown analysis via RNA-interference of the *fgf1* gene, which is not included in the fly genome, revealed its critical function for specifying extraembryonic and embryonic fate along the anterior-posterior axis in the beetle. For that I carefully described the spatio-temporal expression of various marker genes involved in extraembryonic tissue formation and compared their highly dynamic expression profiles from wildtype- and FGF-knockdown embryos. This is the first demonstration of the FGF pathway being required for axis formation in a non-vertebrate animal.

In addition, I also find that Fgf8 that signals through the single Fgf-receptor is the prerequisite for mesoderm differentiation during gastrulation in *Tribolium*. The finding that embryos lacking *Tc-fgfr* function are severely affected in both mesoderm- and in tracheal development shows that different to *Drosophila* a single FGF-receptor regulates these processes in *Tribolium*.

In the context of evolution of development ("Evo-Devo") my results reveal the plasticity of the FGF cell-signalling pathway during embryogenesis of animals.

1   Chapter 1: General Introduction

1.1 FGF-Signalling

1.1.1 Preface

Cell-cell communication, precisely governed by various signal-transduction pathways, is the fundamental process of development and morphogenesis in multicellular organisms. Although, at least 17 different cell-signalling pathways have been recognised in complex metazoans (vertebrates, nematodes, insects), only five of these pathways are essentially required for early developmental processes (Gerhart, 1999; Pires-daSilva and Sommer, 2003). Fibroblast growth factor (FGF) signalling, an evolutionary conserved pathway, is one of them and has been reported to be involved in a variety of cellular processes such as cell proliferation and differentiation, cell migration, axes specification, cell fate determination, and mesoderm formation and morphogenesis (Borland et al., 2001; Böttcher and Niehrs, 2005; Dorey and Amaya, 2010; Muha and Müller, 2013). The deregulation of FGF signalling could lead to various human diseases including cancer (Itoh and Ornitz, 2011; Turner and Grose, 2010; Wesche et al., 2011). A signal-transduction pathway is generally triggered by the binding of an extracellular signal molecule ("ligand") to a transmembrane protein ("receptor"), which leads to the modification of some cytoplasmic proteins ("downstream transducers"). These modified downstream molecules further activate transcription factors that can alter gene expression.

1.1.2 Fibroblast growth factors (FGFs)/Ligands

FGFs are mostly secreted signalling polypeptide growth factors with diverse biological activities. The size of FGFs ranges from 17 to 34 kDa in vertebrates, to 84 kDa in *Drosophila*. The FGFs protein family in humans and mouse is comprised of 22 members and most of them share a central core domain of 120-130 amino acids with 28 highly conserved and six identical amino acids (Fig. 1.1A) (Böttcher and Niehrs, 2005; Itoh and Ornitz, 2011; Ornitz and Itoh, 2001). These core domains have high affinity to bind to the extracellular immunoglobulin (Ig) domain of their membrane-associated tyrosine kinase receptors (FGFRs). FGFs also have affinity for membrane-bound heparan sulfate proteoglycan (HSPG) molecules or their soluble form heparin, which protects FGFs from thermal denaturation and proteolysis and allow a stable interaction with FGFRs (Ornitz, 2000; Ornitz and Itoh, 2001). On behalf

of their structure, function and biochemical properties, vertebrate FGFs are grouped into seven different subfamilies (Itoh and Ornitz, 2004; Popovici et al., 2005).
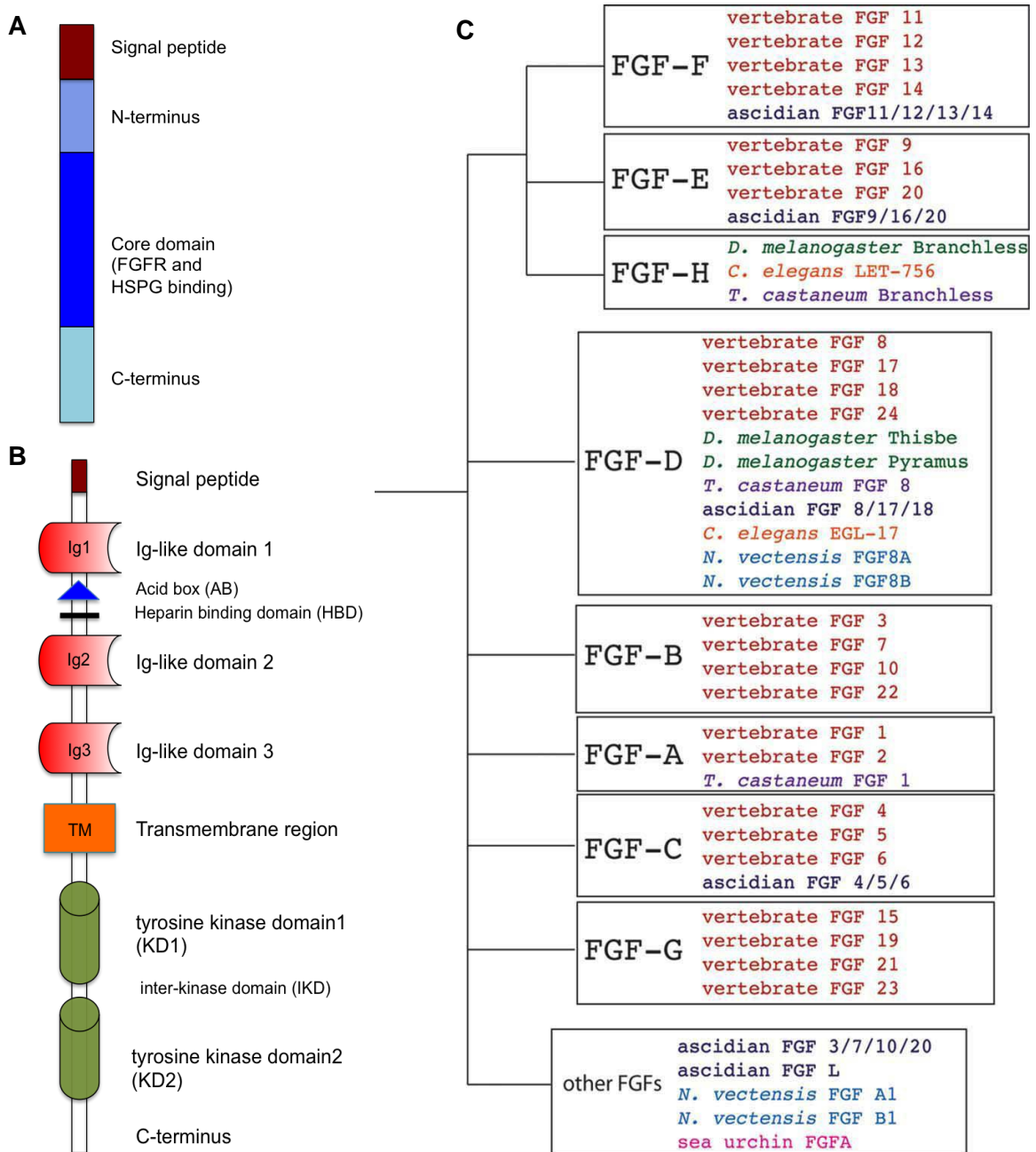
Figure 1.1: Schematic overview of the basic structure of the FGF (**A**) and FGFR (**B**) proteins. (**C**) A phylogenetic classification of all the FGF family members in vertebrates and invertebrates. The image is taken from (Tulin and Stathopoulos, 2010) and based on the 8 group classification described in (Popovici et al., 2005). Ascidian, (*C.intestinalis*; sea squirt), *S. purpuratus* (sea urchin), *D. melanogaster* (fruit fly), *T. castaneum* (red flour beetle), *C. elegans* (nematode worm), *N. vectensis* (sea anenome).

In comparison to vertebrates, only few FGFs have been identified in the genome of non-vertebrates model organisms (Fig. 1.1C; Table 1). While most of these FGFs also possess a complete core sequence that allow them to be grouped with vertebrate FGFs, some FGFs including Branchless in *Drosophila* and *Tribolium* and LET-756 in *C. elegans* lack this core domain and hence were classified to a separate

subfamily (FGF-H), which is thought to be lost in deuterostomes lineage during the course of evolution (Popovici et al., 2005). Additionally, few FGFs from different species could not be assigned to any particular FGF subfamily (Tulin and Stathopoulos, 2010).

Table 1: Overview of *FGFs* and *FGFRs* present in some vertebrate and invertebrate *species*.

	Fgf family	*FGFRs*	References
Human	*FGF1-FGF14, FGF16-FGF23*	*FGFR1-FGFR4*	Itoh and Ornitz, 2011; Itoh, 2007; Ornitz, 2000
Mouse	*Fgf1-18, Fgf20-23*	*Fgfr1-Fgfr4*	Itoh and Ornitz, 2011
Zebrafish	*fgf1-fgf5, fgf6a, fgf6b, fgf7, fgf8, fgf10a, fgf10b, fgf11-14, fgf16, fgf17a, fgf17b, fgf18a, fgf18b, fgf19, fgf20a, fgf20b, fgf21-fgf24*	*fgfr1-fgf4*	Itoh and Ornitz, 2011; Ota, et al., 2009
Drosophila	*pyramus (pyr), thisbe(ths), branchless (bnl)*	*heartless (htl), breathless (btl)*	Klämbt et al., 1992; Sutherland, et al., 1996; Gryzik and Müller, 2004, Stathopoulos, et al., 2004
Tribolium	*Tc-fgf8, Tc-fgf1a, Tc-fgf1b, Tc-branchless (Tc-bnl)*	*Tc-fgfr*	Beerman and Schröder, 2008
C.elegans	*egl-17, let-756*	*egl-15*	Burdine, et al., 1997; Burdine, et al., 1998
C.intestinalis	*Ci-Fgf4-like, Ci-Fgf5-like, Ci-Fgf8-like, Ci-Fgf9-like, Ci-Fgf10-like, Ci-Fgf13-like*	*Ci-FGFR*	Satou et al., 2002; Imai et al., 2002; Shi, et al., 2009; Itoh and Ornitz, 2011
N. vectensis	*NvFGF8a, NvFGF8b, NvFGFa1, NvFGFa2*	*NvFGFRa, NvFGFRb*	Matus et al., 2007; Rentzsch et al., 2008
sea urchin	*fgfA*	*FGFR1, FGFR2*	Röttinger et al., 2008

1.1.3 Fibroblast growth factor receptors (FGFRs)

As members of the receptor tyrosine kinase superfamily, FGFRs also contain an extracellular ligand binding domain, a single-pass transmembrane domain and an intracellular tyrosine kinase domain that transmits the signal toward the interior of the cell (Fig. 1.1B) (Böttcher and Niehrs, 2005; Ornitz and Itoh, 2001; Turner and Grose, 2010). Each extra-cellular domain is comprised of three immunoglobulin-like (Ig-like) domains (Ig1-Ig3), a stretch of specific (serine-rich) amino acids sequence between Ig1 and Ig2 ("acid box", AB) and a heparin-binding domain (HBD) (Fig. 1.1B) (Böttcher and Niehrs, 2005; Thisse and Thisse, 2005). While the Ig2- Ig3 domains of FGFR are necessary for ligand binding and specificity, the Ig1 domain and the acid box are thought to have a receptor autoinhibition function (Beenken and Mohammadi, 2009). The FGFR gene family in vertebrates consists of four closely related genes *FGFR1*, *FGFR2*, *FGFR3* and *FGFR4* that share 55% to 72% identity in their encoded amino acid sequence (Groth and Lardelli, 2002). In addition, a fifth member of the FGFR family *FGFR5* or *FGFR-like1* (*FGFRL1*) has also been identified that has no tyrosine kinase domain in the encoded protein but has the

ability to bind FGFs and hence considered more as a negative regulator (Turner and Grose, 2010; Wiedemann and Trueb, 2000). Besides, alternative splicing of FGFR mRNA, creating various isoforms of FGFRs further adds structural and functional diversity to the FGFR gene family (Groth and Lardelli, 2002; Johnson and Williams, 1993). Particularly, the alternative splicing of part of the Ig3 domain of FGFR1–3 produces different isoforms (FGFR1b–3b) and (FGFR1c–3c) with distinct binding specificities (Johnson et al., 1991) that are expressed in different tissues i. e. epithelial and mesenchymal respectively (Orr-Urtreger et al., 1993). However, unlike FGFR1-3, no alternative splicing in this region for FGFR4 has been documented (Vainikka et al., 1992). The other splice variant from of the FGFR where the missing Ig1 domain alone or together with the acid box region does not affect the FGFR function because neither Ig1 nor the acid box region are essential for FGF-FGFR binding. Rather, their deletion might enhance the binding of the receptor to the FGF and heparin (Wang et al., 1995).

Unlike vertebrates, the FGFR gene family is far less complex in non-vertebrate model organisms and consists of mainly either one or a maximum two *fgfr* genes (Table 1). Moreover, alternate splice forms of FGFRs, a symbolic feature in vertebrates, has not been reported to contribute additional specificity to its members except in the case of the nematode *C.elegans* (Goodman et al., 2003; Tulin and Stathopoulos, 2010). In *C. elegans*, two isoforms of the receptor EGL-15 {EGL15 (5A) and EGL-15 (5B)} has been identified that binds to each specific ligand: egl-15 (5A) with egl-17 and egl-15 (5B) with let-756 and stimulate two different responses (Goodman et al., 2003; Huang and Stern, 2005). In *Drosophila*, while the receptor *Breathless* has no splice variant, the two isoforms of the *Heartless* gene, generated through the splicing of exon I and exon II respectively, can not provide additional variability as the complete coding sequence for both the transcripts are entirely contained within the last exon III (Ito et al., 1994; Klämbt et al., 1992; Shishido et al., 1993).

1.1.4   Role of HSPGs in FGF-FGFR interaction

HSPGs are complex macromolecules present on the cell surface and in the extracellular matrix. They consist of a core protein to which two to three linear polysaccharides chains of sulphated glycosaminoglycans (GAGs) are attached (Ruoslahti and Yamaguchi, 1991; Thisse and Thisse, 2005). An enormous amount of structural diversity in HSPGs can be generated through the modification of attached chains via differential sulfation of GAGs (Pellegrini et al., 2000; Schlessinger et al., 2000), which in turn could lead to different binding specificity for FGFs and FGFRs

(Ornitz, 2000; Pownall and Isaacs, 2010). The principle role of HSPG molecules is the stabilisation and enhancement of the half-life of FGF/FGFR dimers and allows formation of a ternary complex (Plotnikov et al., 1999; Spivak-Kroizman et al., 1994a). In addition, HSPGs also protect FGFs from denaturation and proteolysis by providing a large number of binding sites for free FGFs (Gospodarowicz and Cheng, 1986).

The role of HSPGs in modulation of FGF signalling is evident in both vertebrates and invertebrates (Lin, 2004). Isolation of HSPG mutants provides genetic proofs to that fact, which shows that HSPG mutants phenocopy the FGF or FGFR mutations in both vertebrates and invertebrates (Lin et al., 1999; Nybakken and Perrimon, 2002).

1.1.5 Mechanism of Signal Transduction

The key event in the FGF signal transduction is the formation of a HSPG-FGF-FGFR ternary complex (2:2:2) following binding of two FGF molecules connected by two HSPG molecules to the extracellular Ig2 and Ig3 domains of specific FGFR monomers that then lead to receptor dimerization and subsequently its activation (Fig. 1.2) (Beenken and Mohammadi, 2009; Böttcher and Niehrs, 2005; Turner and Grose, 2010). This dimerization of FGFR triggers trans auto-phosphorylation of specific intracellular tyrosine residues and these phosphorylated tyrosine residues then function as docking sites for intracellular adaptor proteins containing SH2 (Src homology 2) or PTB (phosphotyrosine binding) domains, which ultimately lead to the activation of multiple signal transduction pathways that are described below (Fig. 1.2) (Ullrich and Schlessinger, 1990).

Ras/MAPK Pathway

The main intracellular pathway activated in all cell types through the stimulation of FGFRs is the Ras/MAP kinase pathway (Fig. 1.2) (Dailey et al., 2005). A membrane-anchored docking protein, the FGFR substrate/α (FRS2α) is important for activation of the Ras/MAP kinase pathway (Kouhara et al., 1997). FRS2α binds to the juxtamembrane region of the FGFR through its PBT domains, and upon activation of the receptor it becomes phosphorylated on several tyrosine residues, which further creates docking sites for additional adaptor proteins. The phosphorylated FRS2α sites then recruit the adaptor protein growth factor receptor-bound2 (GRb2) that exists in complex with the nucleotide exchange factor Son of sevenless (Sos) and leads to the activation of the GTP-binding protein Ras through catalysis of GDP to GTP by Grb-2/Sos complex (Ong et al., 2000). The activated Ras then leads to the stimulation of a cascade of phosphorylation events involving downstream proteins

Raf, MEK and MAP kinases (ERK1, 2), the last member of which ultimately enter the nucleus and phosphorylates target transcription factors (TFs) (Sternberg and Alberola-IIa, 1998). Members of the ETS family are most noted TFs activated by MAPK cascade (Randi et al., 2009). These TFs possess a winged helix-loop-helix domain with which they can bind to DNA as monomers and regulate gene expression downstream of MAPK pathway (Nentwich et al., 2009; Wasylyk et al., 1998). The genes, which are transcribed in response to ETS proteins and other transcription factors activated by this pathway, are considered as FGF target genes. This pathway is instrumental in mediating different key cellular responses such as cell proliferation and cell cycle arrest indicating the final effect of growth factor stimulation (Maher, 1999; Raucci et al., 2004).
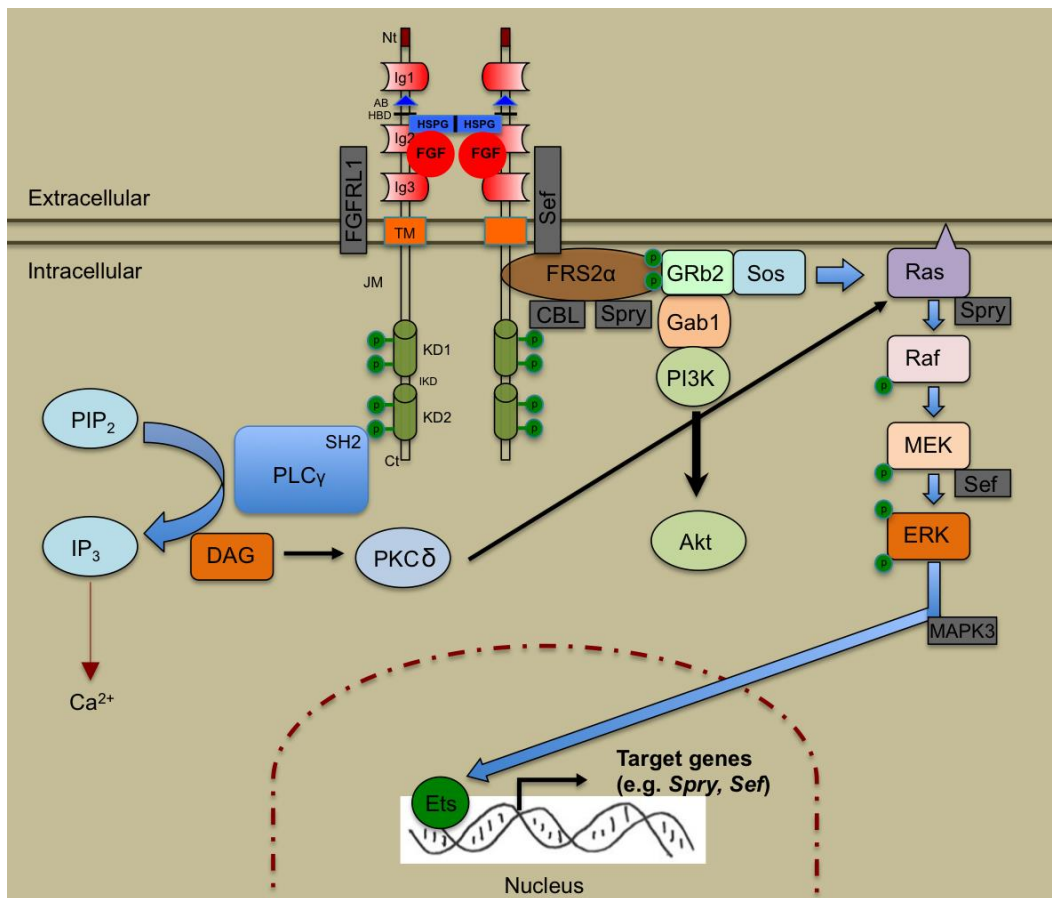
Figure 1.2: Schematic overview of the FGF signal transduction pathways, along with the negative regulators (inspired from Thisse and Thisse, 2005 and Turner and Grose, 2010).

PI3 kinase/Akt pathway

This pathway is activated by recruitment of GRb2 associated binding protein 1 (GAb1) protein by the docking protein GRb2, which leads to activation of phosphoinositide-3 (PI3) kinase pathway that activate downstream antiapoptotic protein kinase Akt/protein kinase B (Fig. 1.2). One of the main roles of this pathway is cell survival by exerting an apoptotic activity in normal development and is

important in the context of cancer (Altomare and Testa, 2005; Nicholson and Anderson, 2002).

PLC/Ca²⁺ Pathway

Independent of FRS2 binding, this pathway is activated by the binding of SH2 domain of protein phospholipase Cγ (PLCγ), which possess intrinsic catalytic activity, to a phosphotyrosine residue (Y766) towards the carboxyl terminus of activated FGFR (Fig. 1.2). The activated form of PLCγ protein hydrolyses phosphatidylinositol 4,5-biphosphate (PIP_2) to phosphatidylinositol 3,4,5-triphosphate (PIP_3) and diacylglycerol (DAG). While DAG is an activator of protein kinase C (PKC), PIP_3 induces release of intracellular calcium (Ca^{2+}). The activated protein kinase C-δ (PKCδ) can further lead to the activation of MAPK pathway by directly phosphorylating Raf protein (Ueda et al., 1996). The physiological role of this pathway is not clear as its attenuation does not affect either mitogenesis (Peters et al., 1992) or cell differentiation (Spivak-Kroizman et al., 1994b). However, some data suggest that it may be necessary for cell adhesion, in some specific cell types (Kolkova et al., 2000).

Apart from these pathways, there are also many other signalling molecules that have been reported to be activated by FGFRs, including the p38 MAPK and Jun N terminal kinase pathways, signal transducer and activator of transcription (STAT) signalling (Hart et al., 2000) and ribosomal protein S6 kinase 2 (RSK2) (Kang et al., 2009).

1.1.6 Deregulation of FGF signalling

Considering a multiple range of biological effects stimulated by the FGF signalling cascade through activation of different intracellular pathways, a tight regulation of this pathway is essential with regards to timing, duration and spread of the signal. A precise regulation can be achieved by both positive and negative feedback loops. FGF signalling can be regulated at both extracellular and intracellular level (Thisse and Thisse, 2005; Turner and Grose, 2010). However, the mechanisms of attenuation and negative feedback control of FGFR signalling have not been completely understood. Here I briefly describe the most common regulators of FGF signalling.

Sprouty (Spry) Protein

Sprouty (Spry) is an intracellular protein (Casci et al., 1999) and the first regulator identified as an antagonist of FGF signalling in *Drosophila* mutants (Hacohen et al.,

1998). In *spry* mutants, an ectopic apical branching of tracheae was observed due to high levels of FGF activity (Hacohen et al., 1998). Later, four members of Spry family (Spry 1, 2, 3, 4) were also identified in mammals (Dikic and Giordano, 2003). These proteins possess a conserved C-terminal cysteine-rich domain, necessary for their specific localization and function. At their amino-terminus, they possess a conserved tyrosine residue, which is essential for the inhibitory actions of the Spry proteins (Cabrita and Christofori, 2008; Mason et al., 2006). A mutation in this tyrosine residue resulted in dominant negative Spry protein that enhances MAPK signalling downstream of FGF (Hanafusa et al., 2002). However, the mechanism of Spry inhibition of FGF signalling is not fully understood, some studies suggest that Spry acts upstream of Ras and competes with FRS2 for binding to Grb2/SOS complex (Hanafusa et al., 2002), while others have shown that Spry proteins inhibit Raf activation (Sasaki et al., 2003). Induction of *Spry* expression through FGF signalling creates a negative feedback loop, where FGF restricts its own activity by activating the expression of *Spry* (Branney et al., 2009; Hacohen et al., 1998; Sivak et al., 2005).

MAP kinase phosphatase 3 (MKP3)

MKP3 proteins negatively regulate the MAP kinase pathway through dephosphorylation of activated MAPK proteins (Alonso et al., 2004). These proteins contain two distinct domains, the N-terminal domain, which has high affinity to bind Erk/MAP kinase protein and the C-terminal domain, which possess dual phosphatase activity (Stewart et al., 1999; Zhang et al., 2003; Zhao and Zhang, 2001). Binding of activated MAPKs to the N-terminal domain of MKP3 triggers a conformational activation of C-terminal phosphatase that leads to the inactivation of MAPKs (Thisse and Thisse, 2005). In *Xenopus*, overexpression of MKP3 blocks mesoderm induction by FGF in specific tissues (Branney et al., 2009; Umbhauer et al., 1995).

Sef

Sef (Similar Expression to FGF) protein is another negative regulator of FGF signalling that resides in the transmembrane region (Kondoh et al., 2005). This protein has been originally identified in zebrafish and later also in mouse and human but not in invertebrates and hence seems to be conserved only in vertebrates (Fürthauer et al., 2002; Tsang et al., 2002). The mode of action of Sef protein is also not very clear. Several reports suggest that Sef acts as a negative regulator of Ras/MAP kinase pathway by inhibiting the phosphorylation of ERK1/2 downstream

effectors and thereby stop signals to enter into the nucleus (Fürthauer et al., 2002; Preger et al., 2004). In contrast, other studies show that Sef acts upstream of Ras by binding to FGF receptor (Kolkova et al., 2000; Ren et al., 2007; Xiong et al., 2003). XFLRT3, CBL are among few other modulators of FGF signalling (Böttcher et al., 2004; Thien and Langdon, 2001).

1.2 Biological significance of FGF Signalling

A multitude of biological responses, including mesoderm patterning, morphogenesis, cell differentiation and regulation of cell proliferation or migration, have been attributed to different FGFs in both vertebrates and invertebrates. Here I discuss some of the functions of FGF signalling that are specifically more relevant in the context of this study.

1.2.1 FGFs and mesoderm development

Mesoderm induction and patterning is one of the earliest events during vertebrate body axes formation and FGF signalling has been found critical for this process. The first evidence came from the studies on *Xenopus laevis*, where basic fibroblast growth factor (FGF2) showed mesoderm inducing capacity equivalent to the ventrovegetal (VV) signal that induces ventral mesoderm (Kimelman and Kirschner, 1987; Slack et al., 1987). Following this discovery, a huge amount of data has been generated to elucidate details of mesoderm development through various FGFs in both vertebrates and invertebrates (Amaya et al., 1991; Bae et al., 2012; Borland et al., 2001; Burdine et al., 1998; Draper et al., 2003; Green et al., 2013; Gryzik and Müller, 2004; Kim and Nishida, 2001; Lea et al., 2009; Lo et al., 2008; Shishido et al., 1993; Tulin and Stathopoulos, 2010) suggesting this function of FGFs as an evolutionary conserved one.

Most of the early experiments carried out in *Xenopus* and zebrafish have shown that FGF signalling is a prerequisite for the formation of mesodermal subtypes, axial mesoderm (which later forms notochord) and paraxial mesoderm (which brings about axial skeleton, skeletal muscles and dermis) (Amaya et al., 1991; Amaya et al., 1993; Griffin et al., 1995). However, it was not clear whether FGF signalling is required during the initial induction or in the maintenance of these mesodermal subtypes. Especially, when compelling evidences suggest that members of the TFGβ signalling family, *Xenopus* nodal related (Xnr1, 2, and 4) (Agius et al., 2000; Kofron et al., 1999) and Vg1 (Birsoy et al., 2006; Weeks and Melton, 1987) are the potent endogenous mesoderm-inducing factors. Furthermore, several studies have also

reported that activin-mediated mesoderm induction in *Xenopus* animal caps, can be blocked by a dominant negative FGFR suggesting that FGF is required in the response to mesoderm induction (Cornell and Kimelman, 1994; LaBonne and Whitman, 1994).

A recent study in *Xenopus* has specifically addressed this question and showed that FGF signalling is essential only for the induction of paraxial mesoderm, for axial mesoderm it is mainly required for the maintenance, not for the induction (Fletcher and Harland, 2008). Additionally, this study also confirms a previously described role of FGF signalling in maintaining a positive feedback loop with the pan-mesodermal transcription factor *Brachyury* (*Xbra*) in *Xenopus* (Isaacs et al., 1994; Schulte-Merker and Smith, 1995; Smith JC, 1991). Though, this study also describes a role of FGF signalling in the initiation of *Xbra* expression (Fletcher and Harland, 2008). The ligand Fgf8 is particularly important for mesoderm development in *Xenopus* and zebrafish (Fletcher et al., 2006; Draper et al., 2003). A loss of both *Fgf8* and its paralog *Fgf24* result in posterior mesoderm defects (Draper et al., 2003).

However, not only FGFs but also different components of the FGF signalling pathway such as FGFRs, HSPGs, FRS2, Grb2 and the Ras downstream cascade have been reported to be required for mesoderm development in *Xenopus*, (Amaya et al., 1991; Neilson KM, 1996; Itoh, K. 1994; Whitman and Melton, 1992; MacNicol et al., 1993; Umbhauer et al., 1995; LaBonne, 1995; Gotoh, 1995). While the inhibition of these components blocks mesoderm formation and induces posterior and gastrulation defects, their overexpression lead to phenocopy elevated FGF signalling effects. A crucial role for FGF signalling in mesoderm formation and maintenance of mesodermal gene expression has also been described in other vertebrates including mammals, birds, and fish (Herrmann BG, 1990; Ciruna and Rossant, 2001; Griffin et al., 1995; Mathieu et al., 2004).

In addition, FGF signalling is also involved in mesoderm formation in primitive chordates. In amphioxus, FGF signalling is essential for the development of anterior somites (Bertrand et al., 2011), and in ascidians it is crucial for mesenchyme, notochord and secondary muscle development (Kim and Nishida, 1999; Kim et al., 2000; Darras and Nishida, 2001; Kim and Nishida, 2001; Imai et al., 2002; Miya and Nishida, 2003; Yasuo and Hudson, 2007). Furthermore, a recent study on the hemichordate *Saccoglossus kowalevskii* also shows involvement of FGF signalling in mesoderm specification (Green, 2013).

Outside of the vertebrate system, FGF signalling has been functionally characterized in only few model organisms for its role in the context of mesoderm development.

Interestingly, in *Drosophila*, FGF signalling was found indispensable for migration of mesodermal cells during gastrulation, but no role of FGFs has been identified in early mesoderm specification. Instead, a high activity of the transcription factor Dorsal, was found essential for mesoderm induction in the fly (Jiang et al., 1991; Ip et al., 1992). In *Drosophila*, the two *Fgf8*-like ligands *pyramus* (*pyr*) and *thisbe* (*ths*) and the receptor *Heartless* play an essential role in mesoderm morphogenesis and differentiation (Stathopoulos et al., 2004; Kadam et al., 2009; McMahon et al., 2010; Tulin and Stathopoulos, 2010). In the short-germband insect *Tribolium*, the *Fgf8*-like ligand *Tc-fgf8* and the only identified receptor *Tc-fgfr* are also implicated in mesoderm development on the basis of their complimentary expression domains in epithelial and mesenchymal territories (Beermann and Schröder, 2008). The further experimental results on mesoderm specification in *Tribolium* are described in Chapter 4 (pp. 88-90; Fig. 4.9).

In the nematode *C. elegans*, a role of FGF signalling in the specification of larval sex myoblasts, a small subset of mesoderm is established (Burdine et al., 1998; DeVore et al., 1995; Goodman et al., 2003; Lo et al., 2008). However, for early mesoderm specification Notch signalling is essential (it acts through T-box transcription factors TBX-37 and TBX-38) (Good et al., 2004). The single *Fgf* ligand in the sea urchin *fgfA*, *Strongylocentrotus purpuratus* is needed for gastrulation, directed migration of mesenchymal cells and for the morphogenesis but not for early specification of mesoderm (Röttinger et al., 2008; Tulin and Stathopoulos, 2010).

1.2.2 FGFs and morphogenesis

Gastrulation

Morphogenesis is the process by which cells during development, in response to signals, move by changing their behaviour and cytoskeletal structures and ultimately alters tissue shape and the relative positions of different cell types. For morphogenesis, convergent extension (CE) is a key process required for early cellular movements during gastrulation. However, for proper gastrulation a suitable coordination between mesoderm specification and morphogenetic movements is necessary (Pownall and Isaacs, 2010). Interestingly, FGF signalling plays an important role in both mesoderm specification and coordination of cell movements during gastrulation.

In earlier studies in *Xenopus*, when FGF signalling impaired using overexpression of a dominant-negative FGFR, most of the embryos failed to gastrulate due to impaired cellular movements (Amaya et al., 1991). However, then it was not clear whether the

observed phenotype was due to an indirect failure of mesoderm specification or due to a direct defect in cell movements (Amaya et al., 1991).

This issue was resolved by identification of two modulators proteins of FGF signalling, Sprouty and Spred in *Xenopus* (Nutt et al., 2001; Sivak et al., 2005). Instead of blocking complete FGF signalling, these proteins were found to inhibit different intracellular pathways that are required for mesoderm specification and morphogenetic movements respectively (Nutt et al., 2001; Sivak et al., 2005). While Sprouty proteins mainly inhibit the PLCγ/PKC/Ca^{2+} pathway and does not affect Ras/ERK pathway, which is needed for early mesoderm specification, Spred proteins mainly target Ras/Erk pathway and leave the PLCγ/PKC/Ca^{2+} pathway unaffected, which is crucial for morphogenetic movements (Nutt et al., 2001; Sivak et al., 2005). This is confirmed, when overexpression of FGF antagonist *Xenopus sprouty2* resulted in defects related to convergent extension movements but largely unaffected mesoderm induction and patterning (Nutt et al., 2001). Likewise, overexpression of *Xenopus spred2* resulted in defects related to mesoderm specification but largely unaffected gastrulation movements (Sivak et al., 2005). These studies have provided some clue for how a primary FGF signal can lead to both the initial specification of cells as mesoderm and later for their passage to undergo morphogenetic movements. Other studies in mouse and zebrafish, where an impairment of FGFR function resulted in embryos with severe defects in cell migration during gastrulation, further corroborate a role of FGF signalling in gastrulation movements (Ciruna and Rossant, 2001; Deng et al., 1994; Griffin et al., 1995; Sun et al., 1999; Yamaguchi et al., 1994).

This feature of FGF signalling appears to be evolutionarily conserved and most compelling evidence to support this fact came from research on *Drosophila*. In *Drosophila*, a mutation in the FGF receptor gene *heartless* leads to the failure of several mesodermal lineages to differentiate and migrate from the midline during gastrulation without affecting initial mesoderm invagination (Beiman et al., 1996; Gisselbrecht et al., 1996; Muha and Müller, 2013). Moreover, the *Fgf8*-like ligands *pyramus* and *thisbe* are also crucial for mesoderm morphogenesis during gastrulation (Gryzik and Müller, 2004; Kadam et al., 2009; Klingseisen et al., 2009). Interestingly, unlike vertebrates, Sprouty protein in *Drosophila* blocks Ras/Erk pathway activated by both Htl and Bnl signalling and thereby pathway specific responses are difficult to recognize (Reich et al., 1999). To further extend our knowledge, I studied the role of *Tc-fgf8* and *Tc-fgfr* in mesdoerm development in *Tribolium* and describe those results in Chapter 4 (pp. 88; Fig. 4.9).

Branching Morphogenesis

Many vertebrate organs like the kidney, the lungs and the vasculature possess branched tubular networks but the development of tracheal system in *Drosophila* is best-understood example of such type of branched tubular networks (Ghabrial et al., 2003; Metzger and Krasnow, 1999). Branches usually start to develop from a simple epithelial purse that undergoes reiterative budding to form a complex, tree-like array. An important role of FGF signalling in branching morphogenesis was first established for the development of the tracheal system in *Drosophila* embryo (Klämbt et al., 1992). In this study, loss-of-function mutations in the FGFR homolog *breathless* (*btl*), which expresses on developing tracheal cells, prevent tracheal branching. Later the FGF ligand *branchless*, which activates *btl* and also expresses in cells surrounding the epithelial trachea, also found essential for branching pattern (Sutherland et al., 1996). The FGF antagonist protein Sprouty in *Drosophila* was first identified due to its effects on branching morphogenesis (Hacohen et al., 1998). *spry* is also expressed in the cells located in close vicinity to *branchless* expressing cells and is critical for locally preventing secondary branching.

For the development of the mouse lung, FGF signalling has also been found as a key regulator of branching morphogenesis (Metzger et al., 2008). The ligand FGF9 in mouse is specifically expressed in mesothelium and epithelial layer of the developing lung and when knocked out shows loss of mesenchymal proliferation as well as reduced branching (Abler et al., 2009; Arman et al., 1999; Colvin et al., 2001). Similarly, while FGF10 is expressed in the lung mesenchyme, FGFR2 is expressed in the lung epithelium and loss of function of either of these genes results in a total loss of branching (Min et al., 1998).

Heart Development

The development of the heart in insects and vertebrates share some common evolutionary features. For example, both the *Drosophila* dorsal vessel (the insect heart) and the vertebrate heart derive from lateral mesodermal cells and develop as a linear tube in the beginning (Bodmer and Venkatesh, 1998; Chen and Fishman, 2000; Frasch, 1999). Moreover, the underlying molecular pathways that regulate the development of cardiovascular tissues are very similar in the fly and in vertebrates. Both the structures share a similar function of pumping hoemolymph or blood in the body respectively. In recent times, the *Drosophila* heart has emerged as a powerful model system for cardiovascular research primarily due the less complex structure of the dorsal vessel and partly due to availability of sophisticated genetic tools (Seyres et al., 2012).

The first step in *Drosophila* heart development is the specification of the dorsal mesoderm after gastrulation (Klapper et al., 1998), which will further give rise to both visceral and cardiac musculature (Cripps and Olson, 2002; Rizki and Rizki, 1978; Zaffran and Frasch, 2002). The *Drosophila* homolog of BMPs, *decapentaplegic* (*dpp*) that is expressed in the dorsal ectoderm plays an instrumental role in this process (Frasch, 1995). The specification of cardiac mesoderm from the dorsal most mesodermal cells depends on the activity of (some) intrinsic transcription factors like Tinman (Tin), Dorsocross (Doc), Pannier (Pnr) and also on the activity of Wingless (Wg) and Dpp signalling in neighboring ectodermal cells (Bodmer et al., 1990; Gajewski et al., 1999; Staehling-Hampton et al., 1994; Yin et al., 1997). Especially, the expression of *tinman* in the dorsal mesoderm is critical for the development of visceral mesoderm, heart cells and dorsal muscles (Azpiazu and Frasch, 1993; Bodmer, 1993). When the function of *tinman* is taken away a severe loss of dorsal mesodermal structures including cardioblasts and pericardial cells occurred (Azpiazu and Frasch, 1993; Bodmer, 1993).

The role of FGF signalling in heart development is identified in *Drosophila heartless* (*htl*) mutants, which show a severe loss of mesodermal cell fate. In these mutants, mesodermal cells fail to migrate towards dorsal margins, and cells do not receive the instructive Dpp signal from ectodermal cells. Subsequently, dorsal mesodermal cell fate is not specified and as a result the cardiac and visceral muscle cells are lost (Beiman et al., 1996; Gisselbrecht et al., 1996; Shishido et al., 1997). In addition, mutations in the components of the FGF signalling pathway, the genes involved in HSPG synthesis *sugarless* and *sulfateless* and the downstream adaptor gene *dof*, also cause mesoderm migration defects consequently the loss of dorsal mesoderm derivatives providing further support for the specific role of FGF signalling in mesoderm migration (Lin et al., 1999; Vincent et al., 1998).

In the vertebrate developing embryo, there are two distinct sources of heart precursor cells: the first heart field (FHF) that forms the cardiac crescent during the primitive streak stage and the secondary heart field (SHF) that remains as progenitor until they migrates and incorporates into the heart, using the FHF as a scaffold (Buckingham et al., 2005; Srivastava, 2006). These precursor cells are also of mesodermal origin and the function of *Nkx2.5*, *BMP2/4*, and *GATA* genes appear to play similar roles in heart development as the *Drosophila* orthologs *tin*, *dpp*, and *pnr* respectively (Bodmer and Venkatesh, 1998; Chen and Fishman, 2000). Several studies in mice and zebrafish also describe an important role of FGF signalling in the regulating different aspects of heart development (Marques et al., 2008; Park et al., 2008; Reifers et al., 2000).

1.2.3 FGF signalling and axes specifications

The dorso-ventral (DV) axis

The roles of FGF signalling in patterning dorso-ventral (DV) axis are not completely understood, though several studies suggest that it plays an active role in DV patterning by inhibiting BMP signalling (Fürthauer et al., 1997; Fürthauer et al., 2004). The genetic analysis has revealed that Bmp2b and Bmp7 and their antagonist chordin, are required for proper DV patterning in zebrafish embryos (Schmid et al., 2000). The *bmp2b* and *bmp7* genes initially express in the whole blastula but later become progressively confined to the ventral domain. This ventral limitation of BMP activity coincides with the spreading of expression of *fgf3*/*fgf8*/*fgf24* genes from the dorsal side of the embryo, suggesting an implication of FGF signalling in the down regulation of BMP activity at dorsal side. In accordance, activation of FGF signalling pathway leads to a dorsalisation of the embryo via inhibition of ventral Bmp gene expression. Conversely, inhibition of FGF signalling results in dorsal expansion of Bmp gene expression, which leads to an expansion of ventral cell fates. However, *fgf8* depletion alone does not cause a strong ventralization of embryos; rather its depletion in *chordino* mutant embryos shows an enhancement of the ventralization phenotype. These results suggest a functional redundancy between the *fgf* genes and also show that Chordin normally masks a specific role of Fgf8 in DV patterning (Fürthauer et al., 1997; Fürthauer et al., 2004; Langdon and Mullins, 2011). In *Xenopus*, the DV axis aligns with animal-vegetal axis of the embryos and FGF signalling also seems to play an important role in specifying the animal-vegetal axis by promoting dorsal fates in the animal sector of the marginal zone of the *Xenopus* embryo (Kumano et al., 2001; Kumano and Smith, 2002a; Kumano and Smith, 2002b). Additionally, there are some data that discusses FGF signalling as an organizer during DV axis formation, through downstream regulation of β-catenin, a component of the canonical Wnt pathway (Maegawa et al., 2006).

In the invertebrate model *Drosophila*, no direct roles of FGF signalling in the specification of the DV axis has been described. However, the FGF receptor, Heartless (Htl), and its two ligands, Pyramus (Pyr) and Thisbe (Ths), are direct targets of the transcription factor Dorsal, which is crucial for early mesoderm specification (Reeves and Stathopoulos, 2009; Stathopoulos et al., 2004).

The antero-posterior (AP) axis

In addition to its role in specifying the DV axis, FGF signalling also plays an important role in the establishment of the AP axis of the early embryo. Many gain- and loss-of-

function experiments in different vertebrates including *Xenopus*, zebrafish, chick and mouse embryos suggest a function of FGF signalling in AP patterning (Amaya et al., 1991; Christen and Slack, 1997; Davidson et al., 2000; Draper et al., 2003; Griffin et al., 1995; Isaacs et al., 1992; Ota et al., 2009; Partanen et al., 1998; Storey et al., 1998). Specifically, FGFs have a strong posteriorizing effect that allows them to convert anterior neural fate to more posterior neural cell types (Cox and Hemmati-Brivanlou, 1995; Holowacz and Sokol, 1999; Lamb and Harland, 1995; Ribisi et al., 2000; Umbhauer et al., 2000). This posteriorizing effect of FGFs is partly executed through their regulation of the ParaHox and Hox genes (Bel-Vialar et al., 2002; Cho and De Robertis, 1990; Haremaki et al., 2003; Isaacs et al., 1998; Northrop and Kimelman, 1994; Partanen et al., 1998; Pownall et al., 1996). Moreover, expression of *FGF4* and *FGF8* in posterior mesoderm of many vertebrate species can act as endogenous posteriorizing factors (Christen and Slack, 1997; Crossley and Martin, 1995; Dubrulle and Pourquie, 2004; Isaacs et al., 1992; Shamim and Mason, 1999). Now it is apparent from several studies that FGF signalling is critical for the AP patterning in all germlayers i.e. neuroectoderm, mesoderm and endoderm (Cox and Hemmati-Brivanlou, 1995; Dessimoz et al., 2006; Lamb and Harland, 1995; Partanen et al., 1998; Pownall et al., 1996; Wells and Melton, 2000; Xu, X. et al., 1999).

FGF signalling does not regulate AP axis formation on its own, rather a coordinated action of several signalling molecules including FGFs, retinoic acid (RA) and Wnts pattern the AP axis (Bayha et al., 2009; Doniach, 1995; Kiecker and Niehrs, 2001; McGrew et al., 1997; McGrew et al., 1995; Takada et al., 1994). Particularly, FGF signalling seems to regulate more posterior Hox genes, whereas RA preferentially regulates more anterior Hox genes (Bel-Vialar et al., 2002). There is an antagonistic relationship between FGF and RA, where RA down-regulates the expression of *Fgf8* and FGF signalling inhibits the expression of *Raldh2*, which encodes for an enzyme essential for RA synthesis (Diez del Corral et al., 2002; Diez del Corral et al., 2003; Diez del Corral and Storey, 2004). Moreover, FGF signalling modulates *Raldh2* expression through *Wnt8c* (Olivera-Martinez and Storey, 2007).

The mutual inhibition of FGF and RA signalling to pattern body structures along the AP axis seems to be evolutionary conserved. In the primitive chordate *Ciona*, the antagonism of RA and the FGF/MAPK signals is required to control the anteroposterior patterning of the tail epidermis (Pasini et al., 2012). No such type of relationship has been identified in the insect model *Drosophila*. However, I describe here, that in the beetle *Tribolium* the ligand *Tc-fgf1b* that has no homolog in *Drosophila* plays a crucial role during specification of the AP axis in the early embryo.

This topic is covered in Chapter 3 of this dissertation (pp. 55-59; Figs. 3.16, 3.17 and 3.18).

1.2.4 FGF signalling and the nervous system

Neural induction

Neural induction is the process in which naive ectodermal cells are instructed to undertake a neural fate that ultimately leads to the generation of nervous system in vertebrates. Several studies on neural induction, mainly from *Xenopus*, have led to the concept of "the default model", which suggests that ectodermal cells are actually fated to become neural by default. According to this model, the default neural fate of ectodermal cells is normally inhibited by BMPs that are expressed in the ectoderm, and this inhibition must be released to transpire neural induction (Böttcher and Niehrs, 2005; Thisse and Thisse, 2005; Weinstein and Hemmati-Brivanlou, 1999). Following this model, several BMP inhibitors, which are secreted by organiser cells, have been found to play a critical role in neural induction in *Xenopus* (Hemmati-Brivanlou et al., 1994b; Lamb et al., 1993; Sasai et al., 1995).

However, in recent times there are increasing evidences that suggest a pivotal role of FGF signalling in neural induction in both vertebrates and invertebrates (Bertrand et al., 2003; Cebria et al., 2002; Lemaire et al., 2002; Matus et al., 2007; Streit et al., 2000). Especially, evidences from the chick embryo suggest that FGF signalling provides the initiating neural fate determining signal that prepare the prospective neural plate for further neural-inducing signals (Sheng et al., 2003; Streit et al., 2000; Wilson et al., 2000). Though, the exact mode of action of FGF signalling in neural induction is debatable. Studies on the chick report, that FGF signalling induces neural fate by repressing *Bmp4* and *Bmp7* expression. Conversely, when FGF signalling is inhibited, *Bmp4* and *Bmp7* mRNA expression is maintained and neural fate is blocked (Wilson et al., 2000). Studies on mouse ES cells suggest that FGF signals appear to act very early as a competence factor for neural induction (Stavridis et al., 2010). Moreover, in *Xenopus*, there are contradictory results with regards to the role of FGF signalling in neural induction. Several studies support a direct role of FGFs in neural induction (Bertrand et al., 2003; Hongo et al., 1999; Launay et al., 1996; Streit et al., 2000; Wagner and Levine, 2012), whereas others report that inhibition of FGF signalling does not affect neural induction (Holowacz and Sokol, 1999; Kroll and Amaya, 1996; McGrew et al., 1997; Ribisi et al., 2000). Despite these differences, a consensus is emerging that FGF signalling indeed plays an important role specifically during induction of the posterior nervous system (Holowacz and Sokol, 1999; Rentzsch et al., 2008; Wills et al., 2010).

The role of the FGFR gene *heartless* in *Drosophila* in neurogenesis and in both glia migration and morphogenesis implicate a conserved function of FGFs in neural development (Forni et al., 2004; Garcia-Alonso et al., 2000). Moreover, in the nematode *C. elegans*, FGF signalling has also been found to affect axon outgrowth through the action of FGFR splice variant *egl-15 (5A)* (Bulow et al., 2004). Several study in the ascidian *Ciona*, corroborate a role of FGF signalling in anterior neural induction (Bertrand et al., 2003; Wagner and Levine, 2012). Furthermore, FGFRs in the platyhelminth *Dugesia japonica* also play an important role in neurogenesis indicating extension of this conserved role the Lophotrochozoa lineage (Cebria et al., 2002; Mineta et al., 2003).

Brain patterning

The isthmus is a constriction at the midbrain–hindbrain boundary (MHB) that has an organizer activity, which leads to the patterning of midbrain-hindbrain anlage. In vertebrates, *FGF8* is a key component of organizing activity due to its expression in the MHB domain (Crossley et al., 1996). A hypomorphic allele of *Fgf8* in mouse displays the loss of midbrain and cerebellar tissue (Meyers et al., 1998). In the chick, the Fgf8-isoforms, *Fgf8a* and *Fgf8b* are expressed at the MHB though the Fgf8b signal is 100 times stronger than that of Fgf8a (Sato et al., 2001). In the chick, ectopic expression of *Fgf8a* leads to expansion of midbrain, whereas misexpression of Fgf8b transforms midbrain into a cerebellum (Sato et al., 2001). In zebrafish, FGF8 is also detected at the MHB and acts as a morphogen to pattern the midbrain (Reifers et al., 1998). The *Fgf8* mutant *acerebellar* in zebrafish lack a cerebellum and a functional midbrain-hindbrain boundary (MHB). Apart from *Fgf8*, *Fgf17* and *Fgf18* are also expressed at the MHB in the mouse and the loss of *Fgf17* results in the truncation of the posterior midbrain and curtailed proliferation of anterior cerebellum (Maruoka et al., 1998).

A similar function of FGF signalling has been described for the primitive chordate *Ciona intestinalis*. Like in vertebrates, the loss of *Fgf8* patterning activity results in the transformation of hindbrain structures into an expanded mesencephalon in the ascidian (Imai et al., 2002; Imai et al., 2009; Satou et al., 2002). However, no such structure as a midbrain-hindbrain boundary (MHB) organizer has been identified in the diverged insect *Drosophila*. In contrast, on the basis of *fgf8 expression*, the presence of an insect-equivalent to the midbrain–hindbrain boundary (MHB) has been discussed in a more basal holometabolous insect *Tribolium* (Beermann and Schröder, 2008). In *Tribolium*, a fine stripe of *Tc-fgf8*, *Tc-fgfr* and *Tc-dof* expression in each head lobe divides the brain into a larger anterior and a smaller posterior

region (Beermann and Schröder, 2008). Based on these findings, the role of *Tc-fgf8* in brain tissue development has been studied in fixed embryos of *Tc-fgf8* knockdown animals and described in this thesis in Chapter 4. (pp. 86-88; Fig. 4.8).

1.3 The model insect *Tribolium castaneum*

Tribolium castaneum, also known as the Red Flour Beetle, is a basal holometabolous insect that represents the largest order of insects, the Coleoptera. The beetle *Tribolium* is a major pest of stored grains and grain products and distributed all over the world. These beetles are very easy to rear on normal wheat flour and do not require any additional water supply. The beetle has a fairly short life cycle, which spans about 3-4 weeks depending on the incubation temperature, with 30º C as best for the optimum growth. The lifespan of the adult beetles is quite long ranging from 2 to 3 years. These features make *Tribolium* an ideal lab animal (Brown et al., 2009).

For several decades, *Tribolium* was used as an important insect model organism mainly for studying classical genetics, ecology, population biology and the physiology of this insect (Brown et al., 2009; Sokoloff, 1974). However, since the last few decades this beetle has been established as a sophisticated model system for studying Evo-Devo (Evolution of Development) approach of insects that either complement (in most cases) or contradict (in few cases) parallel studies in *Drosophila* (Brown et al., 2009; Klingler, 2004). In the agricultural community, *Tribolium* has also been used to study biological processes like pesticide resistance. Considering the fact that the fruit fly *Drosophila melanogaster* is the most powerful insect model organism for genetic / developmental studies, it is important to know the distinct features in *Tribolium* that establish this beetle to qualify as a second insect model organism. Some of them are described below.

While *Tribolium* and *Drosophila* both belong to the holometabolous group of insects, *Tribolium* has more ancestral features of insects, whereas *Drosophila* shows highly diverged characters. One basic fundamental difference between the two insects is their mode of segmentation. Unlike the *Drosophila*'s long germband mode where all its body segments form almost simultaneously at the blastoderm stage, *Tribolium* has a short germ mode of development where only head and thoracic segments are specified at the blastoderm stage and more posterior segments of the body form sequentially from the growth zone during germband elongation (Handel et al., 2000; Heming, 2003; Tautz et al., 1994). This feature parallels the mode of somitogenesis of vertebrates and allows for an evolutionary comparison of the mechanisms underlying body elongation between insects and vertebrates. Another fundamental

difference lies in the mode of development of the head and the appendages in *Tribolium* and *Drosophila.* Like more basal insects, *Tribolium* possess a non-invaginated head and outgrowing limb buds that facilitate the analysis of head- and limb development in insects during early embryogenesis (Bucher and Wimmer, 2005 ; Posnien et al., 2010).

Moreover, there is a fundamental difference in the blastoderm fate map of *Tribolium* and *Drosophila* in the early embryo (Schröder et al., 2008). While the embryonic head is the anterior most structure in *Drosophila*, this position is occupied in *Tribolium* by the extraembryonic membranes, the serosa and the amnion and the head originates from a medial position in the egg (Lynch and Roth, 2011; Sharma et al., 2013a). In addition, the extensive extraembryonic tissues seen in *Tribolium* and in many basal insects are largely reduced in *Drosophila* (for more details see Introduction in Chapter 5). The early fate map along the DV axis in *Tribolium*, however, is very similar to that of long-germ embryos (Chen et al., 2000). Interestingly, despite these differences in the fate map most of the genes that govern specification of the DV and the AP axes in *Drosophila* have also been identified in *Tribolium* as orthologs and appear to be involved in the same processes with few exceptions (Chen et al., 2000; Nunes da Fonseca et al., 2009; Nunes da Fonseca et al., 2008; Schinko et al., 2008; Schröder, 2003; van der Zee et al., 2005; Van der Zee et al., 2008; van der Zee et al., 2006).

Most importantly, most of the sophisticated tools available for genetic manipulations in *Drosophila*, are also applicable in the beetle *Tribolium*. For example, transgenesis is one of them that facilitate genetic manipulation in *Tribolium* by insertion of transposable elements (e.g. *piggyback* and *Minos*) into the *Tribolium* genome (Berghammer et al., 1999a; Lorenzen et al., 2003; Pavlopoulos et al., 2004). With this tool, misexpression studies are also now feasible with the establishment of the GAL4/UAS system in *Tribolium* (Schinko et al., 2010). Insertional mutagenesis is another established technique in *Tribolium* that allow studying the gene function (Berghammer et al., 1999b). Moreover, the accessibility of the complete *Tribolium genome sequence* further enhances its applicability for developing more sophisticated genetic tools (Richards et al., 2008).

Besides these sophisticated tools, a robust and powerful systemic RNA interference (RNAi) technique to knock down gene function through injection of dsRNA is also feasible in *Tribolium*, which facilitates reverse genetics approach. This method was first introduced in the animal model *C. elegans* (Fire et al., 1998), and since then has been applied to many other invertebrate species. Although, RNAi has some limitations in *Drosophila* (Miller et al., 2008), RNAi in the beetle *Tribolium* is highly

efficient and, like *C. elegans*, systemic in nature (Bucher et al., 2002; Miller et al., 2008). This systemic nature allows injection of double stranded RNA (dsRNA) at every lifecycle stage of the beetle including eggs, larvae, pupae and adults. While injection of dsRNA in preblastoderm eggs {embryonic RNAi (eRNAi)} is useful for the functional characterization of genes with specific zygotic contribution (Brown et al., 1999; Schinko et al., 2008), dsRNA injection at the larval stage {larval RNAi (lRNAi)} is appropriate for decoding the function of genes involved in metamorphosis (Tomoyasu and Denell, 2004). Moreover, dsRNA injection into female pupae or adults {pupal RNAi (pRNAi) / adult RNAi (aRNAi)} can trigger an RNAi response in offspring embryos and this phenomenon is referred as "parental RNAi (pRNAi)" (Bucher et al., 2002). All the experimental results in this study are based on pRNAi knocking down the function of only one (single RNAi) or two (double RNAi) gene products. The primary read-out of gene function is first based on the cuticle of the first instar larva, developed from the egg laid by the mother beetle injected with dsRNA. If a phenotype was observed at this level, further analyses based on the expression of marker genes were performed on fixed embryos of various developmental stages to reveal the molecular basis and eventually the primary cause of the phenotype. According to a recent study, the effectiveness of the RNAi response in *Tribolium* depends on the size and concentration of the dsRNA (Miller et al., 2012). This study further shows that the knockdown of multiple genes through combinatorial injection of dsRNA in *Tribolium* might result in an unspecific effect primarily due to the oversaturation of RNAi machinery and secondly due to competitive inhibition between the injected dsRNAs (Miller et al., 2012). Recently, RNAi was employed for the study of gene functions in a genome-wide manner (iBeetle-Project). Therefore, the availability of forward and reverse genetics screening tools establishes *Tribolium* as an emerging model organism not only for Evo-Devo studies but also for studying basic insect biology (Klingler, 2004).

1.4 Objectives of the dissertation

The conserved nature of the FGF signalling pathway in vertebrates and invertebrates encouraged me to functionally characterize various genes involved in the FGF signalling cascade of the beetle *Tribolium* through pRNAi knockdown. One main goal was to describe similarities and differences between these fundamentally distinct animal phyla in respect of FGF-signalling. Specifically I analysed the function of the ligands FGF1 (Chapter 3) and FGF8 (Chapter 4) and the FGF-receptor (Chapter 4). Another goal of this dissertation was to carefully document the complete spatio-temporal expression profile of various genes involved in the formation or regulation of the extra-embryonic membranes in wildtype and in dsRNA treated embryos (Chapter 5).

2   Chapter 2: Materials and Methods

2.1 Animal husbandry

The wildtype San Bernardino strain of red flour beetle, *Tribolium castaneum*, was used for all the experiments done. Whole-wheat flour supplemented with 5% yeast extract was used to rear the beetles in a 30°C incubator (Sokoloff, 1974). Collection of eggs was performed as previously described (Beermann et al., 2004).

2.2 Candidate gene search and PCR cloning

The search for potential orthologs in the *Tribolium* genome was achieved using reference protein sequences of candidate *Drosophila* or mouse genes available at the NCBI database (http://www.ncbi.nlm.nih.gov/). The sequence alignment step was performed using "BLAST" tool from the Beetle Base, a dedicated server for the *Tribolium* genome database (http://beetlebase.org/blast/blast.html). All the gene-specific primers were designed using "NCBI/ Primer-BLAST" and "Primer-3" software tools (see Appendix 1, Table S1). For cDNA synthesis, total RNA was isolated from a pool of 0-48h staged embryos using PureLink^{TM} Micro-to-Midi^{TM} Total RNA Purification System kit (Invitrogen) and used as a template for random hexamer primers of the Transcriptor First Strand cDNA Synthesis Kit (Roche). Gene specific fragments were amplified using cDNA by standard PCR and the amplified fragments were sub-cloned into the "pCR4-TOPO" plasmid vector of the TOPO-TA Cloning® Kit (Invitrogen) and identified by sequencing using standard T3 (AATTAACCCTCACTAAAGGG), or T7prom (TAATACGACTCACTATAGG) primers (LGC Genomics; Berlin).

2.3 Molecular Biology

For double stranded RNA (dsRNA) synthesis, linearized plasmid DNA containing insert was used as a template to generate sense and anti-sense strands of RNA through T3 and T7 MEGAscript® *in-vitro* transcription kits (Ambion) and the products were cleaned up using MEGAclear^{TM} Purification kit (Ambion). The annealing of two strands synthesized dsRNA that was further purified using the same purification kit (Ambion). The DIG-labelled antisense RNA probes were synthesized using DIG RNA Labelling Mix (Roche) and T3/T7/SP6 RNA polymerases (Roche).

The parental RNAi (pRNAi) was performed by either injecting female pupae or freshly hatched female adults under standard conditions (Bucher et al., 2002;

Schröder, 2003). Due to a high mortality rate observed in pupal injection, most of the functional analysis is based on adult injection. To exclude any unspecific results, a non-overlapping fragment was also injected (see Appendix 1, Table S1). At least two different concentration of dsRNA were used for each RNAi experiment (see Appendices 3 and 4).

2.4 Fixation of embryos

A mixture of 0-18h, 12-36h and 24-48h old egg-lays was used for fixation (Schinko et al., 2009) to provide a spectrum of all the various developmental stages for wildtype as well as for RNAi treated embryos. In case of RNAi affected embryos, from each egg lay collected, a larger amount of eggs was taken for the fixation purpose (to further perform *in situ* hybridization or immunolocalisation studies) while the remaining eggs were allowed to develop a cuticle by incubating them at 30 °C for several days.

2.5 Histological Examination

For mRNA and protein detection, *in-situ* hybridization and immunolocalisation studies were performed respectively as previously described (Patel et al., 1994; Tautz and Pfeifle, 1989).

The details of each RNA probe used in this study are described in Table S2 (Appendix 1). For immunolocalization studies, the Even-skipped monoclonal antibody (obtained from the Developmental Studies Hybridoma Bank) and the rabbit polyclonal phosphorylated-MAD (pMAD; Mother Against Dpp) antibody (a gift from Dr. Morata, Centro de Biologia Molecular, Madrid, Spain) were used at a dilution of 1:100 and 1:200 respectively.

For single probe staining NBT/BCIP (blue) and for double probe staining NBT/BCIP (blue) and INT/BCIP (red) were used as substrates for alkaline phosphatase. To achieve minimum background noise, a rigorous calibration of each gene specific probe and each antibody was performed prior to the final analysis. Embryos were counterstained for nuclear DNA with Hoechst 33342 stain (Applichem).

For quantitative comparisons of signal intensities in both wildtype and affected RNAi embryos, each *in-situ* hybridization or antibody staining was performed strictly in parallel condition and the time allowed for colour development was kept equal for both. In addition, to judge a fate map shift of the expression pattern, a minimum of 5 stage matched WT and affected embryos were analysed. All other molecular techniques were performed according to the instructions of the suppliers or following standard protocols (Sambrook et al., 1989).

2.6 Cuticle preparations and mounting of stained embryos

The first instar wildtype and RNAi-affected larvae were initially dechorionized in bleach (DanKlorix) containing 5% Sodiumhypochloride, washed in water and incubated in lactic acid/Hoyer's medium (1:1) at 65 °C overnight (Bucher and Klingler, 2004). Embryos stained by in situ hybridization or antibody staining, were initially stored in 60% glycerol but mounted in 100% glycerol when prepared free from yolk particles.

2.7 Microscopic Analysis

Photographs were taken using AxioCam MRc (for colour images) and AxioCam MRm (for black and white images) cameras on an AxioImager Z1 Zeiss microscope and processed with AxioVision 4.8.1 software. Cuticle analysis was mainly done using fluorescence microscopy while coloured embryos were analysed using DIC, Brightfield and fluorescence microscopy. Most of the embryonic images were taken without a cover slip as it facilitates the turning of the embryo manually to document each axial view (ventral, lateral and dorsal). The symmetry and asymmetry of any gene specific expression was only possible to judge when rotating the same embryo in all possible axial views (ventral, lateral, dorsal view). All the pictures shown in one panel of each marker originate from the same staining reaction to be able to judge differences in stage specific expression levels. Whenever required, different focal planes pictures of the same specimen were merged into one picture using Photoshop CS5 to show a larger viewpoint for that embryo.

2.8 Mock Injection and Positive Control

To judge the efficacy and specificity of RNAi in *Tribolium*, a negative control (by water injection) and two positive control (by injecting *Tc-dll*, *Tc-byn* dsRNA) experiments were performed. While water injection did not show any visible effect, *Tc-dll* and *Tc-byn* knockdown resulted in the same cuticle phenotypes described in previous studies respectively (see Appendix 1, Figure S1) (Beermann et al., 2001; Berns et al., 2008).

2.9 RNAi-based Off-Target effects

RNA interference (RNAi), mediated by small 21-23 bp short interfering RNAs (siRNAs), is one of the widely used techniques trusted for suppressing the gene function in plants and animals (Filipowicz, 2005; Rana, 2007). Although, sometimes RNA interference machinery in addition to generating gene specific target siRNAs also generate some non-specific siRNAs that leads to unintended gene silencing,

which can results in producing false positive results (Jackson et al., 2006). Therefore, to exclude any off-target effects, if any, in a performed RNAi experiment, the sequence of that particular injected fragment was blasted against the *Tribolium* genome (http://beetlebase.org/blast/blast.html). In most of the cases the off-target sequences were shorter than 21 nucleotides. However in few cases the off-target sequences were found longer than 21 nucleotides that can potentially produce some off-target effects but further characterization revealed that either these off-target sequence binds to intronic region or intergenic regions, hence can not serve as off-target effects. To further experimentally exclude off-target effects, at least two non-overlapping fragments (NOFs) for each gene (see Appendix 1, Table S1) were injected and the same range of phenotypes were observed for both the injections.

2.10 TUNEL Assay

The TUNEL (**T**dT mediated d**U**TP **n**ick **e**nd **l**abeling) assay is one of the widely used methods to detect apoptosis in cells (Gavrieli et al., 1992). Apoptosis is the programmed cell death and unlike necrosis is not triggered by accidental damage to the cell. Instead, apoptosis is a highly conserved process that plays a major role in the development and regeneration of tissues and is controlled by complex regulatory networks within the cell (Jin and El-Deiry, 2005). The early characteristics of apoptotic cells are the structural changes in nucleus and cytoplasm that includes rapid blebbing of plasma membrane and nuclear disintegration. This nuclear collapse leads to extensive damage to chromatin and degradation of DNA by endonucleases into oligonucleosomal length DNA fragments. These DNA fragments are the basis of detection of apoptosis by TUNEL method. The DNA fragments were labelled by terminal deoxynucleotidyl transferase (TdT) enzyme, which catalyzes polymerization of labeled nucleotides (dUTPs) to free 3'-OH DNA ends in a template-independent manner. The labeled nucleotides can then be detected by AP conjugated anti-fluorescein antibody. Finally, the colour reaction with the substrate NBT/BCIP was used to exactly pinpoint the site of apoptosis. For the TUNEL Experiment the *In Situ* Cell Death Detection Kit (Roche, Mannheim) was used, which works with fluorescein as a marker. The protocol for the TUNEL is adapted from "TUNEL for *Tribolium*" (Kotkamp et al., 2010) and "TUNEL for *Cupiennius*" (Prpic and Damen, 2005) with some modifications.

Fixed *Tribolium* embryos (stored at -20°C in methanol) were gradually rehydrated by successive incubations in 75, 50 and 25% methanol in PBS-Tween (PBT) for 3-5 minutes each then finally washing twice with 100% PBT for 5 minutes each. The embryos were then treated with proteinase K (1ml PBT + 1.0 µl proteinase K; 14-22

mg/ml) for 2 minutes and washed thrice with PBT. Postfixation of the embryos with formaldehyde by incubating them in 1ml PBT + 140 μl of formaldehyde (37%) for 15 minutes was followed with several washing steps with PBT afterwards. At this point, as a positive control, wildtype embryos were treated with DNaseI (0.06 U / μl) for 30-45 min at 37°C, before being washed three times in DNaseI Buffer. This treatment is sufficient to cause fragmentation of genomic DNA. Here, the positive control was strictly separated from the other samples, in order to prevent contamination of the samples with DNaseI. The embryos were then washed three times with TdT buffer and incubated at 37°C in Tdt buffer containing 20 μM DIG-UTP and 0.3 U/μl TdT enzyme (In Situ Cell Death Detection Kit; Roche). In case of the negative control embryos, the TdT enzyme treatment was excluded. All the embryos were washed thrice with TdT buffer for 10 min each and then thrice with BST buffer for 5 min each and finally incubated in BST buffer at 70°C for 20 min to inactivate TdT enzyme. Embryos were again washed three times for 5 min each with PBT and then washed with PBT containing Boehringer- Blocking- Reagent (1 %) for 1 hour to block the reaction. The embryos were then incubated in PBT with Boehringer-Blocking-Reagent (1 %) + 1:2000 anti-fluorescein antibody for overnight at 4°C. The overnight incubation of the embryos were followed by three time washing with BST buffer for 5 min each and then for several times washing for almost 2 hour with PBT to completely remove any unspecific or unbounded product. The embryos were washed a couple of times with staining buffer and followed by NBT/BCIP staining (20 μl NBT/BCIP in 1 ml PBT). After colour development, repeated washing with PBT stopped staining and then the embryos were postfixed with 4% formaldehyde. After Hoechst nuclear counter-staining, the embryos were stored in 60% glycerine at RT.

2.11 Rapid Amplification of cDNA Ends - Polymerase Chain Reaction (RACE-PCR)

A full-length clone of cDNA derived from the target mRNA sequence is the preferred choice to precisely map that protein-coding gene onto the genomic DNA sequence. However, until the introduction of RACE-PCR in late 1980s, a common problem combated in making cDNA libraries was the amplification of partial clones that lack sequences corresponding to either 5' end or 3' end of the target transcript. An incomplete reverse transcription of the mRNA was thought to be the reason for generation of these partial clones (Frohman et al., 1994). Such type of difficulties were overcome, to some extent, by advent of a new PCR-based cDNA cloning

procedure called as RACE-PCR or One sided PCR or Anchored PCR (Frohman et al. 1988).

Unlike conventional PCR, the main advantage of this technique is the need for only a short stretch of sequence information (28-34 bp) within any region of the target mRNA to clone full-length cDNA of that transcript (Figure. 2.1).
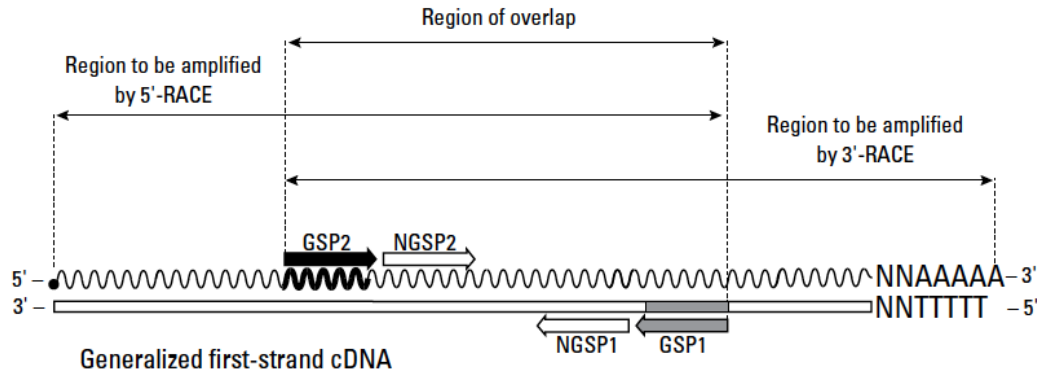
Figure 2.1: A schematic overview of the relationship between gene-specific primers and the cDNA template in RACE-PCR. Gene-specific primers (GSP) lead to produce overlapping RACE products. These products can further controlled by an additional nested-PCR reaction using nested-GSPs (NGSPs). The first strand cDNA template (RNA/DNA hybrid) shown here does not represent either the 5'-RACE-Ready or 3'-RACE-Ready cDNAs (figure taken from SMARTer™ RACE cDNA Amplification Kit User Manual).

While the known sequence can serve as a binding template for the gene specific primer (GSP), an additional anchor sequence supplemented at the end of the cDNA can serve as a binding template for the synthetic universal primer. This procedure is also very efficient in identifying various transcripts of a single gene derived from the alternative splicing of the exons of a functional mRNA. Here I used "SMARTer™ RACE cDNA Amplification Kit (Clontech)" and "Advantage® 2 PCR Kit (Clontech)" to identify the actual 3' or 5' end of the *Tc-fgf1a* or the *Tc-fgf1b* gene through RACE-PCR reactions. The kit protocol was strictly followed, the essence of which is briefly described below:

Step 1: Generation of RACE-Ready cDNA

➢ In the first step, two separate 5' RACE-Ready cDNA and 3' RACE-Ready cDNA templates were synthesized from the isolated total RNA (lab) using 5'-RACE CDS Primer A/ 3'-RACE CDS Primer A, SMARTer II A Oligonucleotides (only for 5' RACE-Ready cDNA) and SMARTScribe™ Reverse Transcriptase (all provided with the kit). For further details see Appendix 1, Figure S2 (steps 1-3) and Figure S3 (steps 1-2).

Step 2: RACE-PCR reaction

➢ In the second step, the 5' RACE-Ready cDNA and the 3' RACE-Ready cDNA were used as templates for binding of gene specific primers (GSPs) extending in either 5' or 3' direction from a particular position and kit supplied Universal Primer A Mix (UPM) at the end of cDNA. The UPM consists of a long UP sequence and a short UP sequence. Since the 3' sequence of long UP and the 5' sequence of SMARTer II A Oligonucleotides (used in 5'-RACE cDNA) or 3'-RACE CDS Primer A (used in 3'-RACE cDNA) are complementary sequences, long UP always binds at the end of cDNA irrespective of the orientation. The short UP sequence however complement the 5' sequence of the long UP and thereby allow the unknown sequence to be flanked by the primer pair of GSP and UPM. For further details see Appendix 1, Figure S2 (steps 4-7) and Figure S3 (steps 3-7).

Step 3: Nested-PCR Reaction

➢ In the third step, to exclude the background noise or non-specific amplification, the amplified products obtained from the 5' RACE-PCR or the 3' RACE-PCR reactions were subjected for further characterization using nested-PCR reactions through nested gene-specific primer (NGSPs). The amplified products of nested reactions were then sub-cloned into a pCR4-TOPO vector and confirmed by sequencing. This step is optional as there are other methods available (i.e. Southern Blot Analysis) that can be adopted for characterization of RACE-PCR products.

3 Chapter 3

Characterization of Fgf1-like genes (*Tc-fgf1a* and *Tc-fgf1b*) in the beetle *Tribolium*

Text is partly taken from *Sharma et al; Developmental Biology 381 (2013) 121–133* with some modifications

3.1 Introduction

The fibroblast growth factor (FGF) signalling-pathway is important for many processes during embryogenesis as different as axis formation, cell migration and organ specification in both vertebrates and invertebrates (Böttcher and Niehrs, 2005; Dailey et al., 2005; Dorey and Amaya, 2010; Muha and Müller, 2013; Tulin and Stathopoulos, 2010).

One of the main events in early embryogenesis is the specification of the main body axes, the anterior-posterior (AP) and the dorsal-ventral (DV) axes. In insects and vertebrates, these processes are not regulated by a single factor alone. Rather, a network that connects various signalling pathways patterns the early embryo in a concerted fashion. One of these pathways is the fibroblast growth factor (FGF) signalling pathway, which is involved in patterning both the axes (Perrimon et al., 2012). In the early *Xenopus*- and zebrafish embryo, FGF signalling promotes dorsal fate by inhibiting BMPs (bone morphogenic protein) in the dorsal mesoderm and thereby restricting BMP expression to the ventral mesoderm (Fletcher and Harland, 2008; Fürthauer et al., 2004; Londin et al., 2005). During the development of the AP axis in vertebrates, FGF8 together with Wnt3a act as posteriorizing signals by antagonizing the retinoic acid (RA) signalling pathway at the posterior of the embryo (Bayha et al., 2009; Diez del Corral and Storey, 2004; Kiecker and Niehrs, 2001). In addition, FGF signalling is also required for the specification of anterior neural structures and the brain (Bertrand et al., 2003; Dorey and Amaya, 2010; Fletcher et al., 2006; Ota et al., 2009; Yang et al., 2002) and moreover the absence of Wnt-signalling activity is a prerequisite to attain this process (Petersen and Reddien, 2009). The down regulation of Wnt-activity, which allows for anterior development, is achieved by FGF-activated *Sox* genes that negatively interfere with the Wnt signalling pathway (Mansukhani et al., 2005; Murakami et al., 2000; Petersen and Reddien, 2009). In *Xenopus*, Sox17 acts as direct Wnt antagonist by binding to the armadillo-repeats of beta-catenin leading to its immediate degradation (Zorn et al., 1999).

In the model organism *Drosophila* a role of FGF signalling in mesoderm morphogenesis and tracheal development is evident (Muha and Müller, 2013) but a specific role in early axis formation has not been described in insects. Compared to *Drosophila*, *Tribolium* has a different blastoderm fatemap along its anterior-posterior axis. In the beetle embryo the most anterior structures specified at the blastoderm stage give rise to the extraembryonic structures serosa and amnion whereas the embryo proper forms in the posterior half of the egg. In contrast, in *Drosophila* the

single extraembryonic membrane, the amnioserosa, is of dorsal origin and the embryonic structures comprise the whole egg, with the embryonic head anlage as the most anterior structure represented at the blastoderm stage (Nunes da Fonseca et al., 2009).

The presence of 22 different FGF ligands and 4 FGF receptors in vertebrates facilitate complex FGF signalling, whereas in *Drosophila* only three Fgf ligands, representing two Fgf subfamilies and two Fgf receptors are present (Tulin and Stathopoulos, 2010). The genome of the red flour beetle *Tribolium castaneum* however contains four Fgf ligands with homology to three Fgf subfamilies and only one FGF receptor (*Tc-fgfr*) that is most similar to the *Drosophila heartless* gene (Beermann and Schröder, 2008).

Notably, the vertebrate Fgf1 subfamily, which is represented by two genes *Tc-fgf1a* and *Tc-fgf1b* in the *Tribolium* genome is absent in the *Drosophila* genome and also has not been found in other dipteran genomes like that of *Anopheles*. However, a single *Fgf1* – like gene has been identified in the hymenopterans genomes of the honeybee (*Apis mellifera*) and the wasp (*Nasonia vitripennis*) but their function(s) have yet to be characterized (The Honeybee Genome Sequencing Consortium, 2006; Tulin and Stathopoulos, 2010; Werren et al., 2010). In vertebrates, the *fgf1* genes are ubiquitously expressed but no distinct function in respect to embryonic patterning has been described (Beenken and Mohammadi, 2009; Beermann and Schröder, 2008). The *Tribolium fgf1* genes are also ubiquitously expressed (see Appendix 3, Figure S10) but their functional role is yet to be revealed (Beenken and Mohammadi, 2009; Beermann and Schröder, 2008).

The analysis of the genomic region containing the two *Fgf1*-like genes, *Tc-fgf1a* and *Tc-fgf1b*, in *Tribolium* has revealed some degree of synteny when compared to *Drosophila* and suggested a loss of *Fgf1* in flies. Furthermore, while the gene structure of *Tc-fgf1a* represents a complete *Fgf* gene like features as it is composed of three exons (Itoh and Ornitz, 2011), a two exon specific structure for *Tc-fgf1b* gene raises some doubts of its gene integrity (Beermann and Schröder, 2008). To date, it is not clear whether these two orthologs (*Tc-fgf1a* and *Tc-fgf1b*) represent a beetle specific gene duplication event or whether they represent splice variants of a single *Fgf1* gene.

3.2 Aim

The background knowledge and the relevance of FGF signalling components in the beetle *Tribolium* in the context of "Evo-Devo" motivated me to study some specific projects, with the following objectives:

1. A thorough examination of the genomic structure of both the *Fgf1* like genes *Tc-fgf1a* and *Tc-fgf1b* using the 3' and 5' RACE-PCR technique.

2. To functionally characterize *Tc-fgf1a* and *Tc-fgf1b* genes using RNA interference (RNAi) first at the cuticle level and later at the molecular (embryonic) level through in-situ hybridization/immunostaining techniques to reveal the expression of marker genes.

3.3 Results

3.3.1 RACE-PCR analyses to identify full length transcripts of *Tc-fgf1a* and *Tc-fgf1b* genes

The two *Fgf1*-like orthologs, *Tc-fgf1a* and *Tc-fgf1b* are clustered within a region of 2 kb on the chromosomal linkage group 8 (Beermann and Schröder, 2008). In this study, by performing a series of 3' and 5' RACE-PCR and nested PCR reactions, I aimed for identifying the actual 3' and 5' ends of both the genes.

A general overview of each accomplished RACE-PCR reaction is shown by schematic drawings (e.g. Fig 3.1). The first part (i) of each drawing explains: (a) the orientation of the RACE-PCR reaction (b) the region of template amplified using a gene specific primer (GSP) and a universal primer A mix (UPM) from the RACE-Ready-cDNA kit (company). The second part (ii) of each drawing illustrates the characterization of the amplified RACE-product by different nested PCR reactions. For a nested PCR the amplified product was further used as a template to generate short and specific fragments within the amplified region with the help of different gene specific nested primers (NGSPs) and a common Nested Universal Primer A (NUP). The third part (iii) of each drawing shows the results obtained from each nested PCR reaction. The identity of the amplified fragments was confirmed by sequencing (all the primers used as GSPs and NGSPs in this study are listed in Table S3, Appendix 1).

3.3.1.1 3' RACE-PCR analysis for *Tc-fgf1a* (TC006602)

At first, a combination of three different 3' RACE-PCR and nested PCR reactions were performed to identify the actual 3' end of the transcripts generated from the *Tc-fgf1a* exon assembly (TC006602) and also to explore a possible interconnection between the two exon assemblies of *Tc-fgf1a* and *Tc-fgf1b* (Fig 3.1).

In a first 3' RACE-PCR reaction (Fig. 3.1A), a forward primer (5'®3') starting in the first exon a_1 of *Tc-fgf1a* (primer #11) was used as GSP1 to generate a gene specific fragment with added 3' end (Fig. 3.1A, (i)). This amplified product was then characterized with the help of four different nested PCR reactions (Fig. 3.1A, (ii)). In nested reactions a forward primer (5'®3') in each exon of the *Tc-fgf1a* exon assembly (primer #142 for exon a_1; primer #12 for exon a_2 and primer #14 for exon a_3) and a forward primer (5'®3') in first exon of the two *Tc-fgf1b* exon assembly were used as NGSP1 to NGSP4 respectively (Fig. 3.1A, (ii)).

The results of two nested PCR reactions showed amplification of two short fragments containing 3' UTR and poly(A) tail at the end (Fig. 3.1A, (iii)). While the amplified product with NGSP2 (a primer in exon a_2) was larger and covered sequences from both the exons (exons a_2 and exons a_3) (see Appendix 2.1), a shorter fragment was amplified with NGSP3 (a primer in exon a_3) that contained only exon a_3 specific sequence (see Appendix 2.2).
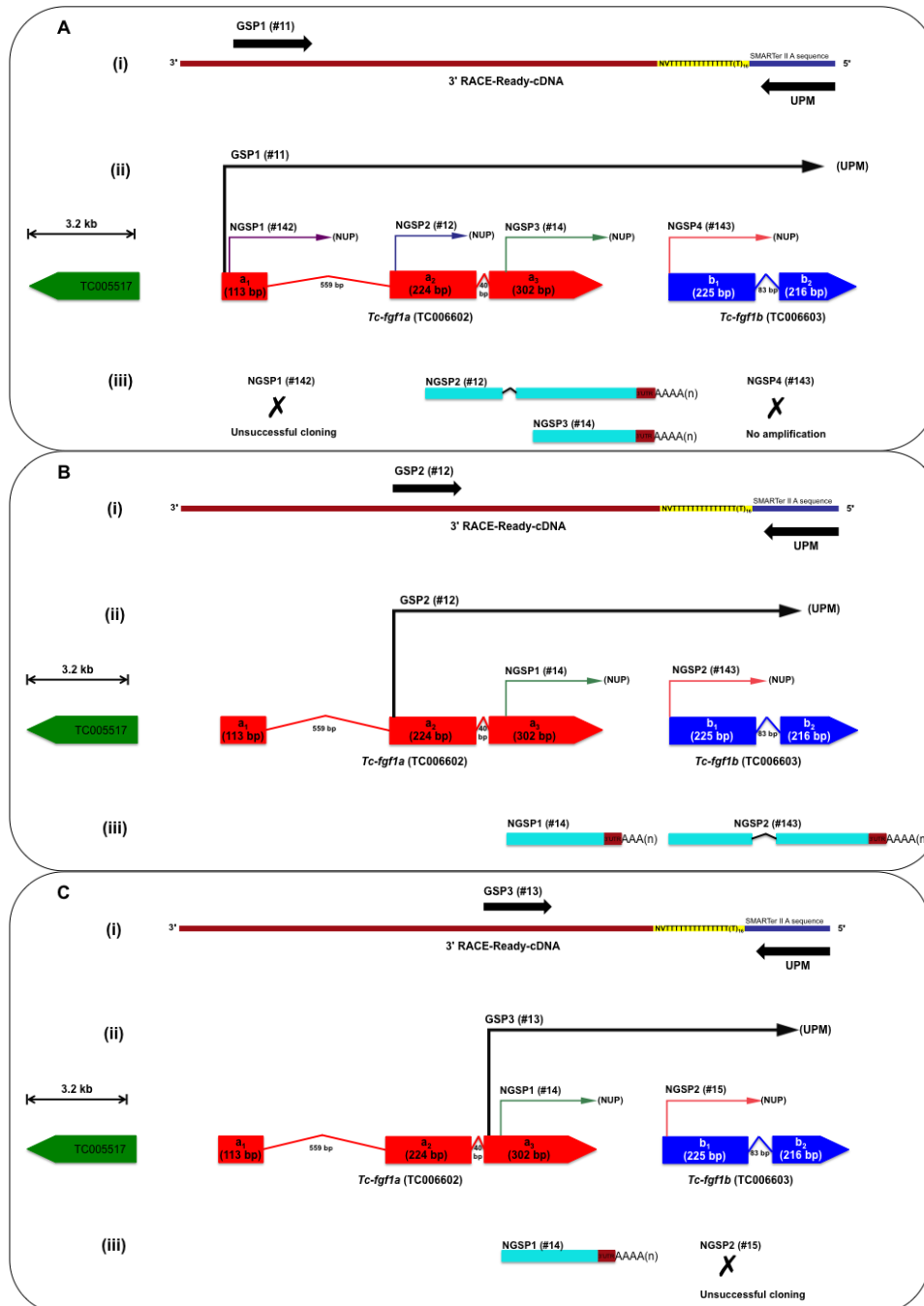
Figure 3.1: Schematic overview of three different 3' RACE-PCR/nested-RACE-PCR reactions performed to identify 3' ends of *Tc-fgf1a* (TC006602) gene and the obtained results. **(A)** In the first 3' RACE-PCR reaction (i) an "exon a_1" specific primer (#11) used as GSP1 to amplify the gene fragment from 3' RACE-Ready-cDNA. In further nested-PCR reactions (ii) a forward primer (5'➔3') from each exon of *Tc-fgf1a* assembly and one from "exon b_1" (#143) of *Tc-fgf1b* assembly were used as NGSPs to generate

short and specific fragments. (iii) Nested reactions with NGSP2 and NGSP3 successfully resulted in amplification of two specific fragments having 3' UTR and Poly(A) tail at the end. While reactions with NGSP1 resulted in non-specific amplification, no product was amplified with the primer NGSP4. **(B)** For second 3' RACE-PCR reaction (i) "exon a_2" specific primer (#12) was used as GSP2 to amplify the gene fragment from 3' RACE-Ready-cDNA. For nested-PCR reactions (ii) a forward primer (5'➔3') from "exon a_3" was used as NGSP1 and the primer from "exon b_1" (#143) was used as NGSP2 to generate short and specific fragments. (iii) Both the nested reactions resulted in amplification of exon specific fragments with 3' UTR and Poly(A) tail at the end. **(C)** In the third attempt (i) "exon a_3" specific primer (#13) was used as GSP3 to amplify the gene fragment from 3' RACE-Ready-cDNA. For nested-PCR reactions (ii) again a forward primer (5'➔3') from "exon a_3" was used as NGSP1 and another primer from "exon b_1" (#15) was used as NGSP2 to amplify short and specific fragments. (iii) An exon a_3 specific fragment with 3' UTR and Poly(A) tail was successfully amplified for the nested reactions with NGSP1. Reaction with NGSP2 resulted in unsuccessful cloning. (GSP, Gene Specific Primer; NGSP, Nested Gene Specific Primer; UPM, Universal Primer A Mix; NUP, Nested Universal Primer A; 3' UTR, 3' Untranslated region; left-right arrow to bar in (ii) represents 3.2 kb of genomic region covering *TC005517*, *Tc-fgf1a* and *Tc-fgf1b* genes)

No clear results were observed from other nested reactions as the reaction with NGSP1 (primer #142) resulted in non-specific amplification and no product was amplified from the reaction with NGSP4 (primer #142) (Fig. 3.1A, (iii)). These initial results support the predicted organisation of exons in *Tc-fgf1a* gene and also did not reveal any physical interconnection between the exon assemblies of *Tc-fgf1a* and *Tc-fgf1b*.

In a second attempt (Fig. 3.1B), when a forward primer (5'®3') starting in the second exon a_2 of *Tc-fgf1a* (primer #12) was used as GSP2 (Fig. 3.1B, (i)) and the primers starting in the third exon a_3 of *Tc-fgf1a* (primer #14) and the first exon b_1 of *Tc-fgf1b* (primer #143) were used as NGSP1 and NGSP2 respectively (Fig. 3.1B, (ii)), a different result was observed. While the nested PCR reaction with primer NGSP1 (#14) again resulted in amplification of an exon a_3- specific short fragment (see Appendix 2.3), a longer fragment covering both the exons of *Tc-fgf1b* (b_1 and b_2) was also amplified in nested reaction with primer NGSP2 (#143) (Fig. 3.1B, (iii)) (see Appendix 2.4). Note, both the fragments contain a 3' UTR and a poly(A) tail at the 3' end.

In a third attempt (Fig. 3.1C), a different forward primer (5'®3') starting in the last exon a_3 of *Tc-fgf1a* (primer #13) was used as GSP3 (Fig. 3.1C, (i)). For nested PCR reactions, the same primer starting in the third exon a_3 of *Tc-fgf1a* (primer #14) was used as NGSP1 and a second primer starting in the first exon b_1 of *Tc-fgf1b* (primer #15) was used as NGSP2 (Fig. 3.1C, (ii)). Even with a different GSP, the result of the nested reaction with NGSP1 was the same. A short exon a_3- specific fragment with 3' UTR and poly(A) tail was amplified (Fig. 3.1C, (iii)) (see Appendix 2.5). But the reaction with NGSP2 (#15) failed to amplify the gene specific product (Fig. 3.1C, (iii)).

3.3.1.2   5' RACE-PCR for *Tc-fgf1a* (TC006602)

In a 5' RACE-PCR and few nested PCR reactions I aimed to identify the actual 5' end of the transcripts generated from the *Tc-fgf1a* exon assembly (TC006602).

In this reaction, a reverse primer (3'®5') starting in the last exon a_3 of *Tc-fgf1a* (Primer#131) was used as GSP1 to amplify the gene specific fragment with added 5' sequence (Fig. 3.2 (i)). This amplified RACE product was then analysed using different nested PCR reactions. For nested PCR reactions, a reverse primer in each of the three exons was used as NGSPs (primer #132 for exon a_3 as NGSP1, primer #133 for exon a_2 as NGSP2 and primer #134 for exon a_1 as NGSP3) (Fig. 3.2 (ii)).

Figure 3.2: A schematic overview of single 5' RACE-PCR and few nested PCR reactions performed to identify 5' end of *Tc-fgf1a* (TC006602) gene and the obtained results. (i) In first step an "exon a_3" specific reverse (3'➜5') primer was used as GSP1 to amplify a gene specific fragment from 5' RACE-Ready-cDNA with the help of forward primer UPM. (ii) In second step three different 5' nested RACE-PCR reactions were performed to characterize the amplified RACE product using exon specific reverse primers as NGSPs and a common NUP. (iii) A positive result was seen only in nested reaction with NGSP2 where a short fragment covering exon a_1 and exon a_2 of *Tc-fgf1a* gene was successfully amplified. Nested reactions with NGSP1 and NGSP3 resulted in unsuccessful cloning. (GSP, Gene Specific Primer; NGSP, Nested Gene Specific Primer; UPM, Universal Primer A Mix; NUP, Nested Universal Primer A; left-right arrow to bar in (ii) represents 2.9 kb of genomic region)

Finally, only the nested PCR reaction with primer NGSP2 (#134) showed amplification of a specific fragment covering the region from exon a_2 to exon a_1 of *Tc-fgf1a* gene (Fig. 3.2 (iii)) (see Appendix 2.6). The 5' end of this fragment was still within the exon a_1. The results of other nested reactions (with NGSP1 and NGSP3) were inconclusive as both of them resulted in non-specific amplification (Fig. 3.2 (iii)). Additionally two more attempts were also made to characterize the 5' end of *Tc-fgf1a* but both of them were unsuccessful in the end (see Appendix 2, Figure S4).

Nevertheless, the only visible result from this reaction clearly shows an interconnection between exon a_1 and exon a_2 of the *Tc-fgf1a* gene and therefore provides further support for the existing gene model for *Tc-fgf1a,* with three exons (exon a_1 at the 5' end, exon a_2 and exon a_3 at the 3' end).

3.3.1.3   3' RACE-PCR for *Tc-fgf1b* (TC006603)

For characterizing the actual 3' end of the transcripts generated from the *Tc-fgf1b* (TC006603) exon assembly, a 3' RACE reaction followed by a set of nested PCR reactions were performed.

For this 3' RACE-PCR reaction, a forward primer (5'®3') in exon b_1 (primer #143) was used as GSP to generate a gene specific fragment using 3' RACE-Ready cDNA (Fig. 3.3 (i)). For the nested reactions a pair of primers in each *Tc-fgf1b* exon were used as NGSPs (e.g. primer #15 and primer #144 in exon b_1 as NGSP1 and NGSP2 and primer #145 and primer #146 in exon b_2 as NGSP3 and NGSP4) (Fig. 3.3 (ii)).
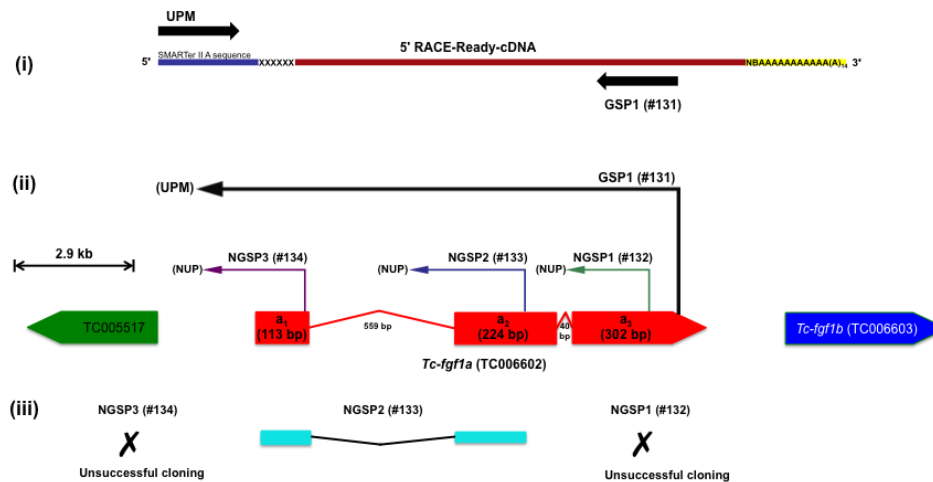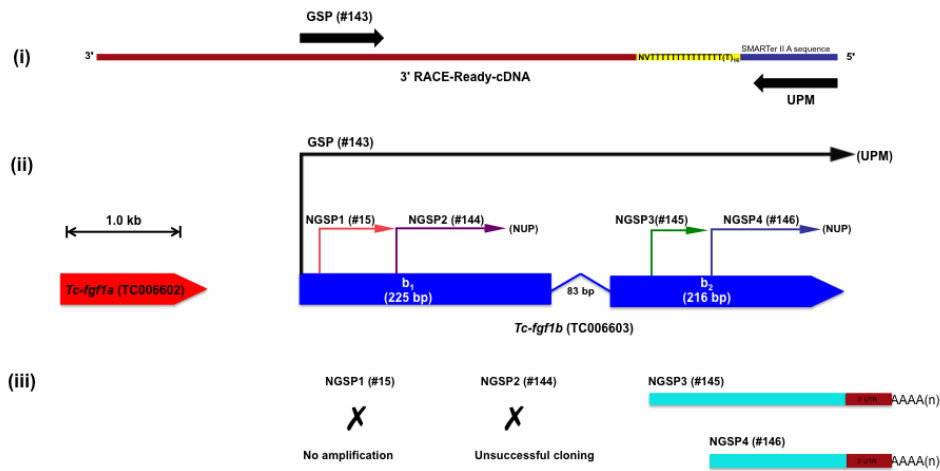

Figure 3.3: A schematic overview of single 3' RACE-PCR and four nested RACE-PCR reactions performed to identify 3' end of *Tc-fgf1b* (TC006603) gene and the obtained results. (i) In first step "exon b_1" specific forward (5'➔3') primer was used as GSP to amplify a gene specific fragment from 3' RACE-Ready-cDNA with the help of reverse primer UPM. (ii) For further nested RACE-PCR reactions four different exon specific forward primers were used as NGSPs along with a common NUP to characterize amplified RACE product. (iii) In results, two exon b_2 specific fragments with 3' UTR and Poly(A) tail were successfully amplified for the nested reactions with NGSP3 and NGSP4 primers. Reaction with NGSP1 and NGSP2 resulted in no amplification and unsuccessful cloning respectively. (GSP, Gene Specific Primer; NGSP, Nested Gene Specific Primer; UPM, Universal Primer A Mix; NUP, Nested Universal Primer A; 3' UTR, 3' Untranslated region; left-right arrow to bar in (ii) represents 1.0 kb of genomic region)

The nested PCR reactions with the primers NGSP3 and NGSP4 resulted in amplification of two exon b_2- specific fragments of variable length each with 3' UTR and poly(A) tail (Fig. 3.3 (iii)) (see Appendices 2.7 and 2.8). The starting position of each fragment was in agreement to the binding position of respective primers (NGSP3 and NGSP4) within the exon b_2. The results of other two nested PCR reactions were inconclusive. While no amplification occurred with the primer NGSP1, primer NGSP2 resulted in non-specific amplification (Fig. 3.3 (iii)). Taken together, these results also favour a predicted two-exon assembly model for *Tc-fgf1b* gene.

3.3.1.4   5' RACE-PCR for *Tc-fgf1b* (TC006603)

Next, I aimed to identify the actual 5' end of the *Tc-fgf1b* gene in a series of 5' RACE-PCR and nested PCR reactions.
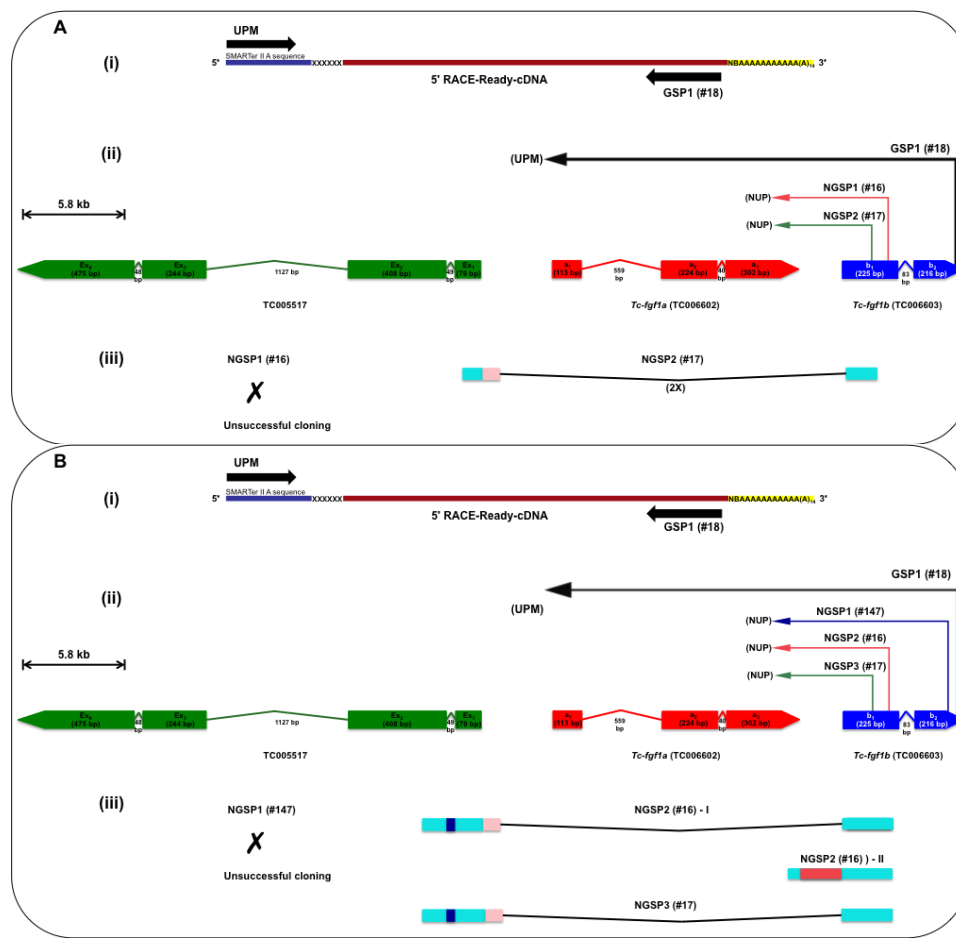
Figure 3.4: Schematic overview of two different 5' RACE-PCR/nested-RACE-PCR reactions performed to identify 5' ends of *Tc-fgf1b* (TC006603) gene and the obtained results. **(A)** In the first 5' RACE-PCR reaction (i) an "exon b_2" specific reverse (3'→5') primer (#18) was used as GSP1 to amplify the gene fragment from 5' RACE-Ready-cDNA with additional sequence at the 5' end. (ii) In 5' nested-PCR reactions, two different reverse primers (3'→5') from exon b_1 of *Tc-fgf1b* were used as NGSPs along with a common NUP to characterize amplified RACE product. (iii) For the nested reaction with the primer NGSP2, a short fragment covering exon b_1 of *Tc-fgf1b* and first exon (Ex_1) of TC005517 was amplified and cloned twice (2X). Non-specific amplification occurred in reaction with NGSP1. **(B)** In repeated 5' RACE-PCR reaction (i) again the reverse primer in "exon b_2" (primer #18) was used as GSP1 to amplify the gene fragment from 5' RACE-Ready-cDNA. (ii) For nested-PCR reactions, one additional reverse primer in "exon b_2" (primer #147) was used as NGSP1. The other two reverse primers from exon b_1 were now used as NGSP2 and NGSP3 respectively (iii) The results of nested reactions with primer NGSP2 and NGSP3 showed amplification of short fragment covering exon b_1 of *Tc-fgf1b* and two exons (Ex_1 and Ex_2) of TC005517. A second fragment was also amplified with NGSP2 showing extension of exon b_1 into exon a_3 of *Tc-fgf1a*. Non-specific amplification occurred in reaction with NGSP1.(GSP, Gene Specific Primer; NGSP, Nested Gene Specific Primer; UPM, Universal Primer A Mix; NUP, Nested Universal Primer A; left-right arrow to bar in (ii) represents 5.8 kb of genomic region)

In first attempt, a reverse primer (3'®5') starting in the last exon b_2 of *Tc-fgf1b* (Primer #18) was used as GSP1 to amplify a gene specific fragment that included the 5' end (Fig. 3.4A (i)). For further nested PCR reactions, two nested primers (primer #16 and primer #17) both starting in exon b_1 in 3'®5' direction, were used as NGSP1 and NGSP2 respectively (Fig. 3.4A (ii)). While the nested reaction with NGSP1 (#16) resulted in non-specific amplification, a surprising result was obtained for the nested reaction with primer NGSP2 (#17). In this reaction a short fragment was amplified

that after sequencing revealed a connection between the exon b_1 of *Tc-fgf1b* gene and the first exon (Ex_1) of the predicted gene TC005517, which is located 5´ to the *Tc-fgf1a* gene ((Fig. 3.4A (iii)) (see Appendix 2.9). Some non-coding sequence from the 5' region of *TC005517* gene was also a part of this amplified fragment.

To check the reproducibility of this result, a second 5' RACE-PCR reaction was also performed (Fig. 3.4B (i)). But this time an additional forward nested primer starting in the exon b_2 (primer #147) was used as NGSP1 while the other nested primers used in previous reaction were used as NGSP2 (primer #16) and NGSP3 (primer #17) respectively (Fig. 3.4B (ii)).

Indeed, similar results were obtained for the nested PCR reactions with NGSP2 (#16) and NGSP3 (#17). In both cases, a short fragment was amplified that started in the region of *Tc-fgf1b* gene and ends in the region of predicted *TC005517* gene (Fig. 3.4B (iii)). The only noticeable difference in these results was the extended length of this amplified fragment at the 5' end, which in this case covered the first two exons (Ex_1 and Ex_2) of *TC005517* gene including the intronic sequence ("blue box"; Fig. 3.4B (iii)) (see Appendix 2.10). In addition, a second fragment was also amplified with the nested primer NGSP2 (#16) that did not show an interconnection between *Tc-fgf1b* and *TC005517* (see Appendix 2.11). It rather showed an extension of exon b_1 of *Tc-fgf1b* into the small 3' region of exon a_3 of *Tc-fgf1a* gene including the intragenic sequence ("brown box") between them (Fig. 3.4B (iii); NGSP2-II). The nested reaction with an additional primer NGSP1 (#147) however resulted in non-specific amplification. Moreover a third 5' RACE-PCR reaction was also executed using two reverse primers (3'®5') in the first exon b_1 of *Tc-fgf1b* as GSP2 (#16) and NGSP (#17) respectively. But this reaction failed to provide any result (see Appendix 2, Figure S5). In summary, these results clearly show an interconnection between the exons located at the 5' end of both the oppositely orientated genes, *Tc-fgf1b* and *TC005517*.

3.3.1.5   3' RACE-PCR using Ex_1 of TC005517 as starting point

Since the 5' end of *Tc-fgf1b* was extended to the 5' region of *TC005517* gene, this 3' RACE-PCR experiment was particularly designed to independently confirm such an unexpected interconnection. For that task, a reverse primer (3'®5') starting in Ex_1 of *TC005517* pointing to the *Tc-fgf1b* gene was used as GSP1 (primer #129) to amplify a fragment from 3' RACE-Ready-cDNA (Fig. 3.5A (i)). For characterisation of the amplified product, a second reverse primer (3'®5') in Ex_1 of *TC005517* (primer #130) and a forward primer (5'®3') in exon b_1 of *Tc-fgf1b* (primer #15) were used as NGSP1 and NGSP2 respectively for nested PCR reactions (Fig. 3.5A (ii)).

Interestingly, in the nested reaction with primer NGSP1 a long fragment consisting of a large intragenic sequence ("brown box") flanked between a short Ex_1 (*TC005517*) specific sequence at the 5' end and a short exon a_1 (*Tc-fgf1a*) specific sequence at the 3' end was amplified (Fig. 3.5A (iii)) (see Appendix 2.12). Notably, a poly(A) tail was also identified at the 3' end of this fragment (Figure 8c). With another nested primer NGSP2, a non-specific fragment was amplified (Fig. 3.5A (iii)).
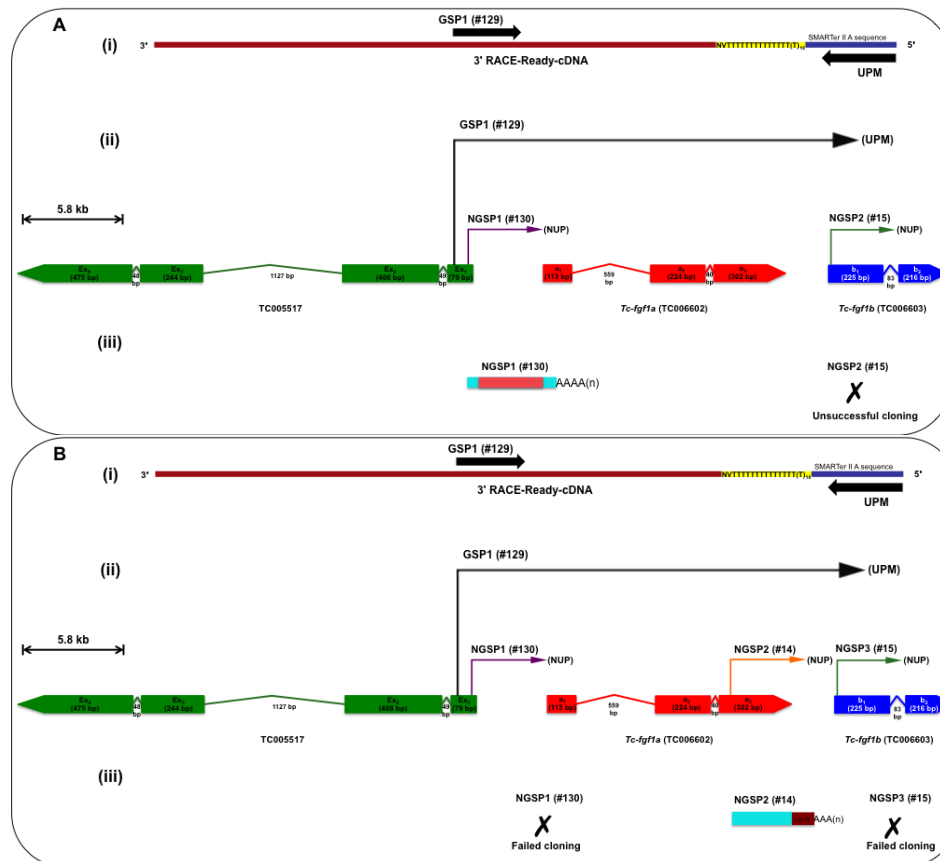
Figure 3.5: Schematic overview of the two 3' RACE-PCR and nested RACE-PCR reactions designed to find out connection between *TC005517* and *Tc-fgf1b* and their results. **(A)** In the first 3' RACE-PCR reaction (i) an "Ex_1" of TC005517 specific reverse (3'➔5') primer (#129) that extends in 3' direction of *Tc-fgf1b* was used as GSP1 to amplify long fragment from 3' RACE-Ready-cDNA. (ii) For nested PCR reactions, two different primers, a second reverse primer (3'➔5') in Ex_1 of TC005517 (#130) and a forward primer (5'➔3') in exon b_1 of *Tc-fgf1b* (#15) were used as NGSP1 and NGSP2 respectively to characterize amplified RACE product. (iii) From the nested reaction with NGSP1, a long fragment covering a large intragenic sequence between Ex_1 of *TC005517* and exon a_1 of *Tc-fgf1a* and flanking exon sequence at either end with a Poly(A) tail at the 3' end was amplified. With NGSP2 a non-specific product was amplified. **(B)** In repeated reaction (i) the reverse primer in "Ex_1" of TC005517 (primer #129) was again used as GSP1 to amplify long fragment from 3' RACE-Ready-cDNA. (ii) For nested PCR reactions, an additional forward primer (5'➔3') in "exon a_3" of *Tc-fgf1a* (primer #14) was used as NGSP2. The other two primers in Ex_1 of TC005517 (#130) and exon b_1 of *Tc-fgf1b* (#15) were used as NGSP1 and NGSP3 respectively (iii) In result, an exon a_3 specific fragment with 3' UTR and Poly(A) tail was amplified from the nested reactions with NGSP2. Unfortunately, cloning was failed for the nested reactions with NGSP1 and NGSP3. (GSP, Gene Specific Primer; NGSP, Nested Gene Specific Primer; UPM, Universal Primer A Mix; NUP, Nested Universal Primer A; left-right arrow to bar in (ii) represents 5.8 kb of genomic region)

To assure that the long fragment amplified in previous 3' RACE-PCR reaction was not an artefact, a second 3' RACE-PCR reaction was performed (Fig. 3.5B). A minor

change applied to this reaction was the use of an additional nested primer starting in exon a_3 and extends in 5'®3' direction (primer #14) as NGSP2 to further check the interconnection between *TC00517* and *Tc-fgf1a* (Fig. 3.5B (ii)). The other nested primers used in a previous reaction were now used as NGSP1 (primer #130) and NGSP3 (primer #15) respectively (Fig. 3.5B (ii)). Interestingly, this time no long fragment was amplified with nested primer NGSP1 instead an exon a_3- specific fragment with 3' UTR and poly(A) tail at the end was amplified from the nested reaction with additional primer NGSP2 (Fig. 3.5B (iii)) (see Appendix 2.13). The result of a nested PCR reaction with NGSP3 was again inconclusive (Fig. 3.5B (iii)). The inconsistency between the two results allowed me to perform more 3' RACE-PCR reactions with certain changes. In a first reaction, the second reverse primer (3'®5') in Ex_1 of *TC005517* (primer #130) was used as GSP2 and the forward primer (5'®3') in exon b_1 (primer #15) was used as NGSP. In a second reaction, the first reverse primer (3'®5') in Ex_1 of *TC005517* (#129) was again used as GSP1 while the second reverse primer (3'®5') in Ex_1 (primer #130) was used as NGSP1. In addition, a forward primer in exon a_1 (primer #142) as well as in exon b_1 (primer #143) was used as NGSP2 and NGSP3 respectively to crosscheck the interconnection. But unfortunately both the reactions failed to provide any positive result (see Appendix 2, Figure S6).

3.3.1.6   5' RACE-PCR for predicted gene *TC005517*
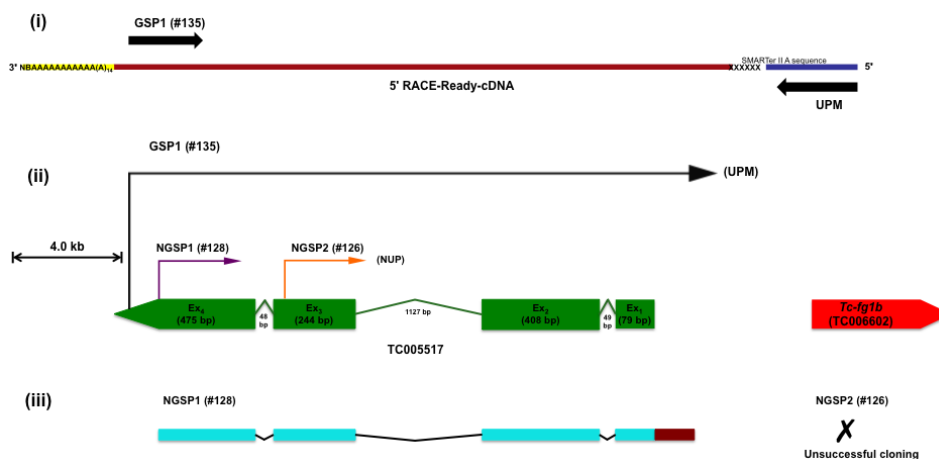
Figure 3.6: A schematic overview of 5' RACE-PCR and nested RACE-PCR reactions performed to identify the exon assembly of *TC005517* gene and the obtained results. (i) For 5' RACE-PCR a reverse primer (3'➔5') in the last exon "Ex_4" of *TC005517* was used as GSP1 to amplify a gene specific fragment from 5' RACE-Ready-cDNA. (ii) For further nested reactions, two more reverse primers (3'➔5') one in Ex_4 and otherin Ex_3 were used as NGSP1 and NGSP2 along with a common NUP to characterize amplified RACE product. (iii) From the nested reaction with primer NGSP1, a long fragment covering Ex_1 to Ex_4 of *TC005517* gene with addition sequence at the 5' end was amplified. Nested reaction with NGSP2 resulted in non-specific amplification. (GSP, Gene Specific Primer; NGSP, Nested Gene

Specific Primer; UPM, Universal Primer A Mix; NUP, Nested Universal Primer A; left-right arrow to bar in (ii) represents 4.0 kb of genomic region)

Since a direct connection was observed between the exon b_1 of *Tc-fgf1b* and the exons Ex_1 and Ex_2 of *TC005517*, this 5' RACE-PCR reaction was performed mainly to support the predicted gene model for *TC005517*.

For the 5' RACE-PCR reaction, a reverse primer (3'®5') in Ex_4 of *TC005517* (primer #135) was used as GSP1 to amplify a gene specific fragment from 5' RACE-Ready-cDNA (Fig. 3.6, (i)). For the nested PCR based analysis, a second reverse primer (3'®5') in Ex_4 (primer #128) and another reverse primer (3'®5') in Ex_3 (primer #126) were used as NGSP1 and NGSP2 respectively (Fig. 3.6, (ii)).

The reaction with the nested primer NGSP1 resulted in a long fragment containing all the four exons of *TC005517* with additional sequence at the 5' end (most likely the 5' UTR) (Fig. 3.6, (iii)) (see Appendix 2.14). The other nested reaction with primer NGSP2 resulted in non-specific amplification (Fig. 3.6, (iii)). Nevertheless, the result obtained in this experiment completely supports the gene structure for *TC005517*.

3.3.2 Functional characterization of *Tc-fgf1a* and *Tc-fgf1b* genes

3.3.2.1 Reference control experiments

3.3.2.1.1   Cuticles of the wildtype larval structures
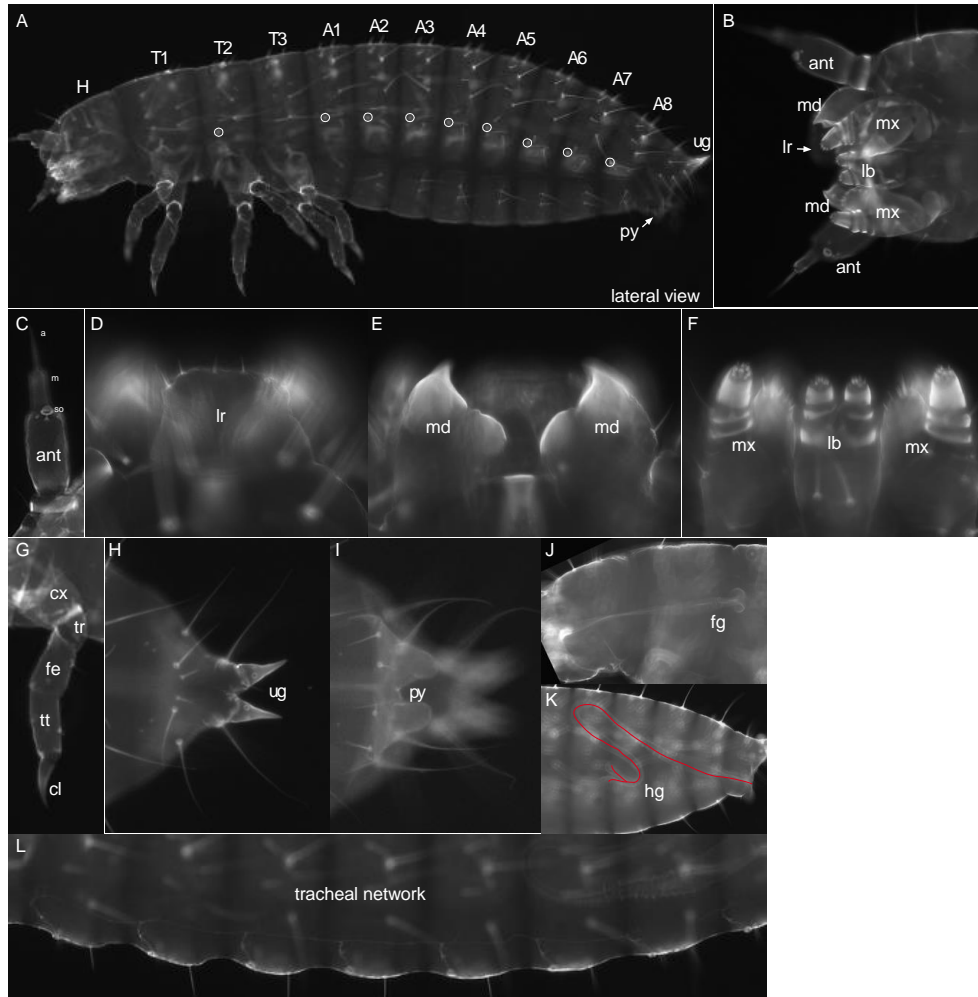
Figure 3.7: Cuticle overviews of a wildtype (WT) first instar larva and the larval structures. (A) Lateral view of a complete WT larval cuticle showing a head capsule with anteriorly localized mouthparts, three thoracic segments (T1-T3) each having a pair of legs, eight alike abdominal segments (A1-A8) each with a pair of tracheal openings (marked by circles) and the last segment having a pair of urogomphi (ug) and pygopodia (py). An additional pair of tracheal openings is the hallmark of T2 segment. (B-F) WT head showing the assembly of head structures (B) and their detailed morphological overview (C-F). (G) A WT first instar larval leg composed of different proximal to distal segments (H-I) A detailed overview of posterior most structures *ug* and *py*. (J-K) The shape of WT foregut (fg) and hindgut (hg). (L) A WT tracheal network connecting the tracheal openings of abdomen. (H, head; T1-T3, thoracic segments 1-3; A1-A8, abdominal segments 1-8; lr, labrum; ant, antenna; md, mandible; mx, maxilla; lb, labium; cx, coxa; tr, trochanter; fe, femur; tt, tibiotarsus; cl, pretarsal claw; a, arista; m, middle part; so, sense organ of the antennae).

To clearly figure out the differences between the wildtype (WT) and the RNAi-affected embryos at the cuticle level, I carefully examined the morphology of a number of WT first instar larvae. The analysis showed that a WT larva is composed of a large head capsule (H), three thoracic segments (T1-T3), eight abdominal segments (A1-A8) and a terminal segment containing the dorsal specific urogomphi

(ug) and the ventral specific pygopodia/anal legs (py) (Fig. 3.7A) (Dönitz et al., 2013). In addition, a pair of tracheal openings in each abdominal segment (A1-A8) and a single pair exclusively in the second thoracic segment (T2) are also evident.

A further analysis showed that a WT head capsule is consisted of the head appendages (antennae) and the mouthparts (labrum, mandibles, maxillae, and labium) (Fig. 3.7B) and each head structure has a unique morphology (Fig. 3.7C-F). A WT leg in *Tribolium* however is an assembly of five different interconnected proximal to distal segments i.e. coxa, trochanter, femur, tibiotarsus and pretarsal claw respectively (Fig. 3.7G). Moreover, the urogomphi (ug) is a solid V-shaped structure with a broad distal base and two proximally pointed arms each with a specific sensory opening (Fig. 3.7H), whereas the pygopodia (py) are fluffy U-shaped paired structures that function as anal legs (Fig. 3.7I). A clear distinction is visible between the foregut and the hindgut (Fig. 3.7J-K). Lastly, a tracheal network that interconnects all the abdominal tracheal openings in a WT larval cuticle is also clearly recognisable (Fig. 3.7L).

3.3.2.1.2 Larval hatching ratio in wildtype eggs
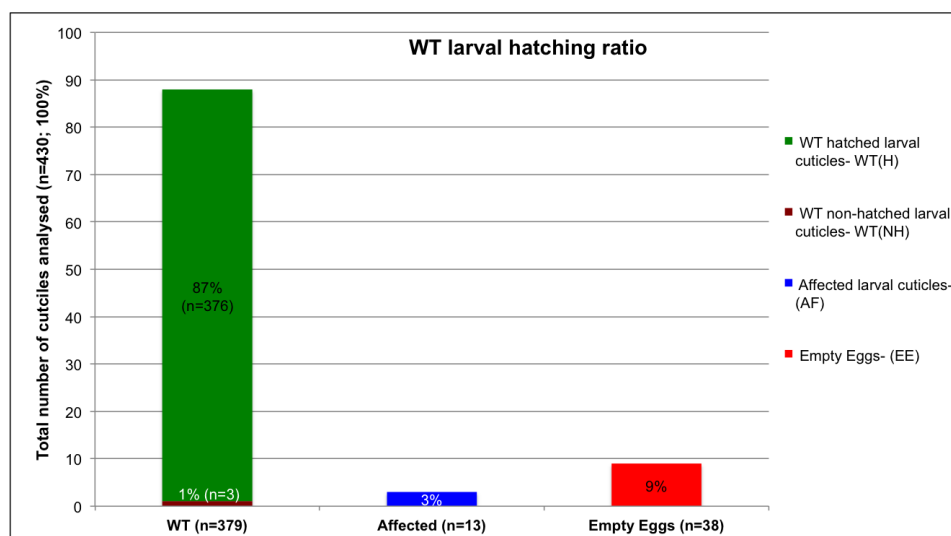
Figure 3.8: Statistical analysis of larval hatching/nonhatching ratio in wildtype eggs.

To study the larval hatching/non-hatching ratio during WT embryogenesis, a pool of counted WT eggs (n=430) were kept at 30°C (in an incubator) to allow for standard growth and were observed regularly for the larval hatching.

The result showed a very high hatching/non-hatching ratio during WT embryogenesis. While 87% (n=376) of the eggs were able to hatch into larvae that were indistinguishable from the wildtype, only the remaining 13% (n=54) eggs stay non-hatched (Fig. 3.8). Within these non-hatched, most of the eggs (n=38, 70%) failed to develop a cuticle and hence described as "empty eggs" (Fig. 3.8). A cuticle

formation was only visible in the remaining non-hatched eggs (n=16, 30%) though many of them (n=13) developed with some malformations (Fig. 3.8). These malformed cuticles were classified as "Affected larval cuticles" (Fig. 3.8). Only few non-hatched cuticles (n=3) resembled wildtype in respect to their head, thorax and abdomen formation and therefore labelled as "WT non-hatched larval cuticle" (Fig. 3.8).

Interestingly, the affected cuticles showed some weak to strong phenotypes (Fig. 3.9). While in weakly affected cuticles (n=2) only the appendages were malformed (Fig. 3.9A), a strong reduction of the appendages formation along with the truncation of the posterior segments (A5-A8) was observed in intermediate cuticle aberrations (n=5) (Fig. 3.9B). In strongly affected cuticles (n=6), only a cuticle sphere was detectable that has one or two identifiable appendages like antenna or legs (Fig. 3.9C). Empty eggs as previously described did not show any cuticle formation (Fig. 3.9D).
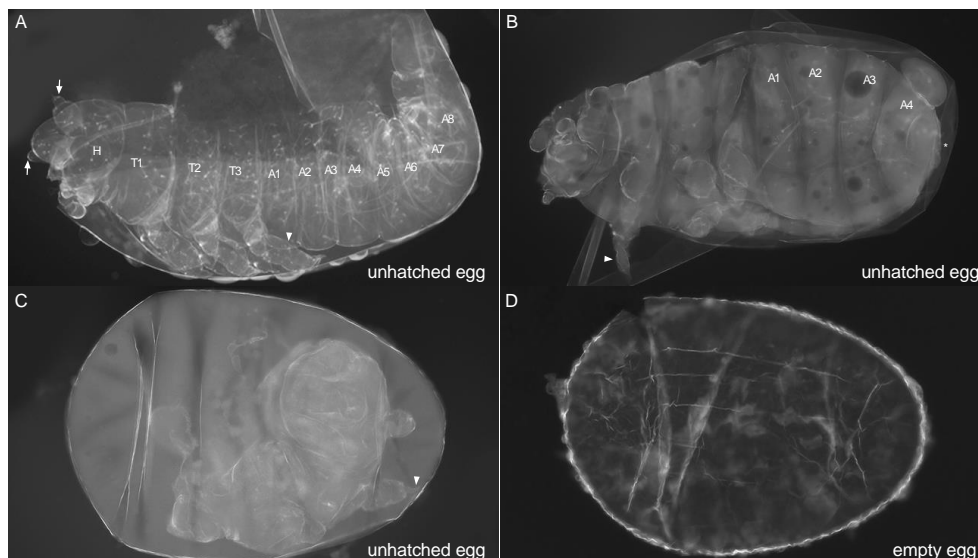
Figure 3.9: Embryonic cuticles of non-hatched and un-injected WT eggs. (A) A weak aberration includes misshaped antennae (white arrow), legs (white arrowhead) and posterior appendages in a fully segmented cuticle (n=2). (B) Cuticle with intermediate aberration showing complete malformation of head and leg appendages (white arrowhead) with a severe posterior truncation (asterisk) (n=5). (C) Strongly affected cuticle sphere with only identifiable leg claw (white arrowhead) (n=6). (D) Auto fluorescence image of empty egg (n=38).

3.3.2.2 No major impact on embryogenesis after *Tc-fgf1a* knockdown

When one of the two *Tribolium* Fgf1-like ligands, *Tc-fgf1a,* was knockdown using different NOFs (see Appendix 3, Figure S7), no major effect was visible on *Tc-fgf1a*[RNAi] embryos (Fig. 3.10) compared to the WT embryos (Fig. 3.8). Like WT, the hatching/non-hatching ratio was high in *Tc-fgf1a*[RNAi] embryos. Most of the eggs (73%; n=855) without *Tc-fgf1a* function were able to hatch as larvae and resemble as wildtype (Figs. 3.10 and 3.11A). But the frequency of empty eggs (17%; n=202) after

Tc-fgf1a-knockdown was almost double the WT eggs, the frequency of affected cuticle however remained same (3%, n=36) in *Tc-fgf1a*^RNAi embryos (compare Figs. 3.8 and 3.10). A slight increase in the number of "WT non-hatched larvae" (7%; n=85) was also obvious after the *Tc-fgf1a*-knockdown (Fig. 3.10).

Figure 3.10: Statistical analysis of *Tc-fgf1a*^RNAi eggs.

The affected *Tc-fgf1a*^RNAi embryos (n=36, 100%) showed a range of weak to strong cuticles phenotypes (Fig. 3.11; for specific details see Appendix 3, Table S4). In weakly affected embryos (n=6, 16%), a malformation of embryonic appendages that include abnormal shapes of the antennae or the legs (asterisk and arrow in Fig. 3.11B) and a loss of antennal spikes was mainly observed. The affected cuticles with intermediate effect (n=17, 47%) showed relatively strong malformation of head appendages, stumpy or shortened legs and a dorsal opening (dotted circles) in a fully segmented embryo but with abnormal shape (Fig. 3.11C-F). These cuticles were either slightly curved or arc-shaped. The stumpy legs described here, in principle, were also made up of five distal to proximal segments but the border between each segment especially between the femur (fe) and the tibio-tarsus (tt) was poorly defined (Fig. 3.11J-L).

Interestingly, 25% (n=9) of the affected cuticles showed a posterior truncation of the body axis as strong phenotype. While in weak posterior truncations the head, thorax and few abdominal segments were detectable (Fig. 3.11G), in strongly truncated cuticles only the head and the thorax developed (Fig. 3.11H). A poor development of the head appendages and the legs was also obvious in these strongly truncated *Tc-fgf1a*^RNAi cuticles (Fig. 3.11H). In addition, in a couple of *Tc-fgf1a*^RNAi embryos (n=2, 6%), a unique short abdomen phenotype was also documented. In these embryos, head, thorax and few anterior abdominal segments build normally but the remaining

posterior abdominal segments (arrowhead) along with terminal structures (arrow) were wrinkled and internalized within the short anterior abdomen (Fig. 3.11I).
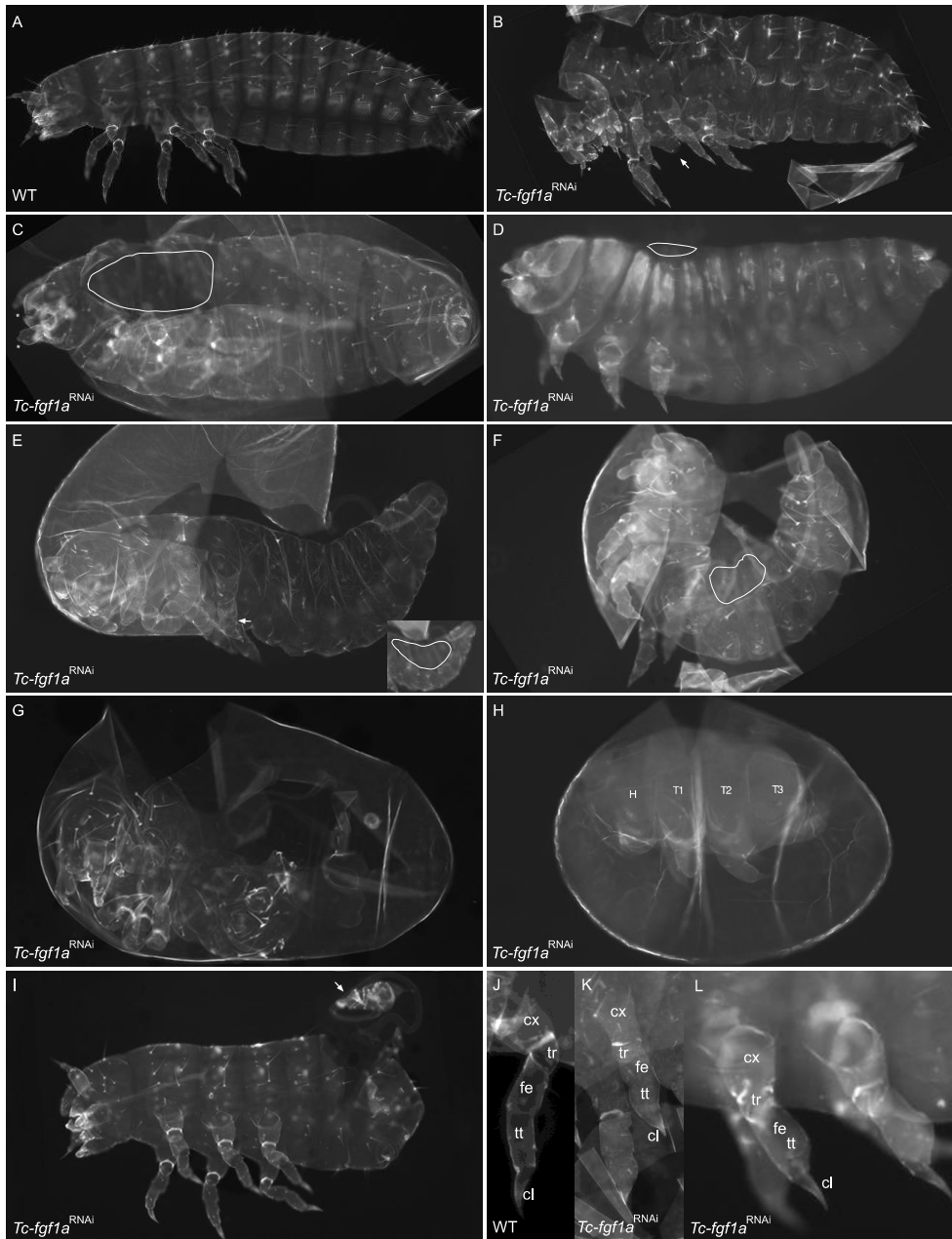
Figure 3.11: *Tc-fgf1a*^{RNAi} cuticle phenotypes. (A) A wildtype larval cuticle. (B-C) Cuticles with weak *Tc-fgf1a*^{RNAi} phenotypes: irregular shape antennae (asterisk, B), a misshaped leg (arrow, B), loss of antennal spikes (asterisk, C) and a dorsal opening (dotted circle; C). (D-F) Cuticles with intermediate phenotypes: irregular and curved shape body, malformed appendages, stumpy/shortened legs and dorsal opening (dotted circle). (G) Cuticle with a unique short abdomen phenotype where posterior structure (arrow) and remaining abdominal segments (arrowhead) were internalized. (H-I) Strongly affected *Tc-fgf1a*^{RNAi} cuticles showing posterior truncation. (J-L) Comparative analysis between the WT (J) and the affected legs (K-L). (cx, coxa; tr, trochanter; fe, femur; tt, tibiotarsus; cl, pretarsal claw)

Therefore this phenotype can be called as "virtual short abdomen phenotype". Furthermore, few cuticles (n=2, 6%) were also found either partially or completely everted ("inside-out phenotype") after *Tc-fgf1a* knockdown. In summary, in-spite of a

high larval hatching in *Tc-fgf1a*[RNAi] embryos, an increase in the number of empty eggs and some specific larval phenotypes were observed.

3.3.2.3   *Tc-fgf1b* RNAi results in dorsally open and curved larval cuticles.

Most surprisingly, when the second Fgf1-like ligand in *Tribolium*, *Tc-fgf1b,* was knocked down, a severe impact on the development of *Tc-fgf1b*[RNAi] embryos was clearly evident (see Appendix 3, Figure S8). This was in complete contrast to the previous result of *Tc-fgf1a*[RNAi]. While, most of the *Tc-fgf1b*[RNAi] eggs (77%, n=821) failed to develop a cuticle and remained as "empty eggs", in almost 12% (n=132) cases a cuticle was produced but with some weak to severe aberrations (Fig. 3.12). Only 11% (n=113) of the *Tc-fgf1b*[RNAi] eggs could develop into the larvae that looked indistinguishable from the WT (Fig. 3.12).

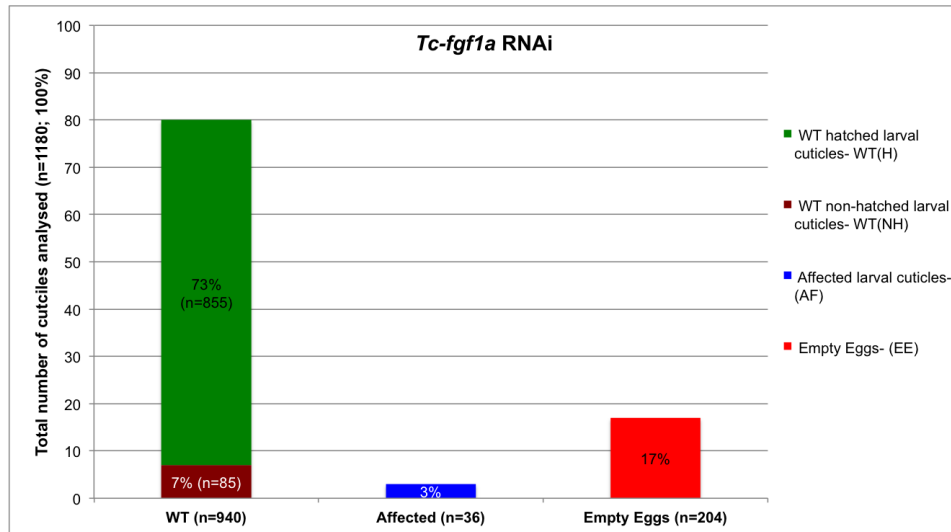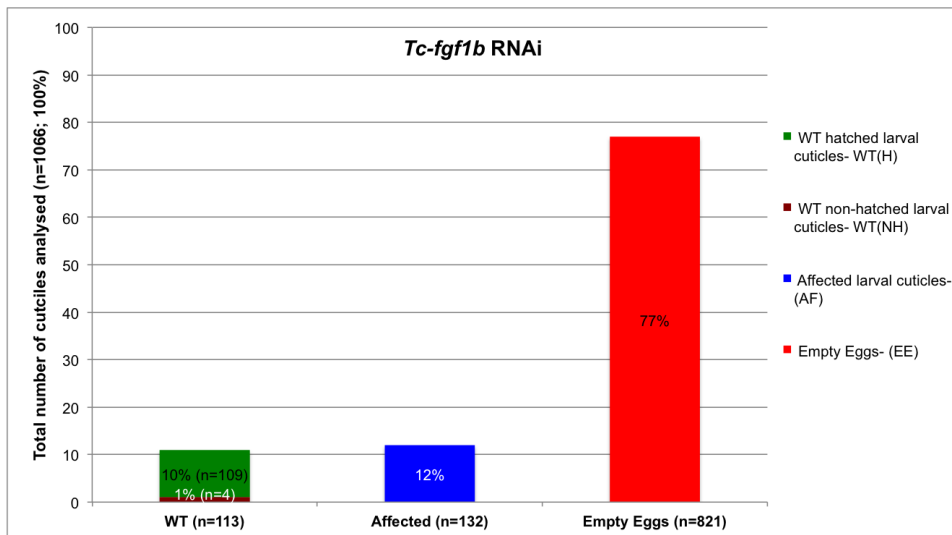Figure 3.12: Statistical analysis of *Tc-fgf1b*[RNAi] eggs.

The affected *Tc-fgf1b*[RNAi] cuticles (n=132, 100%) showed a series of weak to strong phenotypes and grouped into five different classes I-V (Fig. 3.13; for specific details see Appendix 3, Table S5). Class I cuticles (n=25, 19%) showed weakly malformed appendages and a dorsal opening in an otherwise wildtype looking embryonic cuticle (Fig. 3.13B). Class II cuticles (n=18, 14%) were short, dorsally curved and – within the vitelline membrane – posteriorly positioned (Fig. 3.13C). These cuticles also had a dorsal opening and weakly affected leg appendages. Class III cuticles (n=32, 24%) represented intermediate phenotypes where in addition to the dorsal opening and the dorsal curve formation, the shape of the head appendages, the legs and the abdomen were abnormal (Fig. 3.13D). In strongly affected Class IV cuticles (n=21, 16%), a gradual loss of the anterior embryonic structures in a dorsally curved and open cuticle was evident (Fig. 3.13E-F). Cuticles with the headless phenotype (n=6)

(Fig. 3.13G) and a less frequently observed gap phenotype (n=5) (Fig. 3.13H) were also grouped in Class IV.

Figure 3.13: Phenotypic series of *Tc-fgf1b*^{RNAi} cuticles. (A) A wildtype larval cuticle. (B) Class I cuticle with dorsal opening (dotted circle) and malformed urogomphi (arrow). (C) Class II: dorsally curved cuticle with dorsal opening (dotted line) and mildly affected leg (arrowhead). (D) Class III: dorsally curved cuticle with dorsal opening (dotted line) and strongly affected head, leg appendages (arrows) and mis-shaped body. (E-H) Class IV: dorsally open (open arrowheads) and curved cuticles with partial loss of the head (ant, md, lb) and the leg appendages (arrowhead) (E), strong reduction of head structures (F), headless cuticle with missing T1 and T2 and swollen hindgut (G) and cuticle with gap phenotype showing a loss of head and thoracic structures (H). (I-J) Class V: cuticle with malformed head and thorax only (I) and thorax only cuticle sphere (J). (T1-T3, thoracic segments 1-3; lr, labrum; ant, antenna; md, mandible; mx, maxilla; lb, labium; ug, urogomphi; hg, hindgut)

The most frequently visible (n=36, 27%) extreme phenotypes in class V cuticles included either a cuticle with visible head and thoracic structures but with no

posterior structures (Fig. 3.13I) or a cuticle sphere with outgrowing leg appendages only (Fig. 3.13J). A huge number of the eggs (77%) that did not develop a cuticle ("empty eggs") (Fig. 3.12) were classified as the strongest *Tc-fgf1b*[RNAi] - phenotype. While the egg lay rate was close to wildtype after the injection of *Tc-fgf1b* ds-RNA, no larval hatching was observed throughout the first ten egg lays over 3 weeks after the injection.

3.3.2.4   *Tc-fgf1a*/*Tc-fgf1b* double knockdown phenotypes

After observing the contrasting results for the single knockdown of both the *Fgf1*-like genes, a combined knockdown of *Tc-fgf1a* and *Tc-fgf1b* was also performed to check the functional redundancy between these two genes (see Appendix 3, Figure S9). Interestingly, in the double knockdown, almost half of the *Tc-fgf1a*/*Tc-fgf1b*[RNAi] eggs (47%, n=714) were able to develop into the larvae that looked WT (Fig. 3.14). From the remaining 53% (n=800) eggs, while 32% (n=479) eggs failed to produce a cuticle ("empty eggs"), almost 21% (n=310) eggs developed into a cuticle that showed some weak to strong morphological aberrations (Fig. 3.14).
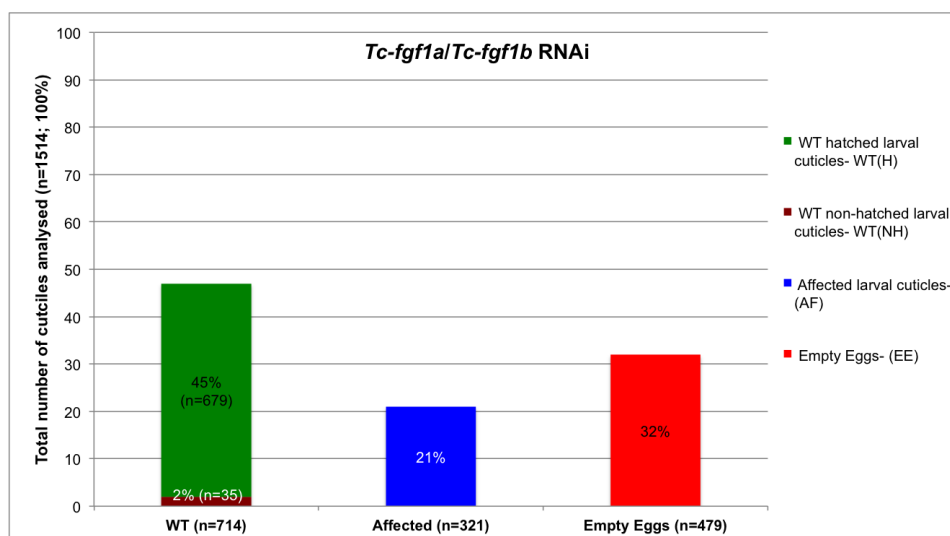
Figure 3.14: Statistical analysis of *Tc-fgf1a*/*Tc-fgf1b*[RNAi] phenotypes.

After the double knockdown, a variety of cuticle phenotypes, ranging from mild defects of appendicular development to severe truncations of the body axes were observed in *Tc-fgf1a*/*Tc-fgf1b*[RNAi] embryos (Fig. 3.15). Based on their phenotypic characterization, these cuticles were grouped into seven different classes (I-VII) (Fig. 3.15; see specific details in Appendix 3, Table S6). While most of the cuticle phenotypes from the double knockdown (from Class I-V; Fig. 3.15B-H) looked very similar to the cuticle phenotypes of single *Tc-fgf1b*[RNAi] (Fig. 3.13), class VI and VII cuticles (Fig. 3.15I-J) showed some phenotypic similarity with single *Tc-fgf1a*[RNAi] cuticles (Fig. 3.11G). Interestingly, the frequency of cuticles with "inside-out

phenotype" (class VI cuticles) was found higher (18/1514; 1.2%) in the double knockdown embryos when compared to single *Tc-fgf1a*[RNAi] (2/1180; 0.2%) (Fig. 3.15I).
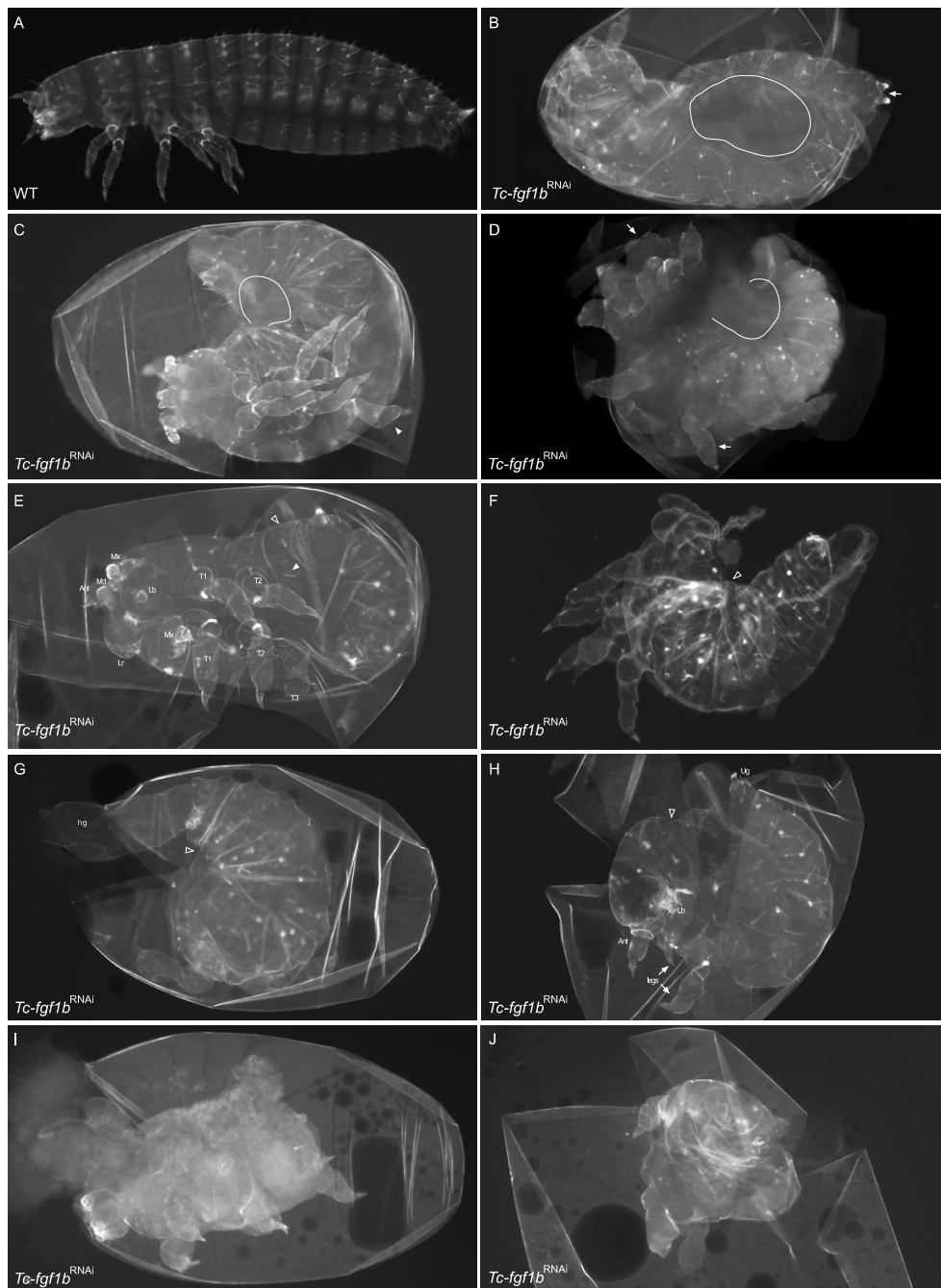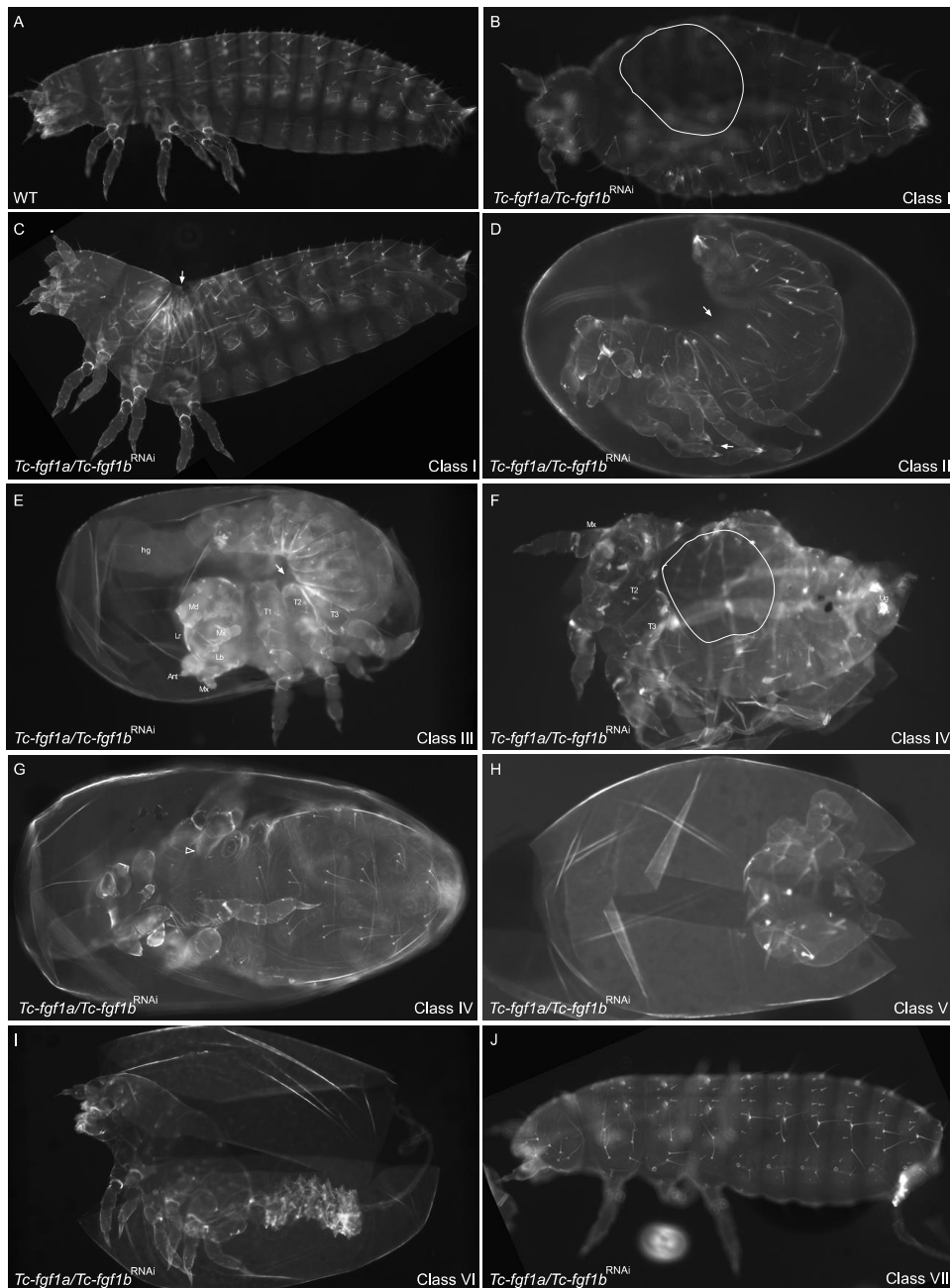

Figure 3.15: Phenotypic series of *Tc-fgf1a/Tc-fgf1b*[RNAi] cuticles. (A) A wildtype larval cuticle. (B-C) Class I cuticle with dorsal opening (dotted circle) and malformed urogomphi (arrow). (C) Class II: dorsally curved cuticle with dorsal opening (dotted line) and mildly affected leg (arrowhead). (D) Class III: dorsally curved cuticle with dorsal opening (dotted line) and strongly affected head, leg appendages (arrows) and mis-shaped body. (E-H) Class IV: dorsally open (open arrowheads) and curved cuticles with partial loss of the head (ant, md, lb) and the leg appendages (arrowhead) (E), strong reduction of head structures (F), headless cuticle with missing T1 and T2 and swollen hindgut (G) and cuticle with gap phenotype showing a loss of head and thoracic structures (H). (I-J) Class V: cuticle with malformed head and thorax only (I) and thorax only cuticle sphere (J). (T1-T3, thoracic segments 1-3; lr, labrum; ant, antenna; md, mandible; mx, maxilla; lb, labium; ug, urogomphi; hg, hindgut)

Class VII cuticles (n=4) showed "virtual short abdomen phenotype" that was first described in single *Tc-fgf1a*[RNAi] embryos. In summary, these results clearly indicate

that while *Tc-fgf1b* function appeared critical for the embryonic development, no clear role of *Tc-fgf1a* identified at this stage. In addition, the double knockdown also indicates that there is no functional redundancy between these two genes.

Since *Fgf1* subfamily is not represented in the *Drosophila* genome and the results of *Tc-fgf1b* knockdown in *Tribolium* were remarkable at the cuticle level, I further aimed to investigate the *Tc-fgf1b*[RNAi] cuticle phenotypes at the embryonic level by analysing various tissue specific marker genes expressions.

3.3.3 Molecular analysis of *Tc-fgf1b*[RNAi] larval phenotypes

3.3.3.1   *Tc-fgf1b*[RNAi] embryos develop with a disorganized serosa and fail to undergo morphogenetic movements

To get an overview on the development of *Tc-fgf1b*[RNAi] embryos, I analysed various developmental stages of affected embryos by Hoechst nuclear staining and compared them to the corresponding wildtype stages.

In the late differentiated blastoderm stage wildtype embryo, the embryonic cells condense at the posterior–ventral region of the egg to form the germ rudiment while the anterior 70% are covered by the extraembryonic serosa, clearly recognizable by the evenly distributed and widely spaced large nuclei (Fig. 3.16A). At this stage, the head anlage occupies a mid-ventral position (Fig. 3.16A; white arrowhead). In fixed embryos derived from the females injected with *Tc-fgf1b* ds-RNA (*Tc-fgf1b*[RNAi] embryos) no single embryo with a properly organized differentiated blastoderm was observed. While embryonic cells also condensed at the posterior end in *Tc-fgf1b*[RNAi] embryos, serosal nuclei were highly disorganized and fewer in number (Fig. 3.16B). In addition, no posterior invagination occurred in affected embryos (Fig. 3.16B; asterisk). At the time of early gastrulation in the wildtype embryo, the extraembryonic membranes fold over and cover the germ rudiment (Fig. 3.16C) (Handel et al., 2000). In *Tc-fgf1b*[RNAi] embryos, the germ disc developed at the surface of the yolk with no sign of coverage by extraembryonic membranes (Fig. 3.16D). During further steps of germband elongation in wildtype embryos, the position of the head progressively shifts towards the anterior pole and the remaining body elongates posteriorly along AP axis (Fig. 3.16E and G). In contrast, the head anlage of *Tc-fgf1b*[RNAi] germbands never translocated to the anterior pole. Instead, it remained at a more posterior (Fig. 3.16F) or at a midventral position (Fig. 3.16H) and elongated around the posterior pole resulting in a curved-shape body (Fig. 3.16F and H). In strongly affected cases an additional kink in the body was also observed (Fig. 3.16F). This morphological

examination of differently staged embryos clearly revealed that anomalies in *Tc-fgf1b*^RNAi embryos started already during early embryogenesis.

3.3.3.2 Expression of extraembryonic marker genes is significantly reduced in *Tc-fgf1b*^RNAi embryos
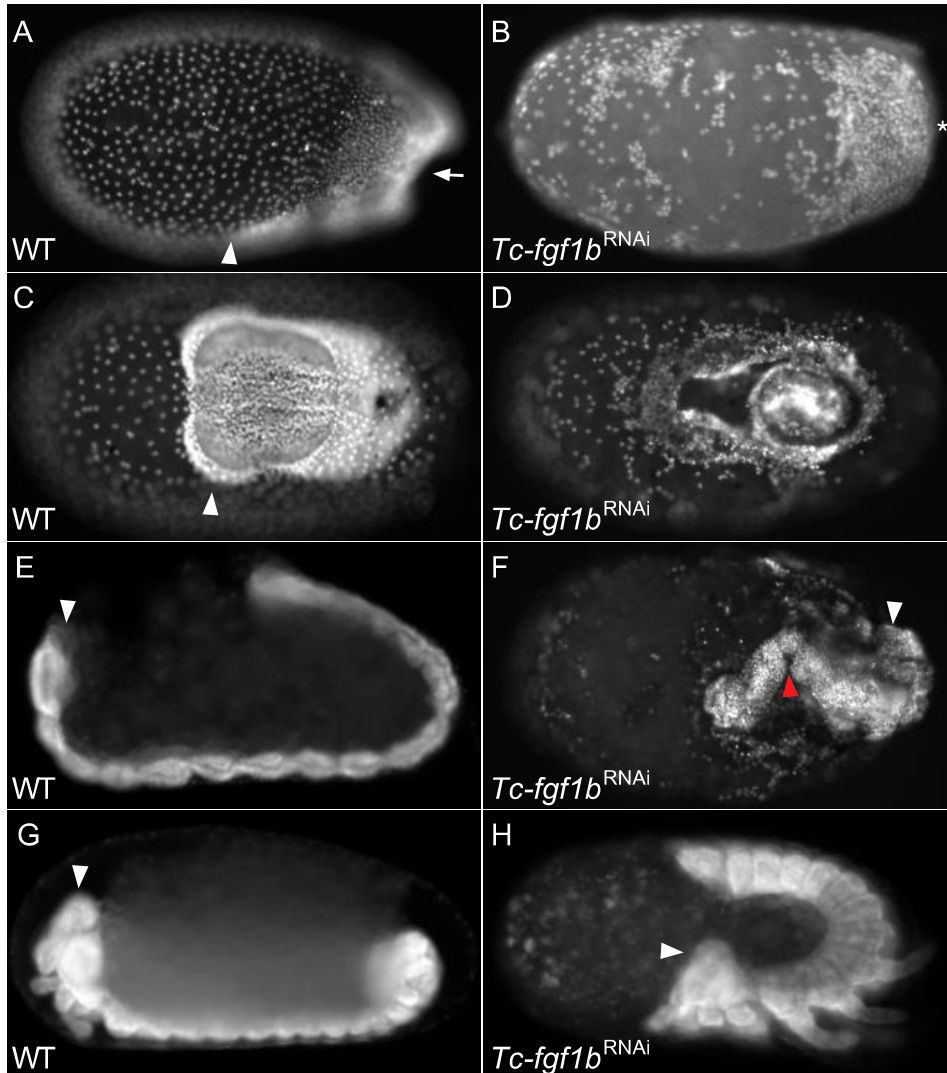
Figure 3.16: Serosa-reduction and posterior arrest of the germ rudiment during morphogenesis in *Tc-fgf1b*^RNAi embryos. Hoechst stained wildtype (A,C,E,G) and *Tc-fgf1b*^RNAi embryos (B,D,F,H). (A) A wildtype late differentiated blastoderm embryo, showing widely spaced and evenly distributed nuclei of the serosa in the anterior two third and the condensed nuclei of the germ rudiment undergoing invagination (arrow) at the posterior pole. The primordium of the head-anlage occupies a mid-ventral position (white arrowhead) at this stage. (B) In *Tc-fgf1b*^RNAi embryos an irregular distribution of fewer serosal nuclei and no posterior invagination of the germ rudiment (asterisk) observed. (C) At gastrulation in the wildtype, the extraembryonic membranes close over the embryonic anlage. White arrowhead points to the still mid-ventrally positioned head-anlage. (D) In *Tc-fgf1b*^RNAi embryos, a germ disc of irregular shape surrounded by a disorganized serosa formed at the surface ("floating embryo"). During germband elongation (E) and -retraction (G) the head in wildtype embryos takes an anterior position (white arrowheads). In *Tc-fgf1b*^RNAi embryos the position of anterior structures (white arrowheads in F and H) is not fixed. In strongly affected germbands, the head-anlage takes a more posterior position while the body elongated around the pole with formation of a kink (red arrowhead; F). In weakly affected germbands, the head remained at a mid-ventral position and the body developed in a typical curved shape form around the posterior pole (H). All views lateral except (C,D) ventral and (F) dorsal.

Morphological examinations of *Tc-fgf1b*[RNAi] embryos at the embryonic level clearly revealed that the formation of the extraembryonic tissue serosa was affected already during early stages (Fig. 3.16B). It is now of interest to know how early the anlage of the serosa became specified in *Tc-fgf1b*[RNAi] embryos. For this question, I analysed the expression pattern of the exclusive serosa marker *Tc-zerknüllt1* (*Tc-zen1*) (Falciani et al., 1996; van der Zee et al., 2005) in wildtype and experimental embryos.

In the wildtype late blastoderm stage embryo, *Tc-zen1* expression marks the presumptive serosa in a dorsally tilted asymmetric cap domain (Fig. 3.17A). Compared to the wildtype, *Tc-zen1* expression was still present as an asymmetric cap, but reduced to a much smaller anterior domain in *Tc-fgf1b*[RNAi] embryos (Fig. 3.17B). Next, I examined whether the second extraembryonic membrane in *Tribolium*, the amnion, might also be affected in *Tc-fgf1b*[RNAi] embryos. To that end, I analysed the expression of the amnion marker *Tc-iroquois* (*Tc-iro*) (Kotkamp et al., 2010; Nunes da Fonseca et al., 2008). In the wildtype, *Tc-iro* marks the precursor of the amnion in the early blastoderm stage in an anteriorly positioned and dorsally open ring domain, slightly tilted along the DV axis (Fig. 3.17C) (Sharma et al., 2013a). The expression strength of this early anterior *Tc-iro* domain was found significantly reduced in *Tc-fgf1b*[RNAi] embryos (Fig. 3.17D). The study of both these marker genes showed that the primordia of both the extraembryonic membranes were severely disrupted in *Tc-fgf1b*[RNAi] embryos.

3.3.3.3   Anterior shift of the embryonic fate map in *Tc-fgf1b*[RNAi] embryos

Since the primordia for anterior extraembryonic tissues were considerably reduced in *Tc-fgf1b*[RNAi] embryos, I questioned whether the anterior-most embryonic anlage was also affected. I analysed the *Tc-orthodenticle1* (*Tc-otd1*) mRNA expression and Even-skipped (*Tc*-Eve) protein expression during early blastoderm formation in wildtype and in affected embryos. While *Tc-otd1* marks the anterior-most embryonic head anlage (Schinko et al., 2008; Schröder, 2003), primary Eve stripes formation represents the origin of blastodermal gnathal segments in *Tribolium* (Patel et al., 1994). Indeed, I observed an altered expression pattern of both these embryonic markers in *Tc-fgf1b*[RNAi] embryos. Compared to wildtype, the expression strength of *Tc-otd1* mRNA was reduced in affected embryos (Figs. 3.17E, E´ and F, F´). In addition, a slight shift (6% of the egg length; N=5) of *Tc-otd1* expression towards a more anterior position was also evident (Figs. 3.17E and F). I also observed an anterior shift of the primary Eve stripes to a more anterior position (13% of the egg length) in *Tc-fgf1b*[RNAi] embryos (Figs. 3.17G and H).
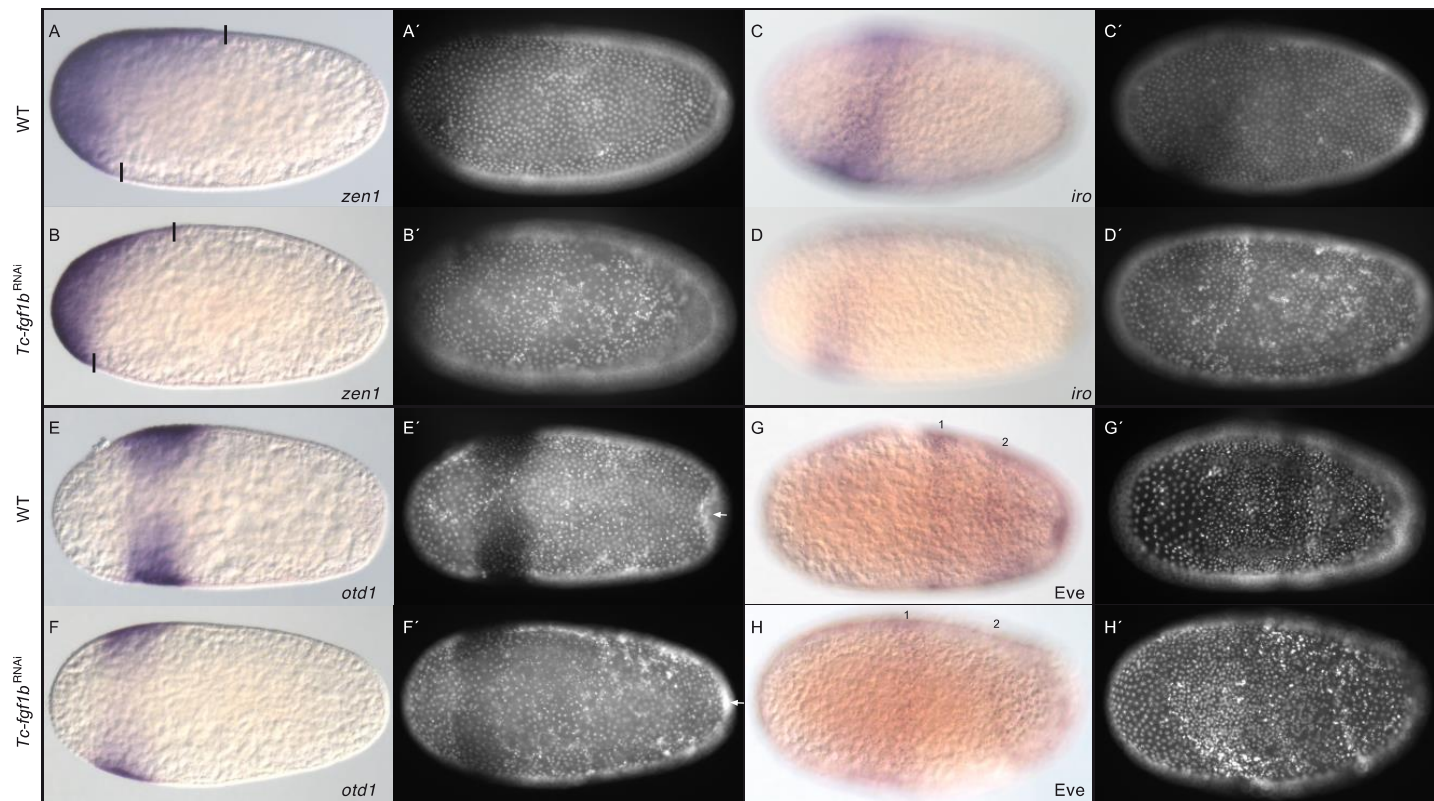
Figure 3.17: Expression analysis of extraembryonic (*Tc-zen1*, *Tc-iro*) and embryonic (*Tc-otd1*, *Tc-*Eve) markers in wildtype and *Tc-fgf1b*^RNAi embryos. (A,C,E,G) wildtype; (B,D,F,H) *Tc-fgf1b*^RNAi embryos; stained for *Tc-zen1* mRNA (A,B), *Tc-iro* mRNA (C,D), *Tc-otd1* mRNA (E,F) and *Tc-*Eve antibody (G,H). (A-H) DIC images of blastoderm stages embryos; (A′-H′) Hoechst nuclear-counterstain. (A-D): lateral views with dorsal upside; (E-H): ventral views. (A) *Tc-zen1* expression in wildtype embryos at the uniform blastoderm stage marks the presumptive serosa that is dorsally tilted. (B) In *Tc-fgf1b*^RNAi embryos the *Tc-zen1* expression domain is strongly reduced but the asymmetry along the dorsal–ventral axis is maintained. (C) During wildtype blastoderm formation, the amnion marker *Tc-iro* is expressed as a dorsally open ring at 80% egg length. In *Tc-fgf1b*^RNAi embryos expression strength of *Tc-iro* is highly reduced (D). (E and F) A comparison of *Tc-otd1* expression in stage-matched wildtype (E) and *Tc-fgf1b*^RNAi embryos (F) revealed a clear reduction with an anterior shift in RNAi treated embryos. In addition no posterior pit formation is obvious (compare white arrow in E′ and F′). (G and H) During early blastoderm formation, an anterior shift of the first primary Eve-stripe is also evident in *Tc-fgf1b*^RNAi embryos (G) as compared to the wildtype embryos (H)

These changes of marker gene expression in the early blastoderm embryo hint for a fate map shift and indicate an important role of FGF signalling in anterior patterning during early development in *Tribolium*.

3.3.3.4   Anterior embryonic structures were affected in *Tc-fgf1b*^{RNAi} embryos
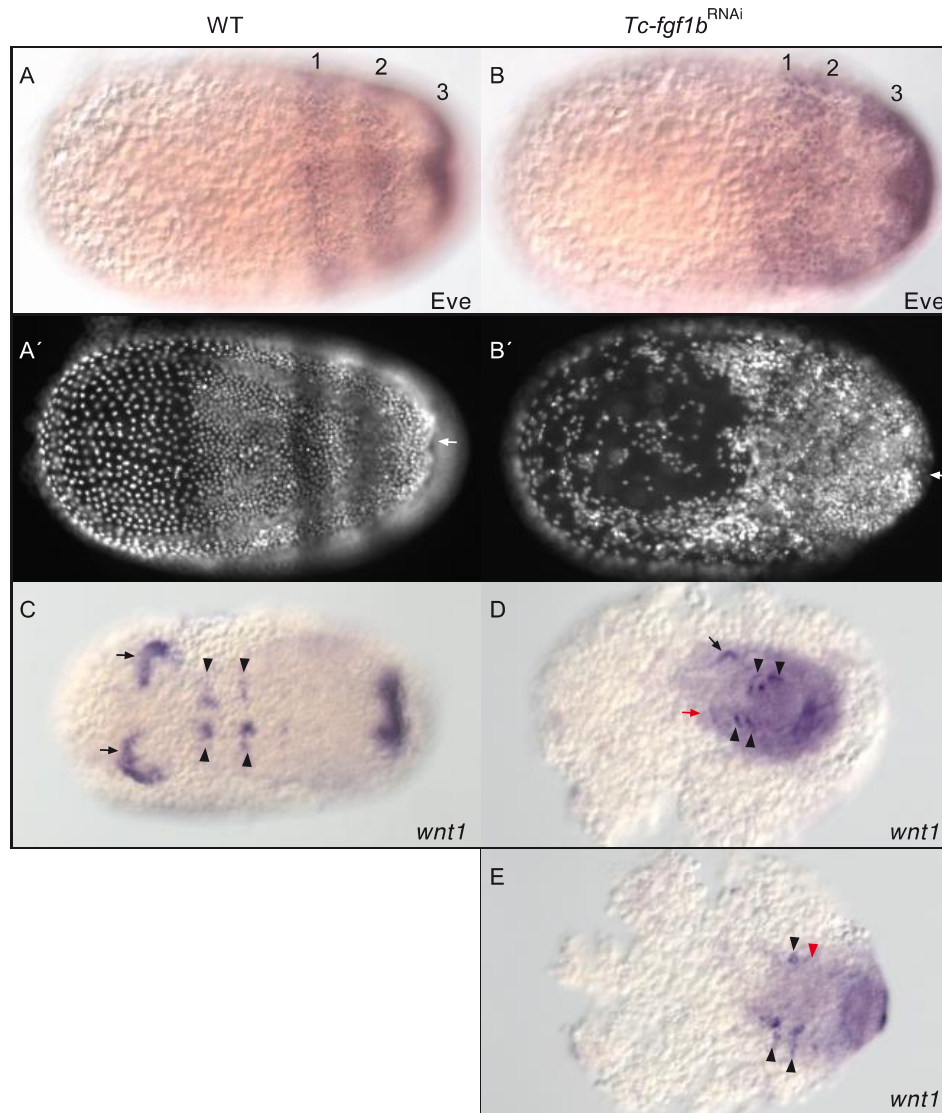
Figure 3.18: Loss of anterior embryonic structures in *Tc-fgf1b*[RNAi] embryos. (A,C) wildtype; (B,D,E) *Tc-fgf1b*[RNAi] embryos; stained for *Tc*-Eve antibody (A,B) and *Tc-wnt1* mRNA (C-E)). (A-E) DIC images; (A′,B′) Hoechst nuclear-counterstain of (A,B), respectively. All embryos are shown in ventral views. (A-B) During early gastrulation in wildtype embryos, both the primary Eve-stripes 1 and 2 mark the early gnathal segments (maxillary and first thoracic segments) and the emerging third primary stripe marks the future growth zone region (A). In *Tc-fgf1b*[RNAi] embryos, both the primary Eve-stripes formed but are irregular and partially fused (B). No posterior pit formation is seen in *Tc-fgf1b*[RNAi] embryos (compare white arrow in A′ and B′). (C) *Tc-wnt1* expression in the wildtype embryo in the head lobes (black arrows) and early segmental stripes (black arrowheads) during germband extension. A posterior expression domain marks the early growth zone region. (D-E) In weakly affected *Tc-fgf1b*[RNAi] embryos, *Tc-wnt1* expression shows the misplacement of the growing germ disc with partial loss of anterior structures (red arrow; D). A more severely affected embryo: complete loss of both anterior head stripes and affected segmentation marked by *Tc-wnt1* expression (red arrowhead; E).

Since an altered expression of different extraembryonic and embryonic markers was observed during early blastoderm patterning, I studied whether these early alterations have an impact on late stages of the embryogenesis as well. To that point, I further analysed the expression patterns of Eve in gastrulating embryos and *Tc-wnt1* expression (a segmental marker) in young extending germbands. Both these markers showed irregularities in *Tc-fgf1b*[RNAi] embryos at the level of segmentation (Fig. 3.18). In early gastrulating wildtype embryo, both the primary Even-skipped stripes 1 and 2 were clearly visible with the third Even-skipped stripe emerging from the future growth zone region (Fig. 3.18A and A´). In *Tc-fgf1b*[RNAi] embryos, both the primary Even-skipped stripes 1 and 2 were principally formed but irregular and partially fused (Fig. 3.18B and B´). The third Eve-stripe seemed not to be affected. The analysis of *Tc-wnt1* expression in extending germbands further revealed the loss of anterior structures and a partial failure of segment formation in *Tc-fgf1b*[RNAi] embryos (Fig. 3.18C-E). When compared to the wildtype (Fig. 3.18C), only a partial loss of anterior head stripes was observed in weakly affected embryos (Fig. 3.18D), whereas, in strongly affected embryos, a complete loss of both the anterior head stripes and a partial loss of segmental stripes were evident (Fig. 3.18E). These results clearly showed that the early anterior patterning defects seen at the blastoderm stages were also observed during gastrulation and germband extension. This further suggests a stable impact of FGF1b-based signalling in formation of anterior structures.

3.3.3.5 Analysis of the dorsal-ventral axis in *Tc-fgf1b*[RNAi] embryos

In contrast to *Drosophila* where the head anlage is exclusively of anterior origin, the head anlage in *Tribolium* initially forms at the anterior and becomes positioned ventrally later during embryogenesis (Lynch and Roth, 2011). Thus, head formation in *Tribolium* depends on both, a functional anterior (Schinko et al., 2008; Schröder, 2003) and a functional DV system (van der Zee et al., 2006). However, in a recent study on *Tc-otd1* function it has been discussed that anterior patterning is solely influenced by the DV system (Kotkamp et al., 2010). In *Tc-fgf1b*[RNAi] affected embryos, a loss of anterior embryonic structures in correlation with reduced *Tc-otd1* expression was also observed. Hence, to analyse the impact of the DV-system on the observed *Tc-fgf1b*[RNAi] phenotype, I looked at the integrity of this system with appropriate marker genes.

In *Tribolium, short gastrulation* (*Tc-sog*) has previously been described as an inhibitor of Dpp signalling that is required to direct the Dpp activity towards the dorsal side of the embryo (van der Zee et al., 2006). During early differentiation of the

blastoderm in wildtype embryos, *Tc-sog* expression was detected in a broad central domain at the ventral surface that narrowed and extended towards the posterior pole (Fig. 3.19A) (van der Zee et al., 2006). Interestingly, the central *Tc-sog* expression domain in *Tc-fgf1b*[RNAi] embryos appeared weaker with no posterior extension indicating an irregular functioning DV system (Fig. 3.19B).

Additionally, I also found *dpp* mRNA expression in *Tc-fgf1b*[RNAi] embryos at a notably higher level at an anterior-ventral position of the blastoderm egg than in the wildtype at the corresponding stage (Fig. 3.19C and D). To show whether this high ventral *Tc-dpp* expression has an impact on the Dpp activity as such, I monitored the activity of the Dpp signalling cascade by antibody staining against phosphorylated MAD (Mothers against Dpp). During blastoderm differentiation in wildtype embryos, pMAD was detected in a broad anterior domain covering the complete serosa primordium and hence is not exclusively dorsal (Sharma et al., 2013a) that continues in a narrow posterior dorsal domain covering the germ rudiment (Fig. 3.19E). In *Tc-fgf1b*[RNAi] embryos, in principal, the pMAD protein was found restricted to the dorsal side in the embryonic domain (Fig. 3.19F and G) but in addition to that a strong reduction in the posterior dorsal embryonic Dpp-activity was also observed in few severely affected embryos (Fig. 3.19G).

The loss of asymmetry of the border between the serosa and the germ rudiment has been described as the consequence of a disrupted DV-system (Nunes da Fonseca et al., 2008; van der Zee et al., 2006). Although slight deviations of DV marker genes from the wildtype pattern were obvious in *Tc-fgf1b*[RNAi] embryos, I did not observe symmetric *Tc-zen1* expression in affected embryos. To further check the integrity of the DV system in relation to symmetry / asymmetry I analysed *Tc-iro* expression at late stages. *Tc-iro* marks the anterior and the dorsal amnion as well as the dorsal ectoderm (Nunes da Fonseca et al., 2010; Nunes da Fonseca et al., 2008), in wildtype (Fig. 3.19H) and *Tc-fgf1b*[RNAi] embryos (Fig. 3.19I and J). Again, I found that *Tc-iro* was still asymmetrically expressed in the anterior amnion and the expression in the dorsal domain was significantly reduced in weakly affected embryos (Fig. 3.19I). In strongly affected embryos, a severe reduction of *Tc-iro* expression in the anterior and the dorsal amnion was observed (Fig. 3.19J).

These findings indicate that the principle set up of the DV axis is not disturbed in *Tc-fgf1b*[RNAi] embryos. However, posterior dorsal structures (dorsal amnion) are sensitive to the loss of FGF1b- dependent signalling.
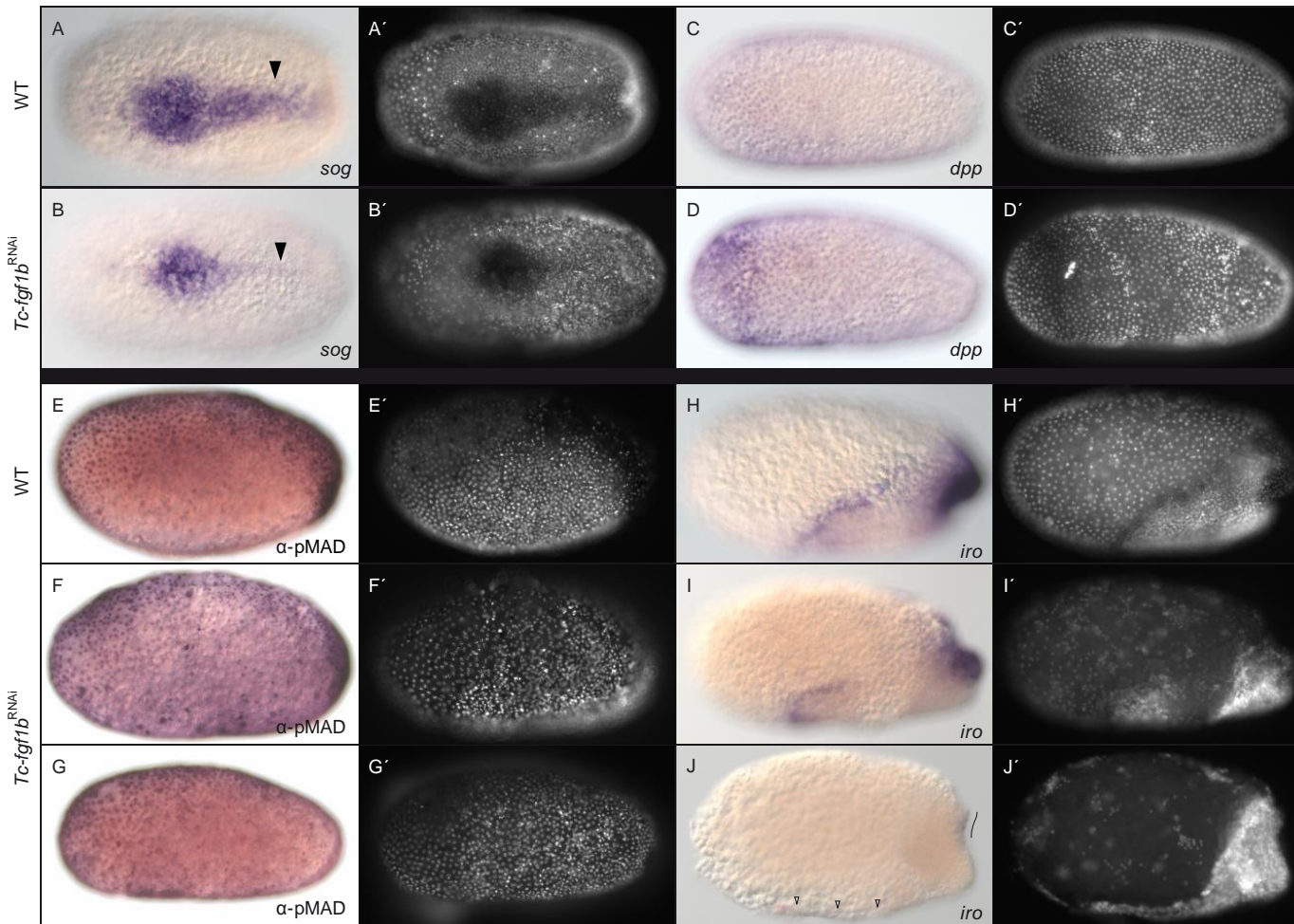
Figure 3.19: The DV-axis is not affected in *Tc-fgf1b*[RNAi] embryos. (A,C,E,H) wildtype embryos; (B,D,F,G,I,J) *Tc-fgf1b*[RNAi] embryos. (A-J) DIC images of blastoderm stages embryos; (A′-J′) Hoechst nuclear-counterstain, respectively. Embryos shown in (A-D) are ventral views and in (E-J) are lateral views with dorsal upside. (A) Wildtype, differentiated blastoderm embryo: *Tc-sog* expression in a broad anterior and narrow posterior ventral domain. A weak anterior and strong posterior reduction (compare arrowheads in A and B) of *Tc-sog* expression is evident in *Tc-fgf1b*[RNAi] embryos (B). (C) Early wildtype blastoderm embryo showing anterior-ventral *Tc-dpp* expression. (D) The level of *Tc-dpp* expression is increased in *Tc-fgf1b*[RNAi] embryos compared to wildtype. (E) Wildtype differentiated blastoderm embryo: nuclear pMAD monitors Dpp activity in a broad anterior and narrow posterior dorso-lateral domain. (F and G) In *Tc-fgf1b*[RNAi] embryos, no ectopic nuclear pMAD detected. A slight decrease in the dorsal domain of Dpp activity is visible in strongly affected embryos (G). (H) Wildtype embryo undergoing invagination: *Tc-iro* expression marks the anterior amnion (present at the asymmetric border between the serosa and the germ rudiment), the dorsal amnion (high level of expression) and the dorsal ectoderm (lower level dorsal expression). (I-J) In *Tc-fgf1b*[RNAi] embryos, a weak (I) to severe ((J); open arrowheads and marked line indicate traces of expression) reduction of anterior as well as dorsal amnion without any loss of asymmetry of the germ rudiment border spotted.

3.3.3.6 The dorsal epidermis is expanded in *Tc-fgf1b*[RNAi] embryos.

In *Drosophila*, the integrity of the dorsal epidermis is required for closing the embryo dorsally over the yolk at the end of embryogenesis (Zahedi et al., 2008). To understand the molecular basis of the dorsal open phenotype seen in *Tc-fgf1b*[RNAi] affected cuticles, I analysed the expression of *Tc-dpp* and *Tc-iro* during later stages of germ band extension where they mark the dorsal epidermis (Nunes da Fonseca et al., 2010; van der Zee et al., 2006).

During early germband extension in the wildtype embryo, weak *Tc-dpp* expression was initially detected in cells around the serosal window (Fig. 3.20A). In the further extended embryo, *Tc-dpp* was expressed in few groups of ectodermal cells of the lateral edge destined to contribute to the dorsal epidermis (Fig. 3.20B) (Sanches-Salazar, 1996). In *Tc-fgf1b*[RNAi] embryos, *Tc-dpp* was expressed at a significantly higher level in broad lateral domains and ectopically at the anterior margin (Fig. 3.20C and D). The quantification was done in strictly controlled parallel staining reactions of experimental and wildtype embryos.

In the wildtype young germband, *Tc-iro* expression was detected between the head lobes and in segmental stripes (Fig. 3.20E). Later during germband extension, strong *Tc-iro* expression was found in the anterior dorsal epidermis and faintly in the emerged stripes near the posterior growth zone in wildtype embryos (Fig. 3.20F) (Nunes da Fonseca et al., 2010). At the young germband stage in *Tc-fgf1b*[RNAi] embryos, *Tc-iro* expression was detected in segmental stripes and ectopically at the margins of the posterior growth zone (Fig. 3.20G). At a more advanced stage, strong *Tc-iro* expression in the expanded dorsal epidermis was also evident in *Tc-fgf1b*[RNAi] embryos (Fig. 3.20H). In summary, the expression of both the marker genes *Tc-dpp* and *Tc-iro* was upregulated and detected in an irregular and clearly expanded domain in the dorsal epidermis and also ectopically in the head and at the margin of the growth-zone in *Tc-fgf1b*[RNAi] embryos.
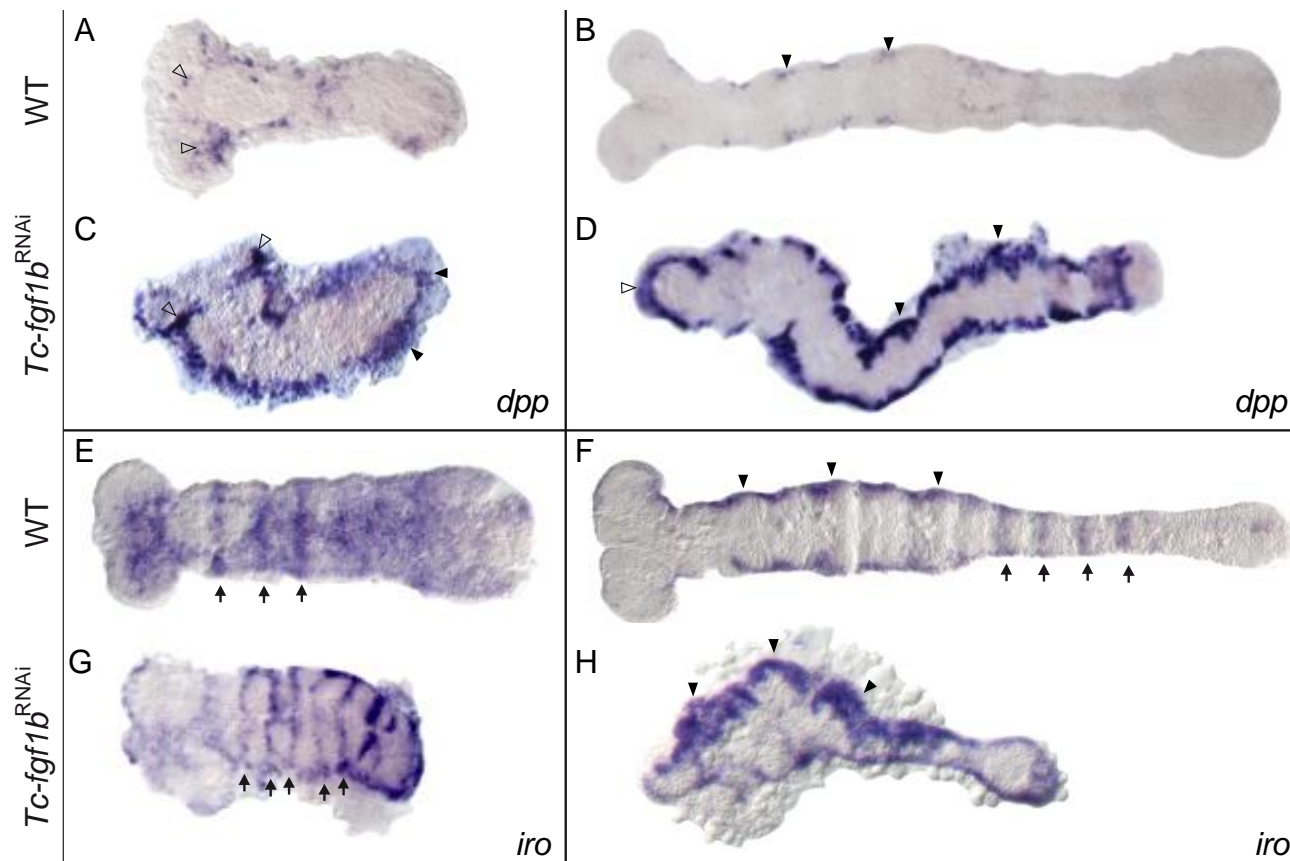
Figure 3.20: Expansion of the dorsal epidermis in *Tc-fgf1b*^RNAi embryos. (A,B,E,F) wildtype embryos; (C,D,G,H) *Tc-fgf1b*^RNAi embryos; transcript detection for *Tc-dpp* (A-D) and *Tc-iro* by in situ hybridization (E-H). All embryos oriented ventral, anterior to the left. (A, B) Germband extension: *Tc-dpp* mRNA initially expressed around the serosal window (open arrowheads in A) and later in the dorsal epidermis of the germband (black arrowheads in B). (C, D) *Tc-fgf1b* RNAi embryos: a significant increase of *Tc-dpp* expression in the expanded dorsal epidermis (black arrowheads) and ectopically at the anterior margin of the head (open arrowheads) evident. (E) Elongating embryo: *Tc-iro* initially expressed in the head and in stripes within the emerging segments (black arrows). (F) Germband extension: *Tc-iro* expressed in the anterior dorsal epidermis (black arrowheads) and faintly in segmental stripes (black arrows) posteriorly. (G, H) *Tc-fgf1b*^RNAi embryos: *Tc-iro* is expressed in stripes and ectopically around the posterior growth zone in the elongating embryo (arrows in G) and in a broad domain of the dorsal epidermis (black arrowheads in H).

3.3.3.7   The mesoderm marker *Tc-twist* is upregulated in *Tc-fgf1b*^{RNAi} embryos.
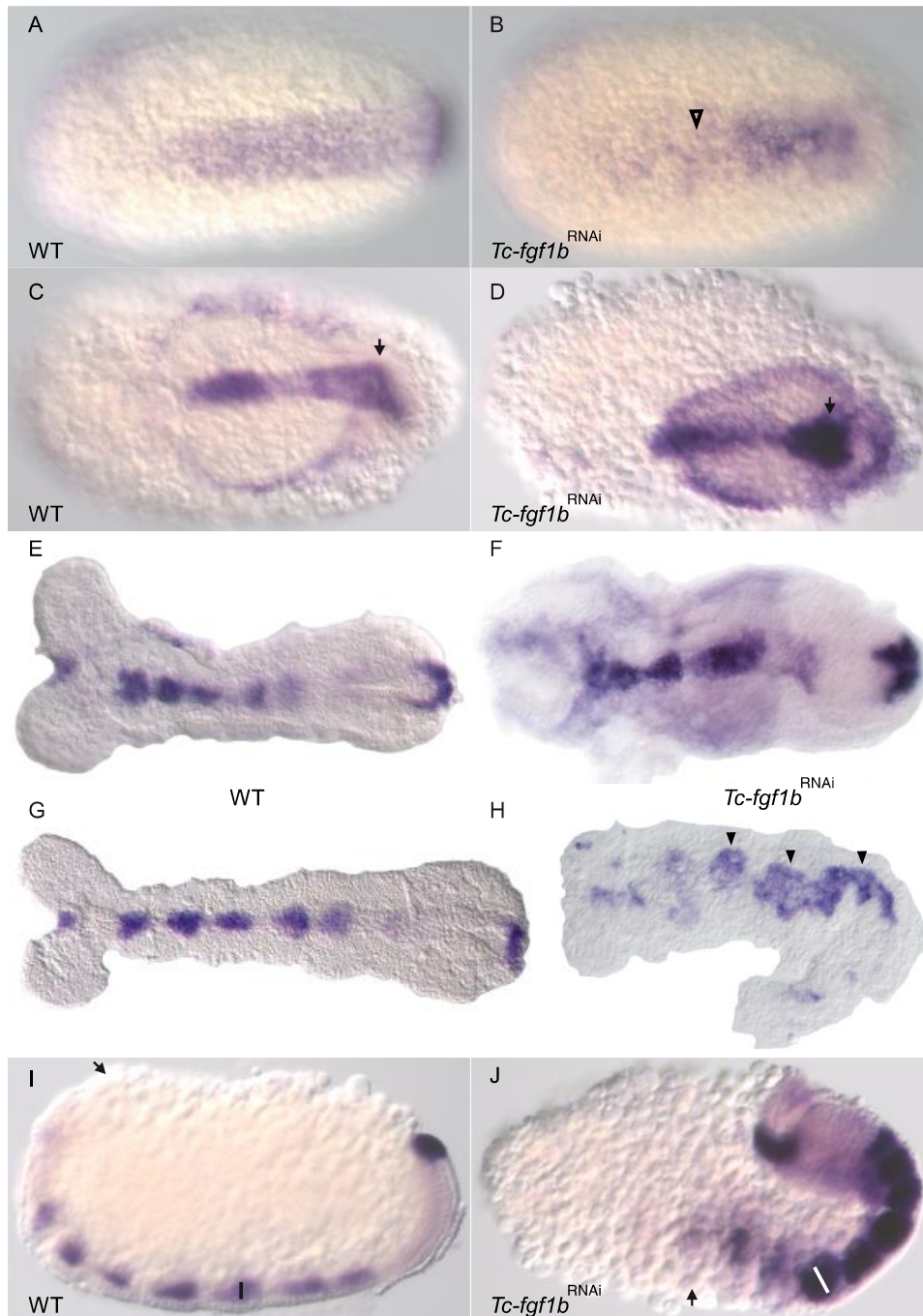
Figure 3.21: The mesoderm marker *Tc-twist* is upregulated in *Tc-fgf1b*^{RNAi} embryos. (A,C,E,G,I) wildtype; (B,D, F,H,J) *Tc-fgf1b*^{RNAi} embryos analysed for *Tc-twist* expression. All embryos are of ventral view except (I) and (J) (lateral view with dorsal upside). (A) Wildtype embryo, late blastoderm: *Tc-twist* is expressed in a ventral stripe of future mesodermal cells towards the boundary between serosa and embryonic anlage. (B) *Tc-fgf1b*^{RNAi}: *Tc-twist* expression in the ventral stripe is irregular and fuzzy in the posterior egg with a reduced anterior domain (open arrowhead). (C, D) Wildtype and *Tc-fgf1b*^{RNAi} (D) embryos: *Tc-twist* is expressed in a mid-ventral stripe (arrow) marking the developing mesoderm with highest expression levels at the posterior end in affected embryos (D, arrow). The complete germ disc of the *Tc-fgf1b*^{RNAi} embryo floats on the surface of the yolk and is not emerged in it. (E) Germband extension, wildtype: *Tc-twist* is expressed in patches in the gnathal region and at the posterior end. (F) Germband extension, *Tc-fgf1b*^{RNAi}: *Tc-twist* is expressed in fused compartments of gnathal and thoracic segments and in a broad patch at the posterior end. (G, H) Elongation of the wildtype and affected germbands: *Tc-twist* is expressed in distinct segmental packages (G). In *Tc-fgf1b*^{RNAi} embryos of the

similar stage, head lobes are fused and *Tc-twist* expression is seen as a partially fused irregular stripe (arrowheads) along the curved body axis (H). (I, J) In comparison to the wildtype (I), an expansion of the mesoderm packages (compare the black and white bar) is observed in *Tc-fgf1b*[RNAi] embryos (J). Additionally, the arrest of head anlage at a midventral position is clearly visible (compare arrows in I and J)..

FGF-signalling in *Drosophila* was shown to influence the behaviour of different cell types including the mesoderm (Bae et al., 2012; Muha and Müller, 2013). I therefore asked whether mesoderm development was also affected in *Tc-fgf1b*[RNAi] embryos and analysed the expression of the mesoderm marker *Tc-twist* in experimental embryos.

In wildtype embryos, *Tc-twist* was expressed in a mid-ventral stripe marking the developing mesoderm during formation of the blastoderm and in the germ rudiment (Fig. 3.21A and C) (Handel et al., 2005; van der Zee et al., 2006). In *Tc-fgf1b*[RNAi] embryos, the anterior part of the *Tc-twist* expression domain was found highly reduced in strength while the posterior domain appeared fuzzy with no sharp boundary at the edges (Fig. 3.21B). In the germ disc that floats at the surface, *Tc-twist* was highly expressed at the posterior pole (Fig. 3.21D).

During germband extension in the wildtype, *Tc-twist* expression was detected as a faint single patch at the anterior end between the head lobes, in groups of cells located in the gnathal region and in a prominent domain at the posterior pole (Fig. 3.21E). In *Tc-fgf1b*[RNAi] embryos of the similar stage, *Tc-twist* expression was detected in fused compartments of gnathal and thoracic segments and as a broad patch at the posterior end (Fig. 3.21F). During elongation of the wildtype germ rudiment, packages of *Tc-twist* expression were distinctly visible in the newly formed segments, in conjunction with a small patch at the anterior and at the posterior end (Fig. 3.21G). In staged matched *Tc-fgf1b*[RNAi] embryos, *Tc-twist* expression was found weak and patchy in the anterior embryo and in a fused domain of irregular shape and width along the curved body axis (Fig. 3.21H).

In the extended germband of the wildtype, *Tc-twist* expression was visible in thin mesodermal packages within each segment (black bar, Fig. 3.21I). In a *Tc-fgf1b*[RNAi] embryo, the packages of mesoderm were partially fused and broadly expanded with a considerably higher mRNA level as compared to the wildtype (white bar, Fig. 3.21J). Note, that in this *Tc-fgf1b*[RNAi] embryo the head remained at a mid-ventral position.

3.4 Discussion

3.4.1 Complexity of the genomic region containing *Fgf1*-like genes

Since its invention, the RACE-PCR technique has been widely used to characterize 3' and 5' ends of cDNA generated from a single gene specific primer (Frohman et al., 1988; Scotto-Lavino et al., 2006a; Scotto-Lavino et al., 2006b; Yeku et al., 2009). In this study, I executed a series of RACE-PCR experiments to define the actual 3' and 5' ends of *Tc-fgf1a* and *Tc-fgf1b* gene.

In the first series of 3' RACE-PCR reactions (Fig. 3.1A), an amplification of "exon a_2" specific fragment and repeated amplification of "exon a_3" specific fragments all with a 3' UTR and a poly(A) tail from different GSPs (Fig. 3.1A-C, (iii)) clearly suggest that the 3' end for *Tc-fgf1a* gene lies between the intergenic region of *Tc-fgf1a* and *Tc-fgf1b*. In addition, these results also demonstrate that there is no interconnection between the exon assemblies of *Tc-fgf1a* and *Tc-fgf1b*. However, the amplification of *Tc-fgf1b* specific fragment from *Tc-fgf1a* specific template (Fig. 3.1B, (iii)) could be an artefact generated due to genomic DNA contamination. This is obvious as the other two reactions with the same objective failed to produce such a fragment (Fig. 3.1A,C, (iii)). Moreover, a direct connection between "exon a_1" and "exon a_2" of *Tc-fgf1a* gene, which could not be established with 3' RACE-PCR reactions (Fig. 3.1A, (i)), was clearly evident in the fragment amplified in the 5' RACE-PCR reaction for *Tc-fgf1a* (Fig. 3.2). Therefore, these results strongly support the predicted three-exon gene model for the *Tc-fgf1a* gene with "exon a_1" at the 5' end and "exon a_3" at the 3' end.

Similarly, the amplification of two "exon b_2" specific fragments with a 3' UTR and a poly(A) tail from the second set of 3' RACE-PCR reaction (Fig. 3.3), favours "exon b_2" as the terminal exon of the two exon-gene model of the *Tc-fgf1b* gene. However, a surprising result obtained repeatedly in independent 5' RACE-PCR reactions (Fig. 3.4A,B) was the extension of the 5' end of *Tc-fgf1b* gene into the 5' region of *TC005517* gene, which is located in opposite orientation just upstream of the *Tc-fgf1a* gene. This result has revealed an overlapping of sequence between the assumed 5' UTR of *Tc-fgf1b* gene and the coding/non-coding sequence in the 5' region of *TC005517* gene. A similar situation has been described in human and mice where a large number of overlapping genes were identified that show an overlap either between the UTRs of two genes or between the coding sequences of two genes or between the UTR and the coding sequences of two genes (Veeramachaneni et al., 2004). In addition, this study also reports that more than

30% of the overlapping genes were overlapped between their 5' region (Head to head), a scenario that parallels the observed result. A by-product was also amplified in this reaction that contains a large intergenic sequence flanked by exon specific sequences of both *Tc-fgf1a and Tc-fgf1b* genes (Fig. 3.4B, (iii)). Conversely, when the same interconnection was explored in the 3' direction using a GSP that start in the first exon of *TC005517* and move towards *Tc-fgf1b*, no conclusive result was obtained (Fig. 3.5A,B). While none of the amplified products showed a real interconnection between *TC005517* and *Tc-fgf1b*, amplification of an exon a_3 specific fragment from these RACE-PCR reactions rather indicate an indirect connection between *Tc-fgf1a* and *TC005517* (Fig. 3.5B, (iii)). A long non-coding RNA was also amplified from these reactions that flanked sequences from *TC005517* and *Tc-fgf1a* gene (Fig. 3.5A, (iii)).

In conclusion, although a continuous run between the exon assemblies of *Tc-fgf1a* and *Tc-fgf1b* in either 3' or 5' directions was not perceived in any of the experiments, it will be too early to judge that *Tc-fgf1a* and *Tc-fgf1b* are two independent genes. Instead, a direct overlap found between the 5' region of *Tc-fgf1b* and *TC005517* and an indirect connection between *Tc-fgf1a* and *TC005517* rather add more complexity to the present understanding of this region. A possible scenario could be that the 5' region of *TC005517* is the common 5' UTR for various splice products of these two exons assemblies. To prove that a thorough analysis of this region with another series of 3' or 5' RACE-PCR reactions using additional primers and contamination free cDNA should be performed to clarify the exact status... Added to that, it is also suggestive to sequence a higher number of RACE-PCR products in the current study. Nevertheless, a consistently visible 3' UTR and a poly(A) tail at the end of the fragments that generated from exon a_3 and exon b_2 strongly support the current exons-assembly for the two orthologs *Tc-fgf1a* and *Tc-fgf1b*.

3.4.2 No functional redundancy between *Tc-fgf1a* and *Tc-fgf1b*

It is clearly evident from the single knockdown of both the *Fgf1*-like genes in *Tribolium* that while the function of *Tc-fgf1b* is critically essential for the early embryonic patterning, *Tc-fgf1a* function appeared dispensable for normal embryonic development because a large number of *Tcfgf1a*[RNAi] eggs developed and hatched into WT larvae (Fig. 3.10) in contrast to *Tcfgf1b*[RNAi] eggs (Fig. 3.12). Moreover, no enhancements of the phenotype in the *Tc-fgf1a*/*Tc-fgf1b* double knockdown embryos (Fig. 3.14) further indicate that there is no redundancy of functions between these two genes. A possible scenario that could explain this situation is that both the genes probably are two independent genes evolved during the beetle lineage as discussed

in our last study (Beermann and Schröder, 2008) and one copy (in this case *Tc-fgf1a*) became non-functional, a usual fate of a duplicated gene pair predicted in most studies (Lynch and Conery, 2000; Zhang, 2003). In addition, a weaker effect observed in the double knockdown embryos appeared as an artefact, which can be explained by the competitive inhibition of dsRNA (Miller et al., 2012) injected through a combined mix for both the genes.

3.4.3 FGF1b-dependent signalling organizes anterior patterning in *Tribolium* embryos

In all bilaterian animals, the primary step in development is the establishment of the anterior-posterior (AP) axis, that represents the most ancient body axis (Kimelman and Martin, 2012). In the model insect *Drosophila*, the molecular mechanism that leads to the specification of the AP axis during development is fairly well understood and has been described in detail (Nasiadka et al., 2002). In contrast, in other arthropods, there is only limited knowledge on the gene network responsible for the formation of the AP axis. However, the evolutionarily conserved head-gap gene *orthodenticle* (*otd*), has been shown to be an important regulator of anterior patterning in many arthropods (Birkan et al., 2011; Buresi et al., 2012; Janssen et al., 2011; Lynch et al., 2006; Nakao, 2012; Schetelig et al., 2008; Schröder, 2003; Wilson and Dearden, 2011).

In this study I have shown that in *Tribolium*, FGF1b- dependent signalling has an influence on *Tc-otd1* expression during early blastoderm formation (Fig. 3.17F). The reduction of the early *Tc-otd1* expression domain in *Tc-fgf1b*[RNAi] embryos could largely explain the loss of anterior fate that is composed of embryonic as well as extraembryonic primordia. The loss of anterior structures was obvious by the irregular expression patterns of marker genes like *Tc-zen1* (Fig. 3.17B), *Tc-iro* (Fig. 3.17D), Eve (Figs. 3.17H and 3.18B) and *Tc-wnt1* (Fig. 3.18D, E) in *Tc-fgf1b*[RNAi] embryos and also by the larval cuticles displaying head and thoracic defects (Fig. 3.13E-G). Further, to overrule any possible implication of early cell death in causing irregularities in these affected embryos, I supplemented our analyses with the TUNEL assay to detect apoptosis at different developmental stages in *Tc-fgf1b*[RNAi] embryos. No excess cell death was observed during any developmental stages in *Tc-fgf1b*[RNAi] embryos that could account for the observed loss of extraembryonic and embryonic structures (see Appendix 3, Figure S11).

In *Tc-fgf1b*[RNAi] embryos, the serosa primordium is severely reduced but not completely lost, confirmed by the remnants of *Tc-zen1* expression at the anterior pole (Fig. 3.17B) and also by the presence of serosal nuclei (Fig. 3.16B, D) in affected

embryos. This parallels the situation in *Tc-otd1*[RNAi] embryos that develop with a partial, but malformed serosa (Kotkamp et al., 2010; Schröder, 2003). Only with the impairment of both, the anterior-posterior and the terminal systems, a complete loss of *Tc-zen1* domain can be achieved and this has been nicely shown in *Tc-otd1 /Tc-torso-like* double RNAi embryos (Kotkamp et al., 2010). Therefore, it can be presumed that the remaining *Tc-zen1* domain seen at the anterior pole of *Tc-fgf1b*[RNAi] embryos is likely due to the activity of the unaffected terminal system. Importantly, the asymmetry of the *Tc-zen1* domain still seen in early stages of *Tc-fgf1b*[RNAi] embryos (Fig. 3B) indicates an unaffected, functional DV-system (discussed below in detail).

Thus, FGF1b-dependent signalling in *Tribolium* broadly organizes the anterior-posterior axis of the blastoderm embryo. Mechanistically, two possible scenarios could explain this important role of FGF signalling in *Tribolium*. First, *Tc-fgf1b* in *Tribolium* could regulate the transcription of *Tc-otd1* via a largely unknown mechanism as a similar mechanism of *Otx*/*Otd* regulation by FGF signalling has been described in the ascidian *Ciona intestinalis* for the induction of anterior neural tissue (Bertrand et al., 2003). In this species, FGF acts via the maternal transcription factors Ets1/2 and GATAa to activate *Otx* required for early neural development (Bertrand et al., 2003).

In the second scenario, the loss of anterior structures could be explained by ectopic activation of the Wnt signalling pathway. In most vertebrates and invertebrates, the inhibition of Wnt activity in the anterior region of the egg is required to allow for the formation of anterior structures (Petersen and Reddien, 2009). In *Tribolium*, RNAi depletion of the WNT inhibitor *Tc-axin* in the anterior blastoderm embryo resulted in severe head defects that has been explained by the failure of downregulating Wnt signalling at the anterior (Fu et al., 2012). In vertebrates, FGF dependent negative regulation of Wnt signalling can be achieved via the activation of *Sox* genes that itself act as Wnt inhibitors in various vertebrate tissues (Dailey et al., 2005; Mansukhani et al., 2005; Murakami et al., 2000; Zorn et al., 1999). On the basis of these scenarios I hypothesize that ubiquitous FGF signalling in *Tribolium* down-regulates a posterior-to-anterior Wnt signalling gradient at the anterior pole to a level that allows the formation of anterior structures. At the posterior, Wnt-signals remain high enough to account for the formation of posterior structures.

It is still unknown whether FGF1 signals through *Tc*-FGFR alone since the *Tc-fgfr*[RNAi] cuticles I analysed so far do not correspond to the strong *Tc-fgf1b*[RNAi] phenotypes described here (described in next chapter). Rather, a further FGF-receptor-like gene

that I detected recently in the *Tribolium* genome, which is ubiquitously expressed in the early embryo (not shown), could serve as an FGF1b receptor.

3.4.4 Extraembryonic tissues are important for early morphogenetic movements during *Tribolium* development.

Extraembryonic membranes are indispensable for normal development of early embryos in vertebrates and invertebrates (Panfilio, 2008). In the wildtype insect embryo extraembryonic membranes are required for positioning the growing embryo within the egg to its final position before hatching (Handel et al., 2000; Panfilio, 2008; Panfilio and Roth, 2010). The complex morphogenetic movements like anatrepsis or katatrepsis in hemimetabolous insects can only take place if the continuity (= physical connection) of extraembryonic and embryonic tissues is maintained. Only then, pulling / pushing forces can be transferred to the embryo (Panfilio, 2008; Panfilio et al., 2006; Panfilio and Roth, 2010).

Tc-fgf1b[RNAi] embryos lack the integrity of both the extraembryonic membranes, serosa and amnion, which can be seen morphologically (Figs. 3.16B, D; 3.18B´ and 3.19B´, I´ J´) as well as through marker-gene expression analyses (Figs. 3.17B, D). This has consequences for embryonic development. First, the embryonic anlage is unable to shift to an anterior position (Figs. 3.16E, G and 3.21I). Instead, it remains posteriorly localized from where it elongates its body around the posterior pole resulting in the formation of a curved body (Figs. 3.13C; 3.16F, H and 3.21J). Second, with no support by both intact extraembryonic membranes, the growing germ disc is not "anchored" and thus "floats" at the surface of the yolk (Figs. 3.16D; 3.18D and 3.21D). In support, previous studies have also shown that the integrity of both extraembryonic membranes is crucial for shifting the germ anlage to the anterior pole during embryogenesis. In *Tc-dpp*[RNAi]- as well as in *Tc-otd*[RNAi] embryos, where both the extraembryonic membranes are affected, a shift of the germ anlage to the anterior pole does not take place and embryos develop in a posterior position within the egg (Kotkamp et al., 2010; van der Zee et al., 2006). However, the complete loss of only one extraembryonic membrane, the serosa, did not show any severe effects on morphogenesis. *Tc-zen1*[RNAi] embryos, without a functional serosa, still developed normally in respect to patterning and morphogenetic movements, possibly organized by the function of the amnion alone (van der Zee et al., 2005).

3.4.5 FGF and DV: is the dorsal-ventral axis affected in *Tc-fgf1b*[RNAi] embryos?

In vertebrates a tight connection of FGF signalling with the BMP signalling pathway has been demonstrated (Dorey and Amaya, 2010; Guo and Wang, 2009). It has been discussed recently that the loss of *Tc-otd1*-function results in a non-functional dorsal-ventral (DV) system in *Tribolium* (Kotkamp et al., 2010). Since I also observed a reduction of *Tc-otd1* expression in *Tc-fgf1b*[RNAi] embryos I explored a possible influence of FGF signalling on the DV system in *Tribolium*. To that end I carefully analysed the expression domains of various DV markers such as *Tc-dpp*, pMAD, *Tc-sog* and *Tc-iro* (Nunes da Fonseca et al., 2010; Nunes da Fonseca et al., 2008; Sanches-Salazar, 1996; van der Zee et al., 2006) in embryos with a reduced FGF signalling pathway. I found that *Tc-sog* expression was weakly reduced in the anterior domain but lost posteriorly similar to what has been described for *Tc-otd1*[RNAi] embryos (Kotkamp et al., 2010). It has been shown previously, that the complete loss of *Tc-sog* expression resulted in a dorsalized phenotype (van der Zee et al., 2006). However, in *Tc-fgf1b*[RNAi] embryos, the DV system in principle seems not to be affected in that *Tc-zen1* (Fig. 3.17B) and *Tc-iro* (Figs. 3.17B and 3.19I) are still asymmetrically expressed and no ectopic nuclear pMAD was detected (Fig. 3.19F, G) although *Tc-dpp* expression was upregulated anteriorly (Fig. 3.19D). Thus, the residual anterior activity of *Tc-sog* observed in *Tc-fgf1b*[RNAi] embryos was sufficient to transport Dpp towards the dorsal side and finally ensured the formation of a functional DV axis. A partial loss of *Tc*-Dpp activity was observed at the posterior likely due to the loss of posterior *Tc-sog* expression. As a result, the dorsal amnion, as marked by *Tc-iro* (Fig. 3.19I, J) was also lost in *Tc-fgf1b*[RNAi] embryos.

Interestingly, in vertebrates FGF signalling was shown to be required for the continued expression of the BMP antagonist *chordin* (Branney et al., 2009; Londin et al., 2005) and for the inhibition of BMP ligands (Delaune et al., 2005; Fürthauer et al., 2004) in an ERK-dependent manner (Eivers et al., 2008). Thus, the inhibition of FGF signalling results in an upregulation of BMP signalling (Dorey and Amaya, 2010). Such an antagonistic relation between FGF and BMPs seems to be conserved also in *Tribolium*. Here, the expression of the *chordin*-ortholog *Tc-sog* was found strongly reduced along the anterior-posterior axis while the *Tribolium* BMP ortholog *Tc-dpp* was upregulated. This illustrates possible parallels of the cross-inhibitory effect between FGF- and BMP signalling in both, vertebrates and *Tribolium* and points to the conservation of this regulatory event during evolution.

3.4.6   The expansion of the dorsal epidermis

The process of dorsal closure (DC) has been intensely studied in *Drosophila* and numerous pathways regulating this process have been described (Heisenberg, 2009; Jacinto and Martin, 2001; Jacinto et al., 2002). Dorsal closure is the result of cooperation between the extraembryonic membrane and the leading edge cells of the dorsal epidermis (Zahedi et al., 2008). In *Tribolium*, I showed so far that in *Tc-fgf1b*[RNAi] embryos both the serosa and the amnion are severely reduced. This alone could already serve as an explanation at the cellular level for the failure of dorsal closure.

Additionally, I also observed high amounts of *Tc-dpp* expression within the dorsal epidermis in *Tc-fgf1b*[RNAi] embryos (Fig. 3.20C, D). In *Drosophila*, Dpp is required in a proper dosage to ensure dorsal closure. If Dpp signalling is impaired such as in mutants for the Dpp-receptor *thickveins*, dorsal closure is incomplete (Affolter et al., 1994). In addition, the downregulation of Dpp in the dorsal most epidermal cells is necessary for the completion of dorsal closure (Martin-Blanco et al., 1998). Thus, the fine-tuning of the Dpp dosage in dorsal epidermal cells is critical for dorsal closure. By interfering with *Tc-fgf1b* function I observed an overexpression of *Tc-dpp* in the leading edge cells (Fig. 3.20A-D). Similarly, high levels of Dpp activity in the leading edge cells in *Drosophila* also result in the failure of dorsal closure (Martin-Blanco et al., 1998). Our results suggest that in *Tribolium* like in *Drosophila* the correct Dpp-level is crucial for the integrity of the leading edge cells and for dorsal closure. In addition, it appears that the number of leading edge cells in *Tc-fgf1b*[RNAi] embryos is higher than in the wildtype as illustrated by *Tc-dpp* (Fig. 3.20C, D) and also by another leading edge cell marker *Tc-iro* (Fig. 3.20G, H).

3.4.7   FGF signalling in mesoderm formation

Among the various roles of FGF signalling, the control of mesoderm formation and patterning is one of the earliest developmental processes that are evolutionarily conserved among metazoans (Dorey and Amaya, 2010; Muha and Müller, 2013). In invertebrates and vertebrates FGF8-dependent signalling was found to be required for mesodermal cell induction and migration (Birnbaum et al., 2005; Gryzik and Müller, 2004; Imai et al., 2002; Kimelman and Kirschner, 1987; Röttinger et al., 2008; Slack et al., 1987; Stathopoulos et al., 2004; Wilson et al., 2005).

In *Tribolium* the role of *Tc-fgf8* in mesoderm development has been presumed on the basis of its expression domain at the border of the presumptive mesoderm (Beermann and Schröder, 2008). Here I describe the role of another FGF ligand, *Tc-fgf1b*, in mesoderm formation in *Tribolium*. The continued expression of the *Tc-twist*

(*Tc-twi*) indicates that ventral mesodermal fate is not lost in *Tc-fgf1b*[RNAi] embryos (Fig. 3.21). However, the expression domain was found to be irregular and patchy and the margins of *Tc-twi* expression were not clearly defined. The lack of anterior *Tc-twi* domain (Fig. 3.21B) in blastoderm embryos likely is due to a reduced level of *Tc-sog* expression (Fig. 3.19B) in *Tc-fgf1b*[RNAi] embryos, as this has been described in *Tc-sog*-RNAi experiments (van der Zee et al., 2006). At the germband stage, mesodermal tissue was expanded in affected embryos (Fig. 3.21J).

We conclude that *fgf1b* in *Tribolium* is not required during early mesoderm induction but fine-tunes mesoderm differentiation during later stages of development. Like in *Tribolium*, FGF signalling in vertebrates is required primarily for the maintenance of axial mesoderm but not for its induction (Fletcher and Harland, 2008). The irregularities of *Tc-twist* expression observed in *Tc-fgf1b*[RNAi] embryos could be explained by an altered behaviour of mesodermal cells in respect to migration or cell adhesion. This would parallel the situation in *Drosophila*, where FGF8-like ligands are required for spreading of mesodermal cells during late gastrulation (Gryzik and Müller, 2004; Kadam et al., 2012; Kadam et al., 2009; Klingseisen et al., 2009; McMahon et al., 2010; Muha and Müller, 2013).

In summary, this study shows that in *Tribolium* FGF1b (but not FGF1a)-dependent FGF signalling is essential for normal embryogenesis at various developmental stages. During early embryogenesis, FGF1b is crucial for patterning the anterior-posterior axis of the blastoderm embryo including extraembryonic- and embryonic tissues. Later in development, FGF1b plays an important role in regulating the formation of the mesoderm and in the dorsal epidermis. Also with this study an important role of FGF signalling in axis formation in an insect has been discussed.

3.4.8 Outlook

Here I have revealed the unexpected role of FGF1b-dependent signalling in AP-axis formation of the beetle *Tribolium*. But the exact mechanism how *Tc-fgf1b* regulates AP axis formation in early embryos is still a puzzle that needs to be solved in the future. Within that context, expression analysis of some more marker genes that are expressed during early blastoderm formation and are involved in patterning the embryo along the AP-axis (like *Tc-axin*, *Tc-mex3*, *Tc-caudal*) or along the DV axis (like *Tc-dorsal*, *Tc-gremlin*) would certainly help to understand the phenotype in a broader dimension. Furthermore, cell-division studies during early embryogenesis in fixed and in living embryos using life-imaging techniques should give further insight into *fgf1*-function in *Tribolium* at the cellular level.

4 Chapter 4

Functional characterization of the ligand *Tc-fgf8*, the receptor *Tc-fgfr* and the downstream molecules *Tc-dof* and *Tc-csw* in the red flour beetle *Tribolium castaneum*

4.1 Introduction

The complexity of the fibroblast growth factor (FGF) signalling pathway is evident by the number and the variety of molecules involved that function as ligands, receptors, signal transducers and downstream effectors (Böttcher and Niehrs, 2005; Dorey and Amaya, 2010). Especially in vertebrates, the high number of extracellular ligands and the variety of their receptors allow for numerous ligand/receptor combinations (Ornitz, 2000). While these various ligand/receptor combinations enable FGFs to play many diverse and essential roles during development of the animals at various stages, the complexity of the *Fgf* gene family in vertebrates impedes functional studies through possible redundant contributions (Tulin and Stathopoulos, 2010). The presence of fewer Fgf homologs in invertebrates however facilitates functional studies because of its low genetic redundancy.

In comparision to 22 FGF ligands and 4 FGF-receptors (FGFRs) in humans, only three FGF ligands {*branchless* (*bnl*), *pyramus* (*pyr*) and *thisbe* (*ths*)} representing two *Fgf* subfamily and two FGF-receptors (FGFRs) {*breathless* (*btl*) and *heartless* (*htl*)} have been identified in the *Drosophila* genome (Gryzik and Müller, 2004; Itoh and Ornitz, 2011; Stathopoulos et al., 2004; Sutherland et al., 1996).

The *branchless*/*breathless* ligand/receptor combination has been found to play a key role in determining the pattern of tracheal branching (Sutherland et al., 1996; Yasuo and Hudson, 2007), formation of the air sac in the larva and recruiting mesodermal cells to exclusively male genital discs (Ahmad and Baker, 2002; Min et al., 1998). The other two Fgf ligands in *Drosophila*, *pyramus* and *thisbe*, were phylogenetically classified as *Fgf8*-like genes. Both the ligands *pyr* and *ths* activate the receptor *htl* to control mesoderm formation and development during gastrulation (Gryzik and Müller, 2004; Muha and Müller, 2013; Stathopoulos et al., 2004; Wilson et al., 2005), where *pyr* specifically regulates the specification of the dorsal mesoderm (Sato and Kornberg, 2002). Both these ligands are also required for pericardial cell specification and caudal visceral mesoderm migration (Kadam et al., 2012; Kadam et al., 2009; Klingseisen et al., 2009).

In comparison to *Drosophila,* the genome of the red flour beetle *Tribolium castaneum* contains four *Fgf* ligands *Tc-fgf1a*, *Tc-fgf1b*, *Tc-fgf8* and *Tc-branchless* (Beermann and Schröder, 2008) and only one *Fgf* receptor *Tc-fgfr*. While the presence of two *Fgf1*-like genes (*Tc-fgf1a* and *Tc-fgf1b*) in *Tribolium* and their assumed synteny to *Drosophila* genes suggest a loss of *fgf1* in flies, the presence of single *Tc-fgf8* gene in *Tribolium* (in contrast to *pyr* and *ths* in *Drosophila*) suggests either a duplication of *fgf8* during the divergence of *Drosophila* or a loss of one *fgf8* homolog in *Tribolium*

genome (Beermann and Schröder, 2008; Tulin and Stathopoulos, 2010). Nevertheless, like *pyr* and *ths* in *Drosophila*, the role of *Tc-fgf8* has also been presumed in mesoderm formation on the basis of its shared expression domain with *twist* (a mesoderm marker) during embryogenesis (Beermann and Schröder, 2008). Additionally, a specific expression domain of *Tc-fgf8* at the mid-brain/hind-brain also suggests a role of *Tc-fgf8* during the brain development in the beetle. Furthermore, the expression pattern of *Tc-fgfr* has been observed in close vicinity to *Tc-fgf8* expression domains suggesting its involvement in various key processes including mesoderm development in cooperation with *Tc-fgf8* (Beermann and Schröder, 2008). While the *fgf1*-like genes, *Tc-fgf1a* and *Tc-fgf1b*, in *Tribolium* have recently been characterized (Sharma et al., 2013b), the functional role of *Tc-fgf8* and *Tc-fgfr* gene in *Tribolium* is yet to be determined.

FGFRs are member of the receptor tyrosine kinases (RTKs) family and activate a range of downstream signalling molecules (Zhu et al., 2005). Generally, RTKs signal through a common signalling cassette but FGF signalling requires some specific intracellular proteins for coupling the activated kinase to the downstream signalling mediators (Dossenbach et al., 2001; Schlessinger, 2000). Downstream of FGFR (Dof; also known as Heartbroken or Stumps) is a cytoplasmic protein that is essentially required for the transduction of signals from both the FGF receptors Btl and Htl in *Drosophila.* Dof acts downstream of the FGFR but upstream of Ras, a small GTP-binding protein (Csiszar et al., 2010; Michelson et al., 1998; Petit et al., 2004; Vincent et al., 1998). In *dof* mutant *Drosophila* embryos, a defect in mesoderm-derived structures and impaired development of the tracheal systems were observed (Imam et al., 1999; Michelson et al., 1998; Vincent et al., 1998). A single ortholog of *dof* has also been identified in the *Tribolium* genome (*Tc-dof*) that is expressed in the same vicinity of *Tc-fgfr* expression (Beermann and Schröder, 2008), a situation very similar to *Drosophila dof* (Vincent et al., 1998).

Another downstream molecule in the RTKs signalling cascade in *Drosophila* is *corkscrew* (*csw*), which is the ortholog of SHP2, a protein tyrosine phosphatase (PTP) (Perkins et al., 1992). It has been described that phosphorylation of tyrosine 515 region in Dof triggers the recruitment of the Csw protein that subsequently helps in activating the Ras/MAPK pathway (Petit et al., 2004). In *Drosophila*, the *csw* mutant phenotype resembles the phenotypes of *btl*, *htl* and *dof* mutant embryos (Petit et al., 2004). Considering the importance of *corkscrew* in *Drosophila*, it would be important to know whether *Tribolium* also possesses a *csw* homolog and if so does it share the functional aspects with the *Drosophila csw* gene.

.

4.2 Aim

Since the functional role of *fgf1*-like ligands (*Tc-fgf1a* and *Tc-fgf1b*) has already been described in the previous chapter. The main objectives of this chapter are:

1. The functional characterization of the single *Fgf8*-like ligand "*Tc-fgf8*" and the single FGF-receptor "*Tc-fgfr*" in *Tribolium* in the context of mesoderm development using RNA interference (RNAi) and *in-situ* hybridization/immunostaining techniques to analyse the phenotype.

2. To find out whether the downstream molecule *Tc-dof* also plays a similar role in development of the beetle as described in the fly.

3. The identification and functional characterization of the *corkscrew* homolog in the *Tribolium* genome.

4.3 Results

4.3.1 Larval cuticle analysis of *Tc-fgf8-, Tc-fgfr-, Tc-dof-* and *Tc-csw-* RNAi embryos

4.3.1.1   *Tc-fgf8*^RNAi and *Tc-fgfr*^RNAi embryos failed to hatch into larvae

In order to determine the function of both, the ligand *Tc-fgf8* and the receptor *Tc-fgfr* during embryonic development of the beetle *Tribolium*, a single individual knockdown for each gene was achieved through parental RNAi by injecting *Tc-fgf8* and *Tc-fgfr* dsRNA respectively at various concentrations (see Appendix 4, Figure S12 and S13). To rule out the possibility of off- target effects, different non-overlapping fragments (NOFs) of the same gene were also injected to confirm the precise function of targeted genes.
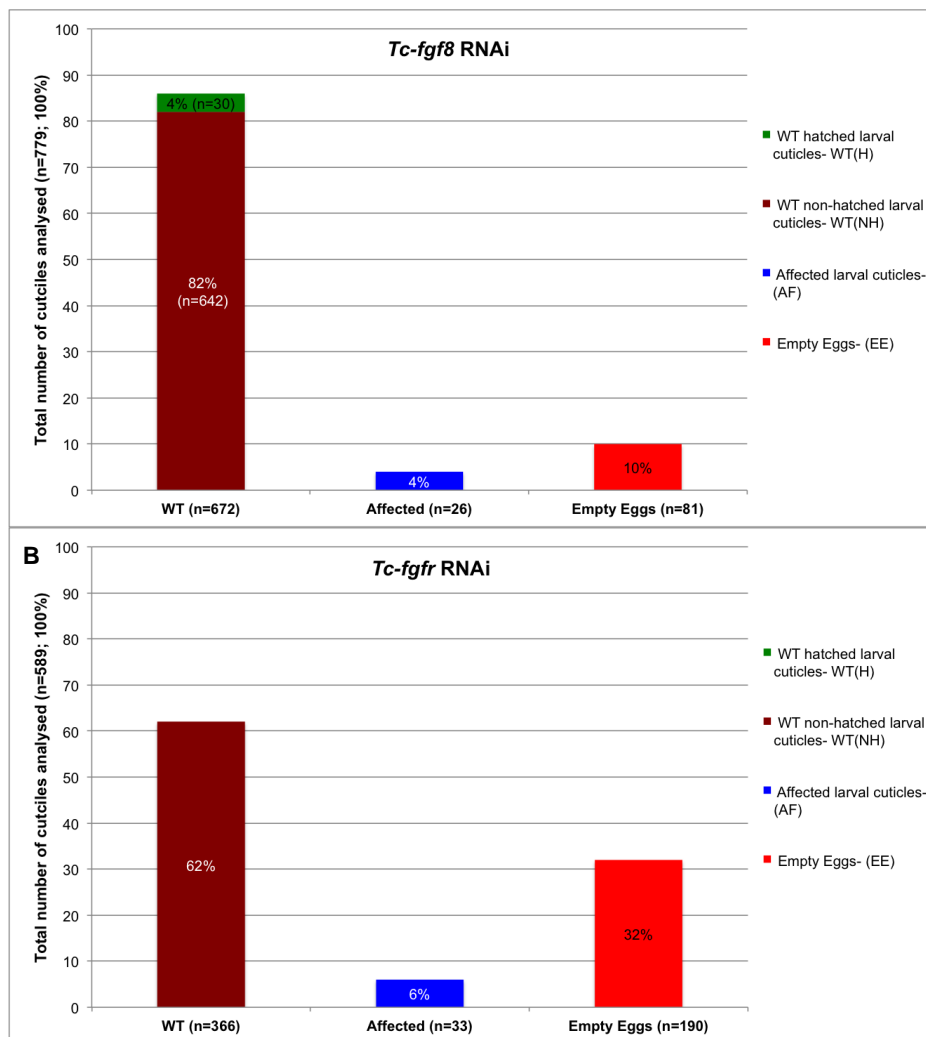
Figure 4.1: Statistical analysis of *Tc-fgf8*^RNAi and *Tc-fgfr*^RNAi eggs.

The single knockdown of either the ligand *Tc-fgf8* or the receptor *Tc-fgfr* (Fig. 4.1A, B) resulted in a situation where a majority of the eggs (82%, n=642 in *Tc-fgf8*^RNAi and

62%, n=366 in *Tc-fgfr*^{RNAi}) developed into larvae, that were indistinguishable from the WT in respect to their main body organization/parts (head, thorax, abdomen and appendages), but failed to hatch from the egg. This class was categorised as "WT non-hatched larval cuticles" (Fig. 4.1A,B). The number of eggs that failed to produce a cuticle ("empty eggs") was three times higher in *Tc-fgfr* knockdown (32%, n=190) when compared to *Tc-fgf8*^{RNAi} (10%, n=81) eggs (Fig. 4.1A, B). This shows that the effect is more severe in *Tc-fgfr*^{RNAi} embryos. A small amount of embryos from both the injections (4%, n=26 in *Tc-fgf8*^{RNAi} and 6%, n=33 in *Tc-fgfr*^{RNAi}) also showed some weak to strong cuticle aberrations and hence described as "affected cuticles" (Fig. 4.1A,B). A small number of *Tc-fgf8*^{RNAi} eggs (4%, n=30) were also able to hatch into larvae (Fig. 4.1A) but could reflect an artefact as those stemmed from one particular injection out of many (for details see Appendix 4, Figure S12 and S13).

4.3.1.2 *Tc-fgf8*^{RNAi} and *Tc-fgfr*^{RNAi} cuticle phenotypes
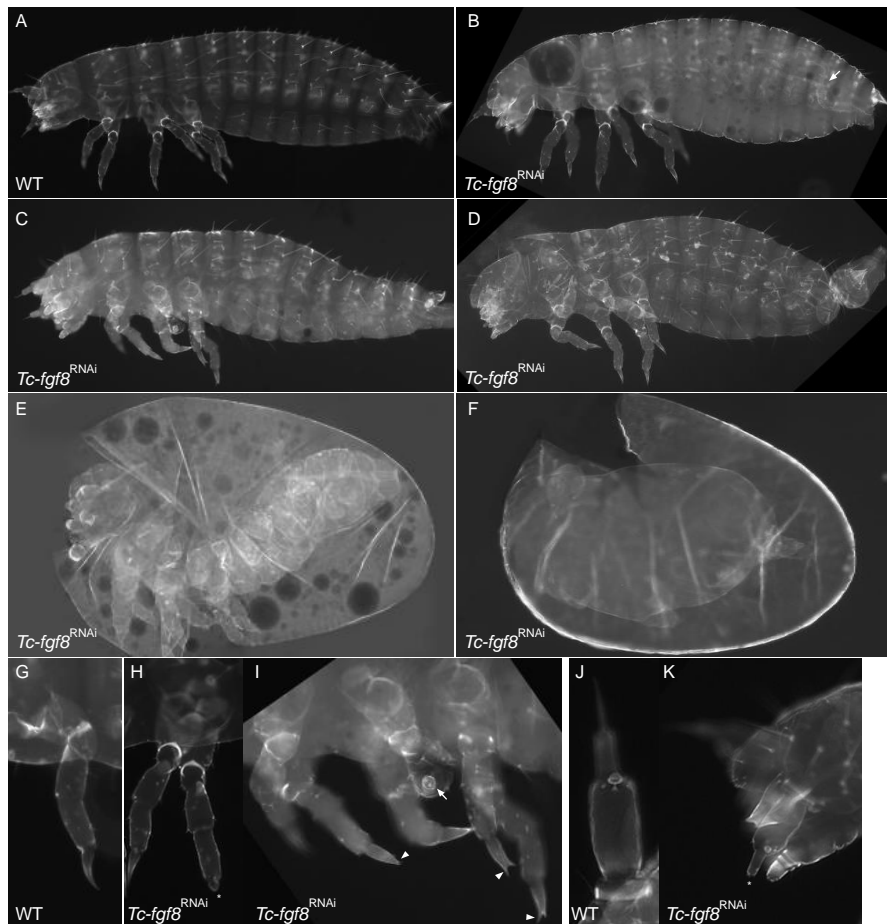
Figure 4.2: *Tc-fgf8*^{RNAi} cuticle phenotypes. (A) A wildtype larval cuticle. (B) A *Tc-fgf8*^{RNAi} non-hatched larval cuticle with irregular shape hindgut (arrow). (C-D) Weakly affected *Tc-fgf8*^{RNAi} cuticles showing appendages malformations (C) and twisted abdomen (D). (E) A strongly affected *Tc-fgf8*^{RNAi} cuticle showing a completely irregular shaped body. (F) Cuticle ball with few visible appendages. (G) A WT larval leg. (H-I) weakly affected legs of *Tc-fgf8*^{RNAi} cuticles: a shortened claw (asterisk, H), bifurcated leg claws (arrowheads, I) or a malformed leg (arrow, I). (J-K) with regard to WT antenna (J), a loss of antennal spike is clearly visible in *Tc-fgf8*^{RNAi} embryo (asterisk, K).
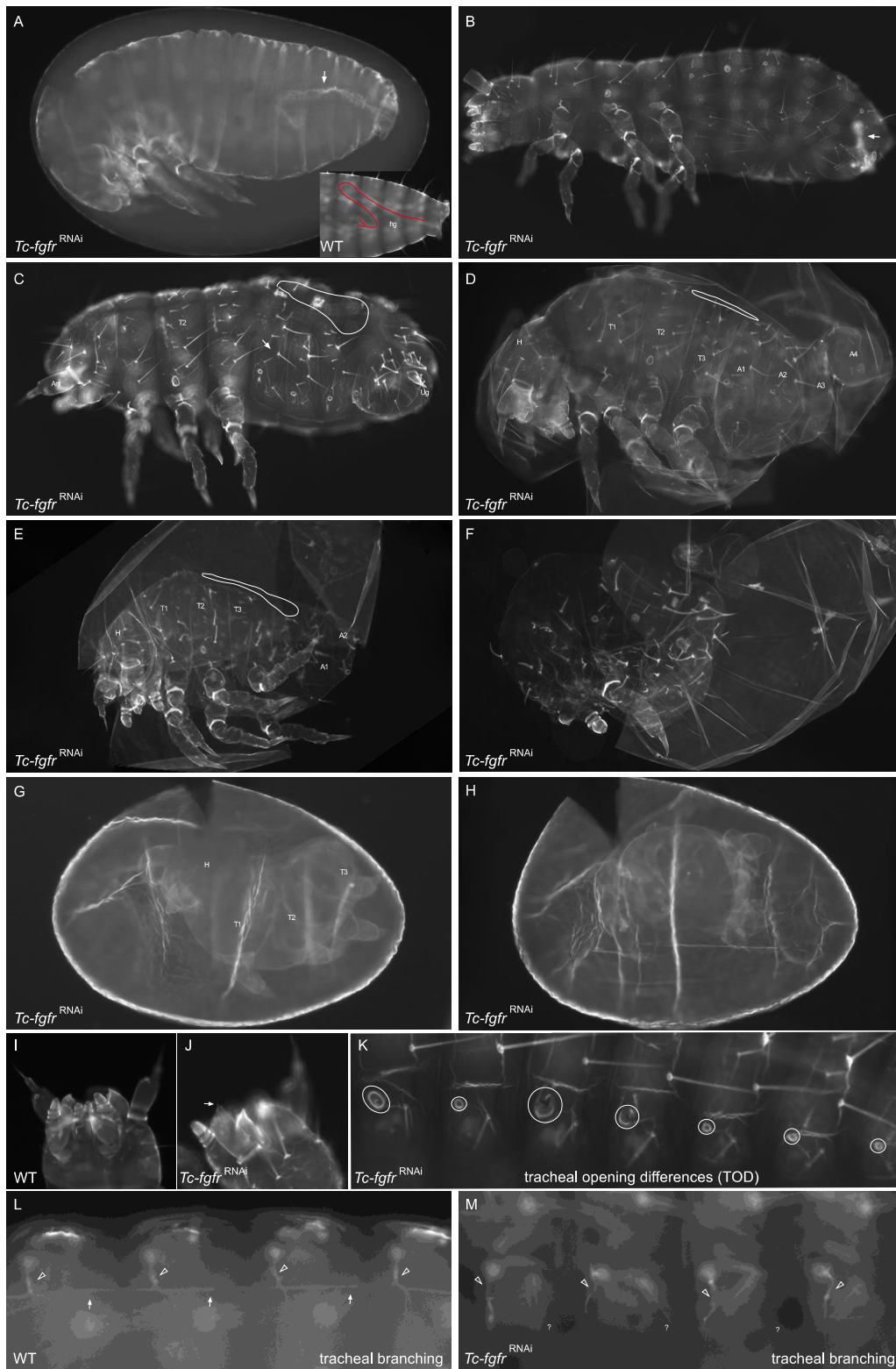
Figure 4.3: Cuticle phenotypes of *Tc-fgfr*RNAi embryos. (A) A non-hatched *Tc-fgfr*RNAi larva shows the hindgut malformation (arrow) compared to I WT hindgut (inset). (B) Cuticle with virtual short abdomen phenotype where remaining segments crumbled within the body (arrow). (C-E) Cuticles with weak to strongly reduced abdominal segments and dorsal opening (dotted circle). (F) Cuticle with rare gap phenotype. (G) Strongly affected cuticle with recognisable head and thoracic structures only. (H) Most severely affected embryo within the egg. (I-J) In weakly affected *Tc-fgfr*RNAi embryo the loss of antennal stigma and spike was obvious. (K-M) Compared to WT (L), an abnormal shape of the tracheal openings (dotted circles, K) and impaired branching of tracheal system (compare white arrows in L with "?" in M) become obvious in *Tc-fgfr*RNAi embryos. (H, Head; T1-T3, thoracic segments 1-3; A1-A8, 1-8 abdominal segments; ug, urogomphi; hg, hindgut; TOD, tracheal opening differences)

A common phenotype that was observed in both *Tc-fgf8*[RNAi] and *Tc-fgfr*[RNAi] embryos was the abnormal shape of the hindgut in all the non-hatched WT larvae (arrow in Fig. 4.2B; Fig. 4.3A). In addition, an irregular shape and size of the tracheal openings (a phenotype termed as tracheal opening differences (TOD)) and a loss of the main tracheal tube that interconnects all the tracheal openings in the tracheal network within each half of the body was exclusively detected in *Tc-fgfr*[RNAi] non-hatched larvae (Fig. 4.3K-M). While the impaired tracheal branching was featured in all the non-hatched larvae, TOD phenotype was observed only in 47% (n=279) *Tc-fgfr*[RNAi] cuticles.

The analysis of "affected cuticles" however showed some phenotypic differences between the *Tc-fgf8*[RNAi] (n=26) and *Tc-fgfr*[RNAi] (n=33) embryos (Figs. 4.2 and 4.3) (for more specific details see Appendix 4, Table S7). Weakly affected *Tc-fgf8*[RNAi] cuticles (n=8) showed loss of antennal spikes (Fig. 4.2D, K), malformation of legs/bifurcated leg-claws (Fig. 4.2C, H-I) and twisted abdomen (Fig. 4.2D). Intermediate class of *Tc-fgf8*[RNAi] cuticles (n=10) showed malformations of the complete body segments and appendages (Fig. 4.2E). The strongly affected *Tc-fgf8*[RNAi] embryos (n=5) were identifiable only by a cuticle sphere with few outgrowing appendages (Fig. 4.2F). The remaining *Tc-fgf8*[RNAi] cuticle (n=3) displayed phenotypes that cannot be included in any of the above category (not shown).

Weakly affected *Tc-fgfr*[RNAi] cuticles (n=5) also showed loss of antennal spike (Fig. 4.3I, J), malformation of legs/bifurcated leg-claws (not shown), TODs (Fig. 4.3K) but no twisted abdomen. However most of the remaining affected cuticles (n=22/28) surprisingly showed a weak to strong reduction/truncation of the posterior segments (Fig. 4.3B-H). While in weakly truncated embryos (n=13) a progressive loss of abdominal segments was obvious (Fig. 4.3B-F), in strongly reduced embryos (n=9) only head and thorax formation was recognizable (Fig. 4.3G). In most severely affected *Tc-fgfr*[RNAi] cuticles (n=6), a cuticle sphere/block was recognisable within the egg that was hard to analyse (Fig. 4.3H) (for more specific details see Appendix 4, Table S8).

In summary, with these results it is obvious that while *Tc-fgf8* does not appear to be essential for early embryogenesis, it certainly has an important role during the late development of the embryo. Similarly the results of *Tc-fgfr* knockdown also provide first evidence that *Tc-fgfr* is functionally required for many vital processes including gut development, tracheal development and abdominal patterning during the development of the beetle *Tribolium*. Nonetheless, these results need to be further confirmed at the embryonic level using expression analysis of some appropriate gene markers like *brachyyenteron*, *wingless* and *trachea-less*.

4.3.1.3 *Tc-dof-*[RNAi] resulted in a diverse range of cuticle phenotypes

After functional characterization of the ligand *Tc-fgf8* and the receptor *Tc-fgfr* at the cuticle level, I further aimed to functionally characterize the downstream molecule *Tc-dof*, which is an intracellular protein specifically required for the transduction of FGF-signalling (Petit et al., 2004; Vincent et al., 1998). In the beetle *Tribolium*, the expression pattern of *Tc-dof* has been detected at sites identical to *Tc-fgfr* expression (Beermann and Schröder, 2008). To find out its function during *Tribolium* development a dose-dependent knockdown of *Tc-dof* was performed through parental RNAi (see Appendix 4, Figure S14).
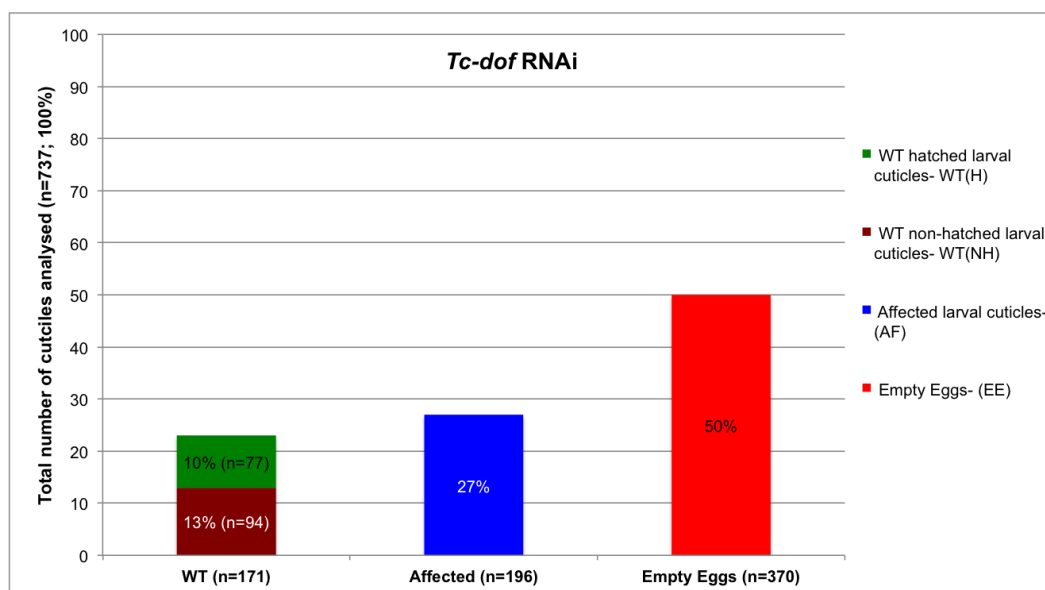
Figure 4.4: Statistical analysis of *Tc-dof* [RNAi] phenotypes.

Interestingly, the result obtained after the single knockdown of *Tc-dof* in *Tribolium* showed clear differences to the result observed after the *Tc-fgfr* knockdown (compare Figs. 4.1B and 4.4). While no cuticle formation was detected in 50% (n=370) of *Tc-dof-*[RNAi] eggs ("empty eggs"), only in 27% (n=196) of *Tc-dof-*[RNAi] eggs a cuticle was realized but with some weak to strong morphological aberrations ("affected cuticles") (Fig. 4.4). Within the remaining 23% (n=171) *Tc-dof-*[RNAi] eggs, 55% (n=94) eggs developed into non-hatching WT larvae (Fig. 4.4). The further remaining 45% (n=77) eggs however successfully hatched into larvae and counted under WT-hatched category because no difference was observed in these cuticles (Fig. 4.4).

A cuticle analysis of all the affected *Tc-dof* [RNAi] embryos (n=196) revealed a multiple range of weak to strong cuticle phenotypes (Fig. 12.2) that were categorized into nine different classes (ClassA-I) (for more specific details see Appendix 4, Table S9). Class A cuticles (weak phenotype; n=49, 25%) showed mild abdominal patterning defects i.e. merging of 2 or more abdominal segments into 1 along with TODs. These

cuticles also show some malformations of head appendages, legs and posterior appendages (Fig. 4.5A-G).
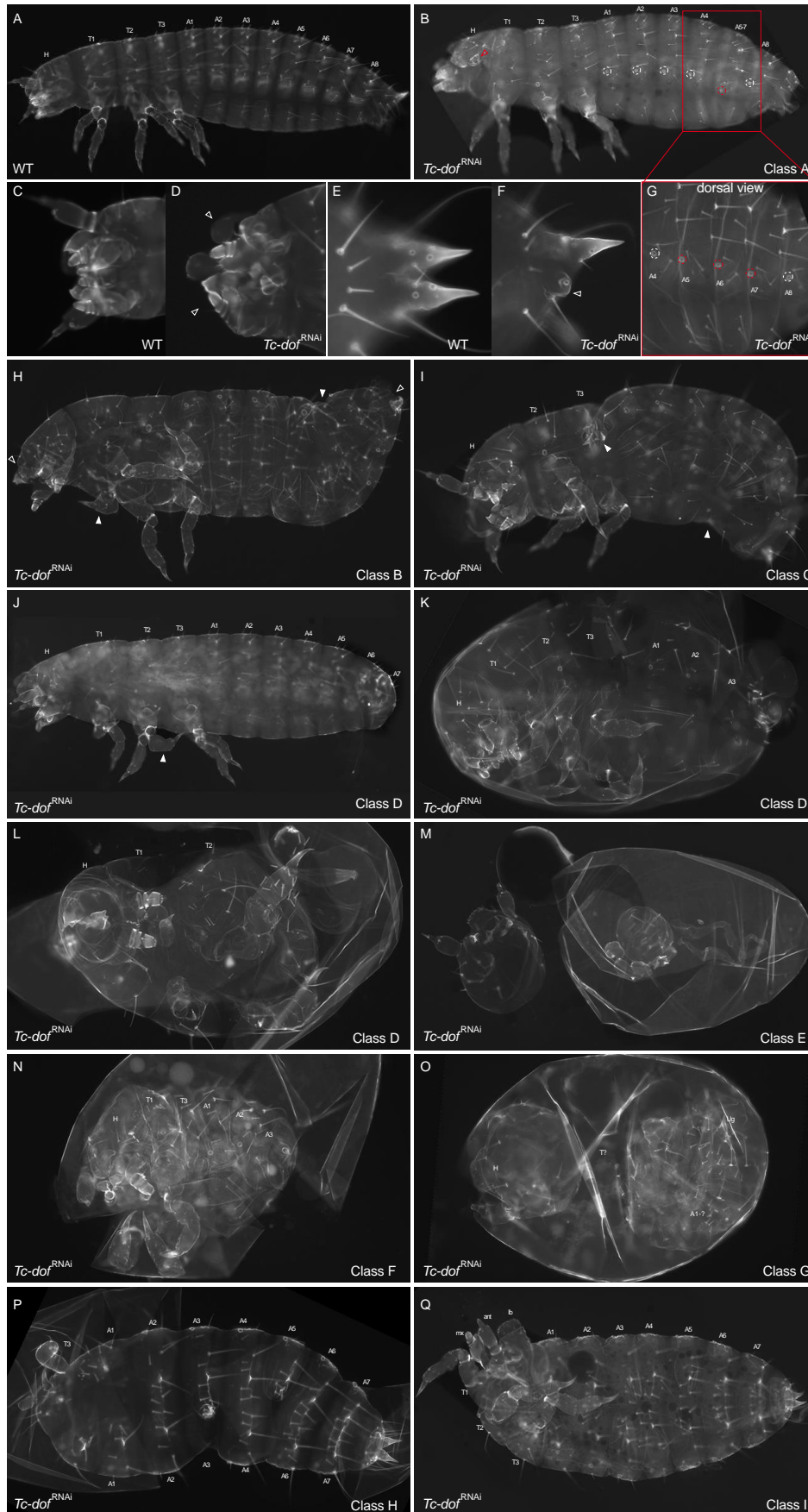
Figure 4.5: *Tc-dof* knockdown results in multiple defects of larval cuticles categorized into 9 different classes. (A) A wildtype larval cuticle. (B) A weakly affected "class A" cuticle with malformed antenna (red open-arrowhead) and incorrectly patterned abdomen where three segments (A5-A7) on one side (dotted red circles in G) merged into a single segment on other side (dotted red circle in B). (C-F) Enlarged view of head appendages and urogomphi in WT (C,E) and affected larva (D,F) showing antennal defects (open arrowheads; D) and loss of urogomphi (open arrowhead; F). (H) A Class B cuticle with multiple defects: loss of antennae (open arrowhead), loss of/malformed leg (white arrowhead), wrongly patterned abdomen (white arrowhead) and loss of urogomphi (open arrowhead). (I) A Class C cuticle with loss of first thoracic segment, poorly developed leg (white arrowhead) and abdominal patterning defect (white arrowhead). (J-L) Class D cuticles with axis elongation phenotype: (J) A weakly truncated cuticle with loss of A8 and posterior structures along with leg deformity and loss of antennal spike. (K) Cuticle with intermediate truncation where formation of head, thorax and only three abdominal segments occured. (L) In strongly truncated cuticle only head and the first two anterior thoracic segments were formed. (M) Most severely affected "class E" cuticle with head only structure. Undefined cuticle spheres along with gut like structure also contribute to this class. (N) A "class F" short cuticle showing loss of central thoracic segment and few abdominal segments similar to "gap-phenotye". (O) A "class G" cuticle partitioned into two spheres showing identity of head and abdomen respectively, thorax is missing here. (P) Class H cuticles show strong anterior truncation where no formation of head and first two thoracic segments occurred. Segmentation defects of abdomen were also visible. (Q) Class I cuticles show left-right asymmetry phenotype: proper formation of appendages on one side while no formation on other side. (H, Head; T1-T3, thoracic segments 1-3; A1-A8, 1-8 abdominal segments; ug, urogomphi; hg, hindgut)

In class B cuticles (n=18, 9%) a fused patterning of head (H) and first thoracic segment (T1) that leads to either loss of one leg or poorly developed legs was apparent in addition to wrongly patterned abdominal segments (Fig. 4.5H). More strongly affected cuticles (Class C; n=13, 7%) showed a complete loss of the first thoracic segment (T1) (Fig. 4.5I). A wrongly patterned abdomen was also visible in these cuticles (Fig. 4.5I). More frequently observed (n=42, 21%) axis elongation phenotype (posterior truncation of the embryo) in *Tc-dof* [RNAi] embryos was the feature of class D cuticles (Fig. 4.5J-L). Within this class a spectrum of weak (partial loss of abdomen; Fig. 4.5J-K) to severe (partial loss of thorax and a complete loss of abdomen; Fig. 4.5L) posterior truncations was evident. Most severely affected embryos display only head formation along with a short cuticle ball (unanalyzable) and a gut like structure and were placed in class E (n=15, 8%; Fig. 4.5M). Additionally in 11% (n=22) of the affected *Tc-dof* [RNAi] embryos a "gap-phenotype" like characteristics was also observed and these cuticles were assigned to a separate class F (Fig. 4.5N). This gap-phenotype like cuticles showed concurrent loss of thoracic and abdominal segments. In other 14% (n=22) affected embryos (Class G), two or more fragmented cuticle spheres were observed with each sphere corresponding to either the head capsule or the thorax or the abdomen. While some of the cuticles spheres were easily identifiable (Fig. 4.5O), for other spheres it was difficult to assign a specific tagma. In few affected *Tc-dof* [RNAi] embryos (n=7, 4%), a headless cuticle phenotype was also observed (Class H; Fig. 4.5P). Lastly, the remaining few affected embryos (n=3, 2%) also showed left-right asymmetry after *Tc-dof* knockdown (Class I; Fig. 4.5P).

Taken together, these results show an involvement of *Tc-Dof* along the AP-axis in properly organizing head, thorax and abdomen formation during *Tribolium* development.

4.3.1.4 *Tc-csw*^{RNAi} leads embryonic lethality and affect egg laying rate

Corkscrew (CSW) is the *Drosophila* ortholog of SHP-2 in vertebrates that functions as signal transducer downstream of multiple RTK pathways including FGF. In *Drosophila, corkscrew* plays an important role in many different processes including tracheal as well as CNS development (Perkins et al., 1996; Perkins et al., 1992). Within the *Tribolium* genome, I identified a single *corkscrew* homolog (*Tc-csw*) using BLAST tools from the NCBI and the BeetleBase and cloned a gene fragment obtained by PCR using gene specific primers (see Appendix 1, Table S1). For functional characterization, dose-dependent knockdown experiments of *Tc-csw* were performed using parental RNAi (pRNAi).

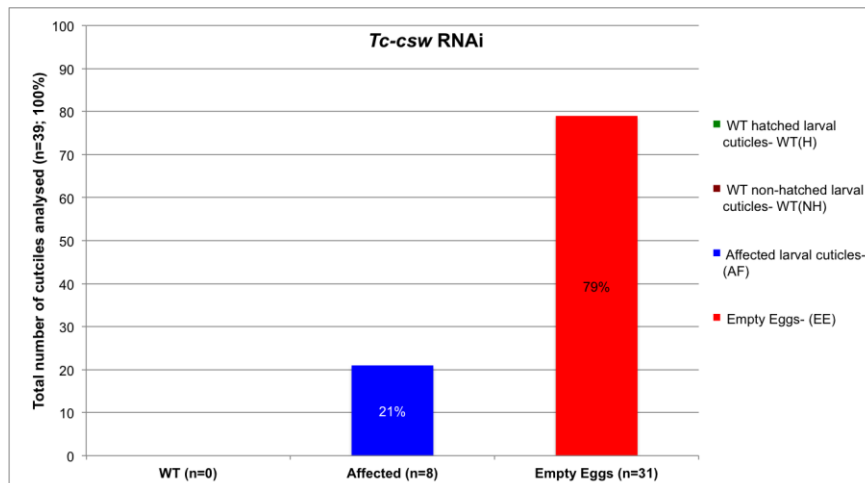Figure 4.6: Statistical analysis of *Tc-csw*^{RNAi} phenotypes.
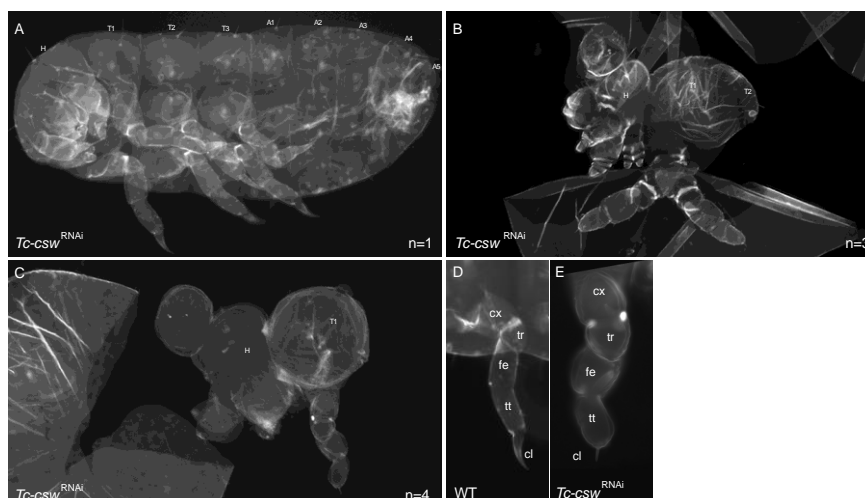

Figure 4.7: Cuticle phenotypes of *Tc-csw*^{RNAi} embryos. (A) A weakly affected *Tc-csw*^{RNAi} embryo showing loss of only posterior abdominal segments (A6-A8). (B, C) Much strongly affected *Tc-csw*^{RNAi} embryos showing severe truncations: (B) In less strongly truncated embryos, a head capsule with

severely malformed antennae and first thoracic segment with a pair of legs were identifiable. (C) In strongest truncations, only posterior head appendages along with one leg were identifiable on a segmented cuticle. A deformity of proximal leg claw was clearly visible in affected embryos (E) when compared to a complete WT leg (D). (H, Head; T1-T3, thoracic segments 1-3; cx, coxa; tr, trochanter; fe, femur; tt, tibiotarsus; cl, pretarsal claw)

An initial impact of the *Tc-csw* knockdown was clearly visible on egg-laying rate of the female adults, which was found strongly reduced after the injection of *Tc-csw* dsRNA. Only few (n=39) *Tc-csw*[RNAi] eggs could be collected from two different independent experiments. 79%(n=31) of eggs did not develop a cuticle (empty eggs) and the remaining 21%(n=8) eggs developed into larval cuticle with severe defects (Fig. 4.6). Most of these showed a severe truncation of the embryonic structures (Fig. 4.7). Only remnants of head and thoracic structures formation were visible in these embryos (Fig. 4.7B, C). Especially the antennae (Fig. 4.7B, C) and the leg claws were severely deformed (Fig. 4.7D, E). In a rarely visible weakly affected embryo only truncation of the posterior abdomen was obvious (Fig. 4.7A).

4.3.2 Molecular analysis of *Tc-fgf8*[RNAi] and *Tc-fgfr*[RNAi] larval phenotypes

From the above knockdown studies, it is clearly apparent that both *Tc-fgf8* and *Tc-fgfr* are functionally important for the late developmental processes. But to further explore the real insights of those cuticle phenotypes at the embryonic level, various molecular markers were analysed in fixed RNAi embryos using *in-situ* hybridization and antibody staining.

4.3.2.1 The embryonic head is not affected in *Tc-fgf8*[RNAi] embryos

The observed high percentage of embryonic lethality (82%) in *Tc-fgf8*[RNAi] embryos and the fact that *Tc-fgf8* is expressed at the midbrain/hindbrain boundary of WT embryos (Beermann and Schröder, 2008) directed me to to study the the embryonic head development in affected embryos.

To address that, the expression pattern of *Tc-orthodenticle1* (*Tc-otd1*) that marks the anterior-most embryonic head anlage (Schinko et al., 2008; Schröder, 2003) was analysed in *Tc-fgf8*[RNAi] embryos. In addition, expression of a segmentation marker *Tc-wingless* (*Tc-wg*/*Tc-wnt1*) (Nagy and Carroll, 1994) was also examined to check the proper development of all the head appendages in late embryos.

Interestingly, no visible differences were observed in the expression profile of *Tc-otd1* and *Tc-wnt1* between wildtype and *Tc-fgf8*[RNAi] embryos. At the blastoderm stage embryo, like in the WT, *Tc-otd1* expression was also seen in two block-like ventral domain that marks the presumptive head lobes in *Tc-fgf8*[RNAi] embryos (Fig. 4.8A, B).
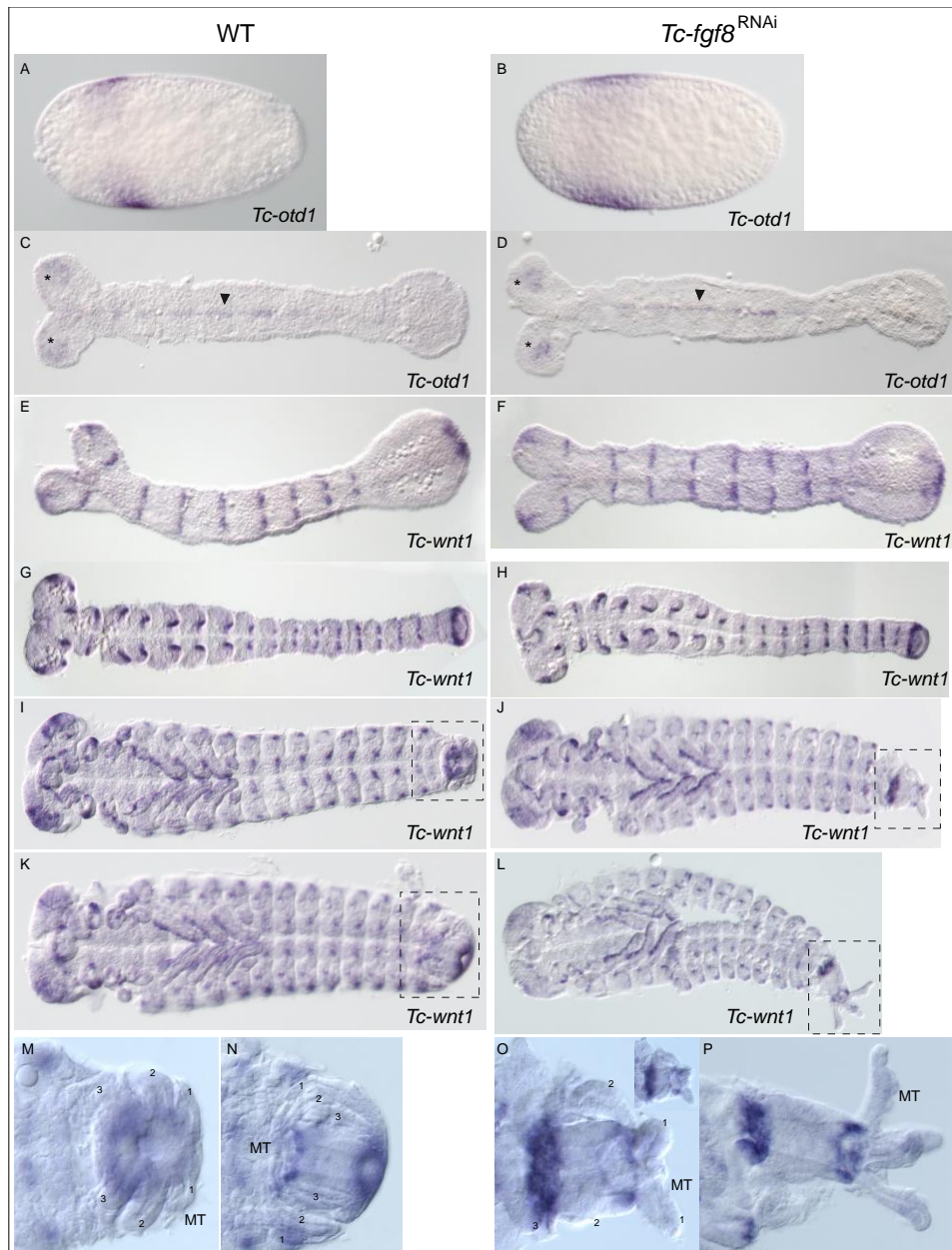
Figure 4.8: Analysis of head (*Tc-otd1*) and segmentation (*Tc-wnt1*) markers in *Tc-fgf8*^RNAi embryos. (A,C,E,G,I,K,M,N) wildtype embryos; (B,D,F,H,J,L,O,P) *Tc-fgf1b*^RNAi embryos; transcript detection for *Tc-otd1* (A-D) and *Tc-wnt1* by in situ hybridization (E-P). Images (M-P) are the enlarged views of boxes in I, K, J, L respectively. All embryos oriented ventral, anterior to the left. (A-B) During blastoderm formation, *Tc-otd1* expression is clearly evident in two broad ventral stripes of the presumptive head lobes in both WT (A) and *Tc-fgf8*^RNAi embryos (B). (C-D) In extended WT germband (C), *Tc-otd1* expression is also visible in the ventral midline (black arrowhead) in addition to the head lobes (aestricks), no obvious difference visible in *Tc-fgf8*^RNAi extended germband (D). (E-H) During successive stages of germband elongation in WT embryos (E, G), *Tc-wnt1* is expressed sequentially in each segment marking the gnathal and the trunk region. A posterior expression domain marks the early growth zone region. No deviation of *Tc-wnt1* expression perceived in corresponding staged *Tc-fgf8*^RNAi embryos (F, H). (I-L) During germband retraction and organogenesis in WT embryos (I, K), *Tc-wnt1* expression also detected in foregut and hindgut anlagen and in the developing legs. In corresponding staged *Tc-fgf8*^RNAi embryos (J, L), *Tc-wnt1* expression also detected in gut anlagen and legs but the shape of the malpighian tubules (MT) was abnormal. (M-P) Enlarged views of gut region in successively older WT embryos (M, N) show three pairs of MT surrounding the tube of the hindgut. In *Tc-fgf8*^RNAi embryos, MTs clearly looked abnormal and failed to surround the hindgut tube.

At the stage-matched extended germband stage, a stable *Tc-otd1* expression was detected in the head lobes and in the domain of ventral midline in both WT and *Tc-*

fgf8^{RNAi} embryos (Fig. 4.8C, D).During successive stages of germband extension in WT (Fig. 4.8E, G) and stage-matched *Tc-fgf8*^{RNAi} embryos (Fig. 4.8F, H), *Tc-wnt1* expression was detected in the head and in each emerging segment that marks the gnathal and the trunk region. A growth zone specific expression was also apparent in both WT and affected embryos (Fig. 4.8E-H).

Later during germband retraction and organ formation, *Tc-wnt1* expression was detected in each head segment (appendages), foregut and hindgut anlagen, in developing legs and in the abdominal segments in WT embryos (Fig. 4.8I, K). In stage-matched *Tc-fgf8*^{RNAi} embryos, *Tc-wnt1* expression was also detected at the identical site and with the same intensity (Fig. 4.8J, L). However, unlike in the WT, the Malpighian tubules (MT) around the hindgut tubes were found completely disorganised in affected embryos (Fig. 4.8M-P). Even a loss of 1 or 2 MT was also observed in some affected embryos.

In summary, no change in the expression pattern of *Tc-otd1* and *Tc-wnt1* during early and late staged *Tc-fgf8*^{RNAi} embryos clearly indicates normal segmental development within the head and the trunk occurred in embryos without *Tc-fgf8* function.

4.3.2.2 Mesoderm morphogenesis is strongly affected in *Tc-fgf8*^{RNAi} and *Tc-fgfr*^{RNAi} embryos

The role of FGF-signalling in mesoderm patterning and development has been described in *Drosophila* (Bae et al., 2012; Muha and Müller, 2013). Both the Fgf8-like ligands in *Drosophila*, Pyr and Ths, and the Fgf-receptor Heartless play an important role in the differentiation of a variety of mesodermal tissues in the gastrulating embryo (Gryzik and Müller, 2004; Stathopoulos et al., 2004). Therefore, I asked whether mesoderm development was also affected in the non-hatched larvae obtained in *Tc-fgf8*^{RNAi} as well as *Tc-fgfr*^{RNAi} experiments. In order to study mesoderm development, I analysed the expression pattern of the mesoderm marker *Tc-twist* (Handel et al., 2005) in both *Tc-fgf8*^{RNAi} and *Tc-fgfr*^{RNAi} embryos.

During blastoderm formation in wildtype embryos, *Tc-twist* is expressed as a mid-ventral stripe marking the prospective mesoderm (Fig. 4.9A). A similar pattern of *Tc-twist* expression domain in mid-ventral stripe was also seen in the blastoderm stage *Tc-fgf8*^{RNAi} (Fig. 4.9E) and *Tc-fgfr*^{RNAi} embryos (Fig. 4.9I). Later during germband extension in WT embryos, mesodermal cells marked by *Tc-twist* were spotted in each emerging segment within the gnathal and the trunk regions (Fig. 4.9B, C). A small patch of mesodermal cells between the head lobes (arrowheads) and a broad patch at the posterior end of growth zone was also visible in extended germbands (Fig. 4.9B, C).
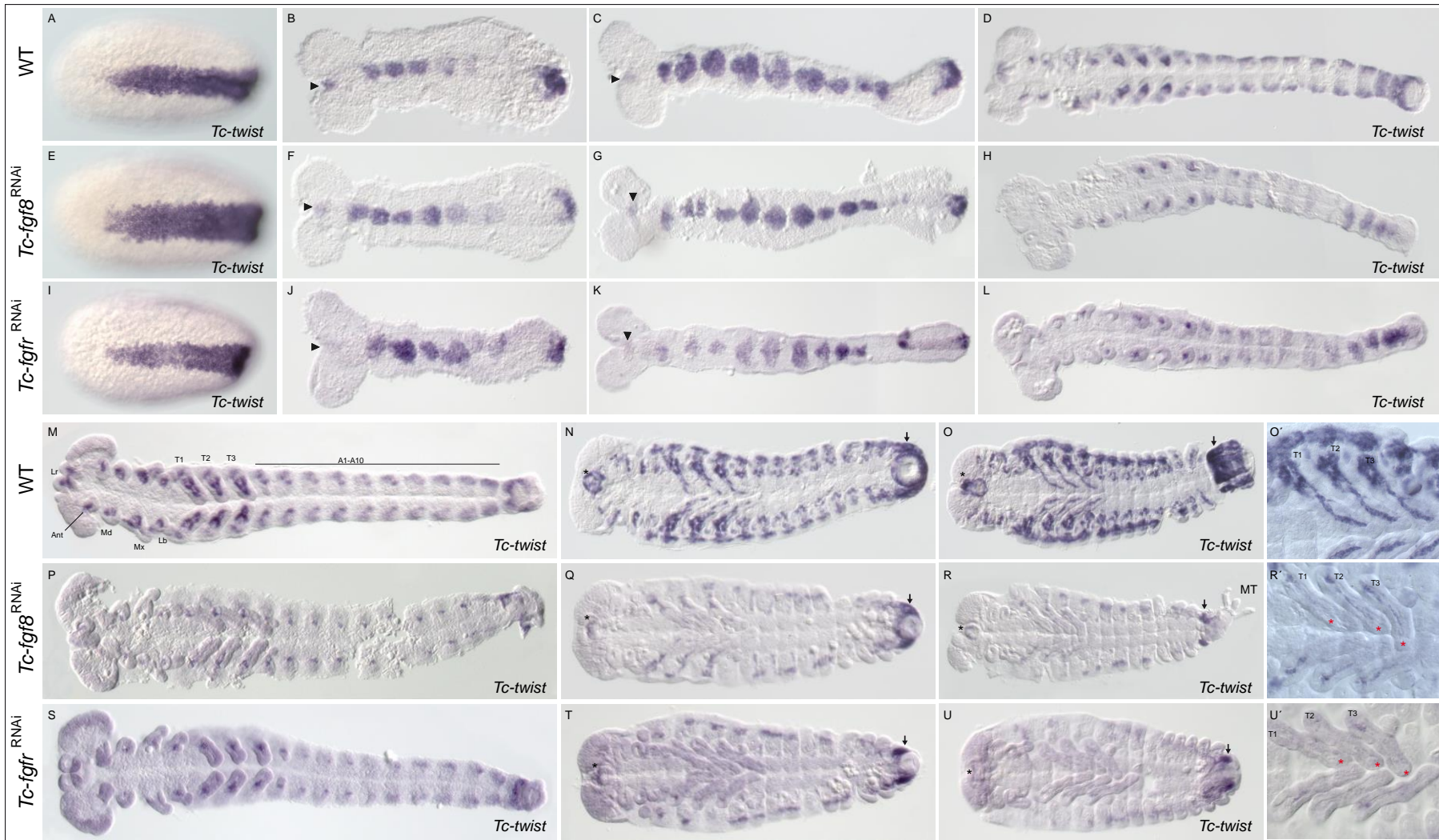
Figure 4.9: Mesoderm development in *Tc-fgf8*[RNAi] and *Tc-fgfr*[RNAi] embryos. (A-D; M-O) wildtype embryos; (E-H; P-R) *Tc-fgf8*[RNAi] embryos and (I-L; S-U) *Tc-fgfr*[RNAi] embryos analysed for *Tc-twist* expression. All embryos oriented ventral, anterior to the left. Images (O´, R´, U´) are the enlarged views of legs visible in O, R and U respectively. (A-C) At the blastoderm stage wildtype embryo, *Tc-twist* is expressed in a ventral stripe of future mesodermal cells (A) that in later stages of germband extension become apparent as a distinct mesodermal packet in each emerging segment and in a broad patch at the posterior end of the growth zone (B, C). A faint patch of mesodermal cells also spotted between the head lobes (arrowheads; B, C). In *Tc-fgf8*[RNAi] (E-G) and *Tc-fgfr*[RNAi] (I-K) embryos, *Tc-twist* expression at the blasoderm and the extended germband stages found identical to wildtype embryos except a slightly diminishing anterior expression in an older stage *Tc-fgfr*[RNAi] embryo (K). (D, M) In fully elongated WT embryos undergoing segmental identity, *Tc-twist* expression is detected in each head appendages, emerging limb buds and at the lateral edges of all the abdominal segments (A1-A10; bars). In stage-matched elongated *Tc-fgf8*[RNAi] (H, P) and *Tc-fgfr*[RNAi] (L, S) embryos, a strong reduction of *Tc-twist* expression in anterior head segments, in emerging legs and in abdominal segments is obvious. (N, O) In further old staged WT embryos, *Tc-twist* expression is detected in a variety of tissues: foregut (black aestricks) and hindgut anlage (arrows), gnathal segments, muscle fibers in legs, spotty domain around tracheal system and in lateral rows of muscle precursor cells. A severely reduced *Tc-twist* expression in all the marking tissues becomes apparent in both *Tc-fgf8*[RNAi] (Q, R) and *Tc-fgfr*[RNAi] (T, U) embryos. Though, few cells around the hindgut in affected embryos retained *Tc-twist* expression. An abnormal shape of malpighian tubules (MT) is also evident in *Tc-fgf8*[RNAi] embryo (R). (O´, R´, U´) Enlarged views of larval legs (red aestricks) showing loss of twist expression in muscle fibers of *Tc-fgf8*[RNAi] (R´) and *Tc-fgfr*[RNAi] (U´) embryos in comparison to WT (O´). (Lr, labrum; Ant, antenna; Md, Mandible; Mx, maxilla; Lb, labium; T1-T3: Thoracic segments; A1-A10, abdominal segments).

Interestingly, no obvious deviation of *Tc-twist* expression from the wildtype embryos was apparent in extended *Tc-fgf8*[RNAi] (Fig. 4.9F, G) and *Tc-fgfr*[RNAi] (Fig. 4.9J, K) germbands. However at the older stages where the germband is fully elongated, a drastic change of *Tc-twist* expression was observed between the WT (Fig. 4.9D, M) and the affected embryos (Fig. 4.9H, P and L, S).

While in WT embryos (Fig. 4.9 M), *Tc-twist* expression can be easily recognised in appendages of the gnathal segments, in the elongating legs and at the lateral edges of abdominal segments, highly reduced *Tc-twist* expression was observed in all these embryonic structures in *Tc-fgf8*[RNAi] (Fig. 4.9H, P) and *Tc-fgfr*[RNAi] (Fig. 4.9L, S) embryos. Especially in the gnathal appendages the expression was severely reduced. Nevertheless, the expression pattern around the hindgut anlage remained visible in affected embryos. In later stage, during retraction of the WT embryos, *Tc-twist* expression becomes more dynamic and clearly marks a variety of tissues including fore- and hindgut anlage, the gnathal appendages, growing muscle fibers in the legs, area surrounding tracheal system and in lateral rows of muscle precursor cells (Fig. 4.9N, O). A very significant loss of *Tc-twist* expression domains was apparent in stage-matched retracted *Tc-fgf8*[RNAi] (Fig. 4.9Q, R) and *Tc-fgfr*[RNAi] (Fig. 4.9T, U) embryos. The enlarged views of larval legs in WT (Fig. 4.9O´), *Tc-fgf8*[RNAi] (Fig. 4.9R´) and *Tc-fgfr*[RNAi] (Fig. 4.9U´) embryos clearly showed a diminishing distal *twist* expression in muscle fibers of affected embryos. However, the expression domain around the hindgut region was found less severely affected. In addition, an abnormal shape of Malpighian tubules was also observed in *Tc-fgf8*[RNAi] embryo (Fig. 4.9R). In summary, embryos without the function of the ligand *Tc-fgf8* and the

receptor *Tc-fgfr* developed with highly reduced mesodermal tissues in the beetle *Tribolium*.

4.3.2.3   Dorsal epidermis is not affected in *Tc-fgf8*[RNAi] and *Tc-fgfr*[RNAi] embryos
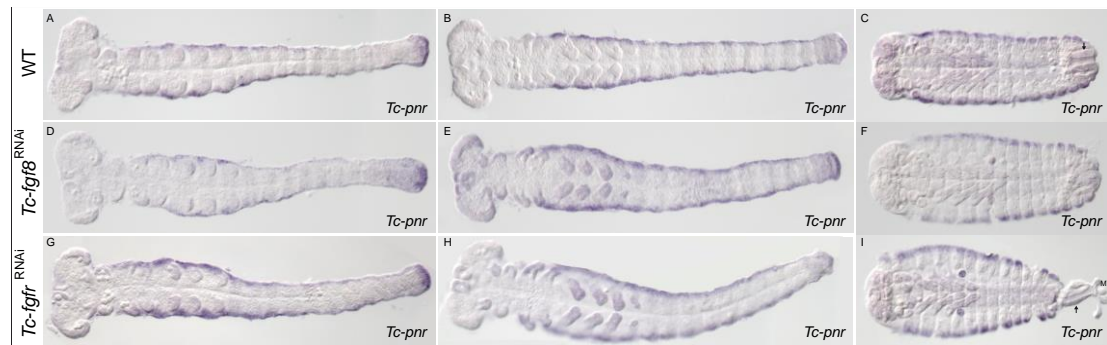
Figure 4.10: Analysis of *Tc-pannier* (*Tc-pnr*) expression in wildtype (A-C), *Tc-fgf8*[RNAi] (D-F) and *Tc-fgfr*[RNAi] (G-I) embryos. All embryos oriented ventral, anterior to the left. (A-C) During successive stages of development in WT embryos, *Tc-pnr* is continually expressed in the dorsolateral epidermal cells. In parallel staged *Tc-fgf8*[RNAi] (D-F) and *Tc-fgfr*[RNAi] (G-I) embryos, *Tc-pnr* also expressed in a similar domain of dorsal epidermis. An outward hindgut tube (marked by arrow) and abnormally shaped malpighian tubules (MT) also visible in *Tc-fgfr*[RNAi] embryo (I).

In *Drosophila*, a homeobox transcription factor *Tinman* (*Tin*) and a GATA transcription factor *Pannier* (*pnr*) have been described to be involved in the differentiation of the cardiac mesoderm (Klinedinst and Bodmer, 2003; Mandal et al., 2004). While *Dm-pnr* is expressed in the dorsal ectoderm and the dorsal mesoderm, *Tribolium pannier* (*Tc-pnr*) expression has only been reported in the dorsolateral epidermis (Nunes da Fonseca et al., 2010; Nunes da Fonseca et al., 2008). Nevertheless, I analysed the expression of *Tc-pnr* in *Tc-fgf8*[RNAi] and *Tc-fgfr*[RNAi] embryos to check whether FGF signalling, like in *Drosophila*, also affects *pnr* expression in *Tribolium* (Cripps and Olson, 2002; Gajewski et al., 1999).

During successive stages of germband elongation and retraction in WT embryos, *Tc-pnr* expression was detected in a progressively stronger dorso-lateral domain of the epidermis (Fig. 4.10A-C). A small *Tc-pnr* domain was also detected at the posterior end of the young extending germband (Fig. 4.10A). In similar staged affected embryos that lack the function of *Tc-fgf8* (Fig. 4.10D-F) or *Tc-fgfr* (Fig. 4.10G-I), a wildtype- like *Tc-pnr* expression profile was documented. However, unlike in WT, the hindgut tube in *Tc-fgf8*[RNAi] (not shown) and *Tc-fgfr*[RNAi] embryos was outwardly pointed (compare arrow in Fig. 4.10C and I) and the Malpighian tubules (MT) were distinctly dissociated from the hindgut tube structure in affected embryos (Fig. 4.10I). These results therefore clearly show that the dorsal epidermis is intact in *Tc-fgf8*[RNAi] and *Tc-fgfr*[RNAi] embryos.

4.4 Discussion

4.4.1 *Tc-fgf8* and *Tc-fgfr* in *Tribolium* are essential for mesoderm differentiation at late embryonic stages

Mesoderm formation and development is one of the key roles of FGF signalling that has been identified in a spectrum of species from both vertebrates and non-vertebrates (Dorey and Amaya, 2010; Muha and Müller, 2013). Especially, FGF8-dependent signalling was found instrumental for mesodermal morphogenesis in metazoans (Birnbaum et al., 2005; Dorey and Amaya, 2010; Fletcher et al., 2006; Fletcher and Harland, 2008; Gryzik and Müller, 2004; Imai et al., 2002; Kimelman and Kirschner, 1987; Röttinger et al., 2008; Slack et al., 1987; Stathopoulos et al., 2004; Wilson et al., 2005).

A previous study has shown the adjacently developing expression domains for the ligand *Tc-fgf8* and the receptor *Tc-fgfr* in *Tribolium*. While *Tc-fgf8* is expressed in the ectodermal domains that closely surround underlying mesoderm territory, *Tc-fgfr* expression was apparent within the mesodermal domain itself. On that basis a role for *Tc-fgf8* and *Tc-fgfr* in mesoderm development has been hypothesized in *Tribolium* (Beermann and Schröder, 2008).

This hypothesis can now be confirmed with the analysis of affected cuticles and the expression pattern of marker genes in embryos without *Tc-fgf8* or *Tc-fgfr* function. The expression analysis of mesoderm marker *Tc-twist* in *Tc-fgf8-* and *Tc-fgfr-* RNAi embryos clearly shows a significant loss of mesodermal cells from various tissues in affected embryos compared to WT (Fig. 4.9). Although this effect was visible only at the late embryonic stages where tissue specification was clearly apparent suggesting a more specific role of FGF signalling in mesoderm morphogenesis of gastrulating embryos (Fig. 4.9D, H, L and M-U´). The analysis of *Tc-twist* expression during early stages of development in WT as well as *Tc-fgf8*[RNAi] or *Tc-fgfr*[RNAi] embryos however revealed no expressional changes in these embroys.. Like WT (Fig. 4.10), a ventral stripe of *Tc-twist* expression marking the mesodermal primordium was also visible in the blastoderm staged *Tc-fgf8*[RNAi] (Fig. 4.9E) and *Tc-fgfr*[RNAi] embryos (Fig. 4.9I). Likewise during the stages of germband extension, the segmental packages of mesodermal cells marked by *Tc-twist* expression were indistinguishable in WT (Fig. 4.9B, C) and *Tc-fgf8*[RNAi] (Fig. 4.9F, G) or *Tc-fgfr*[RNAi] (Fig. 4.9J, K) embryos.

These results therefore clearly show that FGF signalling is not required for the initial specification of the mesoderm and rather plays a critical role in maintaining the mesodermal fate during the later stages of the beetle *Tribolium*. These findings

further corroborate the previous findings in major ecdysozoan model systems (*C. elegans*, *D. melanogaster*) where FGF signalling has no role in mesoderm induction, but is essential for mesoderm migration in gastrulating embryos (DeVore et al., 1995; Kadam et al., 2009; Lo et al., 2008; McMahon et al., 2010; Stathopoulos et al., 2004; Tulin and Stathopoulos, 2010). In contrast, FGF signalling in many vertebrates (*Xenopus*, zebrafish, mouse) and urochordates (ascidians, amphioxus) has been found crucial for mesoderm induction suggesting an ancestral role of FGFs in deuterostome mesoderm specification (Dorey and Amaya, 2010; Fletcher and Harland, 2008; Green et al., 2013). A recent study further supports that hypothesis, FGF signalling was found critically required for early mesoderm specification in the hemichordate *Saccoglossus kowalevskii* (Green et al., 2013). However, whether FGFs play an ancestral role in mesoderm specification of all bilaterians remains elusive, as the current results in the beetle *Tribolium* does not support that model. In future, it will be interesting to know whether the role of FGF signalling in mesoderm induction is confined to the deuterosome lineage or whether this trait is particularly lost during the evolution of ecdysozoans. Therefore, more functional studies on mesoderm specification from the other protostome lineage, the lophotrochozoans, will surely help to understand the evolutionary role of FGFs in mesoderm induction (Green et al., 2013).

4.4.2 FGF signalling in the caudal visceral mesoderm (CVM) and the Malpighian tubules development

A closer observation of *Tc-twist* expression in mesodermal territories of some of the well-specified tissues/organs in the WT as well as in the affected embryos allowed me to understand certain insights of the phenotype (Fig. 4.11). To begin with, a differential effect of FGF signalling on mesoderm patterning along the AP axis was observed in the *Tc-fgf8-* (not shown) or *Tc-fgfr*-knockdown embryos (Fig. 4.11A-B). While in more anteriorly positioned head appendages a complete loss of mesodermal cells was clearly apparent (Fig. 4.11B), a faint expression of *Tc-twist* was visible in a cluster of cells at the proximal bases of more posteriorly positioned gnathal and thoracic appendages in *Tc-fgf8*[RNAi] (not shown) or *Tc-fgfr*[RNAi] embryos (Fig. 4.11B). This finding can be explained in the following ways: (1) that FGF signalling in *Tribolium* indeed differentially regulates mesoderm patterning along the AP axis during gastrulation via some unknown mechanism(s). (2) Like *Drosophila*, FGF signalling also plays an important role in mesoderm cell differentiation and its maintenance in *Tribolium*. Since the head and the gnathal appendages are derived from ontogenetically older segments, a loss of mesodermal domain in these

appendages of affected embryos could be a combined result of impaired cell differentiation and the inability to maintain the differentiated mesodermal cells.
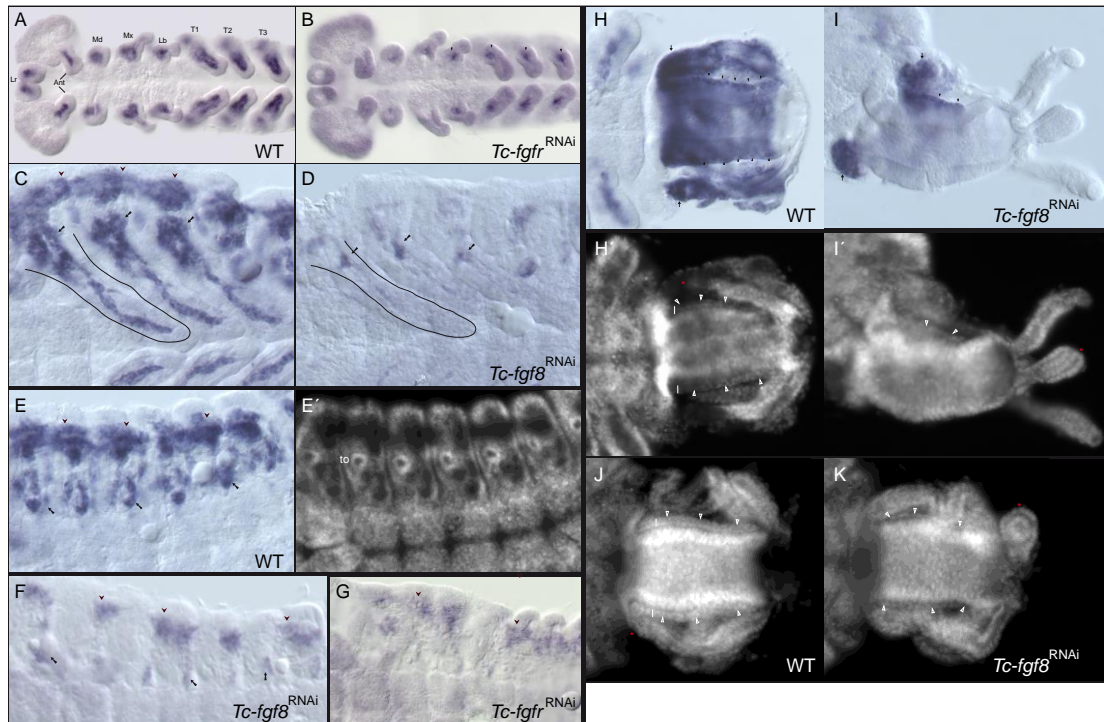
Figure 4.11: Analysis of mesoderm development in some specified tissues of affected embryos. (A, C, E, H, J), WT embryos; (D, F, I, K), *Tc-fgf8*RNAi embryos; (B, G), *Tc-fgfr*RNAi embryo analysed for *Tc-twist* expression. (A-E and F-I) are DIC images, (E´ and H-K) are fluorescent images with E´, I´ as Hoechst nuclear-counterstain of E and I respectively. All embryos oriented ventral with lateral upside. All images are 40X view except A, B and F of 20X view. (A) In young extending WT germband, *Tc-twist* expression lies at the bases of all the gnatham and thoracic appendages. (B) No expression in gnatham appendages except the labium and a highly reduced expression in developing legs apparent in *Tc-fgfr*RNAi embryos. (C-D) Musculature within matured legs (thick arrows) and laterally visible mesodermal tissue in thoracic segment (bifurcated arrowheads) of WT embryos (C) found highly reduced in *Tc-fgf8*RNAi embryos (D). (E-G) In WT embryos, *Tc-twist* expression in lateral mesoderm precursor (bifurcated arrowheads) and in the tissue underlying the tracheal openings (to; thick arrows) is very prominent (E, E´). A common strong reduction of lateral mesodermal tissue (bifurcated arrowheads) is apparent in both affected embryos (F, G). No expression of *Tc-twist* spotted in underlying tracheal tissues of *Tc-fgfr*RNAi (G) embryo, but faintly visible (thick arrows) in *Tc-fgf8*RNAi (F) embryo. (H-K) In mature WT hindgut, *Tc-twist* expression is evident at the tip of malpighian tubules (MT, arrows), in continuous ring around the anus and in caudal visceral mesoderm (arrowheads in H and open arrowheads, bars in H´, J) on either side of hindgut tube. Loss of visceral mesodermal tissue is clear in *Tc-fgf8*RNAi embryos (blackarrowheads and open arrowheads in I, I´, and K). A change in the shape of MT at the distal end is also obvious (compare red aestricks in H, I´ and J, K).

Later in fully retracted WT embryos, analysis of thoracic and abdominal regions distinctly showed a wealth of mesodermal cells (marked by *Tc-twist* expression) in the lateral domain that likely signifies the future heart precursor, at the proximal bases and in growing muscle fibers of the legs (Fig. 4.11C) and in patches underlying the abdominal tracheal openings (Fig. 4.11E, E´). In stage-matched *Tc-fg8*RNAi or *Tc-fgfr*RNAi embryos, a strong reduction of mesodermal cells from all these specific domains was clearly apparent (Fig. 4.11D, F and G). Although, some cells located at the proximal bases of growing legs appeared less severely affected (Fig. 4.11D). In addition, while the expression domain underlying tracheal openings was

completely abolished in *Tc-fgfr*[RNAi] embryos, a faint *twist* expression remained visible in *Tc-fgf8*[RNAi] embryos (curved arrows, Fig. 4.11F).

A possible justification could be that the faint expression domain in the tracheal region is maintained by the unaffected *Tc-bnl* mediated FGF signalling in *Tc-fgf8*[RNAi] embryos. The expression of *bnl* in mesodermal cells of the developing tracheal system of the stage 12 embryo in *Drosophila* has also been described (Sutherland et al., 1996). Besides, the complete loss of *twist* expression and severely damaged tracheal branching observed in *Tc-fgfr*[RNAi] cuticles provide first evidence for the proposed view (Beermann and Schröder, 2008) that *Tc-fgfr* is also likely involved in *Tc-bnl* mediated FGF signalling in *Tribolium*, a role that has been thoroughly studied for *breathless* in the fly *Drosophila* (Ghabrial and Krasnow, 2006; Kondo and Hayashi, 2013; Muha and Müller, 2013; Sutherland et al., 1996).

In broader sense, these results clearly show that in the absence of FGF signalling in *Tribolium*, mesoderm morphogenesis is severely affected during gastrulation. But to specifically point out whether the observed phenotype in affected embryos is due to a defect in basic fundamental processes of mesodermal cell proliferation and differentiation and/or it is specifically due to an aberrant spreading of mesodermal cell, is difficult to discriminate at this preliminary stage. In that context, some recent findings in *Drosophila* that clearly explain the roles of FGF signalling in mesoderm differentiation, migration and morphogenesis will certainly assist us to understand the phenotype in *Tribolium* in greater detail (Bae et al., 2012; Kadam et al., 2009; McMahon et al., 2010).

Another marked phenotype, observed in both *Tc-fg8*[RNAi] or *Tc-fgfr*[RNAi] embryos, was the abnormal shape of the hindgut and irregular organization of the Malpighian tubules (MT) around the hindgut tube (Figs. 4.8J, L, O, P; 4.9R and 4.10I). Instead of pointing towards the posterior opening of the hindgut, the orientation of the MT was upright. Since in *Tribolium* a prominent expression of *Tc-fgf8* and *Tc-dof* has already been described in the hindgut anlagen and in the MT of WT embryos (Beermann and Schröder, 2008), these observed RNAi-phenotypes were expected. In addition, these results also share some similarity and dissimilarity with *Drosophila* where, like in *Tribolium*, FGF signalling also plays a critical role in hindgut development but unlike in *Tribolium* has no impact on development of the Malpighian tubules (Kadam et al., 2012; Lengyel and Iwaki, 2002; Liu et al., 1999). More specifically, in *Drosophila*, it has been described that the musculature around the hindgut called the caudal visceral mesoderm (CVM) is required for proper gut formation and FGF signalling plays an important role in differentiation and migration of the CVM (Kadam et al., 2012; Reim et al., 2012). Indeed, an irregular and disrupted CVM was clearly

recognizable in *Tc-fgf8*^{RNAi} (black arrowheads, Fig. 4.11I) or *Tc-fgfr*^{RNAi} embryos (not shown). While in strongly affected embryos a complete loss of musculature except some residual cells at only one side of the posterior opening of the hindgut was apparent (Fig. 4.11I), in weakly affected embryos instead of a 2-3 cell wide layer only a 1-cell wide layer of the CVM was identifiable at either side of the hindgut tube (white arrowheads, Fig. 4.11K). Notably, these musculature phenotypes in *Tribolium* resembled to the CVM defects observed in *pyr/ths* or *htl* mutant embryos in *Drosophila* (Kadam et al., 2012; Reim et al., 2012). Especially, like *Drosophila*, a loss of CVM cells from the anterior hindgut but localized at the posterior hindgut support the observation that FGF signalling is required for migration of visceral mesoderm in one direction. However, more experimental data are required to support this claim, especially cell tracking experiments and live in-vivo imaging of affected embryos. In summary, these results indicate a conserved and specific role of FGF8-dependent signalling in gut development in insects.

In *Tribolium*, an abnormal shape of the MT at the distal end was often observed in *Tc-fg8*^{RNAi} or *Tc-fgfr*^{RNAi} embryos (red asterisks, Fig. 4.11I´, K), confirming that FGF signalling also has an important role in the development of the MT, the organ mainly responsible for tight regulation of fluid homeostasis in the beetle (Beermann and Schröder, 2008; Huang and Stern, 2005). This has some parallels with the findings in the nematode *C. elegans*, where FGF signalling is involved in the regulation of fluid homeostasis (Huang and Stern, 2005). On that note, one can speculate that fluid homeostasis is also disturbed in embryos with impaired FGF signalling in *Tribolium*. In the future, this statement has to be tested e. g. by activity analysis of ion channels in WT and affected embryos.

4.4.3 The role of the downstream effectors molecules *Tc-dof* and *Tc-csw* in FGF Signalling

In *Drosophila*, Dof is an essential component of FGFR-mediated signalling that acts specifically downstream of the receptors Btl and Htl and upstream of Ras (Petit et al., 2004; Vincent et al., 1998). Like *htl* or *btl* mutants in *Drosophila*, *dof* mutant embryos also showed defects associated with migration and specification of mesodermal and tracheal cells (Michelson et al., 1998; Stathopoulos et al., 2004; Sutherland et al., 1996; Vincent et al., 1998). In the beetle *Tribolium,* like in *Drosophila*, *Tc-dof* is also expressed at the sites of FGF signalling (Beermann and Schröder, 2008). However, primary data collected at the cuticle level through gene-knockdown experiments indicate that the phenotypes of *Tc-fgfr*^{RNAi} and *Tc-dof*^{RNAi} *Tribolium* embryos differ from each other. While the larval non-hatching phenotype was predominant in *Tc-*

fgfr[RNAi] embryos, 50% *Tc-dof*[RNAi] eggs failed to produce a cuticle and those developed a cuticle showed multiple defects in all the three basic tagma formation of the embryo. In addition, unlike *Tc-fgfr*[RNAi], the tracheal branching network was found unaffected in *Tc-Dof*[RNAi] cuticles. Only a small number of *Tc-dof*[RNAi] embryos also displayed a larval non-hatching phenotype and a subsection of cuticles in both *Tc-fgfr*[RNAi] and *Tc-dof*[RNAi] embryos also showed a similar posterior truncation phenotype. These results primarily suggest that, unlike *dof* in *Drosophila*, *Tc-dof* seems to play a much broader (significant) role in the development of the beetle embryo and might not necessarily be confined to FGF-induced responses alone. Clearly, more experimental data are required to draw some direct parallels between *Tribolium* and *Drosophila* with regards to the function of *dof* in these two species. Especially, the analysis of mesoderm marker *Tc-twist* in *Tc-dof*[RNAi] embryos would certainly help in understanding the specificity of Dof towards the FGF-cascade. Furthermore, *Tc-dof* involvement in properly organizing head, thorax and abdomen formation along the AP-axis also hints at a possible cross talk between the different signalling pathways that are required to pattern the embryo.

The functional knockdown of another signal transducer molecule *corkscrew* in *Tribolium* revealed some degree of similarity with the *Drosophila* counterpart. Like *csw* in *Drosophila*, *Tc-csw* has also been found involved in the process of oogenesis in *Tribolium* suggesting a conserved role of *csw* between the two lineages. The few obtained *Tc-csw*[RNAi] cuticle phenotypes however were completely different to the *Drosophila csw* mutant phenotype. Embryonic body formation was severely affected in these *Tc-csw*[RNAi] embryos. Since multiple RTK pathways target Corkscrew as downstream transducer (Perkins et al., 1996; Perkins et al., 1992) and a recent finding that Dof in *Drosophila* also can transduce the signal without recruiting Corkscrew (Csiszar et al., 2010), it is very difficult to draw concrete conclusions from these results.

In summary, the results described in this chapter clearly explain that FGF8/FGFR signalling in *Tribolium* is not required for the mesoderm induction at early developmental stages but plays an essential role in the morphogenesis of the mesoderm in late gastrulating embryos in different tissues and in that plays a similar role as shown for *Drosophila* (Gryzik and Müller, 2004; Kadam et al., 2009; Klingseisen et al., 2009; McMahon et al., 2010; Stathopoulos et al., 2004).

4.4.4 Outlook

In this chapter, I have discussed the role of different ligand (*Tc-fgf8*), receptor (*Tc-fgfr*), and adapter molecules (*Tc-dof* and *Tc-csw*) of FGF signalling in *Tribolium* development. Though some of the primary goals have been achieved with this study, further research is required to address some broader questions. For instance, is heart formation actually affected in *Tc-fgf8*[RNAi] and *Tc-fgfr*[RNAi] embryos? What is the role of other ligand *Tc-bnl* and how is the morphology of tracheal network looks like in *Tc-bnl* knockdown embryos? Is Dof a real FGF- specific signal transducer in *Tribolium*? Is mesoderm development also affected in *Tc-dof*[RNAi] embryos? These unanswered questions need to be addressed in the future by following some of these experiments: (1) the expression analysis of some of the heart specific marker genes (like *tinman*, *c15*, *Eve*) and gut-marker (*Tc-brachyenteron, Tc-byn*) in *Tc-fgf8*[RNAi] and *Tc-fgfr*[RNAi] embryos; (2) pRNAi assisted functional analysis of *Tc-bnl* at the cuticle and the embryonic level; (3) analysis of mesoderm development in *Tc-dof*[RNAi] embryos; (4) examination of the expression profile of *Tc-dof* in *Tc-fgf8*[RNAi] and *Tc-fgfr*[RNAi] embryos.

5 Chapter 5

The dynamic expression of extraembryonic marker genes in the beetle *Tribolium castaneum* reveals the complexity of serosa and amnion formation in a short germ insect

Text of this chapter is taken from *Sharma et al; Gene Expression Patterns (2013) 362–371* with few modifications

5.1 Introduction

Embryonic development in insects has been studied for a long time and by now is best understood at the genetic and at the cellular level in the model organism *Drosophila melanogaster*. In contrast, the analysis of tissues that do not contribute to the embryo proper, the extraembryonic membranes, has long been neglected. Still, these membranes fulfil important functions like assisting the morphogenetic movements, protecting the embryo against physical or mechanical stress and acting as immunological barriers (Jacobs et al., 2013; Jacobs and van der Zee, 2013; Panfilio, 2008). One main reason for the negligence could be the presence of only a single and highly reduced extraembryonic tissue, the amnioserosa in *Drosophila.* However, the presence of two distinct extraembryonic tissues, the serosa and the amnion is a key feature for most insects like *Anopheles*, *Tribolium*, *Nasonia* and *Oncopeltus* (Buchta et al., 2013; Goltsev et al., 2007; Panfilio, 2008; van der Zee et al., 2005). Recently, there has been an increased interest in understanding the processes and mechanisms involved in the formation of extraembryonic membranes (Dearden et al., 2000; Garcia-Solache et al., 2010; Panfilio, 2008; Panfilio et al., 2006; Panfilio and Roth, 2010; Rafiqi et al., 2008; Rafiqi et al., 2012; Schmidt-Ott, 2000; van der Zee et al., 2005).

Whereas the amnioserosa in *Drosophila* derives from the dorsal-most region of the cellular blastoderm under the control of dorsal-ventral patterning system (Moussian and Roth, 2005; Reeves and Stathopoulos, 2009), the extraembryonic tissue serosa in *Tribolium* originates from an anterior region under the control of the anterior-posterior and the terminal patterning systems (Kotkamp et al., 2010; Lynch and Roth, 2011; Schoppmeier and Schröder, 2005). However, the developmental origin of the other extraembryonic tissue - the amnion - remains obscure. Currently it is discussed that the amnion is mainly of embryonic origin and forms undistinguishable from the embryonic anlage late in development (Anderson, 1972; Handel et al., 2000; Panfilio, 2008).In the beetle *Tribolium castaneum*, a detailed microscopic study of embryogenesis has revealed a tight interplay between the extraembryonic tissues, the serosa and the amnion, and the embryonic tissue during the morphogenetic movements of early embryogenesis (Handel et al., 2000).

The formation of the tissues (serosa, amnion and the embryo proper) and their morphogenetic movements in relation to each other is highly dynamic and therefore difficult to visualize in static pictures. However, the morphological dynamics can be followed by systematically analysing the expression pattern of genes expressed in the extraembryonic membranes and their precursor cells (marker genes). Primarily,

zen1 expression in *Tribolium* marks serosal tissue (Falciani et al., 1996; Sanches-Salazar, 1996; van der Zee et al., 2005; van der Zee et al., 2006). The second *zen* gene in *Tribolium Tc-zen2* shows the same expression profile as *Tc-zen1* except for a late amniotic expression domain (van der Zee et al., 2005). For the amnion analysis in *Tribolium*, so far, two marker genes *Tc-pannier* (*Tc-pnr*) and *Tc-iroquois* (*Tc-iro*) have been established (Nunes da Fonseca et al., 2010; Nunes da Fonseca et al., 2008; van der Zee et al., 2005; van der Zee et al., 2006). While *Tc-pnr* is expressed in only a subset of the amnion- the dorsal amnion (van der Zee et al., 2005; van der Zee et al., 2006), *Tc-iro* expression has been described in both the anterior and the dorsal primordium of the amnion (Nunes da Fonseca et al., 2010; Nunes da Fonseca et al., 2008).

The expression pattern of another marker gene *hindsight* in the extraembryonic tissues appears to be evolutionary conserved among the dipterans. In *Drosophila* the *hindsight* (*hnt*) / *pebbled* gene is expressed in the amnioserosa and is required for germband retraction (Frank and Rushlow, 1996; Yip et al., 1997). In other flies that develop with two distinct extraembryonic membranes like *Anopheles* (Goltsev et al., 2007) and *Megaselia* (Rafiqi et al., 2008), *hnt* is expressed early in the blastoderm in a broad domain that includes the tissues, the prospective serosa and the prospective amnion (Goltsev et al., 2007; Rafiqi et al., 2010; Rafiqi et al., 2012). The beetle *Tribolium* also has two distinct extraembryonic membranes but whether its *hindsight* ortholog (*Tc-hnt*) also marks the extraembryonic tissues is yet to be elucidated.

In *Drosophila* and *Tribolium*, the proper formation of extraembryonic membranes requires an input of the dorsal-ventral patterning system and Decapentaplegic (Dpp) is one crucial molecule that regulates the expression and activity of genes in these tissues (Ferguson and Anderson, 1992; Lynch and Roth, 2011; van der Zee et al., 2006). The active sites of Dpp-signalling within the embryo can be visualized by monitoring the expression of the downstream transducer of this pathway, phosphorylated MAD (Mothers against Dpp) / pMAD. In *Drosophila*, *dpp* mRNA expression and Dpp-activity coincide at the dorsal side of the early embryo and later at the dorsal epidermis and the amnioserosa (Dorfman and Shilo, 2001). In contrast, in *Tribolium*, the site of Dpp-activity (marked by the pMAD antibody) has been reported exclusively on the dorsal surface contrasting to the ventral expression of *Tc-dpp* mRNA (Chen et al., 2000; Nunes da Fonseca et al., 2008; Van der Zee et al., 2008; van der Zee et al., 2006). While the early *Tc-dpp* expression in a symmetric anterior polar cap has been described as serosa-specific, the Dpp-activity was found restricted to the dorsal serosal and embryonic tissue at late blastoderm stages (Chen et al., 2000; Sanches-Salazar, 1996; van der Zee et al., 2006).

5.2 Aim

To date, our current knowledge about the well-established extraembryonic-marker genes *Tc-zen1* and *Tc-iro* and their regulators Dpp and pMAD is based on the description of only few embryological stages from mostly lateral views, and is therefore need to be study in more detail. . This is especially obvious for the expression of the amnion marker *Tc-iro* and the Dpp-activity marker pMAD that have been described only at the late differentiated blastoderm stage and during germband extension (Nunes da Fonseca et al., 2010; Nunes da Fonseca et al., 2008). Therefore, in this study I aimed:

1. To provide a comprehensive overview on the tissue-specific gene expression patterns of different marker genes during early wildtype embryogenesis, which will help to understand the dynamics and the topology of the extraembryonic membranes in relation to the embryo in a more complete fashion in *Tribolium*.

2. To elucidate whether *hindsight* in *Tribolium* (*Tc-hnt*) also marks the extraembryonic tissues by analysing its expression pattern during early embryogenesis.

5.3   Results

5.3.1 Expression dynamics of the amnion marker *iroquois* (*Tc-iro*) during blastoderm development

In *Tribolium*, the expression pattern of *iroquois* (*Tc-iro*) has been used as a molecular marker to describe the anterior and the dorsal amnion at late developmental embryonic stages (Kotkamp et al., 2010; Nunes da Fonseca et al., 2010; Nunes da Fonseca et al., 2008). Whether *Tc-iro* expressing amnion precursor cells can be found earlier during embryogenesis is still unknown. I therefore describe the spatio-temporal expression profile of *Tc-iro* during blastoderm maturation.

No maternal contribution of *Tc-iro* mRNA was seen in freshly laid eggs (Fig. 5.1A, A′). The first very weak, ubiquitous *Tc-iro* expression was detected at the start of the early embryonic nuclear divisions (Fig. 5.1B, B′) and became confined to a crescent shape domain at the anterior pole in older stage embryos (Fig. 5.1C, C′). At the uniform blastoderm stage, the *Tc-iro* expression domain broadened and developed into a rotationally symmetric cap (bars, Fig. 5.1D, 1-3′). Later, this *Tc-iro* domain receded (asterisks in Fig. 5.1E) from the anterior pole to transform into a ring-like domain (Fig. 5.1E, 1-3′). When viewed laterally this domain was slightly oblique (Fig. 5.1E, 2-2′), while the ventral and the dorsal domain of that ring remained perpendicular to the anterior-posterior axis of the embryo (Fig. 5.1E, 1-1′ and 3-3′). Quickly thereafter, no *Tc-iro* expression was found at the anterior pole except in a ring domain (Fig. 5.1F, 1-3′). The ring domain persisted only for a short time and a loss of *Tc-ir*o expression at the dorsal surface was observed at an older stage (Fig. 5.1G, 3-3′) that resulted in a horseshoe-shape domain (Fig. 5.1G, 1-2′).

After the differentiation of the blastoderm, a weak expression of *Tc-iro* mRNA was detected in a new domain of dorsal-posterior cells (black arrowheads; Fig. 5.1H, 3-3′). This new *Tc-iro* domain became more profound later in development (black arrowheads; Fig. 5.1I, 3-3′). At the same time, the lateral *Tc-iro* domain receded, leaving a gap between the anterior-lateral and the dorsal domain (black arrow; Fig. 5.1I, 2-2′). During posterior invagination of the blastoderm, *Tc-iro* expression was appeared as a thin stripe at the anterior-lateral border between the serosa and the germ rudiment (Fig. 5.1J, 1-2′). At this stage, the broad dorsal domain of *Tc-iro* expression followed the posterior invagination (Fig. 5.1J, 3-3′).Later at the beginning of germband extension, *Tc-iro* transcripts were visible in extraembryonic cells at the edges around the serosal window that are morphologically indistinguishable from embryonic cells (Handel et al., 2000) (black arrowheads; Fig. 5.5, A-A′).
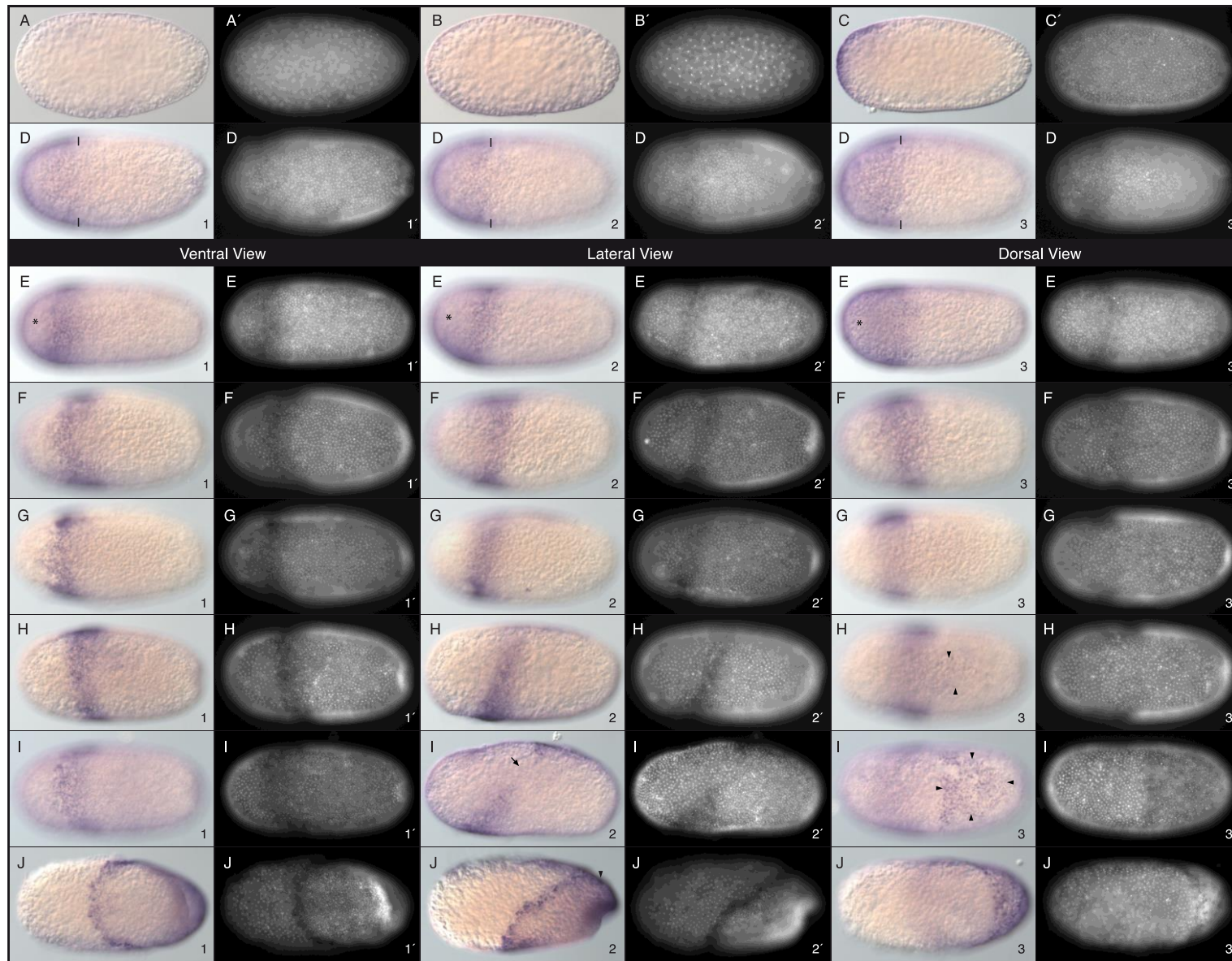
Figure 5.1: The dynamics of *Tc-iro* expression during early embryogenesis. (A, A') No maternal expression of *Tc-iro* mRNA in the young egg. (B-C') During early nuclear divisions, initially a faint ubiquitous expression detected (B, B') that later became confined to the anterior pole in a small crescent shape domain (C, C'). (D1-F3') During blastoderm maturation, *Tc-iro* expression first broadened into a rotationally symmetric cap (bars in D1-D3') and later receded from the anterior pole (asterisks in E1-E3') to result in a slightly tilted ring like domain (E1-E3', F1-F3'). The obliqueness of the ring was only visible in lateral views (E2, F2) but it appeared symmetric along the AP axis in the ventral or the dorsal view (E1, 1', E3, 3'; F1, 1', F3, 3'). (G1-G3') At the late blastoderm stage, *Tc-iro* expression faded dorsally (G3, G3') and resolved into a horseshoe shape domain (G1-G2'). (H1–I3') At differentiated blastoderm stages, *Tc-iro* expression emerged in a group of dorsal-posterior cells (black arrowheads; H3, I3) that shows no connection to the anterior-lateral *Tc-iro* domain (H2; black arrow in I2). (J1-J3') During posterior invagination, the anterior-lateral domain of *Tc-iro* combined with the dorsal *Tc-iro* domain (black arrowhead). All embryos are shown in surface views. Only embryos shown in A-C' represent optical sections.

In addition, *Tc-iro* transcripts were also detected in the emerging segmental stripes in an older extending germband (arrows, Fig. 5.5, D-D´) (Nunes da Fonseca et al., 2010). In summary, I have shown the expression of *Tc-iro* in the blastodermal domain and also this study revealed that how the early anterior cap domain of *Tc-iro* expression progressively resolved into a stripy domain present at the border between the serosa and the germ anlage that likely represents the precursor of the anterior-lateral amnion.

5.3.2 Expression dynamics of the serosa marker *zerknüllt-1* (*Tc-zen1*) during blastoderm development

The *zerknüllt-1* gene in *Tribolium* (*Tc-zen1*) is an exclusive serosa marker (Falciani et al., 1996) and has been used in various functional studies to judge the fate of the serosa (Fu et al., 2012; Kotkamp et al., 2010; Nunes da Fonseca et al., 2008; van der Zee et al., 2005). Here the aim of the study is to provide a complete understanding of *Tc-zen1* expression during early blastoderm formation in wildtype embryos.

In freshly laid eggs, no maternal contribution of *Tc-zen1* transcripts was detected (Fig. 5.2A, A´) as reported previously (Dearden et al., 2000). Only after few nuclear divisions, a weak ubiquitous expression became evident (Fig. 5.2B, B´). At a slightly older stage, the ubiquitous expression receded from the posterior end and developed into a faint, rotationally symmetric cap like domain at the anterior pole (Fig. 5.2C, C´) (Falciani et al., 1996). At the uniform blastoderm stage, the rotationally symmetric cap like domain became much stronger and expanded posteriorly covering the anterior 30% of the egg (Fig. 5.2D, D´). Soon thereafter, symmetry breaking of *Tc-zen1* expression became obvious by a slight tilt of the expression domain visible only in the lateral view (bars; Fig. 5.2E, 2-2´). Before the condensation of the embryonic nuclei starts, the asymmetry of *Tc-zen1* expression in the presumptive serosa became more pronounced (Fig. 5.2F, 1-3´). At this stage the boundary between *Tc-zen1*-positive and *Tc-zen1*-negative cells was still fuzzy (Fig. 5.2F, 1-1´and 3-3´).
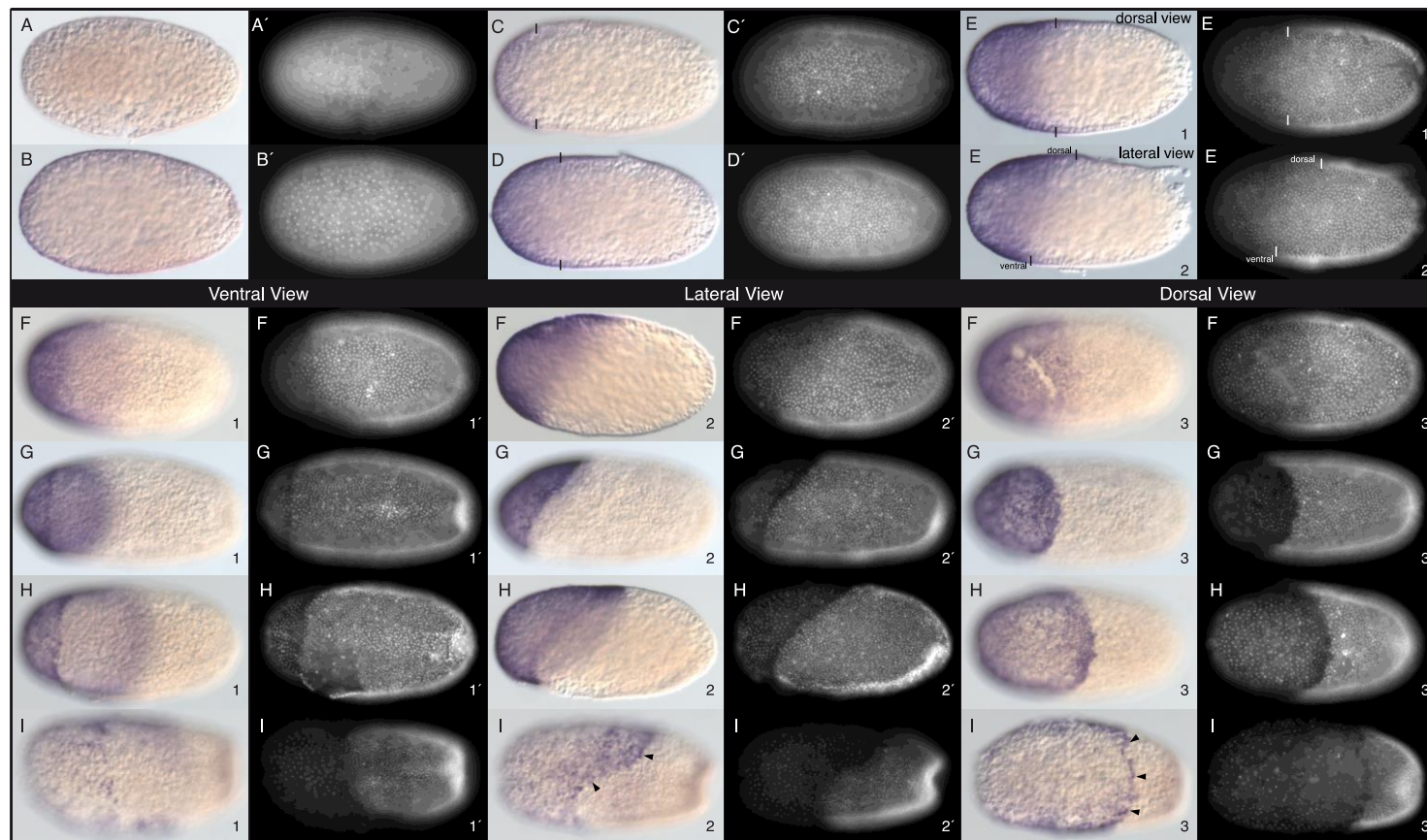
Figure 5.2: *Tc-zen1* expression profile during early embryogenesis. (A, A') No maternal contribution of *Tc-zen1* mRNA in freshly laid eggs. (B-D') During blastoderm maturation, a weak ubiquitous expression of *Tc-zen1* detected at an early stage (B, B') later receded from the posterior pole and resulted in a rotationally symmetric cap at the anterior pole that further extends posteriorly (bars in C, D). (E1-E2') At a slightly older stage, first sign of rotational asymmetry obvious (compare dorsal (1, 1') and lateral views (2, 2') of the same embryo E (bars)). (F1-F3') Asymmetry of *Tc-zen1* expression became more distinct (2, 2'). No sharp border between the serosa and the germ anlage (1-3'). (G1-G3') When the serosa became morphologically distinct, *Tc-zen1* expression intensified in this tissue with a clear border to the germ anlage. (H1-I3') *Tc-zen1* was expressed in the serosa that follows the morphogenetic movements. A clear boundary between the serosa and the germ rudiment was maintained (black arrowheads in I2 and I3). All embryos are shown in surface views. Only embryos shown in A-E2', F2, H2 represent optical sections.

106

After differentiation of the blastoderm, the expression strength of *Tc-zen1* in the morphologically distinct serosa appeared at its maximum with a defined boundary between the serosa and the germ rudiment (Fig. 5.2G, 1-3´). From this stage onwards, the *Tc-zen1* domain appeared symmetric in both the ventral (1, 1') and the dorsal (3, 3') views (Fig. 5.2G-I).

No *Tc-zen1* expression was observed in the germ anlage. Later during successive stages of blastoderm differentiation, *Tc-zen1* expression followed the morphogenetic movements of the *Tribolium* embryo (Fig. 5.2H-2I; 1-3´). A dorsal-posterior shift of the *Tc-zen1* expressing serosal tissue was clearly visible due to the posterior invagination of the germ anlage (black arrowheads; Fig. 5.2I, 2 and 3). The ventral part of the serosa remained in the anterior half at the mid-ventral position (Fig. 5.2I, 2 and 2´). As the serosal cells became polyploid and flattened, *Tc-zen1* expression pattern diminished, confirming previous descriptions (Falciani et al., 1996). As soon as the extraembryonic membranes close over the embryo, *Tc-zen1* transcripts are mainly detected at the outer edges of the serosal window in extending germbands (Fig. S1, B-B´ and E-E´; dotted line marks the inner edges of the serosal window).

This study allowed us to monitor the exact staging of the symmetry-breaking event of *Tc-zen1* expression and therefore to visualize the first influence of the DV-system on serosa morphology.

5.3.3 Co-expression of *Tc-zen1* and *Tc-iro* during blastoderm formation

As shown above in separate expression studies, both the extraembryonic membrane markers, *Tc-iro* (Fig. 5.1) and *Tc-zen1* (Fig. 5.2) revealed early anterior expression domains. To clarify whether these markers are co-expressing in the same set of anterior cells or whether they are expressing in non-overlapping domains, I performed double *in situ* hybridization analysis.

At the early blastoderm stage, an overlapping domain of *Tc-zen1* and *Tc-iro* expression was evident in a small domain at the anterior-most pole of the embryo (Fig. 5.3A, 1-1´, 2). At a slightly older stage, the anterior small domain of both transcripts enlarged into a broad and rotationally symmetric cap domain (Fig. 5.3B, 1-2´) where co-expression of *Tc-zen1* and *Tc-iro* was still observed (Fig. 5.3B, 3). During blastoderm maturation, *Tc-zen1* transcripts stayed in a cap-like domain while *Tc-iro* expression resolved into a posteriorly adjacent, rotational symmetric ring-domain (Fig. 5.3C, 1-2). A gradual border between the anterior *Tc-zen1*- and the posterior *Tc-iro* domain became visible (Fig. 5.3C, 3).
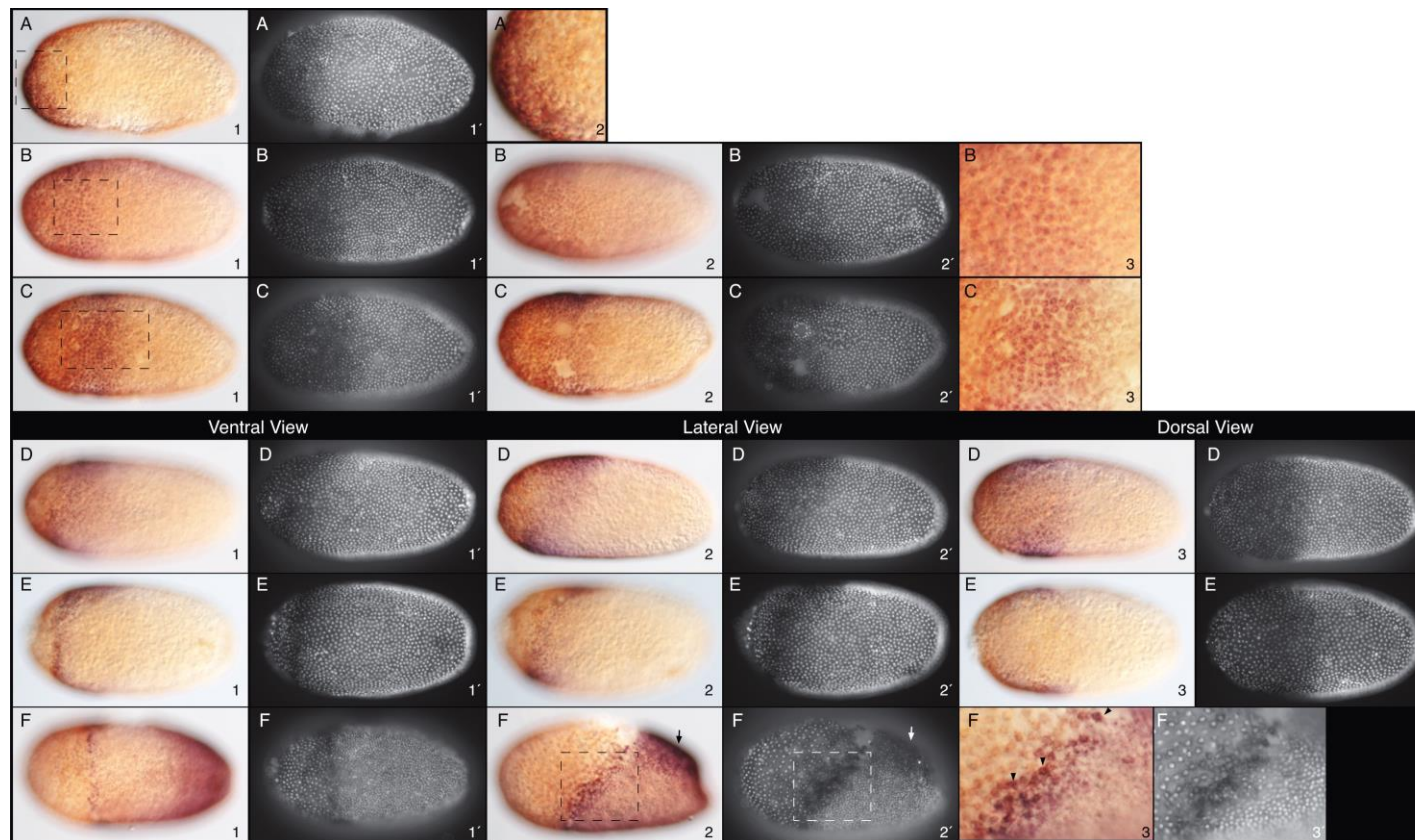
Figure 5.3: Double *in situ* hybridization analysis of *Tc-zen1* and *Tc-iro* during *Tribolium* development. (A1-B3) During early blastoderm formation, *Tc-zen1* (blue) and *Tc-iro* (red) were co-expressed at the anterior pole initially in a small domain (A1-2) and later in a broad rotationally symmetric cap (B1-3). (C1-C3) The symmetric cap domain extended and partitioned into an anterior *Tc-zen1* (red) and a more posterior *Tc-iro* (blue) expression domain (C3) that both retained rotational symmetry (compare C1 and C2). (D1-E3') During late blastoderm formation, the symmetric domains of *Tc-zen1* and *Tc-iro* expression became asymmetric (D2, 2'; E2, 2'); the border between these two domains was much more pronounced (compare D1 and E1). No *Tc-iro* transcripts were detected at the dorsal surface (E3, 3'). (F1-F3') At differentiated blastoderm stage, the ventral border between serosa and germ rudiment was marked by a 2-3 cell-wide *Tc-iro* domain (F1, 1'). The lateral border was slightly thicker (F2, 2') and there some cells still co-expressed *Tc-zen1* and *Tc-iro* (black arrowheads, F3, 3'). All embryos are shown in surface views. *Tc-zen1* is shown in red, *Tc-iro* in blue. A2, B3, C3, F3 and F3' are the enlarged views of boxes in A1, B1, C2, F2 and F2', respectively.

At the late blastoderm stage, *Tc-iro* expression was intensified and two distinct expression domains of *Tc-zen1* and *Tc-iro* with limited overlap became apparent while both domains underwent a transition from symmetric to an asymmetric domain (lateral views; Fig. 5.3D, 1-3´).

Before the condensation of nuclei has begun at the uniform blastoderm, the boundary between *Tc-zen1* and *Tc-iro* expressing cells became more pronounced at the ventral surface (Fig. 5.3E, 1-1´) but stays fuzzy at the lateral side (Fig. 5.3E, 2-2´). The *Tc-iro* domain was lost dorsally at this stage (Fig. 5.3E, 3-3´).

At the differentiated blastoderm stage, clearly distinct domains for both the markers were observed. While *Tc-zen1* expressed only in morphologically distinct nuclei of serosa (red; Fig. 5.3F, 1-2´), *Tc-iro* transcripts were detected differentially at the ventral and the lateral border between serosa and the germ rudiment (blue; Fig. 5.3F, 1-2´). The newly formed posterior-dorsal *Tc-iro* domain was also obvious at this stage (arrow in Fig. 5.3F, 2 and 2´). Few cells at the lateral border were found still unresolved into the *Tc-zen1* or *Tc-iro* specific domains (black arrowheads; Fig. 5.3F, 3-3´).

In summary, during early stages of blastoderm formation the expression pattern of both the marker genes *Tc-zen1* (serosa marker) and *Tc-iro* (amnion marker) share a common anterior territory, which at later stages resolved into two separate domains representing the precursors of the respective extraembryonic tissues.

5.3.4 Expression pattern of *Tribolium-hindsight* (*Tc-hnt*) during early development

To get a broader understanding of the molecular basis for the formation of extraembryonic membranes, I analysed here the expression pattern profile of *hindsight* during early embryogenesis of the beetle *Tribolium*.

From early blastoderm formation to late gastrulation, the dynamics of the *Tc-hnt* expression pattern was found very similar to the expression profile of the serosa marker *Tc-zen1*. Like *Tc-zen1*, *Tc-hnt* transcripts were not maternally supplied (Fig. 5.4A, A´), ubiquitously distributed from the syncytial (Fig. 5.4B, B´) to the cellular blastoderm stage (Fig. 5.4C, C´) and at later stages receded from the posterior pole (Fig. 5.4D, D´) to develop into an anterior rotational symmetric cap (Fig. 5.4E, E´) that enlarged symmetrically towards the posterior (bars; Fig. 5.4F, F´).

At the undifferentiated blastoderm stage, when nuclei are still indistinguishable from each other, an asymmetry of *Tc-hnt* expression was observed in a lateral view (bars; Fig. 5.4G, 2-2´). Ventral and dorsal expression of *Tc-hnt* transcripts in the same embryo remained symmetric (Fig. 5.4G, 1-1´ and 3-3´). At this stage, the boundary of
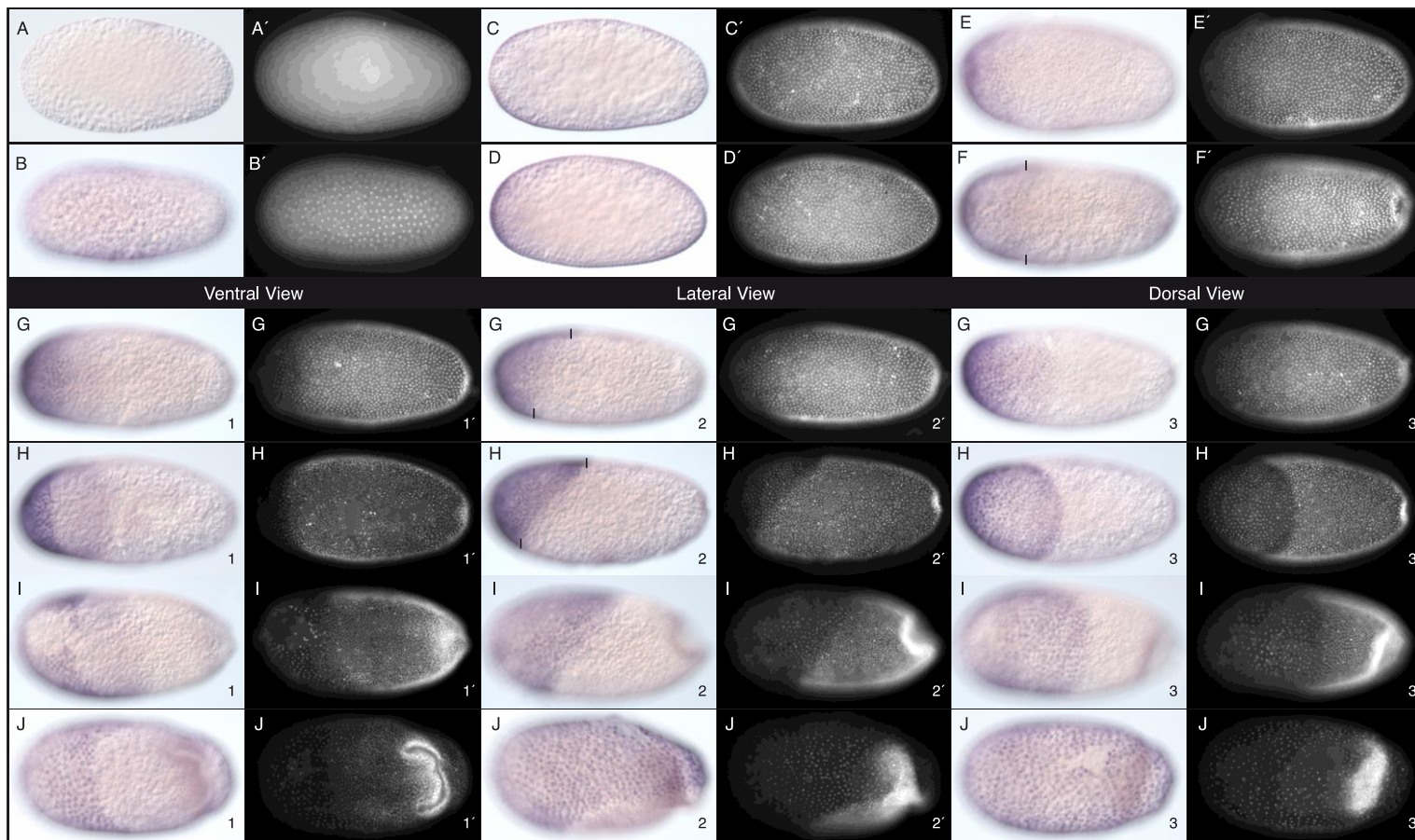
Figure 5.4: The early expression pattern profile of *Tribolium hindsight* during embryogenesis. (A-A') Like *Tc-zen1*, no maternal contribution of *Tc-hnt* mRNA was detected in early embryos. (B-F') During successive stages of blastoderm formation, a weak ubiquitous expression of *Tc-hnt* (B-C') receded from the posterior pole (D, D') and confined to an anterior rotational symmetric cap-like domain (E-F'). (G1-J3') *Tc-hnt* expression followed the dynamics of the developing presumptive serosa like *Tc-zen1* expression (see all ventral, lateral and dorsal views). All embryos are shown in surface views except D, which represents an optical section.
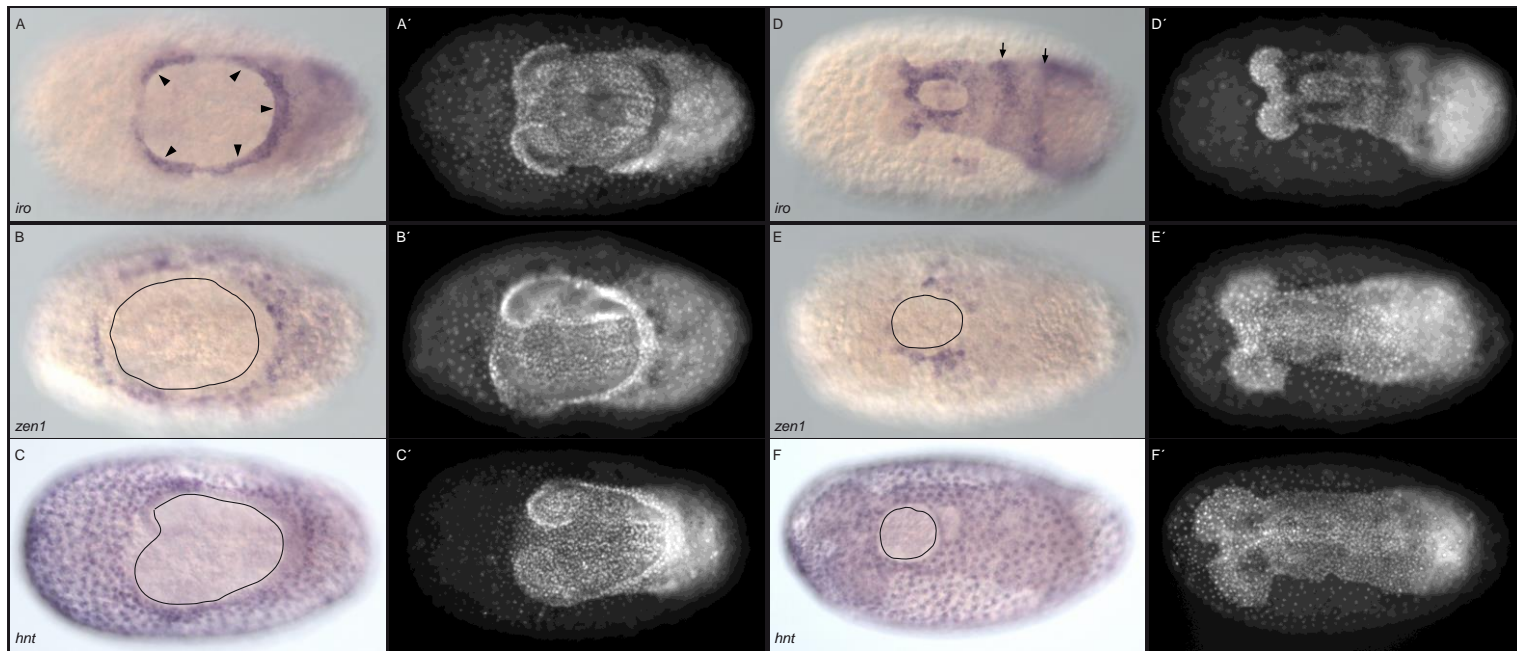
Figure 5.5: *Tc-iro*, *Tc-zen1* and *Tc-hnt* expression in the extending germbands. (A-A´) *Tc-iro* expression was refined to the edges of the serosal window in a young extending germband (arrowheads). (B-C´) At a similar stage, *Tc-zen1* and *Tc-hnt* transcripts were detected at the outer edges of the serosal window but in a non-overlapping domain with *Tc-iro* (dotted circle marks inner edge of the serosal window). (D-D´) In older extending germband embryos, *Tc-iro* was expressed at inner edges of the serosal window and also in stripes (black arrows) in the emerging segments. (E-E´) At a similar age, *Tc-zen1* is only expressed at outer edges of the serosal window. (F-F´) A relatively high expression of *Tc-hnt* in the serosal cell was also detected at this stage. All embryos are shown in surface views.

the *Tc-hnt* expression domain appeared fuzzy (Fig. 5.4G, 1-3´) but became much more defined (Fig. 5.4H, 1-3´) with increased steepness at the lateral surface (bars; Fig. 5.4H, 2-2´) in a slightly older stage embryo.

After differentiation of the blastoderm, *Tc-hnt* transcripts were detected in more distinctly visible and widely spaced serosal nuclei (Fig. 5.4I, 1-3´). During further successive stages of development, *Tc-hnt* transcripts were exclusively detected in the serosa undergoing morphogenetic movements (Fig. 5.4J, 1-3´). No expression of *hnt* mRNA was detected in the germ anlage. In the extending germbands, *Tc-hnt* - like *Tc-zen1* - transcripts were detected only in the covering serosal layer but at a higher level than *Tc-zen1* (Fig. 5.6C-C´ and F-F´).

5.3.5 Early asymmetry of *Tc-dpp* expression during development

Tc-dpp expression has been described at early uniform blastoderm stages as an "anterior cap domain that lacks dorso-ventral asymmetry" (Chen et al., 2000; Sanches-Salazar, 1996; van der Zee et al., 2006) and at late blastoderm stages as an oblique stripe at the border between serosa and the germ rudiment (Chen et al., 2000; van der Zee et al., 2006). Because *Tc*-Dpp is an important regulator for the development of extraembryonic membranes, I carefully analysed its expression dynamics from early blastoderm formation to late differentiation of the blastoderm.

During early blastoderm formation, a weak ubiquitous expression of *Tc-dpp* mRNA was detected (Fig. 5.6A, A´) and after few nuclear divisions that became asymmetric with higher level of expression on one side (Fig. 5.6B, 1-2´). Asymmetry was seen first along the DV-axis (Fig. 5.6B, 1-2´) and further, after receding from the posterior pole, it was also detectable along the AP-axis (Fig. 5.6C, 1-3´). At a later stage, an elevated expression of *Tc-dpp* mRNA was detected in the anterior-ventral 95%-60% of the egg (Fig. 5.6D, 1-1´). Intriguingly, both the poles of the embryo appeared free of *Tc-dpp* transcripts (Fig. 5.6D, 2). During further blastoderm maturation, the broad anterior-ventral *Tc-dpp* domain condensed to a broad stripe covering anterior 82%-60% of the egg length (Fig. 5.6E-5.6F; 1-1´), showing a retraction of *Tc-dpp* expression from the anterior (compare E2, F2 with D2 in Fig. 5.6). A wedge-shape domain of *Tc-dpp* expression narrowing from ventral to dorsal surface became apparent in the lateral views (Fig. 5.6E-5.6F; 2´-2´´). Only weak *Tc-dpp* expression was visible in dorsal most cells (Fig. 5.6E; 3-3´). The asymmetry of *Tc-dpp* expression along the DV axis was only judged when the ventral-, lateral- and dorsal-views within the same embryo were compared.
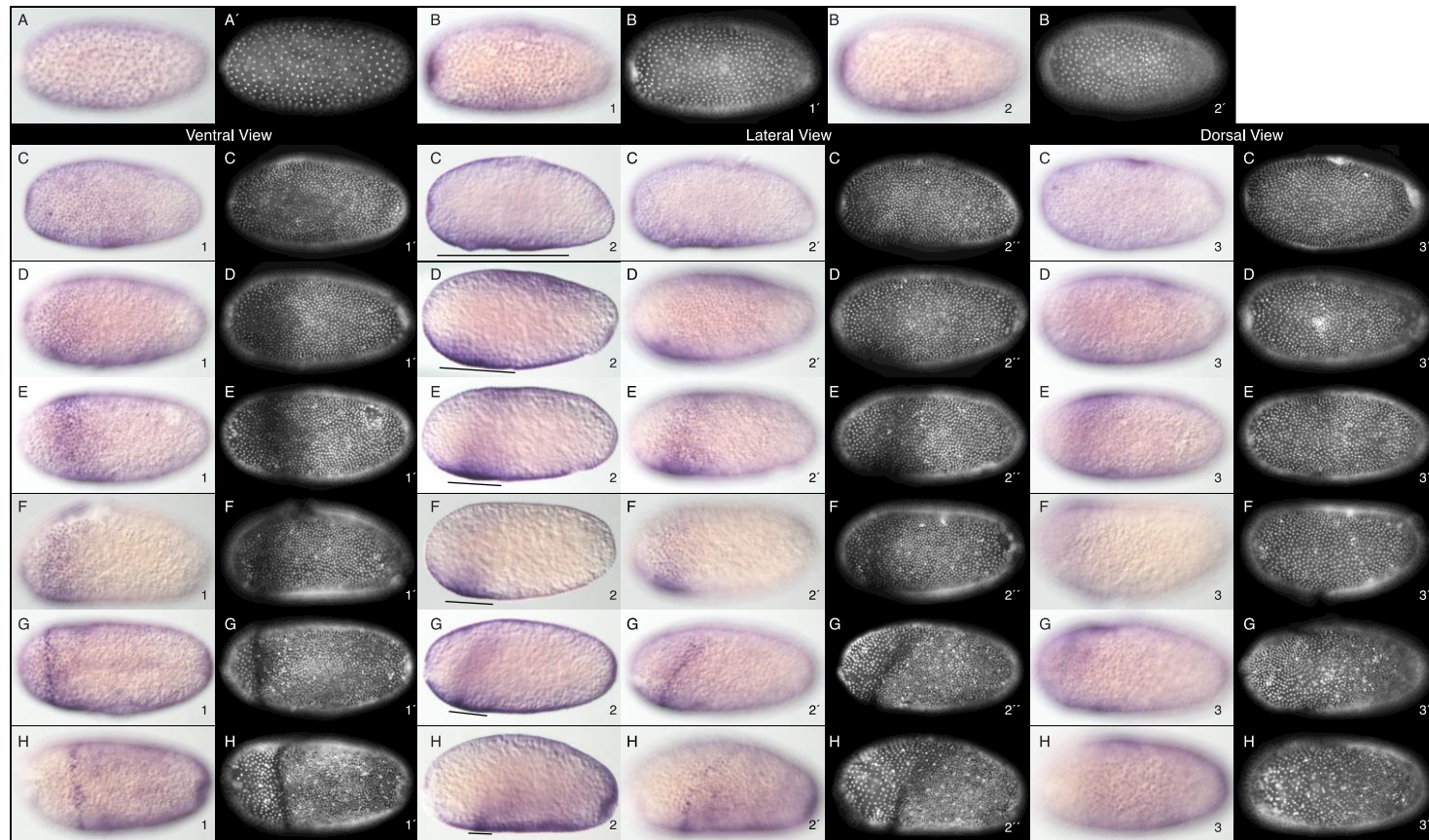
Figure 5.6: Dynamics of *Tc-dpp* expression during *Tribolium* development. (A, A') Ubiquitous expression of *Tc-dpp* at the syncytial blastoderm stage. (B-C3') Asymmetric distribution of *Tc-dpp* transcripts first along the DV axis (B1-B2') and at a later stage along the AP axis (C1-C3'). (D1-F3') The asymmetric expression pattern was visible by comparing ventral (1, 1'), lateral (2–2'') and dorsal views (3, 3') of cellular blastoderm embryos. The quenching of nuclear stain in D-F1' indicated strong ventral mRNA expression. Weak expression of *Tc-dpp* at the dorsal surface was reflected by the absence of quenching (D-F3'). (G1-H3') In differentiated blastoderm embryos, *Tc-dpp* expression resolved into a stripe domain that only appeared symmetric when viewed from ventral side (G1, 1'; H1, 1'). Its obliqueness only became obvious in the lateral views (G2', 2''; H2', 2''). Bars in C2-H2 illustrate the gradual refinement of broad *Tc-dpp* expression into a narrow domain. This refinement can also be observed in the ventral views (C1-H1). All embryos are shown in surface views. Only embryos shown in C2-H2 represent optical sections.

At the successive differentiated blastoderm stages (Fig. 5.6G-5.6H), the broad stripe of *Tc-dpp* expression narrowed significantly from a 12-15 to a 1-2 cell-wide domain that runs along the boundary between the widely spaced serosal cells and the more condensed cells of the germ rudiment (Fig. 5.6G-5.6H, 1-2´´). When viewed ventrally, the *Tc-dpp* domain appeared as a straight line orthogonal to the AP axis (Fig. 5.6G-5.6H, 1-1´) but appeared oblique when viewed laterally (Fig. 5.6G-5.6H, 2-2´´). A low level of *Tc-dpp* expression was also visible in the serosal nuclei (Fig. 5.6G-5.6H, 1, 2´ and 3).

These results show an early gradient of *Tc-dpp* expression along both the axes, the DV-axis and the AP-axis and illustrate how an early asymmetric expression progressively resolved into a 1-2 cell-wide oblique expression domain at the border between the serosa and the germ rudiment.

5.3.6 The dynamics of Dpp-activity as judged by pMAD expression during *Tribolium* development

In addition to *Tc-dpp* mRNA expression profile, I also focused to get a complete survey on the temporal and spatial profile of Dpp-activity during early *Tribolium* development by using an antibody that specifically detects pMAD.

Unlike *Tc-dpp* mRNA expression, no Dpp-activity was observed at the syncytial blastoderm stage (Fig. 5.7A, A´) but at the later stage ubiquitous expression was detected (Fig. 5.7B, B´). Thereafter, a drastic change in the distribution of Dpp-activity was observed at the late blastoderm stage (Fig. 5.7C, 1-3´). At this stage, nuclear pMAD was detected in a broad domain along the complete AP axis covering the entire dorsal surface (Fig. 5.7C, 3-3´). At the lateral side, nuclear pMAD was seen in a broad anterior domain that narrowed towards the posterior (Fig. 5.7C, 2-2´) embracing both, the anterior and the posterior pole. Remarkably, pMAD activity was also detected in a small ventral region of the anterior-most serosa precursor (Fig. 5.7C, 1-1´). During posterior pit formation, nuclear pMAD was detected in all the morphologically distinct nuclei at the dorsal surface (Fig. 5.7D, 3-3´). While on the ventral side nuclear pMAD was only visible in future serosal cells (Fig. 5.7D, 1-1´), the lateral nuclear pMAD was observed in a broad anterior domain of the future serosa and a narrow posterior domain of the future germ rudiment (Fig. 5.7D, 2-2´). At this stage, a significant increase in the activity of Dpp was also detected at the posterior pole (Fig. 5.7D, 1-3´). At the differentiated blastoderm stage, the nuclear pMAD expression became clearly evident in a broad-ventral (Fig. 5.7E, 1-1´), an oblique-lateral (Fig. 5.7E, 2-2´) and large-dorsal domain (Fig. 5.7E, 3-3´) of the presumptive serosal cells.
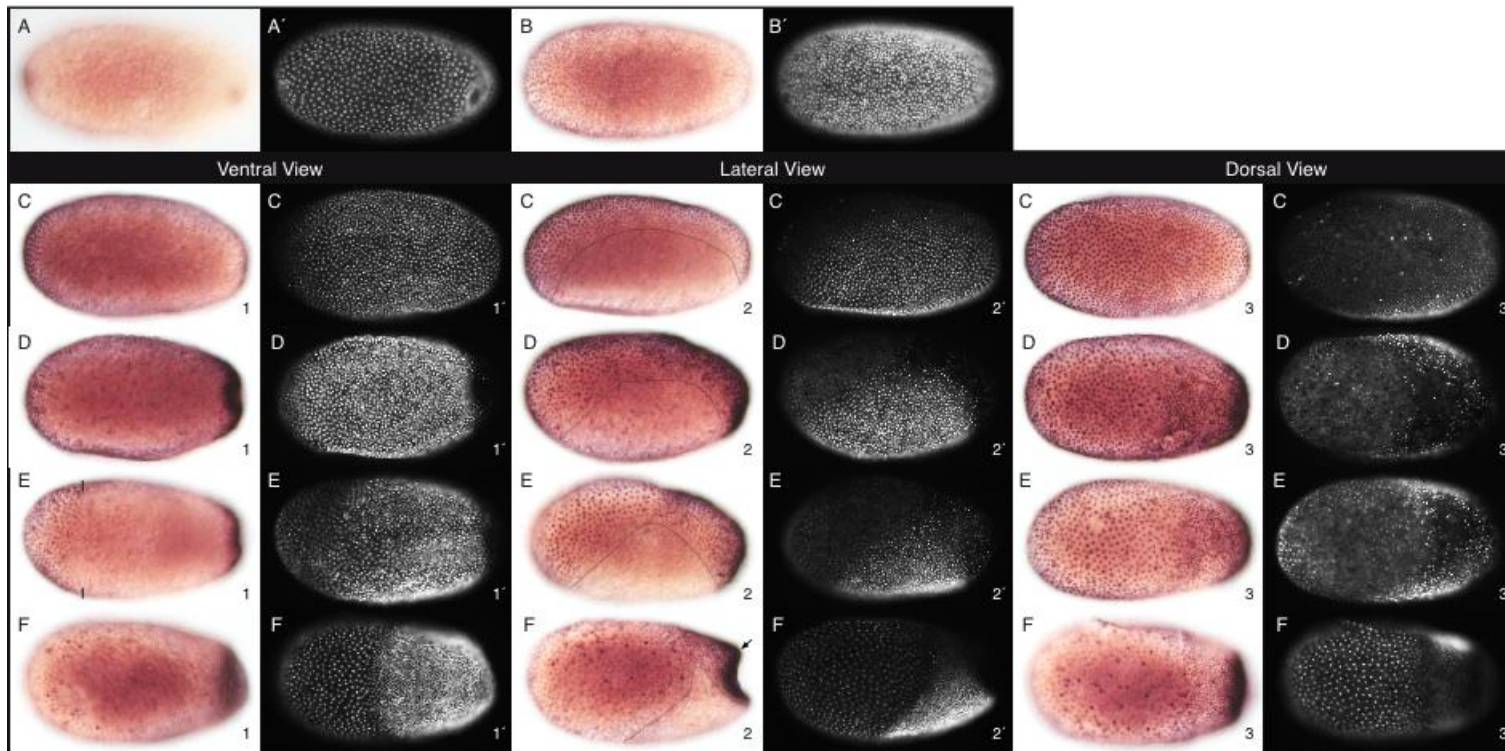
Figure 5.7: Dynamics of pMAD activity detected during *Tribolium* development. (A-B') No pMAD activity was detected at the syncytial blastoderm stage (A, A') but a few nuclear divisions later a transient ubiquitous expression of pMAD was detectable (B, B'). (C1-C3') At this stage, pMAD expression was mainly restricted to a large dorsal domain along the complete AP axis (C3, 3'). In addition, a small symmetric anterior-ventral (C1, 1') and a posterior-narrowing lateral pMAD domain (C2, 2') were observed. (D1-F3') In the extraembryonic anlage pMAD was expressed in all serosal nuclei of ventral, lateral and dorsal fate (compare 1-1', 2-2' and 3-3') whereas in the embryonic anlage pMAD is only active dorsally (compare 2-2' with 3-3'). Lines/bars demarcate the border between pMAD positive and pMAD negative regions. All embryos are shown in surface views.

At this stage, Dpp-activity was also traced in a dorso-lateral domain possibly marking future embryonic cells (Fig. 5.7E, 2-3´). Prior to gastrulation, Dpp-activity in the serosa was faded and only some nuclei displaying a high Dpp-activity level remained (Fig. 5.7F, 1-3´). At this stage, high Dpp-activity was also observed in the dorsal amnion (arrow; Fig. 5.7F, 2-2´). The ventral surface of the germ anlage remained free of Dpp-activity (Fig. 5.7F, 1-1´). In summary, with these results I report a previously undescribed anterior-ventral expression domain of pMAD that remained visible during blastoderm maturation in *Tribolium.*

5.4 Discussion

5.4.1 The anterior-lateral part of the amnion originates from the early anterior blastoderm

In this study I have analysed the expression pattern of *Tc-iro,* a molecular marker for the amnion, from early blastoderm formation to late extending germbands. To my surprise, I found that *Tc-iro* expression was already detectable at the anterior pole during early blastoderm formation (Fig. 5.1C, D). This early anterior expression domain of *Tc-iro* is shared with the early anterior *Tc-zen1* domain that marks the presumptive serosa (Fig. 5.2C, D). A double *in situ* hybridization analysis of *Tc-zen1* and *Tc-iro* expressions indeed confirmed that both these markers are co-expressed at this stage (Fig. 5.3A, B). This indicates that either a distinction of amnion- and serosa precursors has not yet occurred or that the primordia of both tissue types are closely intermingled. As long as *Tc-zen1* and *Tc-iro* are coexpressed in the anterior blastodermal cap, this territory of cells likely is fated to form extraembryonic tissue. Since both the markers are expressed in an early anterior-terminal cap, I hypothesize that like *Tc-zen1* (Kotkamp et al., 2010; Schröder, 2003), the early expression domain of *Tc-iro* is also regulated by the terminal system.

Thus the early blastodermal expression of *Tc-iro* provides a first hint that this group of anterior cells include the precursor cells of the anterior-lateral amnion and therefore this part of the amnion can be considered as of early anterior origin.

5.4.2 Regulatory input of the embryonic patterning systems on *Tc-iro*

During later stages, *Tc-zen1* and *Tc-iro* expression developed into directly adjacent regions representing the respective precursors of the serosa and the amnion. The same topology of flanking of the serosa and the amnion can be seen in the fly model *Megaselia* that also develops with two distinct extraembryonic tissues (Rafiqi et al., 2010; Rafiqi et al., 2012). While the anterior symmetric cap of *Tc-iro* expression (Fig. 5.1D) progressively resolved first into a symmetric ring domain (Fig. 5.3C) that later became asymmetric (Figs. 5.1F and 5.3D), *Tc-zen1* expression stayed as an asymmetric cap at the anterior pole (Fig. 5.2E).

The transformation of the *Tc-iro* cap to a ring-shaped domain (Figs. 5.1D, E and 5.3B, C) can be explained by the negative influence of the terminal system and by sustained upregulation of *Tc-iro* at the same stage under the control of the AP system. The stage, when the *Tc-iro* blastoderm ring (and the anterior *Tc-zen1* domain) becomes tilted (= asymmetric) (Figs. 5.1F and 5.3D) likely reflects the

earliest visible sign of a functional DV system. The transition of the symmetric cap to the asymmetric ring is seen in blastoderm stages of similar nuclear density and thus, seems to occur very quickly.

The complete ring-like domain of *Tc-iro* persists only transiently and opens up at the dorsal side (Figs. 5.1G and 5.3E) while at the same time, *Tc-iro* becomes activated in a nearby new domain that later differentiates into the dorsal amnion (Figs. 5.1H, I and 5.3F). Both these events could be regulated by the DV system that differentially inhibits and activates different target genes along the AP- axis.

5.4.3 What is the origin of the dorsal part of the amnion?

Interestingly, the origin of the dorsal amnion precursor (Fig. 5.1, I3) correlates with a sustained high expression level of pMAD in a dorso-posterior region (Fig. 5.7D-E, 3-3´). These observations support the previous finding that a high level of Dpp signalling is required for the formation of dorsal amnion in wildtype embryos (Nunes da Fonseca et al., 2008; van der Zee et al., 2006). However, the question remains whether the dorsal amnion is of embryonic or extraembryonic origin. Here I provide two possible scenarios that can explain the origin of this tissue: (1) the dorsal amnion precursor gets separated from the germ rudiment when cells at its margin start to express *Tc-iro*. This way of amnion formation represents the traditional view of the embryonic origin of the amnion (Anderson, 1972; Handel et al., 2000). (2) Alternatively, the dorso-posterior region (Fig. 5.1I, 3) - as it develops - is composed of cells with embryonic as well as extraembryonic fates that sort later and hence this region is of mixed origin. Clearly, more amniotic marker genes and lineage-tracing experiments are required to further refine our picture of the development of this tissue.

Taken together, the mature amnion in *Tribolium* is likely a tissue of mixed origin. While the anterior-lateral part of the amnion originates from the anterior blastoderm, the dorsal amnion seems to form de-novo within or near the dorsal embryonic region. Later during development, both parts of the amnion combine with each other to form a continuous tissue that closes over the embryo at the end of embryogenesis.

5.4.4 *Tc-hnt* faithfully marks the serosa in *Tribolium*

In flies like *Drosophila* and *Megaselia*, *hindsight* serves as a general marker for the extraembryonic tissues. By analysing the expression pattern of *Tc-hnt* during early embryogenesis, I tested its reliability as an extraembryonic marker gene in the beetle *Tribolium*.

I found that the spatio-temporal expression dynamics of *Tc-hnt* was more similar to the expression dynamics of the serosa marker *Tc-zen1* than the amnion marker *Tc-iro*. This result has been corroborated by a recent study in *Nasonia* that also reports *zen*-like serosal expression of *Nv-hnt* (Buchta et al., 2013). Therefore, *Tc-hnt* can be considered as an exclusive serosa marker in the beetle *Tribolium*. Although, this is in contrast to *Megaselia*, where *hnt* is expressed in both differentiated tissues serosa and amnion (Rafiqi et al., 2010; Rafiqi et al., 2012). A possible scenario that can explain the serosa-specificity of *hnt* expression in *Tribolium* as well as in *Nasonia* could be that during evolution *hindsight* gained amnion expression aspects and evolved to a more general marker for extraembryonic tissues in flies. To further clarify this point, *hnt* expression needs to be analysed in more basal insects like *Oncopeltus* or *Schistocerca*.

As in *Drosophila* (Yip et al., 1997), no maternal contribution of *hindsight* was detected in *Tribolium*. However, in the late gastrulating embryos a relatively high level of *Tc-hnt* expression in the flattened serosal nuclei (Fig. 5.5, C-C´ and F-F´) suggests its possible role in maintenance of serosa during late development of *Tribolium* embryos, a function described for *Drosophila-hindsight* (Yip et al., 1997).

5.4.5 Further insights from the expression pattern studies of *Tc-dpp* and pMAD

The refined picture of the expression profile of *Tc-dpp* has revealed that there is no symmetric cap domain as reported previously (Chen et al., 2000; Sanches-Salazar, 1996; van der Zee et al., 2006) rather it shows that *Tc-dpp* expression is asymmetric along the DV axis already in the early blastoderm. This expression dynamics is in perfect accordance with previous speculations *Tc-dpp* being activated directly or indirectly by *Tc*-Dorsal (Chen et al., 2000). The asymmetry of *Tc-dpp* expression first along the DV axis and later also along the AP-axis resulted in the ventrally upregulated *Tc-dpp* domain (Fig. 5.6A-D) described previously (Chen et al., 2000).

When pMAD expression was used to monitor the Dpp-activity, I initially detected ubiquitous activity that quickly became dorsal specific. This quick transition can be explained by the blastodermal activity of Sog protein that is required to direct Dpp activity towards the dorsal side of the embryo (van der Zee et al., 2006). Intriguingly, during successive stages of development, Dpp-activity was also detected in some anterior-ventral precursor cells of the serosa (Fig 5.7C-F, 1-1´ and 2-2´) and thus, Dpp-activity cannot be judged as exclusively dorsal. Whether Dpp acitivity has some inputs on the serosal tissue has to be determined in future.

6   Concluding Remarks

The current findings in this dissertation extend our knowledge regarding the roles of FGF signalling in another invertebrate model system the red flour beetle *Tribolium*. With these results I showed that different FGFs are required to govern diverse biological processes during embryogenesis of the beetle *Tribolium*. While the ligand *Tc-fgf1b*, which has no representative within the *Drosphila* genome, was found to be essential for early specification of extraembryonic and embryonic fates along the anterior-posterior axis, the ligand *Tc-fgf8* in cooperation with *Tc-fgfr* was found to be critical for mesoderm development in gastrulating embryos. In addition, specific severe defects in the tracheal system of *Tc-fgfr*[RNAi] embryos were also observed. Thus, a single FGF-receptor regulates these processes in *Tribolium* that are governed in *Drosophila* by two FGF-receptors. This indicates that in *Tribolium* important details of the FGF signalling pathway appear to be fundamentally different when compared to *Drosophila*. In the future, it would be interesting to functionally analyse the combinatory of Fgf / Fgfr in *Tribolium*. The fact that the functional results of *Tc-fgfr*-RNAi experiments are not congruent with the results derived from *Tc-fgf1b* knockdown embryos urges to find the exact mode of action of this signal. Is there a signalling cross talk between FGF/Wnt or FGF/BMP to pattern the early axis of the embryo? Or, is there another FGF-receptor encoded in the *Tribolium* genome that has acquired this function during evolution? How does a single FGF-receptor in *Tribolium* integrate two different ligand-specific responses? These are some of the broader questions that emerged from this study and need to be analysed in the future to reveal more mechanical insights into FGF signalling in *Tribolium*.

Nevertheless, in the context of evolution of development (Evo-Devo) the results presented in this dissertation reveal the plasticity of the FGF cell-signalling pathway during embryogenesis of animals.

7   References

Abler, L. L., Mansour, S. L. and Sun, X. (2009). Conditional gene inactivation reveals roles for *Fgf10* and *Fgfr2* in establishing a normal pattern of epithelial branching in the mouse lung. *Dev Dyn* **238**, 1999-2013.

Affolter, M., Nellen, D., Nussbaumer, U. and Basler, K. (1994). Multiple requirements for the receptor serine/threonine kinase *thick veins* reveal novel functions of TGF beta homologs during *Drosophila* embryogenesis. *Development* **120**, 3105-3117.

Agius, E., Oelgeschlager, M., Wessely, O., Kemp, C. and De Robertis, E. M. (2000). Endodermal Nodal-related signals and mesoderm induction in *Xenopus*. *Development* **127**, 1173-1183.

Ahmad, S. M. and Baker, B. S. (2002). Sex-specific deployment of FGF signaling in *Drosophila* recruits mesodermal cells into the male genital imaginal disc. *Cell* **109**, 651-661.

Alonso, M., Melani, M., Converso, D., Jaitovich, A., Paz, C., Carreras, M. C., Medina, J. H. and Poderoso, J. J. (2004). Mitochondrial extracellular signal-regulated kinases 1/2 (ERK1/2) are modulated during brain development. *Journal of neurochemistry* **89**, 248-256.

Altomare, D. A. and Testa, J. R. (2005). Perturbations of the AKT signaling pathway in human cancer. *Oncogene* **24**, 7455-7464.

Amaya, E., Musci, T. J. and Kirschner, M. W. (1991). Expression of a dominant negative mutant of the FGF receptor disrupts mesoderm formation in *Xenopus* embryos. *Cell* **66**, 257-270.

Amaya, E., Stein, P. A., Musci, T. J. and Kirschner, M. W. (1993). FGF signalling in the early specification of mesoderm in *Xenopus*. *Development* **118**, 477-487.

Anderson, D. T. (1972). The development of hemimetabolous insects. In *Developmental Systems: Insects* (ed. S. J. Counce & C. H. Waddington), pp. 95-163. London: Academic Press.

Arman, E., Haffner-Krausz, R., Gorivodsky, M. and Lonai, P. (1999). *Fgfr2* is required for limb outgrowth and lung-branching morphogenesis. *Proc Natl Acad Sci U S A* **96**, 11895-11899.

Azpiazu, N. and Frasch, M. (1993). *tinman* and *bagpipe*: two homeo box genes that determine cell fates in the dorsal mesoderm of *Drosophila*. *Genes Dev* **7**, 1325-1340.

Bae, Y. K., Trisnadi, N., Kadam, S. and Stathopoulos, A. (2012). The role of FGF signaling in guiding coordinate movement of cell groups: guidance cue and cell adhesion regulator? *Cell adhesion & migration* **6**, 397-403.

Bayha, E., Jorgensen, M. C., Serup, P. and Grapin-Botton, A. (2009). Retinoic acid signaling organizes endodermal organ specification along the entire antero-posterior axis. *PloS one* **4**, e5845.

Beenken, A. and Mohammadi, M. (2009). The FGF family: biology, pathophysiology and therapy. *Nat Rev Drug Discov* **8**, 235-253.

Beermann, A., Aranda, M. and Schröder, R. (2004). The Sp8 zinc-finger transcription factor is involved in allometric growth of the limbs in the beetle *Tribolium castaneum*. *Development* **131**, 733-742.

Beermann, A., Jay, D. G., Beeman, R. W., Hülskamp, M., Tautz, D. and Jürgens, G. (2001). The *short antennae* gene of *Tribolium* is required for limb development and encodes the orthologue of the *Drosophila* Distal-less protein. *Development* **128**, 287-297.

Beermann, A. and Schröder, R. (2008). Sites of Fgf signalling and perception during embryogenesis of the beetle *Tribolium castaneum*. *Dev Genes Evol* **218**, 153-167.

Beiman, M., Shilo, B. Z. and Volk, T. (1996). Heartless, a *Drosophila* FGF receptor homolog, is essential for cell migration and establishment of several mesodermal lineages. *Genes Dev* **10**, 2993-3002.

Bel-Vialar, S., Itasaki, N. and Krumlauf, R. (2002). Initiating Hox gene expression: in the early chick neural tube differential sensitivity to FGF and RA signaling subdivides the *HoxB* genes in two distinct groups. *Development* **129**, 5103-5115.

Berghammer, A., Bucher, G., Maderspacher, F. and Klingler, M. (1999a). A system to efficiently maintain embryonic lethal mutations in the flour beetle *Tribolium castaneum*. *Dev Genes Evol* **209**, 382-389.

Berghammer, A. J., Klingler, M. and Wimmer, E. A. (1999b). A universal marker for transgenic insects. *Nature* **402**, 370-371.

Berns, N., Kusch, T., Schröder, R. and Reuter, R. (2008). Expression, function and regulation of Brachyenteron in the short germband insect *Tribolium castaneum*. *Dev Genes Evol* **218**, 169-179.

Bertrand, V., Hudson, C., Caillol, D., Popovici, C. and Lemaire, P. (2003). Neural tissue in ascidian embryos is induced by FGF9/16/20, acting via a combination of maternal GATA and Ets transcription factors. *Cell* **115**, 615-627.

Birkan, M., Schäper, N. D. and Chipman, A. D. (2011). Early patterning and blastodermal fate map of the head in the milkweed bug *Oncopeltus fasciatus*. *Evolution & development* **13**, 436-447.

Birnbaum, D., Popovici, C. and Roubin, R. (2005). A pair as a minimum: the two fibroblast growth factors of the nematode *Caenorhabditis elegans*. *Dev Dyn* **232**, 247-255.

Birsoy, B., Kofron, M., Schaible, K., Wylie, C. and Heasman, J. (2006). Vg 1 is an essential signaling molecule in *Xenopus* development. *Development* **133**, 15-20.

Bodmer, R. (1993). The gene *tinman* is required for specification of the heart and visceral muscles in *Drosophila*. *Development* **118**, 719-729.

Bodmer, R., Jan, L. Y. and Jan, Y. N. (1990). A new homeobox-containing gene, msh-2, is transiently expressed early during mesoderm formation of *Drosophila*. *Development* **110**, 661-669.

Bodmer, R. and Venkatesh, T. V. (1998). Heart development in *Drosophila* and vertebrates: conservation of molecular mechanisms. *Developmental genetics* **22**, 181-186.

Borland, C. Z., Schutzman, J. L. and Stern, M. J. (2001). Fibroblast growth factor signaling in *Caenorhabditis elegans*. *Bioessays* **23**, 1120-1130.

Böttcher, R. T. and Niehrs, C. (2005). Fibroblast growth factor signaling during early vertebrate development. *Endocr Rev* **26**, 63-77.

Böttcher, R. T., Pollet, N., Delius, H. and Niehrs, C. (2004). The transmembrane protein XFLRT3 forms a complex with FGF receptors and promotes FGF signalling. *Nature cell biology* **6**, 38-44.

Branney, P. A., Faas, L., Steane, S. E., Pownall, M. E. and Isaacs, H. V. (2009). Characterisation of the fibroblast growth factor dependent transcriptome in early development. *PloS one* **4**, e4951.

Brown, S. J., Mahaffey, J. P., Lorenzen, M. D., Denell, R. E. and Mahaffey, J. W. (1999). Using RNAi to investigate orthologous homeotic gene function during development of distantly related insects. *Evolution & development* **1**, 11-15.

Brown, S. J., Shippy, T. D., Miller, S., Bolognesi, R., Beeman, R. W., Lorenzen, M. D., Bucher, G., Wimmer, E. A. and Klingler, M. (2009). The red flour beetle, *Tribolium castaneum* (Coleoptera): a model for studies of development and pest biology. *Cold Spring Harb Protoc* **2009**, pdb emo126.

Bucher, G. and Klingler, M. (2004). Divergent segmentation mechanism in the short germ insect *Tribolium* revealed by giant expression and function. *Development* **131**, 1729-1740.

Bucher, G., Scholten, J. and Klingler, M. (2002). Parental RNAi in *Tribolium* (Coleoptera). *Curr Biol* **12**, R85-86.

Bucher, G. and Wimmer, E. A. (2005). Beetle a-head. *B.I.F. Futura* **20**, 164-169.

Buchta, T., Ozuak, O., Stappert, D., Roth, S. and Lynch, J. A. (2013). Patterning the dorsal-ventral axis of the wasp *Nasonia vitripennis*. *Dev Biol*.

Buckingham, M., Meilhac, S. and Zaffran, S. (2005). Building the mammalian heart from two sources of myocardial cells. *Nature reviews. Genetics* **6**, 826-835.

Bulow, H. E., Boulin, T. and Hobert, O. (2004). Differential functions of the *C. elegans* FGF receptor in axon outgrowth and maintenance of axon position. *Neuron* **42**, 367-374.

Burdine, R. D., Branda, C. S. and Stern, M. J. (1998). *EGL-17(FGF)* expression coordinates the attraction of the migrating sex myoblasts with vulval induction in *C. elegans*. *Development* **125**, 1083-1093.

Buresi, A., Baratte, S., Da Silva, C. and Bonnaud, L. (2012). *orthodenticle/otx* ortholog expression in the anterior brain and eyes of *Sepia officinalis* (Mollusca, Cephalopoda). *Gene expression patterns : GEP* **12**, 109-116.

Cabrita, M. A. and Christofori, G. (2008). Sprouty proteins, masterminds of receptor tyrosine kinase signaling. *Angiogenesis* **11**, 53-62.

Casci, T., Vinos, J. and Freeman, M. (1999). Sprouty, an intracellular inhibitor of Ras signaling. *Cell* **96**, 655-665.

Cebria, F., Kobayashi, C., Umesono, Y., Nakazawa, M., Mineta, K., Ikeo, K., Gojobori, T., Itoh, M., Taira, M., Sanchez Alvarado, A., et al. (2002). FGFR-related gene *nou-darake* restricts brain tissues to the head region of planarians. *Nature* **419**, 620-624.

Chen, G., Handel, K. and Roth, S. (2000). The maternal NF-kappaB/dorsal gradient of *Tribolium castaneum*: dynamics of early dorsoventral patterning in a short-germ beetle. *Development* **127**, 5145-5156.

Chen, J. N. and Fishman, M. C. (2000). Genetics of heart development. *Trends in genetics : TIG* **16**, 383-388.

Cho, K. W. and De Robertis, E. M. (1990). Differential activation of *Xenopus* homeo box genes by mesoderm-inducing growth factors and retinoic acid. *Genes Dev* **4**, 1910-1916.

Christen, B. and Slack, J. M. (1997). FGF-8 is associated with anteroposterior patterning and limb regeneration in *Xenopus*. *Dev Biol* **192**, 455-466.

Ciruna, B. and Rossant, J. (2001). FGF signaling regulates mesoderm cell fate specification and morphogenetic movement at the primitive streak. *Dev Cell* **1**, 37-49.

Colvin, J. S., White, A. C., Pratt, S. J. and Ornitz, D. M. (2001). Lung hypoplasia and neonatal death in Fgf9-null mice identify this gene as an essential regulator of lung mesenchyme. *Development* **128**, 2095-2106.

Cornell, R. A. and Kimelman, D. (1994). Activin-mediated mesoderm induction requires FGF. *Development* **120**, 453-462.

Cox, W. G. and Hemmati-Brivanlou, A. (1995). Caudalization of neural fate by tissue recombination and bFGF. *Development* **121**, 4349-4358.

Cripps, R. M. and Olson, E. N. (2002). Control of cardiac development by an evolutionarily conserved transcriptional network. *Dev Biol* **246**, 14-28.

Crossley, P. H. and Martin, G. R. (1995). The mouse *Fgf8* gene encodes a family of polypeptides and is expressed in regions that direct outgrowth and patterning in the developing embryo. *Development* **121**, 439-451.

Crossley, P. H., Martinez, S. and Martin, G. R. (1996). Midbrain development induced by FGF8 in the chick embryo. *Nature* **380**, 66-68.

Csiszar, A., Vogelsang, E., Beug, H. and Leptin, M. (2010). A novel conserved phosphotyrosine motif in the *Drosophila* fibroblast growth factor signaling adaptor Dof with a redundant role in signal transmission. *Mol Cell Biol* **30**, 2017-2027.

Dailey, L., Ambrosetti, D., Mansukhani, A. and Basilico, C. (2005). Mechanisms underlying differential responses to FGF signaling. *Cytokine Growth Factor Rev* **16**, 233-247.

Davidson, B. P., Cheng, L., Kinder, S. J. and Tam, P. P. (2000). Exogenous FGF-4 can suppress anterior development in the mouse embryo during neurulation and early organogenesis. *Dev Biol* **221**, 41-52.

Dearden, P., Grbic, M., Falciani, F. and Akam, M. (2000). Maternal expression and early zygotic regulation of the *Hox3/zen* gene in the grasshopper *Schistocerca gregaria*. *Evolution & development* **2**, 261-270.

Delaune, E., Lemaire, P. and Kodjabachian, L. (2005). Neural induction in *Xenopus* requires early FGF signalling in addition to BMP inhibition. *Development* **132**, 299-310.

Deng, C. X., Wynshaw-Boris, A., Shen, M. M., Daugherty, C., Ornitz, D. M. and Leder, P. (1994). Murine FGFR-1 is required for early postimplantation growth and axial organization. *Genes Dev* **8**, 3045-3057.

Dessimoz, J., Opoka, R., Kordich, J. J., Grapin-Botton, A. and Wells, J. M. (2006). FGF signaling is necessary for establishing gut tube domains along the anterior-posterior axis in vivo. *Mech Dev* **123**, 42-55.

DeVore, D. L., Horvitz, H. R. and Stern, M. J. (1995). An FGF receptor signaling pathway is required for the normal cell migrations of the sex myoblasts in *C. elegans* hermaphrodites. *Cell* **83**, 611-620.

Diez del Corral, R. and Storey, K. G. (2004). Opposing FGF and retinoid pathways: a signalling switch that controls differentiation and patterning onset in the extending vertebrate body axis. *Bioessays* **26**, 857-869.

Dikic, I. and Giordano, S. (2003). Negative receptor signalling. *Current opinion in cell biology* **15**, 128-135.

Doniach, T. (1995). Basic FGF as an inducer of anteroposterior neural pattern. *Cell* **83**, 1067-1070.

Dönitz, J., Grossmann, D., Schild, I., Schmitt-Engel, C., Bradler, S., Prpic, N. M. and Bucher, G. (2013). TrOn: an anatomical ontology for the beetle *Tribolium castaneum*. *PloS one* **8**, e70695.

Dorey, K. and Amaya, E. (2010). FGF signalling: diverse roles during early vertebrate embryogenesis. *Development* **137**, 3731-3742.

Dorfman, R. and Shilo, B. Z. (2001). Biphasic activation of the BMP pathway patterns the *Drosophila* embryonic dorsal region. *Development* **128**, 965-972.

Dossenbach, C., Rock, S. and Affolter, M. (2001). Specificity of FGF signaling in cell migration in *Drosophila*. *Development* **128**, 4563-4572.

Draper, B. W., Stock, D. W. and Kimmel, C. B. (2003). Zebrafish *fgf24* functions with *fgf8* to promote posterior mesodermal development. *Development* **130**, 4639-4654.

Dubrulle, J. and Pourquie, O. (2004). *fgf8* mRNA decay establishes a gradient that couples axial elongation to patterning in the vertebrate embryo. *Nature* **427**, 419-422.

Eivers, E., Fuentealba, L. C. and De Robertis, E. M. (2008). Integrating positional information at the level of Smad1/5/8. *Curr Opin Genet Dev* **18**, 304-310.

Falciani, F., Hausdorf, B., Schröder, R., Akam, M., Tautz, D., Denell, R. and Brown, S. (1996). Class 3 Hox genes in insects and the origin of *zen*. *Proc Natl Acad Sci U S A* **93**, 8479-8484.

Ferguson, E. L. and Anderson, K. V. (1992). Localized enhancement and repression of the activity of the TGF-beta family member, *decapentaplegic*, is necessary for dorsal-ventral pattern formation in the *Drosophila* embryo. *Development* **114**, 583-597.

Filipowicz, W. (2005). RNAi: the nuts and bolts of the RISC machine. *Cell* **122**, 17-20.

Fire, A., Xu, S., Montgomery, M. K., Kostas, S. A., Driver, S. E. and Mello, C. C. (1998). Potent and specific genetic interference by double-stranded RNA in *Caenorhabditis elegans*. *Nature* **391**, 806-811.

Fletcher, R. B., Baker, J. C. and Harland, R. M. (2006). FGF8 spliceforms mediate early mesoderm and posterior neural tissue formation in *Xenopus*. *Development* **133**, 1703-1714.

Fletcher, R. B. and Harland, R. M. (2008). The role of FGF signaling in the establishment and maintenance of mesodermal gene expression in *Xenopus*. *Dev Dyn* **237**, 1243-1254.

Forni, J. J., Romani, S., Doherty, P. and Tear, G. (2004). Neuroglian and FasciclinII can promote neurite outgrowth via the FGF receptor *Heartless*. *Molecular and cellular neurosciences* **26**, 282-291.

Frank, L. H. and Rushlow, C. (1996). A group of genes required for maintenance of the amnioserosa tissue in *Drosophila*. *Development* **122**, 1343-1352.

Frasch, M. (1995). Induction of visceral and cardiac mesoderm by ectodermal Dpp in the early *Drosophila* embryo. *Nature* **374**, 464-467.

Frasch, M. (1999). Intersecting signalling and transcriptional pathways in *Drosophila* heart specification. *Seminars in cell & developmental biology* **10**, 61-71.

Frohman, M. A., Dush, M. K. and Martin, G. R. (1988). Rapid production of full-length cDNAs from rare transcripts: amplification using a single gene-specific oligonucleotide primer. *Proc Natl Acad Sci U S A* **85**, 8998-9002.

Fu, J., Posnien, N., Bolognesi, R., Fischer, T. D., Rayl, P., Oberhofer, G., Kitzmann, P., Brown, S. J. and Bucher, G. (2012). Asymmetrically expressed *axin* required for anterior development in *Tribolium. Proc Natl Acad Sci U S A* **109**, 7782-7786.

Fürthauer, M., Lin, W., Ang, S. L., Thisse, B. and Thisse, C. (2002). Sef is a feedback-induced antagonist of Ras/MAPK-mediated FGF signalling. *Nature cell biology* **4**, 170-174.

Fürthauer, M., Thisse, C. and Thisse, B. (1997). A role for FGF-8 in the dorsoventral patterning of the zebrafish gastrula. *Development* **124**, 4253-4264.

Fürthauer, M., Van Celst, J., Thisse, C. and Thisse, B. (2004). Fgf signalling controls the dorsoventral patterning of the zebrafish embryo. *Development* **131**, 2853-2864.

Gajewski, K., Fossett, N., Molkentin, J. D. and Schulz, R. A. (1999). The zinc finger proteins Pannier and GATA4 function as cardiogenic factors in *Drosophila. Development* **126**, 5679-5688.

Garcia-Alonso, L., Romani, S. and Jimenez, F. (2000). The EGF and FGF receptors mediate neuroglian function to control growth cone decisions during sensory axon guidance in *Drosophila. Neuron* **28**, 741-752.

Garcia-Solache, M., Jaeger, J. and Akam, M. (2010). A systematic analysis of the gap gene system in the moth midge *Clogmia albipunctata. Dev Biol* **344**, 306-318.

Gavrieli, Y., Sherman, Y. and Ben-Sasson, S. A. (1992). Identification of programmed cell death in situ via specific labeling of nuclear DNA fragmentation. *The Journal of cell biology* **119**, 493-501.

Gerhart, J. (1999). 1998 Warkany lecture: signaling pathways in development. *Teratology* **60**, 226-239.

Ghabrial, A., Luschnig, S., Metzstein, M. M. and Krasnow, M. A. (2003). Branching morphogenesis of the *Drosophila* tracheal system. *Annual review of cell and developmental biology* **19**, 623-647.

Ghabrial, A. S. and Krasnow, M. A. (2006). Social interactions among epithelial cells during tracheal branching morphogenesis. *Nature* **441**, 746-749.

Gisselbrecht, S., Skeath, J. B., Doe, C. Q. and Michelson, A. M. (1996). *heartless* encodes a fibroblast growth factor receptor (DFR1/DFGF-R2) involved in the directional migration of early mesodermal cells in the *Drosophila* embryo. *Genes Dev* **10**, 3003-3017.

Goltsev, Y., Fuse, N., Frasch, M., Zinzen, R. P., Lanzaro, G. and Levine, M. (2007). Evolution of the dorsal-ventral patterning network in the mosquito, *Anopheles gambiae. Development* **134**, 2415-2424.

Good, K., Ciosk, R., Nance, J., Neves, A., Hill, R. J. and Priess, J. R. (2004). The T-box transcription factors TBX-37 and TBX-38 link GLP-1/Notch signaling to mesoderm induction in *C. elegans* embryos. *Development* **131**, 1967-1978.

Goodman, S. J., Branda, C. S., Robinson, M. K., Burdine, R. D. and Stern, M. J. (2003). Alternative splicing affecting a novel domain in the *C. elegans* EGL-15 FGF receptor confers functional specificity. *Development* **130**, 3757-3766.

Gospodarowicz, D. and Cheng, J. (1986). Heparin protects basic and acidic FGF from inactivation. *Journal of cellular physiology* **128**, 475-484.

Green, S. A., Norris, R. P., Terasaki, M. and Lowe, C. J. (2013). FGF signaling induces mesoderm in the hemichordate *Saccoglossus kowalevskii*. *Development* **140**, 1024-1033.

Griffin, K., Patient, R. and Holder, N. (1995). Analysis of FGF function in normal and no tail zebrafish embryos reveals separate mechanisms for formation of the trunk and the tail. *Development* **121**, 2983-2994.

Groth, C. and Lardelli, M. (2002). The structure and function of vertebrate fibroblast growth factor receptor 1. *The International journal of developmental biology* **46**, 393-400.

Gryzik, T. and Müller, H. A. (2004). *FGF8-like1* and *FGF8-like2* encode putative ligands of the FGF receptor Htl and are required for mesoderm migration in the *Drosophila* gastrula. *Curr Biol* **14**, 659-667.

Guo, X. and Wang, X. F. (2009). Signaling cross-talk between TGF-beta/BMP and other pathways. *Cell Res* **19**, 71-88.

Hacohen, N., Kramer, S., Sutherland, D., Hiromi, Y. and Krasnow, M. A. (1998). *sprouty* encodes a novel antagonist of FGF signaling that patterns apical branching of the *Drosophila* airways. *Cell* **92**, 253-263.

Hanafusa, H., Torii, S., Yasunaga, T. and Nishida, E. (2002). Sprouty1 and Sprouty2 provide a control mechanism for the Ras/MAPK signalling pathway. *Nature cell biology* **4**, 850-858.

Handel, K., Basal, A., Fan, X. and Roth, S. (2005). *Tribolium castaneum twist*: gastrulation and mesoderm formation in a short-germ beetle. *Dev Genes Evol* **215**, 13-31.

Handel, K., Grünfelder, C. G., Roth, S. and Sander, K. (2000). *Tribolium* embryogenesis: a SEM study of cell shapes and movements from blastoderm to serosal closure. *Dev Genes Evol* **210**, 167-179.

Haremaki, T., Tanaka, Y., Hongo, I., Yuge, M. and Okamoto, H. (2003). Integration of multiple signal transducing pathways on Fgf response elements of the *Xenopus* caudal homologue *Xcad3*. *Development* **130**, 4907-4917.

Hart, K. C., Robertson, S. C., Kanemitsu, M. Y., Meyer, A. N., Tynan, J. A. and Donoghue, D. J. (2000). Transformation and Stat activation by derivatives of FGFR1, FGFR3, and FGFR4. *Oncogene* **19**, 3309-3320.

Heisenberg, C. P. (2009). Dorsal closure in *Drosophila*: cells cannot get out of the tight spot. *Bioessays* **31**, 1284-1287.

Heming, B. (2003). Insect development and evolution. Cornell University Press, Ithaka, NY

Hemmati-Brivanlou, A., Kelly, O. G. and Melton, D. A. (1994b). Follistatin, an antagonist of activin, is expressed in the Spemann organizer and displays direct neuralizing activity. *Cell* **77**, 283-295.

Holowacz, T. and Sokol, S. (1999). FGF is required for posterior neural patterning but not for neural induction. *Dev Biol* **205**, 296-308.

Hongo, I., Kengaku, M. and Okamoto, H. (1999). FGF signaling and the anterior neural induction in *Xenopus*. *Dev Biol* **216**, 561-581.

Huang, P. and Stern, M. J. (2005). FGF signaling in flies and worms: more and more relevant to vertebrate biology. *Cytokine Growth Factor Rev* **16**, 151-158.

Imai, K. S., Satoh, N. and Satou, Y. (2002). Early embryonic expression of FGF4/6/9 gene and its role in the induction of mesenchyme and notochord in *Ciona savignyi* embryos. *Development* **129**, 1729-1738.

Imai, K. S., Stolfi, A., Levine, M. and Satou, Y. (2009). Gene regulatory networks underlying the compartmentalization of the *Ciona* central nervous system. *Development* **136**, 285-293.

Imam, F., Sutherland, D., Huang, W. and Krasnow, M. A. (1999). *stumps*, a *Drosophila* gene required for fibroblast growth factor (FGF)-directed migrations of tracheal and mesodermal cells. *Genetics* **152**, 307-318.

Isaacs, H. V., Pownall, M. E. and Slack, J. M. (1998). Regulation of Hox gene expression and posterior development by the *Xenopus caudal* homologue *Xcad3*. *The EMBO journal* **17**, 3413-3427.

Isaacs, H. V., Tannahill, D. and Slack, J. M. (1992). Expression of a novel FGF in the *Xenopus* embryo. A new candidate inducing factor for mesoderm formation and anteroposterior specification. *Development* **114**, 711-720.

Ito, M., Matsui, T., Taniguchi, T. and Chihara, K. (1994). Alternative splicing generates two distinct transcripts for the *Drosophila melanogaster* fibroblast growth factor receptor homolog. *Gene* **139**, 215-218.

Itoh, N. and Ornitz, D. M. (2004). Evolution of the *Fgf* and *Fgfr* gene families. *Trends in genetics : TIG* **20**, 563-569.

Itoh, N. and Ornitz, D. M. (2011). Fibroblast growth factors: from molecular evolution to roles in development, metabolism and disease. *J Biochem* **149**, 121-130.

Jacinto, A. and Martin, P. (2001). Morphogenesis: unravelling the cell biology of hole closure. *Curr Biol* **11**, R705-707.

Jacinto, A., Woolner, S. and Martin, P. (2002). Dynamic analysis of dorsal closure in *Drosophila*: from genetics to cell biology. *Dev Cell* **3**, 9-19.

Jackson, A. L., Burchard, J., Schelter, J., Chau, B. N., Cleary, M., Lim, L. and Linsley, P. S. (2006). Widespread siRNA "off-target" transcript silencing mediated by seed region sequence complementarity. *RNA* **12**, 1179-1187.

Jacobs, C. G., Rezende, G. L., Lamers, G. E. and van der Zee, M. (2013). The extraembryonic serosa protects the insect egg against desiccation. *Proceedings. Biological sciences / The Royal Society* **280**, 20131082.

Jacobs, C. G. and van der Zee, M. (2013). Immune competence in insect eggs depends on the extra-embryonic serosa. *Developmental and comparative immunology*.

Janssen, R., Budd, G. E. and Damen, W. G. (2011). Gene expression suggests conserved mechanisms patterning the heads of insects and myriapods. *Dev Biol* **357**, 64-72.

Jin, Z. and El-Deiry, W. S. (2005). Overview of cell death signaling pathways. *Cancer biology & therapy* **4**, 139-163.

Johnson, D. E., Lu, J., Chen, H., Werner, S. and Williams, L. T. (1991). The human fibroblast growth factor receptor genes: a common structural arrangement underlies the mechanisms for generating receptor forms that differ in their third immunoglobulin domain. *Mol Cell Biol* **11**, 4627-4634.

Johnson, D. E. and Williams, L. T. (1993). Structural and functional diversity in the FGF receptor multigene family. *Advances in cancer research* **60**, 1-41.

Kadam, S., Ghosh, S. and Stathopoulos, A. (2012). Synchronous and symmetric migration of *Drosophila* caudal visceral mesoderm cells requires dual input by two FGF ligands. *Development* **139**, 699-708.

Kadam, S., McMahon, A., Tzou, P. and Stathopoulos, A. (2009). FGF ligands in *Drosophila* have distinct activities required to support cell migration and differentiation. *Development* **136**, 739-747.

Kang, S., Elf, S., Dong, S., Hitosugi, T., Lythgoe, K., Guo, A., Ruan, H., Lonial, S., Khoury, H. J., Williams, I. R., et al. (2009). Fibroblast growth factor receptor 3 associates with and tyrosine phosphorylates p90 RSK2, leading to RSK2 activation that mediates hematopoietic transformation. *Mol Cell Biol* **29**, 2105-2117.

Kiecker, C. and Niehrs, C. (2001). A morphogen gradient of Wnt/beta-catenin signalling regulates anteroposterior neural patterning in *Xenopus*. *Development* **128**, 4189-4201.

Kim, G. J. and Nishida, H. (2001). Role of the FGF and MEK signaling pathway in the ascidian embryo. *Development, growth & differentiation* **43**, 521-533.

Kimelman, D. and Kirschner, M. (1987). Synergistic induction of mesoderm by FGF and TGF-beta and the identification of an mRNA coding for FGF in the early *Xenopus* embryo. *Cell* **51**, 869-877.

Kimelman, D. and Martin, B. L. (2012). Anterior–posterior patterning in early development: three strategies. *WIREs Dev Biol* **1**, 253-266.

Klämbt, C., Glazer, L. and Shilo, B. Z. (1992). *breathless*, a *Drosophila* FGF receptor homolog, is essential for migration of tracheal and specific midline glial cells. *Genes Dev* **6**, 1668-1678.

Klapper, R., Holz, A. and Janning, W. (1998). Fate map and cell lineage relationships of thoracic and abdominal mesodermal anlagen in *Drosophila melanogaster*. *Mech Dev* **71**, 77-87.

Klinedinst, S. L. and Bodmer, R. (2003). Gata factor Pannier is required to establish competence for heart progenitor formation. *Development* **130**, 3027-3038.

Klingler, M. (2004). *Tribolium*. *Curr Biol* **14**, R639-640.

Klingseisen, A., Clark, I. B., Gryzik, T. and Müller, H. A. (2009). Differential and overlapping functions of two closely related *Drosophila* FGF8-like growth factors in mesoderm development. *Development* **136**, 2393-2402.

Kofron, M., Demel, T., Xanthos, J., Lohr, J., Sun, B., Sive, H., Osada, S., Wright, C., Wylie, C. and Heasman, J. (1999). Mesoderm induction in *Xenopus* is a zygotic event regulated by maternal VegT via TGFbeta growth factors. *Development* **126**, 5759-5770.

Kolkova, K., Novitskaya, V., Pedersen, N., Berezin, V. and Bock, E. (2000). Neural cell adhesion molecule-stimulated neurite outgrowth depends on activation of protein kinase C and the Ras-mitogen-activated protein kinase pathway. *The Journal of neuroscience : the official journal of the Society for Neuroscience* **20**, 2238-2246.

Kondo, T. and Hayashi, S. (2013). Mitotic cell rounding accelerates epithelial invagination. *Nature* **494**, 125-129.

Kondoh, K., Torii, S. and Nishida, E. (2005). Control of MAP kinase signaling to the nucleus. *Chromosoma* **114**, 86-91.

Kotkamp, K., Klingler, M. and Schoppmeier, M. (2010). Apparent role of *Tribolium orthodenticle* in anteroposterior blastoderm patterning largely reflects novel functions in dorsoventral axis formation and cell survival. *Development* **137**, 1853-1862.

Kouhara, H., Hadari, Y. R., Spivak-Kroizman, T., Schilling, J., Bar-Sagi, D., Lax, I. and Schlessinger, J. (1997). A lipid-anchored Grb2-binding protein that links FGF-receptor activation to the Ras/MAPK signaling pathway. *Cell* **89**, 693-702.

Kroll, K. L. and Amaya, E. (1996). Transgenic *Xenopus* embryos from sperm nuclear transplantations reveal FGF signaling requirements during gastrulation. *Development* **122**, 3173-3183.

Kumano, G., Ezal, C. and Smith, W. C. (2001). Boundaries and functional domains in the animal/vegetal axis of *Xenopus* gastrula mesoderm. *Dev Biol* **236**, 465-477.

Kumano, G. and Smith, W. C. (2002a). The nodal target gene *Xmenf* is a component of an FGF-independent pathway of ventral mesoderm induction in *Xenopus*. *Mech Dev* **118**, 45-56.

Kumano, G. and Smith, W. C. (2002b). Revisions to the *Xenopus* gastrula fate map: implications for mesoderm induction and patterning. *Dev Dyn* **225**, 409-421.

LaBonne, C. and Whitman, M. (1994). Mesoderm induction by activin requires FGF-mediated intracellular signals. *Development* **120**, 463-472.

Lamb, T. M. and Harland, R. M. (1995). Fibroblast growth factor is a direct neural inducer, which combined with *noggin* generates anterior-posterior neural pattern. *Development* **121**, 3627-3636.

Lamb, T. M., Knecht, A. K., Smith, W. C., Stachel, S. E., Economides, A. N., Stahl, N., Yancopolous, G. D. and Harland, R. M. (1993). Neural induction by the secreted polypeptide noggin. *Science* **262**, 713-718.

Langdon, Y. G. and Mullins, M. C. (2011). Maternal and zygotic control of zebrafish dorsoventral axial patterning. *Annu Rev Genet* **45**, 357-377.

Launay, C., Fromentoux, V., Shi, D. L. and Boucaut, J. C. (1996). A truncated FGF receptor blocks neural induction by endogenous *Xenopus* inducers. *Development* **122**, 869-880.

Lea, R., Papalopulu, N., Amaya, E. and Dorey, K. (2009). Temporal and spatial expression of FGF ligands and receptors during *Xenopus* development. *Dev Dyn* **238**, 1467-1479.

Lemaire, P., Bertrand, V. and Hudson, C. (2002). Early steps in the formation of neural tissue in ascidian embryos. *Dev Biol* **252**, 151-169.

Lengyel, J. A. and Iwaki, D. D. (2002). It takes guts: the *Drosophila* hindgut as a model system for organogenesis. *Dev Biol* **243**, 1-19.

Lin, X. (2004). Functions of heparan sulfate proteoglycans in cell signaling during development. *Development* **131**, 6009-6021.

Lin, X., Buff, E. M., Perrimon, N. and Michelson, A. M. (1999). Heparan sulfate proteoglycans are essential for FGF receptor signaling during *Drosophila* embryonic development. *Development* **126**, 3715-3723.

Liu, X., Kiss, I. and Lengyel, J. A. (1999). Identification of genes controlling malpighian tubule and other epithelial morphogenesis in *Drosophila melanogaster*. *Genetics* **151**, 685-695.

Lo, T. W., Branda, C. S., Huang, P., Sasson, I. E., Goodman, S. J. and Stern, M. J. (2008). Different isoforms of the *C. elegans* FGF receptor are required for attraction and repulsion of the migrating sex myoblasts. *Dev Biol* **318**, 268-275.

Londin, E. R., Niemiec, J. and Sirotkin, H. I. (2005). Chordin, FGF signaling, and mesodermal factors cooperate in zebrafish neural induction. *Dev Biol* **279**, 1-19.

Lorenzen, M. D., Berghammer, A. J., Brown, S. J., Denell, R. E., Klingler, M. and Beeman, R. W. (2003). *piggyBac*-mediated germline transformation in the beetle *Tribolium castaneum. Insect molecular biology* **12**, 433-440.

Lynch, J. A., Brent, A. E., Leaf, D. S., Pultz, M. A. and Desplan, C. (2006). Localized maternal *orthodenticle* patterns anterior and posterior in the long germ wasp *Nasonia. Nature* **439**, 728-732.

Lynch, J. A. and Roth, S. (2011). The evolution of dorsal-ventral patterning mechanisms in insects. *Genes Dev* **25**, 107-118.

Lynch, M. and Conery, J. S. (2000). The evolutionary fate and consequences of duplicate genes. *Science* **290**, 1151-1155.

Maegawa, S., Varga, M. and Weinberg, E. S. (2006). FGF signaling is required for β-catenin-mediated induction of the zebrafish organizer. *Development* **133**, 3265-3276.

Maher, P. (1999). p38 mitogen-activated protein kinase activation is required for fibroblast growth factor-2-stimulated cell proliferation but not differentiation. *The Journal of biological chemistry* **274**, 17491-17498.

Mandal, L., Banerjee, U. and Hartenstein, V. (2004). Evidence for a fruit fly hemangioblast and similarities between lymph-gland hematopoiesis in fruit fly and mammal aorta-gonadal-mesonephros mesoderm. *Nat Genet* **36**, 1019-1023.

Mansukhani, A., Ambrosetti, D., Holmes, G., Cornivelli, L. and Basilico, C. (2005). Sox2 induction by FGF and FGFR2 activating mutations inhibits Wnt signaling and osteoblast differentiation. *The Journal of cell biology* **168**, 1065-1076.

Marques, S. R., Lee, Y., Poss, K. D. and Yelon, D. (2008). Reiterative roles for FGF signaling in the establishment of size and proportion of the zebrafish heart. *Dev Biol* **321**, 397-406.

Martin-Blanco, E., Gampel, A., Ring, J., Virdee, K., Kirov, N., Tolkovsky, A. M. and Martinez-Arias, A. (1998). *puckered* encodes a phosphatase that mediates a feedback loop regulating JNK activity during dorsal closure in *Drosophila. Genes Dev* **12**, 557-570.

Maruoka, Y., Ohbayashi, N., Hoshikawa, M., Itoh, N., Hogan, B. L. and Furuta, Y. (1998). Comparison of the expression of three highly related genes, *Fgf8*, *Fgf17* and *Fgf18*, in the mouse embryo. *Mech Dev* **74**, 175-177.

Mason, J. M., Morrison, D. J., Basson, M. A. and Licht, J. D. (2006). Sprouty proteins: multifaceted negative-feedback regulators of receptor tyrosine kinase signaling. *Trends in cell biology* **16**, 45-54.

Matus, D. Q., Thomsen, G. H. and Martindale, M. Q. (2007). FGF signaling in gastrulation and neural development in *Nematostella vectensis*, an anthozoan cnidarian. *Dev Genes Evol* **217**, 137-148.

McGrew, L. L., Hoppler, S. and Moon, R. T. (1997). Wnt and FGF pathways cooperatively pattern anteroposterior neural ectoderm in *Xenopus. Mech Dev* **69**, 105-114.

McGrew, L. L., Lai, C. J. and Moon, R. T. (1995). Specification of the anteroposterior neural axis through synergistic interaction of the Wnt signaling cascade with noggin and follistatin. *Dev Biol* **172**, 337-342.

McMahon, A., Reeves, G. T., Supatto, W. and Stathopoulos, A. (2010). Mesoderm migration in *Drosophila* is a multi-step process requiring FGF signaling and integrin activity. *Development* **137**, 2167-2175.

Metzger, R. J., Klein, O. D., Martin, G. R. and Krasnow, M. A. (2008). The branching programme of mouse lung development. *Nature* **453**, 745-750.

Metzger, R. J. and Krasnow, M. A. (1999). Genetic control of branching morphogenesis. *Science* **284**, 1635-1639.

Meyers, E. N., Lewandoski, M. and Martin, G. R. (1998). An *Fgf8* mutant allelic series generated by *Cre-* and *Flp*-mediated recombination. *Nat Genet* **18**, 136-141.

Michelson, A. M., Gisselbrecht, S., Buff, E. and Skeath, J. B. (1998). Heartbroken is a specific downstream mediator of FGF receptor signalling in *Drosophila*. *Development* **125**, 4379-4389.

Miller, S. C., Brown, S. J. and Tomoyasu, Y. (2008). Larval RNAi in *Drosophila*? *Dev Genes Evol* **218**, 505-510.

Miller, S. C., Miyata, K., Brown, S. J. and Tomoyasu, Y. (2012). Dissecting systemic RNA interference in the red flour beetle *Tribolium castaneum*: parameters affecting the efficiency of RNAi. *PloS one* **7**, e47431.

Min, H., Danilenko, D. M., Scully, S. A., Bolon, B., Ring, B. D., Tarpley, J. E., DeRose, M. and Simonet, W. S. (1998). Fgf-10 is required for both limb and lung development and exhibits striking functional similarity to *Drosophila branchless*. *Genes Dev* **12**, 3156-3161.

Mineta, K., Nakazawa, M., Cebria, F., Ikeo, K., Agata, K. and Gojobori, T. (2003). Origin and evolutionary process of the CNS elucidated by comparative genomics analysis of planarian ESTs. *Proc Natl Acad Sci U S A* **100**, 7666-7671.

Moussian, B. and Roth, S. (2005). Dorsoventral axis formation in the *Drosophila* embryo-shaping and transducing a morphogen gradient. *Curr Biol* **15**, R887-899.

Muha, V. and Müller, H. A. (2013). Functions and mechanisms of fibroblast growthfactor (FGF) signalling in *Drosophila melanogaster*. *International journal of molecular sciences* **14**, 5920-5937.

Murakami, S., Kan, M., McKeehan, W. L. and de Crombrugghe, B. (2000). Up-regulation of the chondrogenic *Sox9* gene by fibroblast growth factors is mediated by the mitogen-activated protein kinase pathway. *Proc Natl Acad Sci U S A* **97**, 1113-1118.

Nagy, L. M. and Carroll, S. (1994). Conservation of *wingless* patterning functions in the short-germ embryos of *Tribolium* castaneum. *Nature* **367**, 460-463.

Nakao, H. (2012). Anterior and posterior centers jointly regulate *Bombyx* embryo body segmentation. *Dev Biol* **371**, 293-301.

Nasiadka, A., Dietrich, B. H. and Krause, H. M. (2002). Anterior–posterior patterning in the *Drosophila* embryo. *Advances in Developmental Biology and Biochemistry* **12**, 155-204.

Nentwich, O., Dingwell, K. S., Nordheim, A. and Smith, J. C. (2009). Downstream of FGF during mesoderm formation in *Xenopus*: the roles of Elk-1 and Egr-1. *Dev Biol* **336**, 313-326.

Nicholson, K. M. and Anderson, N. G. (2002). The protein kinase B/Akt signalling pathway in human malignancy. *Cellular signalling* **14**, 381-395.

Northrop, J. L. and Kimelman, D. (1994). Dorsal-ventral differences in *Xcad-3* expression in response to FGF-mediated induction in *Xenopus*. *Dev Biol* **161**, 490-503.

Nunes da Fonseca, R., Lynch, J. A. and Roth, S. (2009). Evolution of axis formation: mRNA localization, regulatory circuits and posterior specification in non-model arthropods. *Curr Opin Genet Dev* **19**, 404-411.

Nunes da Fonseca, R., van der Zee, M. and Roth, S. (2010). Evolution of extracellular Dpp modulators in insects: The roles of *tolloid* and *twisted-gastrulation* in dorsoventral patterning of the *Tribolium* embryo. *Dev Biol* **345**, 80-93.

Nunes da Fonseca, R., von Levetzow, C., Kalscheuer, P., Basal, A., van der Zee, M. and Roth, S. (2008). Self-regulatory circuits in dorsoventral axis formation of the short-germ beetle *Tribolium castaneum. Dev Cell* **14**, 605-615.

Nutt, S. L., Dingwell, K. S., Holt, C. E. and Amaya, E. (2001). *Xenopus* Sprouty2 inhibits FGF-mediated gastrulation movements but does not affect mesoderm induction and patterning. *Genes Dev* **15**, 1152-1166.

Nybakken, K. and Perrimon, N. (2002). Heparan sulfate proteoglycan modulation of developmental signaling in *Drosophila. Biochimica et biophysica acta* **1573**, 280-291.

Olivera-Martinez, I. and Storey, K. G. (2007). Wnt signals provide a timing mechanism for the FGF-retinoid differentiation switch during vertebrate body axis extension. *Development* **134**, 2125-2135.

Ong, S. H., Guy, G. R., Hadari, Y. R., Laks, S., Gotoh, N., Schlessinger, J. and Lax, I. (2000). FRS2 proteins recruit intracellular signaling pathways by binding to diverse targets on fibroblast growth factor and nerve growth factor receptors. *Mol Cell Biol* **20**, 979-989.

Ornitz, D. M. (2000). FGFs, heparan sulfate and FGFRs: complex interactions essential for development. *Bioessays* **22**, 108-112.

Ornitz, D. M. and Itoh, N. (2001). Fibroblast growth factors. *Genome biology* **2**, REVIEWS3005.

Orr-Urtreger, A., Bedford, M. T., Burakova, T., Arman, E., Zimmer, Y., Yayon, A., Givol, D. and Lonai, P. (1993). Developmental localization of the splicing alternatives of fibroblast growth factor receptor-2 (FGFR2). *Dev Biol* **158**, 475-486.

Ota, S., Tonou-Fujimori, N. and Yamasu, K. (2009). The roles of the FGF signal in zebrafish embryos analyzed using constitutive activation and dominant-negative suppression of different FGF receptors. *Mech Dev* **126**, 1-17.

Panfilio, K. A. (2008). Extraembryonic development in insects and the acrobatics of blastokinesis. *Dev Biol* **313**, 471-491.

Panfilio, K. A., Liu, P. Z., Akam, M. and Kaufman, T. C. (2006). *Oncopeltus fasciatus zen* is essential for serosal tissue function in katatrepsis. *Dev Biol* **292**, 226-243.

Panfilio, K. A. and Roth, S. (2010). Epithelial reorganization events during late extraembryonic development in a hemimetabolous insect. *Dev Biol* **340**, 100-115.

Park, E. J., Watanabe, Y., Smyth, G., Miyagawa-Tomita, S., Meyers, E., Klingensmith, J., Camenisch, T., Buckingham, M. and Moon, A. M. (2008). An FGF autocrine loop initiated in second heart field mesoderm regulates morphogenesis at the arterial pole of the heart. *Development* **135**, 3599-3610.

Partanen, J., Schwartz, L. and Rossant, J. (1998). Opposite phenotypes of hypomorphic and Y766 phosphorylation site mutations reveal a function for *Fgfr1* in anteroposterior patterning of mouse embryos. *Genes Dev* **12**, 2332-2344.

Pasini, A., Manenti, R., Rothbacher, U. and Lemaire, P. (2012). Antagonizing retinoic acid and FGF/MAPK pathways control posterior body patterning in the invertebrate chordate *Ciona intestinalis*. *PloS one* **7**, e46193.

Patel, N. H., Condron, B. G. and Zinn, K. (1994). Pair-rule expression patterns of *even-skipped* are found in both short- and long-germ beetles. *Nature* **367**, 429-434.

Pavlopoulos, A., Berghammer, A. J., Averof, M. and Klingler, M. (2004). Efficient transformation of the beetle *Tribolium castaneum* using the *Minos* transposable element: quantitative and qualitative analysis of genomic integration events. *Genetics* **167**, 737-746.

Pellegrini, L., Burke, D. F., von Delft, F., Mulloy, B. and Blundell, T. L. (2000). Crystal structure of fibroblast growth factor receptor ectodomain bound to ligand and heparin. *Nature* **407**, 1029-1034.

Perkins, L. A., Johnson, M. R., Melnick, M. B. and Perrimon, N. (1996). The nonreceptor protein tyrosine phosphatase *corkscrew* functions in multiple receptor tyrosine kinase pathways in *Drosophila*. *Dev Biol* **180**, 63-81.

Perkins, L. A., Larsen, I. and Perrimon, N. (1992). *corkscrew* encodes a putative protein tyrosine phosphatase that functions to transduce the terminal signal from the receptor tyrosine kinase *torso*. *Cell* **70**, 225-236.

Perrimon, N., Pitsouli, C. and Shilo, B. Z. (2012). Signaling mechanisms controlling cell fate and embryonic patterning. *Cold Spring Harb Perspect Biol* **4**, a005975.

Peters, K. G., Marie, J., Wilson, E., Ives, H. E., Escobedo, J., Del Rosario, M., Mirda, D. and Williams, L. T. (1992). Point mutation of an FGF receptor abolishes phosphatidylinositol turnover and Ca2+ flux but not mitogenesis. *Nature* **358**, 678-681.

Petersen, C. P. and Reddien, P. W. (2009). Wnt signaling and the polarity of the primary body axis. *Cell* **139**, 1056-1068.

Petit, V., Nussbaumer, U., Dossenbach, C. and Affolter, M. (2004). Downstream-of-FGFR is a fibroblast growth factor-specific scaffolding protein and recruits Corkscrew upon receptor activation. *Mol Cell Biol* **24**, 3769-3781.

Pires-daSilva, A. and Sommer, R. J. (2003). The evolution of signalling pathways in animal development. *Nature reviews. Genetics* **4**, 39-49.

Plotnikov, A. N., Schlessinger, J., Hubbard, S. R. and Mohammadi, M. (1999). Structural basis for FGF receptor dimerization and activation. *Cell* **98**, 641-650.

Popovici, C., Roubin, R., Coulier, F. and Birnbaum, D. (2005). An evolutionary history of the FGF superfamily. *Bioessays* **27**, 849-857.

Posnien, N., Schinko, J. B., Kittelmann, S. and Bucher, G. (2010). Genetics, development and composition of the insect head--a beetle's view. *Arthropod structure & development* **39**, 399-410.

Pownall, M. and Isaacs, H. (2010). FGF signalling in vertebrate development. San Rafael (CA): Morgan & Claypool Life Sciences.

Pownall, M. E., Tucker, A. S., Slack, J. M. and Isaacs, H. V. (1996). *eFGF, Xcad3* and Hox genes form a molecular pathway that establishes the anteroposterior axis in *Xenopus*. *Development* **122**, 3881-3892.

Preger, E., Ziv, I., Shabtay, A., Sher, I., Tsang, M., Dawid, I. B., Altuvia, Y. and Ron, D. (2004). Alternative splicing generates an isoform of the human Sef gene with altered subcellular localization and specificity. *Proc Natl Acad Sci U S A* **101**, 1229-1234.

Prpic, N. M. and Damen, W. G. (2005). Cell death during germ band inversion, dorsal closure, and nervous system development in the spider *Cupiennius salei*. *Dev Dyn* **234**, 222-228.

Rafiqi, A. M., Lemke, S., Ferguson, S., Stauber, M. and Schmidt-Ott, U. (2008). Evolutionary origin of the amnioserosa in cyclorrhaphan flies correlates with spatial and temporal expression changes of *zen*. *Proc Natl Acad Sci U S A* **105**, 234-239.

Rafiqi, A. M., Lemke, S. and Schmidt-Ott, U. (2010). Postgastrular *zen* expression is required to develop distinct amniotic and serosal epithelia in the scuttle fly *Megaselia*. *Dev Biol* **341**, 282-290.

Rafiqi, A. M., Park, C. H., Kwan, C. W., Lemke, S. and Schmidt-Ott, U. (2012). BMP-dependent serosa and amnion specification in the scuttle fly *Megaselia abdita*. *Development* **139**, 3373-3382.

Rana, T. M. (2007). Illuminating the silence: understanding the structure and function of small RNAs. *Nature reviews. Molecular cell biology* **8**, 23-36.

Randi, A. M., Sperone, A., Dryden, N. H. and Birdsey, G. M. (2009). Regulation of angiogenesis by ETS transcription factors. *Biochemical Society transactions* **37**, 1248-1253.

Raucci, A., Laplantine, E., Mansukhani, A. and Basilico, C. (2004). Activation of the ERK1/2 and p38 mitogen-activated protein kinase pathways mediates fibroblast growth factor-induced growth arrest of chondrocytes. *The Journal of biological chemistry* **279**, 1747-1756.

Reeves, G. T. and Stathopoulos, A. (2009). Graded dorsal and differential gene regulation in the *Drosophila* embryo. *Cold Spring Harb Perspect Biol* **1**, a000836.

Reich, A., Sapir, A. and Shilo, B. (1999). Sprouty is a general inhibitor of receptor tyrosine kinase signaling. *Development* **126**, 4139-4147.

Reifers, F., Bohli, H., Walsh, E. C., Crossley, P. H., Stainier, D. Y. and Brand, M. (1998). *Fgf8* is mutated in zebrafish *acerebellar (ace)* mutants and is required for maintenance of midbrain-hindbrain boundary development and somitogenesis. *Development* **125**, 2381-2395.

Reifers, F., Walsh, E. C., Leger, S., Stainier, D. Y. and Brand, M. (2000). Induction and differentiation of the zebrafish heart requires fibroblast growth factor 8 (*fgf8/acerebellar*). *Development* **127**, 225-235.

Reim, I., Hollfelder, D., Ismat, A. and Frasch, M. (2012). The FGF8-related signals Pyramus and Thisbe promote pathfinding, substrate adhesion, and survival of migrating longitudinal gut muscle founder cells. *Dev Biol* **368**, 28-43.

Ren, Y., Li, Z., Rong, Z., Cheng, L., Li, Y., Wang, Z. and Chang, Z. (2007). Tyrosine 330 in hSef is critical for the localization and the inhibitory effect on FGF signaling. *Biochemical and biophysical research communications* **354**, 741-746.

Rentzsch, F., Fritzenwanker, J. H., Scholz, C. B. and Technau, U. (2008). FGF signalling controls formation of the apical sensory organ in the cnidarian *Nematostella vectensis*. *Development* **135**, 1761-1769.

Ribisi, S., Jr., Mariani, F. V., Aamar, E., Lamb, T. M., Frank, D. and Harland, R. M. (2000). Ras-mediated FGF signaling is required for the formation of posterior but not anterior neural tissue in *Xenopus laevis*. *Dev Biol* **227**, 183-196.

Richards, S., Gibbs, R. A., Weinstock, G. M., Brown, S. J., Denell, R., Beeman, R. W., Gibbs, R., Bucher, G., Friedrich, M., Grimmelikhuijzen, C. J., et al. (2008). The genome of the model beetle and pest *Tribolium castaneum*. *Nature* **452**, 949-955.

Rizki, T. M. and Rizki, R. M. (1978). Larval adipose tissue of homoeotic bithorax mutants of *Drosophila*. *Dev Biol* **65**, 476-482.

Röttinger, E., Saudemont, A., Duboc, V., Besnardeau, L., McClay, D. and Lepage, T. (2008). FGF signals guide migration of mesenchymal cells, control skeletal morphogenesis and regulate gastrulation during sea urchin development. *Development* **135**, 353-365.

Ruoslahti, E. and Yamaguchi, Y. (1991). Proteoglycans as modulators of growth factor activities. *Cell* **64**, 867-869.

Sambrook, J., Fritsch, E. F. and Maniatis, T. (1989). *Molecular cloning - a laboratory manual*: Cold Spring Harbour Press.

Sanches-Salazar, J., Pletcher, M.T., Bennett, R.L., Brown, S.J., Dandamudi, T.J., Denell, R.E., Dotor, J.S. (1996). The *Tribolium decapentaplegic* gene is similar in sequence, structure, and expression to the *Drosophila dpp* gene. *Dev Genes Evol* **206**, 237–246.

Sasai, Y., Lu, B., Steinbeisser, H. and De Robertis, E. M. (1995). Regulation of neural induction by the Chd and Bmp-4 antagonistic patterning signals in *Xenopus*. *Nature* **377**, 757.

Sasaki, A., Taketomi, T., Kato, R., Saeki, K., Nonami, A., Sasaki, M., Kuriyama, M., Saito, N., Shibuya, M. and Yoshimura, A. (2003). Mammalian Sprouty4 suppresses Ras-independent ERK activation by binding to Raf1. *Nature cell biology* **5**, 427-432.

Sato, M. and Kornberg, T. B. (2002). FGF is an essential mitogen and chemoattractant for the air sacs of the *Drosophila* tracheal system. *Dev Cell* **3**, 195-207.

Sato, T., Araki, I. and Nakamura, H. (2001). Inductive signal and tissue responsiveness defining the tectum and the cerebellum. *Development* **128**, 2461-2469.

Satou, Y., Imai, K. S. and Satoh, N. (2002). Fgf genes in the basal chordate *Ciona intestinalis*. *Dev Genes Evol* **212**, 432-438.

Schetelig, M. F., Schmid, B. G., Zimowska, G. and Wimmer, E. A. (2008). Plasticity in mRNA expression and localization of *orthodenticle* within higher Diptera. *Evolution & development* **10**, 700-704.

Schinko, J., Posnien, N., Kittelmann, S., Koniszewski, N. and Bucher, G. (2009). Single and double whole-mount *in situ* hybridization in red flour beetle (*Tribolium*) embryos. *Cold Spring Harb Protoc* **2009**, pdb prot5258.

Schinko, J. B., Kreuzer, N., Offen, N., Posnien, N., Wimmer, E. A. and Bucher, G. (2008). Divergent functions of *orthodenticle*, *empty spiracles* and *buttonhead* in early head patterning of the beetle *Tribolium castaneum* (Coleoptera). *Dev Biol* **317**, 600-613.

Schinko, J. B., Weber, M., Viktorinova, I., Kiupakis, A., Averof, M., Klingler, M., Wimmer, E. A. and Bucher, G. (2010). Functionality of the *GAL4/UAS* system in *Tribolium* requires the use of endogenous core promoters. *BMC Dev Biol* **10**, 53.

Schlessinger, J. (2000). Cell signaling by receptor tyrosine kinases. *Cell* **103**, 211-225.

Schlessinger, J., Plotnikov, A. N., Ibrahimi, O. A., Eliseenkova, A. V., Yeh, B. K., Yayon, A., Linhardt, R. J. and Mohammadi, M. (2000). Crystal structure of a ternary FGF-FGFR-heparin complex reveals a dual role for heparin in FGFR binding and dimerization. *Molecular cell* **6**, 743-750.

Schmid, B., Fürthauer, M., Connors, S. A., Trout, J., Thisse, B., Thisse, C. and Mullins, M. C. (2000). Equivalent genetic roles for bmp7/snailhouse and bmp2b/swirl in dorsoventral pattern formation. *Development* **127**, 957-967.

Schmidt-Ott, U. (2000). The amnioserosa is an apomorphic character of cyclorrhaphan flies. *Dev Genes Evol* **210**, 373-376.

Schoppmeier, M. and Schröder, R. (2005). Maternal *torso* signaling controls body axis elongation in a short germ insect. *Curr Biol* **15**, 2131-2136.

Schröder, R. (2003). The genes *orthodenticle* and *hunchback* substitute for *bicoid* in the beetle *Tribolium*. *Nature* **422**, 621 – 625.

Schröder, R., Beermann, A., Wittkopp, N. and Lutz, R. (2008). From development to biodiversity-*Tribolium* castaneum, an insect model organism for short germband development. *Dev Genes Evol* **218**, 119-126.

Scotto-Lavino, E., Du, G. and Frohman, M. A. (2006a). 3' end cDNA amplification using classic RACE. *Nature protocols* **1**, 2742-2745.

Scotto-Lavino, E., Du, G. and Frohman, M. A. (2006b). 5' end cDNA amplification using classic RACE. *Nature protocols* **1**, 2555-2562.

Seyres, D., Roder, L. and Perrin, L. (2012). Genes and networks regulating cardiac development and function in flies: genetic and functional genomic approaches. *Briefings in functional genomics* **11**, 366-374.

Shamim, H. and Mason, I. (1999). Expression of *Fgf4* during early development of the chick embryo. *Mech Dev* **85**, 189-192.

Sharma, R., Beermann, A. and Schröder, R. (2013a). The dynamic expression of extraembryonic marker genes in the beetle *Tribolium castaneum* reveals the complexity of serosa and amnion formation in a short germ insect. *Gene expression patterns : GEP* **13**, 362-371.

Sharma, R., Beermann, A. and Schröder, R. (2013b). FGF signalling controls anterior extraembryonic and embryonic fate in the beetle *Tribolium*. *Developmental biology* **381**, 121-133.

Sheng, G., dos Reis, M. and Stern, C. D. (2003). Churchill, a zinc finger transcriptional activator, regulates the transition between gastrulation and neurulation. *Cell* **115**, 603-613.

Shishido, E., Higashijima, S., Emori, Y. and Saigo, K. (1993). Two FGF-receptor homologues of *Drosophila*: one is expressed in mesodermal primordium in early embryos. *Development* **117**, 751-761.

Shishido, E., Ono, N., Kojima, T. and Saigo, K. (1997). Requirements of DFR1/Heartless, a mesoderm-specific *Drosophila* FGF-receptor, for the formation of heart, visceral and somatic muscles, and ensheathing of longitudinal axon tracts in CNS. *Development* **124**, 2119-2128.

Sivak, J. M., Petersen, L. F. and Amaya, E. (2005). FGF signal interpretation is directed by Sprouty and Spred proteins during mesoderm formation. *Dev Cell* **8**, 689-701.

Slack, J. M., Darlington, B. G., Heath, J. K. and Godsave, S. F. (1987). Mesoderm induction in early *Xenopus* embryos by heparin-binding growth factors. *Nature* **326**, 197-200.

Sokoloff, A. (1974). The Biology of *Tribolium. Clarendon Press, Oxford, UK.*

Spivak-Kroizman, T., Lemmon, M. A., Dikic, I., Ladbury, J. E., Pinchasi, D., Huang, J., Jaye, M., Crumley, G., Schlessinger, J. and Lax, I. (1994a). Heparin-induced oligomerization of FGF molecules is responsible for FGF receptor dimerization, activation, and cell proliferation. *Cell* **79**, 1015-1024.

Spivak-Kroizman, T., Mohammadi, M., Hu, P., Jaye, M., Schlessinger, J. and Lax, I. (1994b). Point mutation in the fibroblast growth factor receptor eliminates phosphatidylinositol hydrolysis without affecting neuronal differentiation of PC12 cells. *The Journal of biological chemistry* **269**, 14419-14423.

Srivastava, D. (2006). Making or breaking the heart: from lineage determination to morphogenesis. *Cell* **126**, 1037-1048.

Staehling-Hampton, K., Hoffmann, F. M., Baylies, M. K., Rushton, E. and Bate, M. (1994). *dpp* induces mesodermal gene expression in *Drosophila. Nature* **372**, 783-786.

Stathopoulos, A., Tam, B., Ronshaugen, M., Frasch, M. and Levine, M. (2004). *pyramus* and *thisbe*: FGF genes that pattern the mesoderm of *Drosophila* embryos. *Genes Dev* **18**, 687-699.

Stavridis, M. P., Collins, B. J. and Storey, K. G. (2010). Retinoic acid orchestrates fibroblast growth factor signalling to drive embryonic stem cell differentiation. *Development* **137**, 881-890.

Sternberg, P. W. and Alberola-Ila, J. (1998). Conspiracy theory: RAS and RAF do not act alone. *Cell* **95**, 447-450.

Stewart, A. E., Dowd, S., Keyse, S. M. and McDonald, N. Q. (1999). Crystal structure of the MAPK phosphatase Pyst1 catalytic domain and implications for regulated activation. *Nature structural biology* **6**, 174-181.

Storey, K. G., Goriely, A., Sargent, C. M., Brown, J. M., Burns, H. D., Abud, H. M. and Heath, J. K. (1998). Early posterior neural tissue is induced by FGF in the chick embryo. *Development* **125**, 473-484.

Streit, A., Berliner, A. J., Papanayotou, C., Sirulnik, A. and Stern, C. D. (2000). Initiation of neural induction by FGF signalling before gastrulation. *Nature* **406**, 74-78.

Sun, X., Meyers, E. N., Lewandoski, M. and Martin, G. R. (1999). Targeted disruption of *Fgf8* causes failure of cell migration in the gastrulating mouse embryo. *Genes Dev* **13**, 1834-1846.

Sutherland, D., Samakovlis, C. and Krasnow, M. A. (1996). *branchless* encodes a *Drosophila* FGF homolog that controls tracheal cell migration and the pattern of branching. *Cell* **87**, 1091-1101.

Takada, S., Stark, K. L., Shea, M. J., Vassileva, G., McMahon, J. A. and McMahon, A. P. (1994). *Wnt-3a* regulates somite and tailbud formation in the mouse embryo. *Genes Dev* **8**, 174-189.

Tautz, D., Friedrich, M. and Schröder, R. (1994). Insect embryogenesis - what is ancestral and what is derived? *Development* **Supplement**, 193-199.

Tautz, D. and Pfeifle, C. (1989). A non-radioactive in situ hybridization method for the localization of specific RNAs in *Drosophila* embryos reveals translational control of the segmentation gene *hunchback*. *Chromosoma* **98**, 81-85.

The Honeybee Genome Sequencing Consortium, W. G., Robinson GE, Gibbs RA, Weinstock GM, Robinson GE, Worley KC, Evans JD, Maleszka R, Robertson HM, Weaver DB, Beye M, Bork P, Elsik CG, Evans JD, Hartfelder K, Hunt GJ, Robertson HM, Robinson GE, Ma (2006). Insights into social insects from the genome of the honeybee *Apis mellifera*. In *Nature*, pp. 931-949.

Thien, C. B. and Langdon, W. Y. (2001). Cbl: many adaptations to regulate protein tyrosine kinases. *Nature reviews. Molecular cell biology* **2**, 294-307.

Thisse, B. and Thisse, C. (2005). Functions and regulations of fibroblast growth factor signaling during embryonic development. *Dev Biol* **287**, 390-402.

Tomoyasu, Y. and Denell, R. E. (2004). Larval RNAi in *Tribolium* (Coleoptera) for analyzing adult development. *Dev Genes Evol* **214**, 575-578.

Tsang, M., Friesel, R., Kudoh, T. and Dawid, I. B. (2002). Identification of Sef, a novel modulator of FGF signalling. *Nature cell biology* **4**, 165-169.

Tulin, S. and Stathopoulos, A. (2010). Extending the family table: Insights from beyond vertebrates into the regulation of embryonic development by FGFs. *Birth Defects Res C Embryo Today* **90**, 214-227.

Turner, N. and Grose, R. (2010). Fibroblast growth factor signalling: from development to cancer. *Nature reviews. Cancer* **10**, 116-129.

Ueda, Y., Hirai, S., Osada, S., Suzuki, A., Mizuno, K. and Ohno, S. (1996). Protein kinase C activates the MEK-ERK pathway in a manner independent of Ras and dependent on Raf. *The Journal of biological chemistry* **271**, 23512-23519.

Ullrich, A. and Schlessinger, J. (1990). Signal transduction by receptors with tyrosine kinase activity. *Cell* **61**, 203-212.

Umbhauer, M., Marshall, C. J., Mason, C. S., Old, R. W. and Smith, J. C. (1995). Mesoderm induction in *Xenopus* caused by activation of MAP kinase. *Nature* **376**, 58-62.

Umbhauer, M., Penzo-Mendez, A., Clavilier, L., Boucaut, J. and Riou, J. (2000). Signaling specificities of fibroblast growth factor receptors in early *Xenopus* embryo. *Journal of cell science* **113 (Pt 16)**, 2865-2875.

Vainikka, S., Partanen, J., Bellosta, P., Coulier, F., Birnbaum, D., Basilico, C., Jaye, M. and Alitalo, K. (1992). Fibroblast growth factor receptor-4 shows novel features in genomic structure, ligand binding and signal transduction. *The EMBO journal* **11**, 4273-4280.

van der Zee, M., Berns, N. and Roth, S. (2005). Distinct functions of the *Tribolium zerknüllt* genes in serosa specification and dorsal closure. *Curr Biol* **15**, 624-636.

van der Zee, M., da Fonseca, R. N. and Roth, S. (2008). TGFbeta signaling in *Tribolium*: vertebrate-like components in a beetle. *Dev Genes Evol* **218**, 203-213.

van der Zee, M., Stockhammer, O., von Levetzow, C., Nunes da Fonseca, R. and Roth, S. (2006). Sog/Chordin is required for ventral-to-dorsal Dpp/BMP transport and head formation in a short germ insect. *Proc Natl Acad Sci U S A* **103**, 16307-16312.

Veeramachaneni, V., Makalowski, W., Galdzicki, M., Sood, R. and Makalowska, I. (2004). Mammalian overlapping genes: the comparative perspective. *Genome research* **14**, 280-286.

Vincent, S., Wilson, R., Coelho, C., Affolter, M. and Leptin, M. (1998). The *Drosophila* protein Dof is specifically required for FGF signaling. *Molecular cell* **2**, 515-525.

Wagner, E. and Levine, M. (2012). FGF signaling establishes the anterior border of the *Ciona* neural tube. *Development* **139**, 2351-2359.

Wang, F., Kan, M., Yan, G., Xu, J. and McKeehan, W. L. (1995). Alternately spliced NH2-terminal immunoglobulin-like Loop I in the ectodomain of the fibroblast growth factor (FGF) receptor 1 lowers affinity for both heparin and FGF-1. *The Journal of biological chemistry* **270**, 10231-10235.

Wasylyk, B., Hagman, J. and Gutierrez-Hartmann, A. (1998). Ets transcription factors: nuclear effectors of the Ras-MAP-kinase signaling pathway. *Trends in biochemical sciences* **23**, 213-216.

Weeks, D. L. and Melton, D. A. (1987). A maternal mRNA localized to the vegetal hemisphere in *Xenopus* eggs codes for a growth factor related to TGF-beta. *Cell* **51**, 861-867.

Weinstein, D. C. and Hemmati-Brivanlou, A. (1999). Neural induction. *Annual review of cell and developmental biology* **15**, 411-433.

Wells, J. M. and Melton, D. A. (2000). Early mouse endoderm is patterned by soluble factors from adjacent germ layers. *Development* **127**, 1563-1572.

Werren, J. H., Richards, S., Desjardins, C. A., Niehuis, O., Gadau, J., Colbourne, J. K., et al. (2010). Functional and evolutionary insights from the genomes of three parasitoid *Nasonia* species. *Science* **327**, 343-348.

Wesche, J., Haglund, K. and Haugsten, E. M. (2011). Fibroblast growth factors and their receptors in cancer. *Biochem J* **437**, 199-213.

Wiedemann, M. and Trueb, B. (2000). Characterization of a novel protein (FGFRL1) from human cartilage related to FGF receptors. *Genomics* **69**, 275-279.

Wills, A. E., Choi, V. M., Bennett, M. J., Khokha, M. K. and Harland, R. M. (2010). BMP antagonists and FGF signaling contribute to different domains of the neural plate in *Xenopus. Dev Biol* **337**, 335-350.

Wilson, M. J. and Dearden, P. K. (2011). Diversity in insect axis formation: two *orthodenticle* genes and *hunchback* act in anterior patterning and influence dorsoventral organization in the honeybee (*Apis mellifera*). *Development* **138**, 3497-3507.

Wilson, R., Vogelsang, E. and Leptin, M. (2005). FGF signalling and the mechanism of mesoderm spreading in *Drosophila* embryos. *Development* **132**, 491-501.

Wilson, S. I., Graziano, E., Harland, R., Jessell, T. M. and Edlund, T. (2000). An early requirement for FGF signalling in the acquisition of neural cell fate in the chick embryo. *Curr Biol* **10**, 421-429.

Xiong, S., Zhao, Q., Rong, Z., Huang, G., Huang, Y., Chen, P., Zhang, S., Liu, L. and Chang, Z. (2003). hSef inhibits PC-12 cell differentiation by interfering with Ras-mitogen-activated protein kinase MAPK signaling. *The Journal of biological chemistry* **278**, 50273-50282.

Xu, X., Li, C., Takahashi, K., Slavkin, H. C., Shum, L. and Deng, C. X. (1999). Murine fibroblast growth factor receptor 1alpha isoforms mediate node regression and are essential for posterior mesoderm development. *Dev Biol* **208**, 293-306.

Yamaguchi, T. P., Harpal, K., Henkemeyer, M. and Rossant, J. (1994). *fgfr-1* is required for embryonic growth and mesodermal patterning during mouse gastrulation. *Genes Dev* **8**, 3032-3044.

Yang, X., Dormann, D., Munsterberg, A. E. and Weijer, C. J. (2002). Cell movement patterns during gastrulation in the chick are controlled by positive and negative chemotaxis mediated by FGF4 and FGF8. *Dev Cell* **3**, 425-437.

Yasuo, H. and Hudson, C. (2007). FGF8/17/18 functions together with FGF9/16/20 during formation of the notochord in *Ciona* embryos. *Dev Biol* **302**, 92-103.

Yeku, O., Scotto-Lavino, E. and Frohman, M. A. (2009). Identification of alternative transcripts using rapid amplification of cDNA ends (RACE). *Methods Mol Biol* **590**, 279-294.

Yin, Z., Xu, X. L. and Frasch, M. (1997). Regulation of the *twist* target gene *tinman* by modular cis-regulatory elements during early mesoderm development. *Development* **124**, 4971-4982.

Yip, M. L., Lamka, M. L. and Lipshitz, H. D. (1997). Control of germ-band retraction in *Drosophila* by the zinc-finger protein HINDSIGHT. *Development* **124**, 2129-2141.

Zaffran, S. and Frasch, M. (2002). Early signals in cardiac development. *Circulation research* **91**, 457-469.

Zahedi, B., Shen, W., Xu, X., Chen, X., Mahey, M. and Harden, N. (2008). Leading edge-secreted Dpp cooperates with ACK-dependent signaling from the amnioserosa to regulate myosin levels during dorsal closure. *Dev Dyn* **237**, 2936-2946.

Zhang, J. (2003). Evolution by gene duplication: an update. *TRENDS in Ecology and Evolution* **18**, 7.

Zhang, J., Zhou, B., Zheng, C. F. and Zhang, Z. Y. (2003). A bipartite mechanism for ERK2 recognition by its cognate regulators and substrates. *The Journal of biological chemistry* **278**, 29901-29912.

Zhao, Y. and Zhang, Z. Y. (2001). The mechanism of dephosphorylation of extracellular signal-regulated kinase 2 by mitogen-activated protein kinase phosphatase 3. *The Journal of biological chemistry* **276**, 32382-32391.

Zhu, M. Y., Wilson, R. and Leptin, M. (2005). A screen for genes that influence fibroblast growth factor signal transduction in *Drosophila*. *Genetics* **170**, 767-777.

Zorn, A. M., Barish, G. D., Williams, B. O., Lavender, P., Klymkowsky, M. W. and Varmus, H. E. (1999). Regulation of Wnt signaling by Sox proteins: XSox17 alpha/beta and XSox3 physically interact with beta-catenin. *Molecular cell* **4**, 487-498.

Appendix

Table S 1: Genes / non-overlapping fragments used for pRNAi-based functional analysis.

Gene	Clone	Size	Intronic Sequence	Additional Sequence	Position (CDS)	Forward primer (5´-3´)	Reverse primer (5´-3´)
Tc-fgf1a (a_1a_2)*	288	303 bp	NA	31 bp (5´UTR)	16-287	AAGCAGTGGTATCAACGCAGAGT**	ACGGCGAGGTTGTGTCTAGTTCTG
Tc-fgf1a (a_2a_3)	289	704 bp	NA;	183 bp (3´UTR+PolyA tail)	119-639	GAGTGGAGGACGCTCCCAGTTCA	AAGCAGTGGTATCAACGCAGAGT**
Tc-fgf1a (a_2a_3)	128	462 bp	39 bp	NA	128-550	ACGCTCCCAGTTCACACGCCTCTAT	TTATCCCGATGTACCACCCCAAATG
Tc-fgf1a (a_3)*	290	381 bp	NA	146 bp (3´UTR+PolyA tail)	405-639	CTACGTCGCCATGGACCCCAAAG	AAGCAGTGGTATCAACGCAGAGT**
Tc-fgf1a (a_3)*	281	381 bp	NA	146 bp (3´UTR+PolyA tail)	405-639	CTACGTCGCCATGGACCCCAAAG	AAGCAGTGGTATCAACGCAGAGT**
Tc-fgf1b (b_1b_2)	229	499 bp	75	NA	6-429	CGAAAAGCCAAGCTGGCATGGGA	TAGCTGTTGCAATTCCGCTTCCG
Tc-fgf1b (b_1b_2)	293	1107 bp	39 bp	591 bp (3´UTR+PolyA tail)	1-441	ATGGACGAAAAGCCAAGCTGGCATG	AAGCAGTGGTATCAACGCAGAGT**
Tc-fgf1b (b_2)	295	701 bp	NA	558 bp (3´UTR+PolyA tail)	299-441	ATCATCCGGACTGGTACATTGGGA	AAGCAGTGGTATCAACGCAGAGT**
Tc-fgf1 (a_3b_1)	228	699 bp	179 (a_3-b_1)	NA	343-639 (a_3) 1-223 (b_1)	TTGGAGGTAATGTCGGCTGGGCA	CCGCGTACAAATTTCCCGAATCGT
Tc-fgf1 (a_3b_1)	292	483 bp	179 (a_3-b_1)	NA	590-639 (a_3) 1-223 (b_1)	CCGCGTACAAATTTCCCGAATCGT	AAGCAGTGGTATCAACGCAGAGT**
Tc-fgf1 ($a_3b_1b_2$)	129	791 bp	179 (a_3-b_1) 75 (b_1-b_2)	NA	466-639 (a_3) 1-363 (b_1b_2)	ACCATTTTTATCGAGGCGTTTCAA	CTGCGTCCGTTTTCCATTCTTCAT
Tc-fgf8	167	658 bp	NA	NA	17-674	GAAACATCATAAACCGCACTATTTG	TCATTCATGCTTACACACGTCCAC
Tc-fgf8	125	420 bp	NA	NA	175-594	CATGTAACGTCGGTGTGAGAAA	GTCCGACAAGAAAGAACTATCAC
Tc-fgfr	180	556 bp	NA	NA	166-719	CAAAATGTGGGGCTAAAGGTA	GTCGATAAAGTAAACGTGTGA
Tc-fgfr2	249	846 bp	NA	NA	918-1781	AGAGGAGGAGAACACTGTGCCTG	GGTTCGGAGACATCCTCGTTGGTG
Tc-dof	188	810 bp	NA	NA	-	-	-
Tc-csw	227	769 bp	NA	NA	503-1248	AATACGATGTTGGTGGCGGCGAG	GGTCTGAAGGCACGCCATGATCC
Tc-byn	35	~ 1.2 kb	NA	NA	NA	NA	NA
Tc-dll	2	900 bp	NA	NA	NA	NA	NA

Table S 2: Overview of genes used as molecular markers for expression studies.

Gene	GLEAN_Number	Size	Source	Binding position (CDS)	Clone number
Tc-zen1	TC000921	792 bp	Reinhard Schröder	23–814	1
Tc-iro	TC003632	1097 bp	Self cloned	391–1487	286
Tc-otd1	TC003354	917 bp	Reinhard Schröder	-	17
Tc-wnt1	TC014084	~ 1.6 kb	Reinhard Schröder	-	40
Tc-sog	TC012650	~ 900 bp	Jeremy Lynch	-	297
Tc-dpp	TC008466	702 bp	Jeremy Lynch	248–945	299
Tc-twist	TC014598	514 bp	Reinhard Schröder	-	177
Tc-hnt	TC009560	602 bp	Anke Beermann	1606–2078	303
Tc-fgf1b	TC006603	499 bp	Self cloned	6-429	229

Table S 3: Primers used in RACE-PCR reactions as GSPs and NGSPs.

Stock Number (lab)	Size (bp)	Sequence (5'➔3')	Primer Name	used in
Primer #11	25	TGGAAAACGGGACTAGTGACAGTGA	FGF a1_2-Fw	3' RACE
Primer #142	22	AAACGGGACTAGTGACAGTGAT	FGF A1_6-Fw	3' RACE
Primer #12	23	GAGTGGAGGACGCTCCCAGTTCA	FGF a2_6-Fw	3' RACE
Primer #14	23	CTACGTCGCCATGGACCCCAAAG	FGF a3_68-Fw	3' RACE
Primer #143	25	ATGGACGAAAAGCCAAGCTGGCATG	FGF B1_1-Fw	3' RACE
Primer #13	23	TTGGAGGTAATGTCGGCTGGGCA	FGF a3_6-Fw	3' RACE
Primer #15	23	CGAAAAGCCAAGCTGGCATGGGA	FGF b1_6-Fw	3' RACE
Primer #131	24	ATCGCCTTTTGGCCGTACTTGGTC	FGF a3_268-Rv	5' RACE
Primer #132	24	GCGTACTTTAGGGAGAGATAGGTG	FGF a3_187-Rv	5' RACE
Primer #133	24	ACGGCGAGGTTGTGTCTAGTTCTG	FGF a2_174-Rv	5' RACE
Primer #134	19	CGCAATTCCCCTTTTCGTC	FGF a1_111-Rv	5' RACE
Primer #144	24	ATGGGCACGTTTTGGGCACAAGGG	FGF B1_80-Fw	3' RACE
Primer #145	24	ATCATCCGGACTGGTACATTGGGA	FGF B2_74-Fw	3' RACE
Primer #146	25	GAAGAATGGAAAACGGACGCAGTGG	FGF B2_117-Fw	3' RACE
Primer #18	23	TAGCTGTTGCAATTCCGCTTCCG	FGF b2_182-Rv	5' RACE
Primer #16	24	CCGCGTACAAATTTCCCGAATCGT	FGF b1_200-Rv	5' RACE
Primer #17	23	CGCTCCTTGAATCCTGACATGGG	FGF b1_152-Rv	5' RACE
Primer #147	26	CCGCTTCCGATACATTTCTGTTGGGC	FGF B2_190-Rv	5' RACE
Primer #129	24	GCGTTTTCTCCCTGTTGGTTGTCC	Tc-005517-fgf2-RACE-Fw-17	3' RACE
Primer #130	22	GACATGCTGTGAGGTGATAAGG	Tc-005517-fgf2-RACE-Fw-65	3' RACE
Primer #135	24	GAGGGCCCCGGATGGTTCAGATAG	Tc5517-Rv-1269	5' RACE
Primer #128	22	CGTACTGGGCGATGGGTTGGTG	Tc5517-Rv-1160	5' RACE
Primer #126	22	TGTGCTTGCTTGTAGGTGCGGA	Tc5517-Rv-773	5' RACE

Figure S 1: Mock (water) injection and positive control (*Tc-dll* and *Tc-byn*) injection experiments. (A) Graph showing the statistical analysis for water, *Tc-dll* and *Tc-byn* injection experiments. (B-G) Cuticular analysis of *Tc-dll*[RNAi] (B-F) and *Tc-byn*[RNAi] (G) first instar larvae showing gene specific knockdown phenotypes. (B) A hatched *Tc-dll*[RNAi] larva showing loss of distal appendages in head, legs and urogomphi structures. (C-F) Magnified images clearly show loss of distal part of the antenna (asterisks) in head (C-D), in legs (asterisk)- only coxa and trochanter remains (E) and in the urogomphi (F). (G) A *Tc-byn*[RNAi] first instar larva showing abnormal hindgut (red circle) and urogomphi (white arrows) phenotype.
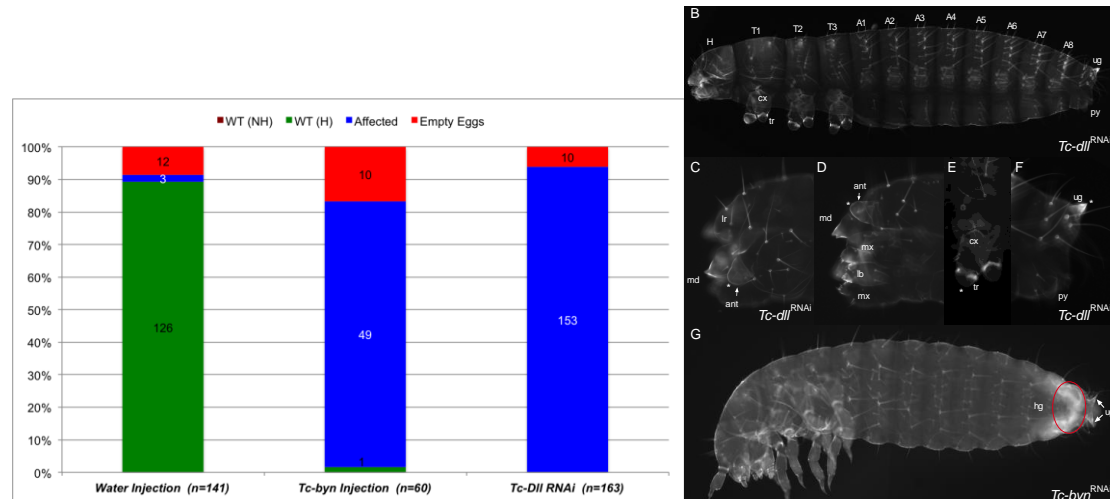
Figure S 2: Overview of 5' RACE-PCR mechanism (image taken from the kit manual).
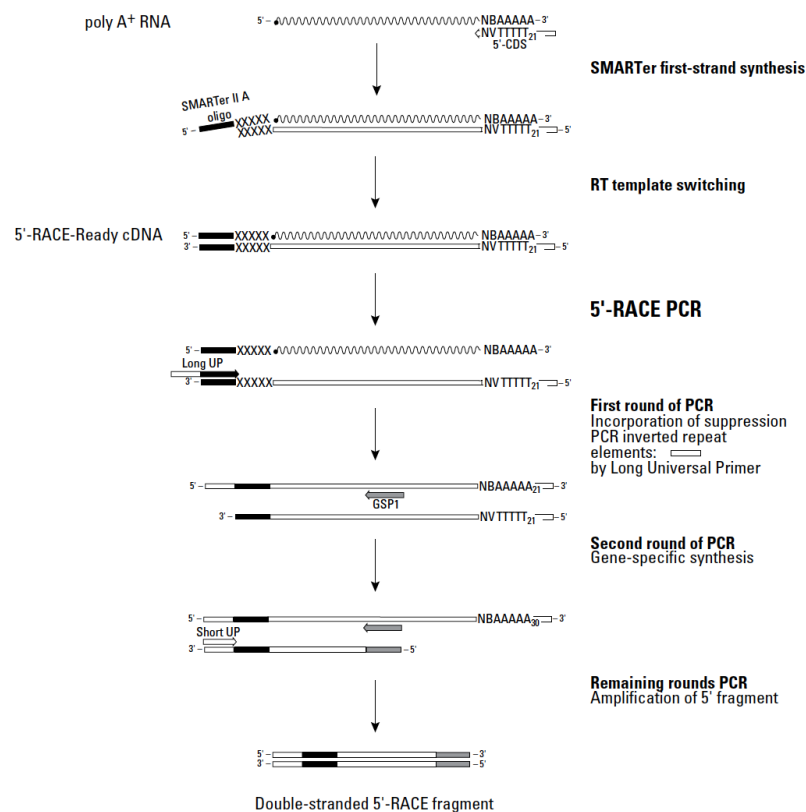
SMARTer II A Oligonucleotide (12 µM)
5'–AAGCAGTGGTATCAACGCAGAGTACXXXXX–3' (X = undisclosed base in the proprietary SMARTer oligo sequence)

5'-RACE CDS Primer A (5'-CDS; 12 µM)

5'–(T)25V N–3' (N = A, C, G, or T; V = A, G, or C)

10X Universal Primer A Mix (UPM)
Long (0.4 μM):   5'–ctaatacgactcactatagggc AAGCAGTGGTATCAACGCAGAGT–3'
Short (2 μM):   5'–ctaatacgactcactatagggc –3'

Nested Universal Primer A (NUP; 10 μM)
5'–AAGCAGTGGTATCAACGCAGAGT–3'Control Reagents

Figure S 3: Overview of 3' RACE-PCR mechanism (image taken from the kit manual).
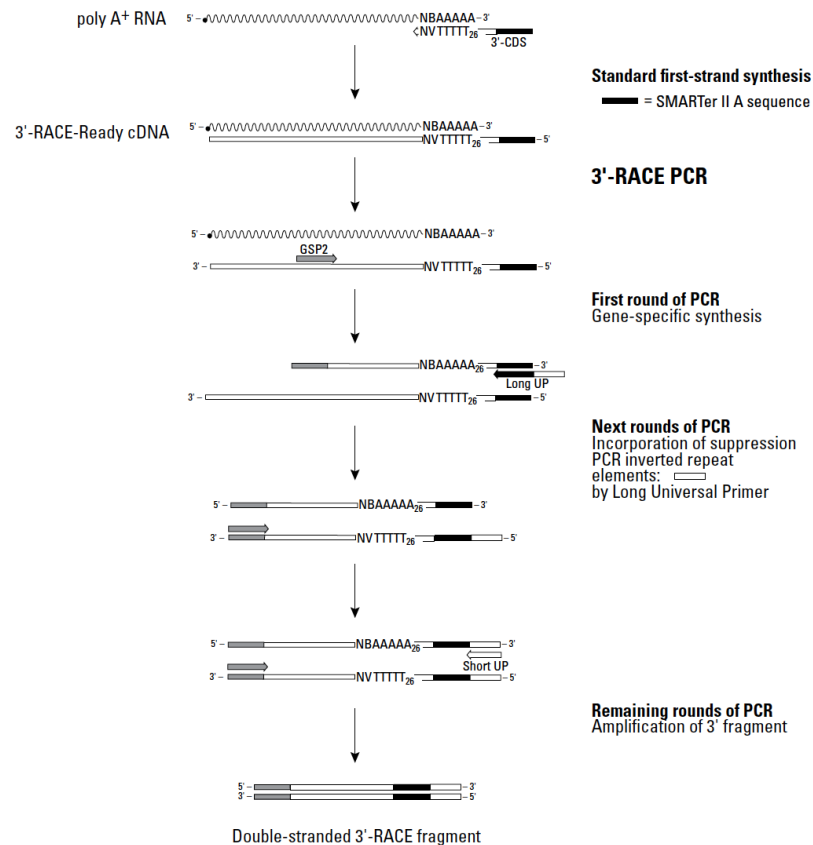
3'-RACE CDS Primer A (3'-CDS; 12 μM)

5'–AAGCAGTGGTATCAACGCAGAGTAC(T)30 V N–3' (N = A, C, G, or T; V = A, G, or C)

10X Universal Primer A Mix (UPM)
Long (0.4 μM):   5'–ctaatacgactcactatagggc AAGCAGTGGTATCAACGCAGAGT–3'
Short (2 μM):   5'–ctaatacgactcactatagggc –3'

Nested Universal Primer A (NUP; 10 μM)
5'–AAGCAGTGGTATCAACGCAGAGT–3'Control Reagents

Figure S 4: Overview of failed 5' RACE-PCR and nested-PCR reactions executed to identify the 5' end of *Tc-fgf1a* (TC006602) gene. All the amplified products from both the nested reactions were found as artefacts as none of them showed desired gene characteristic sequences. (GSP, Gene Specific Primer; NGSP, Nested Gene Specific Primer; UPM, Universal Primer A Mix; NUP, Nested Universal Primer A; left-right arrow to bar in (ii) represents 2.9 kb of genomic region).
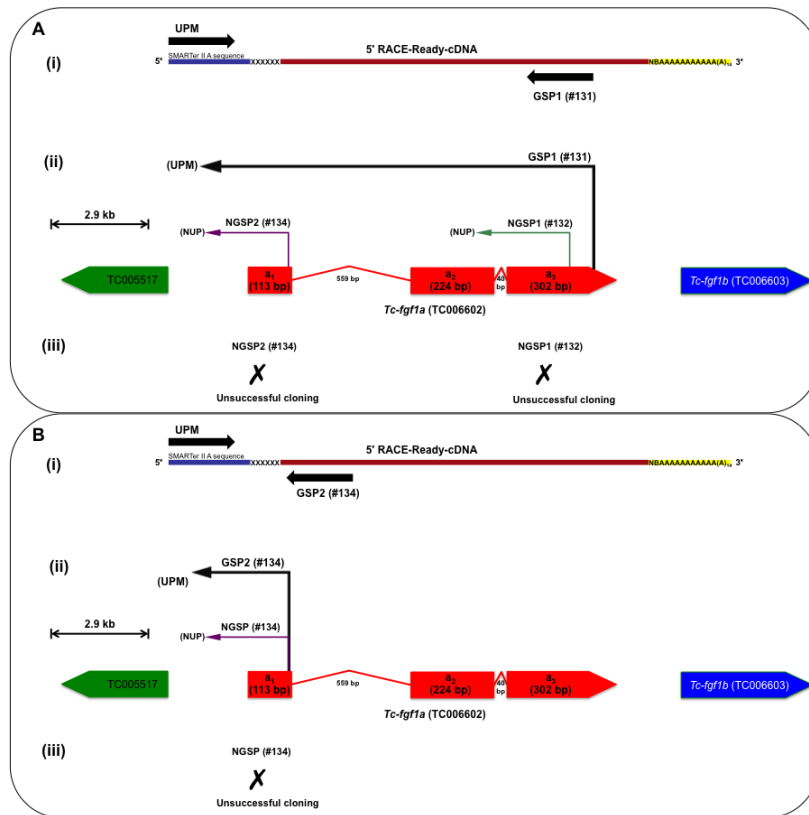
Figure S 5: Overview of failed 5' RACE-PCR and nested-PCR reaction executed to identify the 5' end of *Tc-fgf1b* (TC006603) gene. No amplified product was characterized due to failed cloning. (GSP, Gene Specific Primer; NGSP, Nested Gene Specific Primer; UPM, Universal Primer A Mix; NUP, Nested Universal Primer A; left-right arrow to bar in (ii) represents 5.8 kb of genomic region)
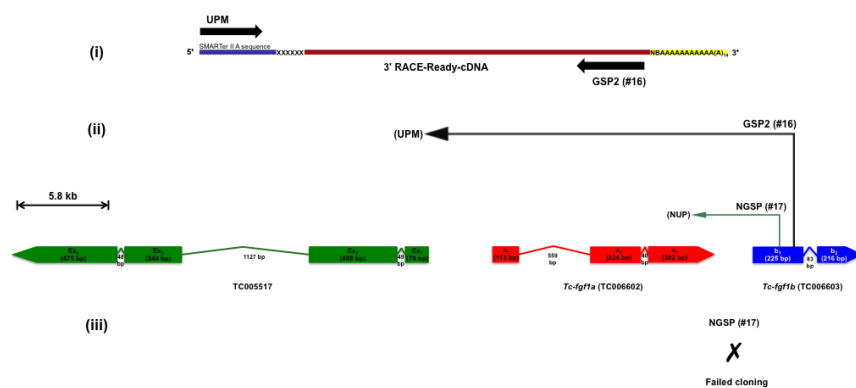
Figure S 6: Overview of failed 3' RACE-PCR and nested-PCR reactions executed in search of an interconnection between *Tc-fgf1b* (TC006603) and *Tc005517* gene also in 3' direction. All the amplified products from both the nested reactions were either artefacts (confirmed by sequencing) or could not be cloned. (GSP, Gene Specific Primer; NGSP, Nested Gene Specific Primer; UPM, Universal Primer A Mix; NUP, Nested Universal Primer A; left-right arrow to bar in (ii) represents 5.8 kb of genomic region)
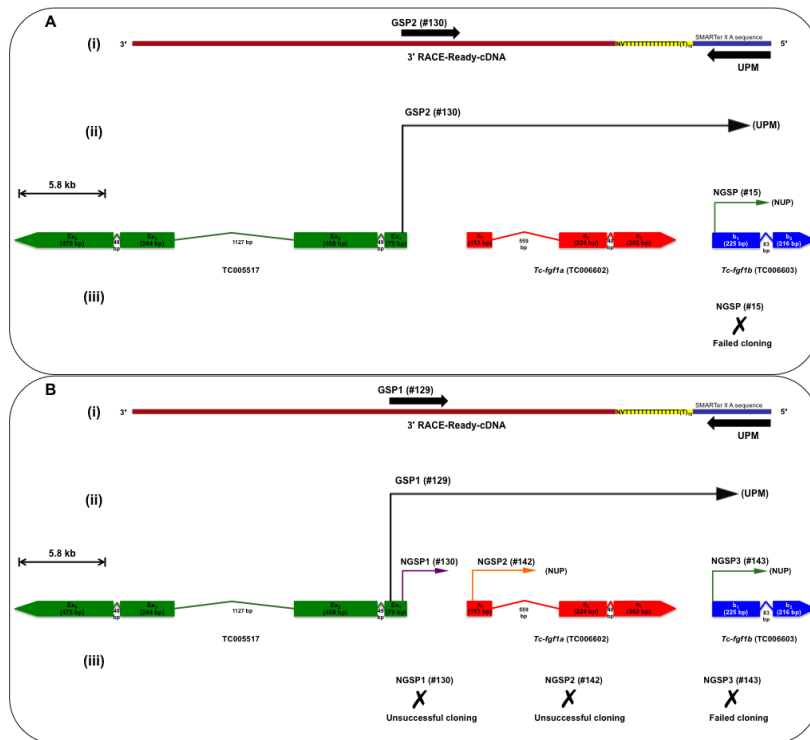
**Klon-Name:** *Tc-fgf1(a₂+ a₃)* **- 3´RACE**

Glean Nr: TC006602

Insert / -länge: 704 bp
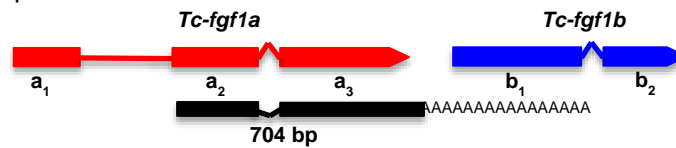
Entstehung: 3´ RACE PCR reaction using Primer#11 & UPM(Clontech)
3´ nested-PCR reaction using Primers:-
NUP(Clontech): 5'–AAGCAGTGGTATCAACGCAGAGT–3' &
NGSP(primer #12): 5´- GAGTGGAGGACGCTCCCAGTTCA -3´ (Romy Weller)

Orientierung: 5´– 3´
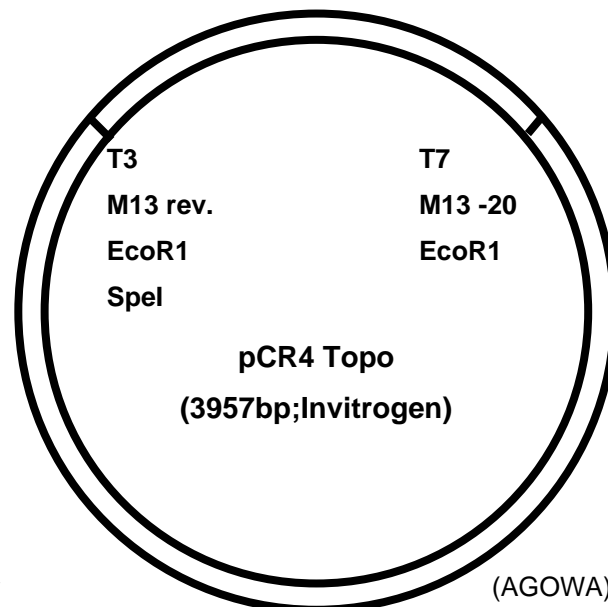
Sequenz: mit T3 Primer   (AGOWA) (02.08.11)

Mini: 29.07.11 (**11+12_E1**)   **Midi:** 06.01.12

Lagerung: -20°C, als pDNA   **back-up**: 20 µl, pDNA (aus Midi)

FGF1(a₂+a₃)-3´RACE 11+12_E1 (02.08.11; Romy Weller)
GAGTGGAGGACGCTCCCAGTTCA(primer#12)CACGCCTCTATTTCCGCGCCCCAAATTT
CCTGGCCCCCCTCCAACCCCAACTCAAACTGGCGCCAACTGCGCCCTGTCCACTTCGGA
AACCCGCTTTTCGGCACAAAAATGCAGCTCTATTCCAGAACTAGACACAACCTCGC C
GTTTATCCGGACGGCGAAGTGCGGGGAACCCCCGACGACGACGACTTGCA CACTTAT
TTGGAGGTAATGTCGGCTGGGCACCCGGGCCACGTGCGCA TTA AGGGCC
TTTTGACAAACCTCTACGTCGCCATGGACCCCAAAGGGCGCTTGTACGGGGAGCCAGAC
ATGACGG ACAATTCTACCATTTTTATCGAGGCGTTT CAAGGCTCTTACAA CACCTAT CT
CTCCCTA AAGTACGCCCATTTGGGGTGGTACATCGGGATAAAAAAATCGGGGAAGTT
CAAGCGCGGGCCCAAGACCAAGTACGGCCAAAAGGCGATCAAGTTTTTTACCGCGCAGA
TCTCGC TTTCAATGAAAACAGTATTAGCATTTGTTATATTTTTTACTCACATTTGTGTAATA
TTCCACACGTGACTCATTTTTAACAATAAATATTGGCAGATTTGAAAAAAAAAAAAAAAAAA
AAAAAAAAAAAAAAAAAATAAAAAAAAAAAAAAAAAAAAAAAAAAAAAAAAAAG**ACTCTGCGT
TGATACCACTGCTT(NUP)**
Translated Blast results in Frame +3 for 6602
Actual size of insert (w/o primers): 658 bp

Klon-Name: *Tc-fgf1(a₃)* - 3´RACE

Glean Nr: TC006602

Insert / -länge: 421 bp

Entstehung: 3´ RACE PCR reaction using Primer#11 & UPM(Clontech)
3´ nested-PCR reaction using Primers:-
NUP(Clontech): 5'–AAGCAGTGGTATCAACGCAGAGT–3' &
NGSP(primer #14): 5´- CTACGTCGCCGACCCCAAAG -3´ (Romy Weller)

Orientierung: 5´– 3´
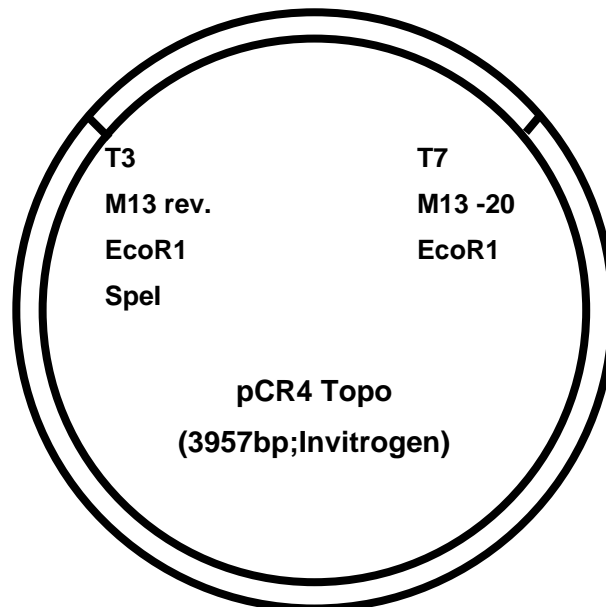
Sequenz: mit T3 Primer (AGOWA) (02.08.11)

Mini: 29.07.11 (**Clone E4**)   **Midi:** ....

Lagerung: -20°C, als pDNA   **back-up**: ....

FGF1(a₃)-3´RACE Clone-E4 (02.08.11; Romy Weller)
CTACGTCGCCATGGACCCCAAAG(primer#14)
GGCGCTTGTACGGGGAGCCAGACATGACGGACAATTCTACCATTTTTATCGAGGCGTTT
CAAGGCTCTTACAACACCTATCTCTCCCTAAAGTACGCCCATTTGGGGGTGGTACATCGG
GATAAAAAAATCGGGGAAGTTCAAGCGCGGGCCCAAGACCAAGTACGGCCAAAAGGCG
ATCAAGTTTTTTACCGCGCAGATCTCGCTTTCAATGAAAACAGCATTAGCATTTGTTATATT
TTTTACTCACATTTGTGTAATATTCCACACGTGACTCATTTTTAACAATAAATATTGGCAGA
TTTGTAAAAAAAAAAAAAAAAAAAAAAAAAAAAAAAAAAAAAAAAAAAAAAGTAAAAAAAAAAAAAAAAAA
AAAAAAAAAAAAGT**ACTCTGCGTTGATACCACTGCTT(NUP)**
Actual size of insert (w/o primers): 375 bp

Klon-Name: *Tc-fgf1(a₃)* **- 3´RACE**

Glean Nr: TC006602

Insert / -länge: 380 bp
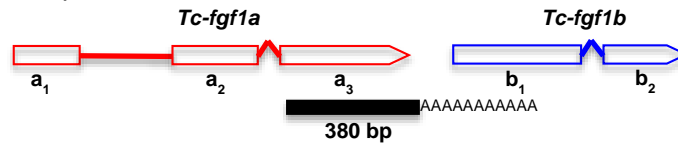
Entstehung: 3´ RACE PCR reaction using Primer#11 & UPM(Clontech)
3´ nested-PCR reaction using Primers:-
NUP(Clontech): 5'–AAGCAGTGGTATCAACGCAGAGT–3' &
NGSP(primer #14): 5´- CTACGTCGCCGACCCCAAAG -3´ (Romy Weller)

Orientierung: 5´– 3´
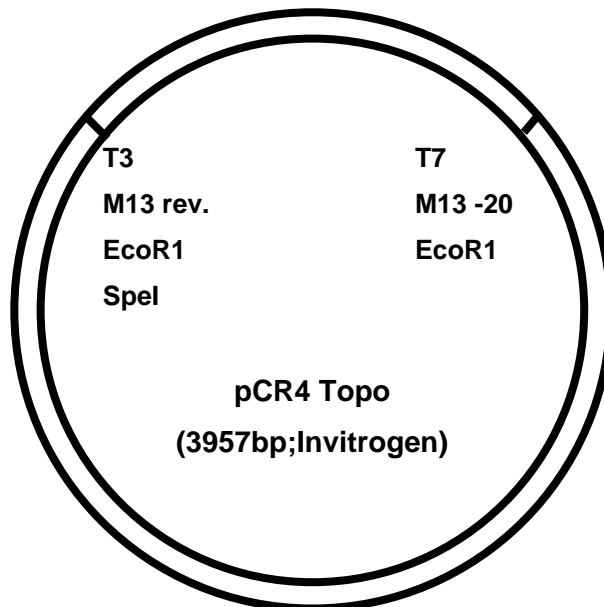
Sequenz: mit T3 Primer (AGOWA) (02.08.11)

Mini: 29.07.11 (**Clone E5**)   **Midi:** ....

Lagerung: -20°C, als pDNA   **back-up**: ....

FGF1(a₃)-3´RACE Clone-E5 (02.08.11; Romy Weller)
CTACGTCGCCATGGACCCCAAAG(primer#14)GGCGCTTGTACGGGGAGCCAGACATGA
CGGACAATTCTACCATTTTTATCGAGGCGTTTCAAGGCTCTTACAACACCTATCTCTCCCT
AAAGTACGCCCATTTGGGGTGGTACATCGGGATAAAAAAATCGGGGAAGTTCAAGCGCG
GGCCCAAGACCAAGTACGGCCAAAAGGCGATCAAGTTTTTACCGCGCAGATCTCGCTTT
CAATGAAAACAGTATTAGCATTTGTTATATTTTTTACTCACATTTGTGTAATATTCCACACG
TGACTCATTTTTAACAATAAATATTGGCAGATTTGCAAAAAAAAAAAAAAAAAAAAAAAAAAA
AAGT**ACTCTGCGTTGATACCACTGCTT(NUP)**
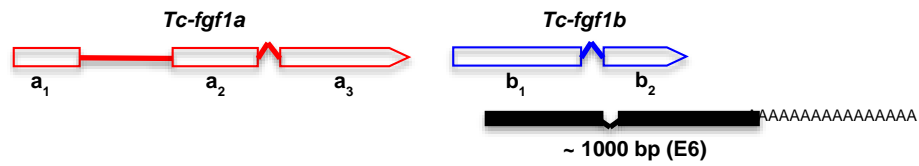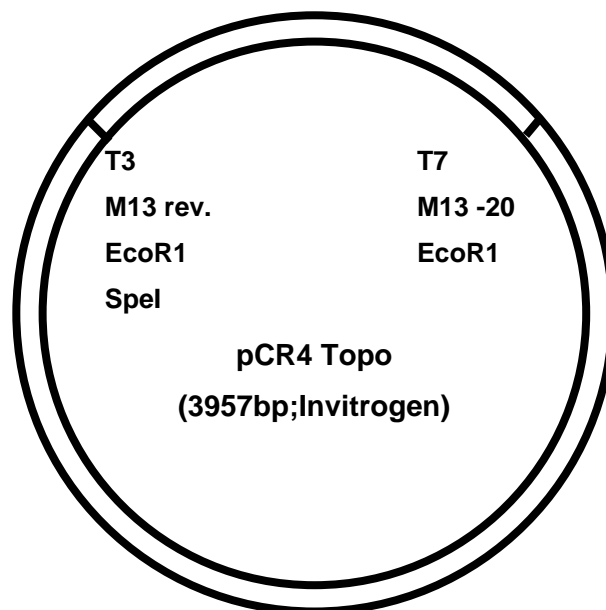Actual size of insert (w/o primers): 334 bp

Klon-Name: *Tc-fgf1(a₃)* - 3´RACE

Glean Nr: TC006602

Insert / -länge: 378 bp
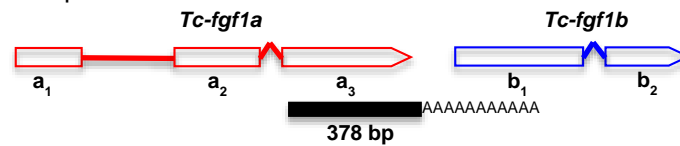
Entstehung: 3´ RACE PCR reaction using Primer#12 & UPM(Clontech)
3´ nested-PCR reaction using Primers:-
NUP(Clontech): 5'–AAGCAGTGGTATCAACGCAGAGT–3' &
NGSP(primer #14): 5´- CTACGTCGCCGACCCCAAAG -3´ (Romy Weller)

Orientierung: 5´– 3´
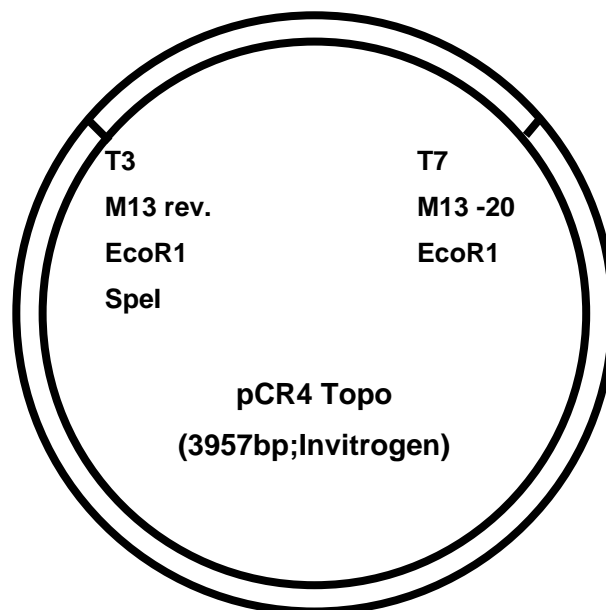
Sequenz: mit T3 Primer (AGOWA) (02.08.11)

Mini: 29.07.11 (**Clone E2**)   **Midi:** ....

Lagerung: -20°C, als pDNA   **back-up**: ....

FGF1(a₃)-3´RACE Clone-E2 (02.08.11; Romy Weller)
CTACGTCGCCATGGACCCCAAAG(primer#14)GGCGCTTGTACGGGGAGCCAGACATGG
CGGACAATTCTACCATTTTTATCGAGGCGTTTCAAGGCTCTTACAACACCTATCTCTCCCT
AAAGTACGCCCATTTGGGGTGGTACATCGGGATAAAAAAATCGGGGAAGTTCAAGCGCG
GGCCCAAGACCAAGTACGGCCAAAAGGCGATCAAGTTTTTACCGCGCAGATCTCGCTTT
CAATGAAAACAGTATTAGCATTTGTTATATTTTTTACTCACATTTGTGTAATATTCCACACG
TGACTCATTTTTAACAATAAATATTGGCAGATTCAAAAAAAAAAAAAAAAAAAAAAAAAAAA
GT**ACTCTGCGTTGATACCACTGCTT(NUP)**

Actual size of insert (w/o primers): 332 bp

Klon-Name: *Tc-fgf1*(*b₁* + *b₂*)**- 3´RACE**

Glean Nr: TC006603

Insert / -länge: ~ 1 kb

Entstehung: 3´ RACE PCR reaction using Primer#12 & UPM(Clontech)
3´ nested-PCR reaction using Primers:-
NUP(Clontech): 5'–AAGCAGTGGTATCAACGCAGAGT–3' &
NGSP(primer #143): 5´- ATGGACGAAAAGCCAAGCTGGCATG -3´ (Romy Weller)

Orientierung: 3´– 5´

Sequenz: mit T3 Primer (AGOWA) (10.08.11)

Mini: 29.07.11 **(Klon -E6)**   **Midi:** 06.10.2011

Lagerung: -20°C, als pDNA   **back-up**: 20 µl, pDNA (aus Midi)

Klon-Name: *Tc-fgf1(a₃)* **- 3´RACE**

Glean Nr: TC006602

Insert / -länge: 382 bp
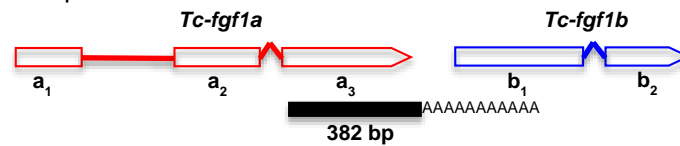
Entstehung: 3´ RACE PCR reaction using Primer#13 & UPM(Clontech)
3´ nested-PCR reaction using Primers:-
NUP(Clontech): 5'–AAGCAGTGGTATCAACGCAGAGT–3' &
NGSP(primer #14): 5´- CTACGTCGCCGACCCCAAAG -3´ (Rahul Sharma)

Orientierung: 5´– 3´
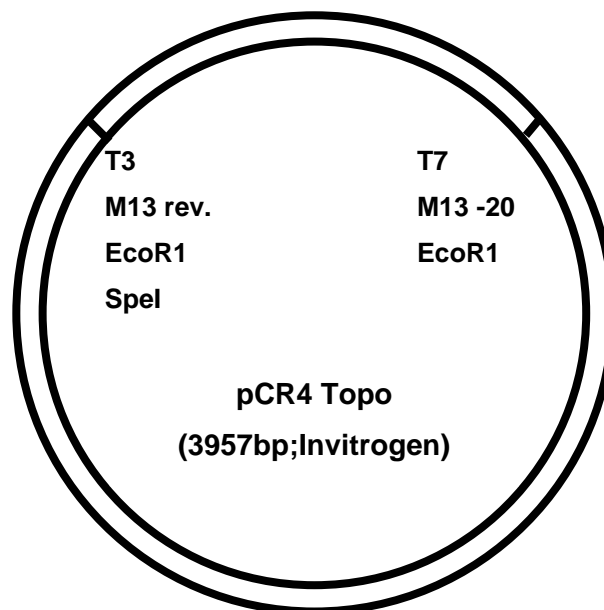
Sequenz: mit T3 Primer (AGOWA) (01.06.10)

Mini: 26.05.10 (**clone 5**)   **Midi:** 10.03.11

Lagerung: -20°C, als pDNA   **back-up**: 20 μl, pDNA (aus Midi)

FGF1(a₃)-3´RACE Clone-5 (01.06.10; Rahul Sharma)
CTACGTCGCCATGGACCCCAAAG(primer#14)GGCGCTTGTACGGGGAGCCAGACATGA
CGGACAATTCTACCATTTTTATCGAGGCGTTTCCAGGCTCTTACAACACCTATCTCTCCCT
AAAGTACGCCCATTTGGGGTGGTACATCGGGATAAAAAAAATCGGGGAAGTTCAAGCGC
GGGCCCAAGACCAAGTACGGCCAAAAGGCGATCAAGTTTTTACCGCGCAGATCTCGCTT
TCAATGAAAACAGTATTAGCATTTGTTATATTTTTTACTCACATTTGTGTAATATTCCACAC
GTGACTCATTTTTAACAATAAATATTGGCAGATTTGAAAAAAAAAAAAAAAAAAAAAAAAAA
AAAAGT**ACTCTGCGTTGATACCACTGCTT(NUP)**
Translated Blast results in Frame +2 for 6602
Actual size of insert (w/o primers): 335 bp

Klon-Name: *Tc-fgf1(a₁+ a₂)* **- 5´RACE**

Glean Nr: TC006602

Insert / -länge: 303 bp
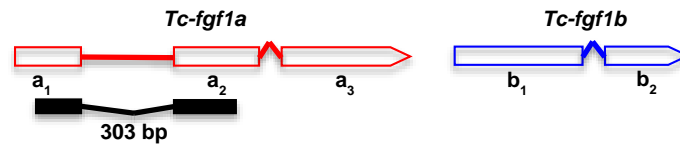
Entstehung: 5´ RACE PCR reaction using Primer#131 & UPM(Clontech)
5´ nested-PCR reaction using Primers:-
NUP(Clontech): 5'–AAGCAGTGGTATCAACGCAGAGT–3' &
NGSP(primer #133): 5´-ACGGCGAGGTTGTGTCTAGTTCTG-3´ (Romy Weller)

Orientierung: 5´– 3´
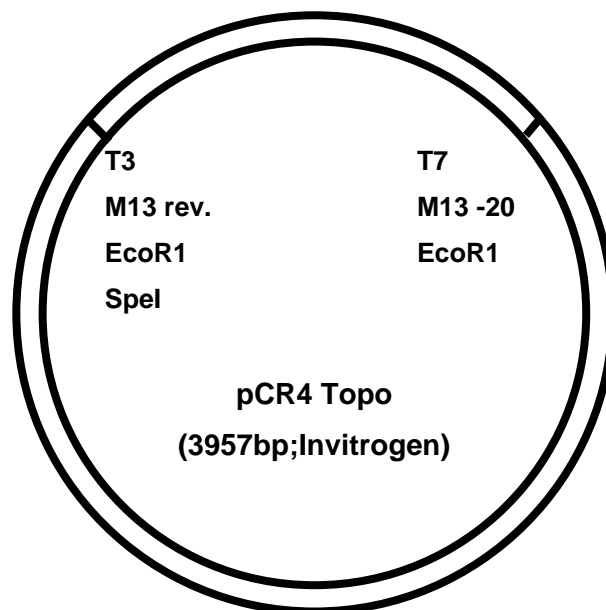
Sequenz: mit T3 Primer (AGOWA) (20.04.11)

Mini: 14.04.11 (**Klon E5_Lane 4**)   **Midi:** 31.05.2011

Lagerung: -20°C, als pDNA   **back-up**: 20 µl, pDNA (aus Midi)

FGF1(a₁+a₂)-5´RACE Clone E5_Lane4 (20.04.11; Romy Weller)
AAGCAGTGGTATCAACGCAGAGT(NUP)ACATGGGG**AGT**GACAGTGATAGTACCGATGT
TGAAAGTTTGAGTGACAGTGATGAGATCGATGAAGGAAAAAATGTGAAAAATAGGACGAA
AAGGGGGAATTGCGTGGTGCGGAGTGGAGGACGCCCCCAGTTCACACGCCTCTATTTCC
GCGCCCCAAATTTCCTGGCCCCCCCTCCAACCCCAACTCAAACTGGCGCCAACTGCGCCC
TGTCCACTTCGGAAACCCGCTTTTCGGCACAAAAATGCAGCTCTATTC**CAGAACTAGAC
ACAACCTCGCCGT(primer#133)**

Translated Blast results in Frame +2 for 6602
Actual size of insert (w/o primers): 256 bp

Klon-Name: *Tc-fgf1(b₂)* - 3´RACE-I
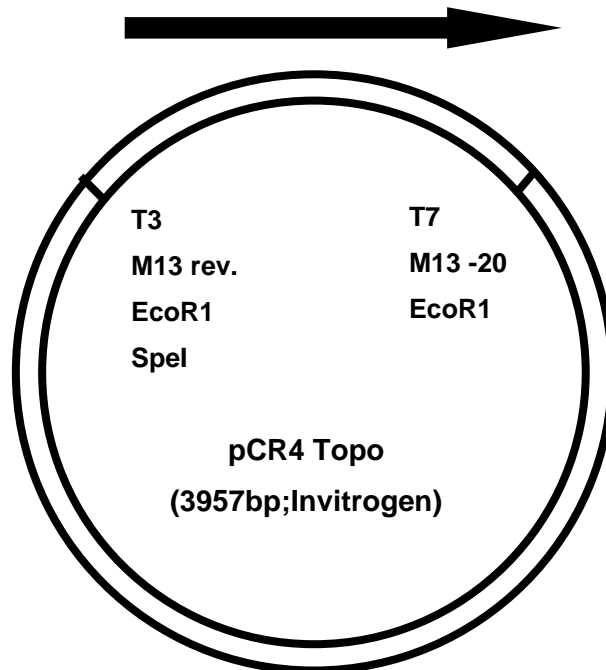
Glean Nr: TC006603

Insert / -länge: 756 bp
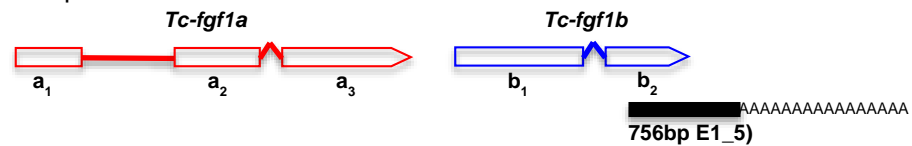
Entstehung: 3´ RACE PCR reaction using Primer#143 & UPM(Clontech)
3´ nested-PCR reaction using Primers:-
NUP(Clontech): 5'–AAGCAGTGGTATCAACGCAGAGT–3' &
NGSP(primer #145): 5´- ATCATCCGGACTGGTACATTGGGA -3´ (Romy Weller)

Orientierung: 5´– 3´

Sequenz: mit T3 Primer (AGOWA) (26.07.11)

Mini: 22.07.11 **(Klon E1_5)**   **Midi:** ....

Lagerung: -20°C, als pDNA   **back-up**: ....

FGF1(a₃)-3´RACE Clone E1_5 (22.07.11; Romy Weller)
ATCATCCGGACTGGTACATTGGGA(primer#145)TTAAAAAAGATGGGAACATGAAGAAT
GGAAAACGGACGCAGTGGGGCAAAAAATCAGTGAAATTTTTGCCCAACAGAAATGTATC
GGGAGCGGAATTGCAACAGCTAGACTCCAGTTGATGTTTTAAATAATTGGGTATTTCTAC
GTAATAAGTATTAGCAGATGTTTAAGCAAAACCTTGAGCGATAGCTCCATAATTAGATTCG
TCTATAATTGTGAGAGGAAGTCGGATTGGCATAAATTTTAACTAGAATTTGAATTTCTTGT
TTATTGGCGGTTTTACTTTGTAAAATTTTATTGTCACGTCAACGCTGTCCAATTATGTTTTT
TTTCGAAGGCTAGGAAAAATGCTGGATATTAAAAAAACAAATGCAGTCACACAAAAGTTA
GATTATTTATTTTATTAAAATAACGAAAGTTAGACATAATTCGTCGATTTCTTTATGTTTTCT
AGTGAAATTTCTTAAGATAAGGAAGTTATTGACTCAGGTACGAGCTGAGTCATTGGCTGA
AATCACCTATACGCACAAAAGTATTTGTTGTATTTTGTATTTATGTTTCTTTCTATCTTTTAT
TTATGTTAATGTTCTAGTACGAAAGGACCGAATGTTAAAATTATATTTTAGAGTTTGAATAA
AGTTAAAAAAAAAAAAAAAAAAAAAAAAAAAAAAAAAATTAATTAAAAAAAAAAAAAAAAAAAAAAAA
AAAAGGTCT**ACTCTGCGTTGATACCACTGGCTT(NUP)**
Translated Blast results in Frame +2 for 6603
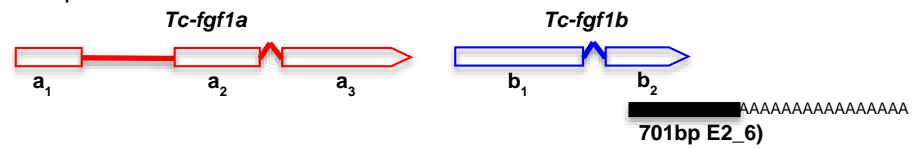Actual size of insert (w/o primers): 709 bp

Klon-Name: *Tc-fgf1(b₂)* - 3´RACE-II

Glean Nr: TC006603

Insert / -länge: 701 bp

Tc-fgf1a   *Tc-fgf1b*

a₁   a₂   a₃   b₁   b₂

AAAAAAAAAAAAAAAA

701bp E2_6)

Entstehung: 3´ RACE PCR reaction using Primer#143 & UPM(Clontech)
3´ nested-PCR reaction using Primers:-
NUP(Clontech): 5'–AAGCAGTGGTATCAACGCAGAGT–3' &
NGSP(primer #145): 5´- ATCATCCGGACTGGTACATTGGGA -3´ (Romy Weller)

Orientierung: 5´– 3´

EcoR1

T3
M13 rev.
EcoR1
SpeI

T7
M13 -20
EcoR1

pCR4 Topo
(3957bp;Invitrogen)
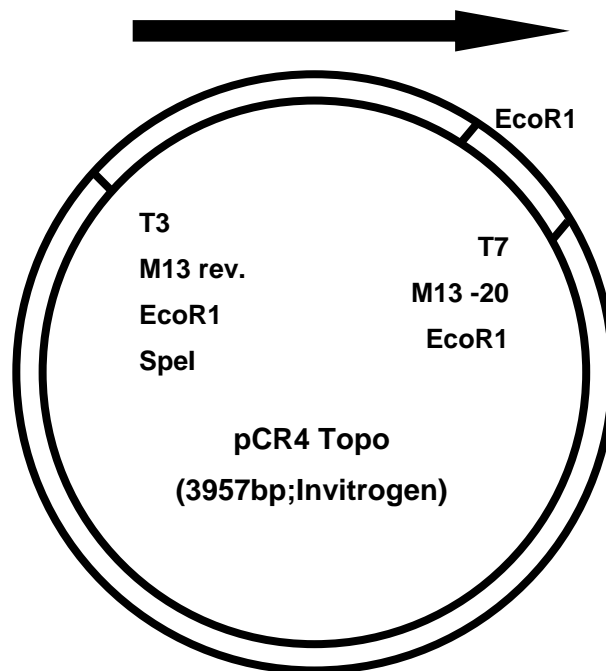
Sequenz: mit T3 Primer (AGOWA) (26.07.11)

Mini: 22.07.11 **(Klon E2_6)**   **Midi:** 07.10.2011

Lagerung: -20°C, als pDNA   **back-up**: 20 μl, pDNA (aus Midi)

FGF1(b₂)-3´RACE Clone 143+145_E2-6 (22.07.11; Romy Weller)
ATCATCCGGACTGGTACATTGGGA(primer#145)TTAAAGAAGATGGGAACATGAAGAAT
GGAAAACGGACGCAGTGGGGCAAAAAATCAGTGAAATTTTTGCCCAACAGAAATGTATC
GGAAGCGGAATTGCAACAGCTAGACTCCAGTTGATGTTTTAAATAATTGAGTATTTCTAC
GTAATAAGTATTAGCAGGTGTTTAAGCAAAACCTTGAGCGATAGCTCCAAAATTAGATTC
GTCTATAATTGTGAGAGGAAGTCGGATTGGCATAAATTTTAACTAGAATTTGAATTTCTTG
TTTATTGGCGGTTTTACTTTGTAAAATTTTATTGTCACGTCAACGCTGTCCAATTATGTTTT
TTTTCGAAGGCTAGGAGAAATGCTGGATATTAAAAAAACAAATGCAGTCACACAAAGTT
AGATTATTTATTTTATTGAAATAACGAAAGTTAGACATAATTCGTCGATTTCTTTATGTTTT
CTAGTGAAATTTCTTAAGATAAGGAAGTTATTGACTCAGGTACGAGCTGAGTCATTGGCT
GAAATCACCTATACGCACAAAGTATTTGTTGTATTTTGTATTTATGTTTCTTTATATCTTTT
ATTTATGTATGGTGTTACATATTGTTTTTTTTGAATATATTTTT**GAATTC**GAAAAAA
AAAAAAAAAAAAAAAAAAAAAAAAAGT**ACTCTGCGTTGATACCACTGCTT(NUP)**
Translated Blast results in Frame +3 for 6602
Actual size of insert (w/o primers): 654 bp
GAATTC is an additional **EcoRI** RE site recognised in the inserted nucleotide fragment.
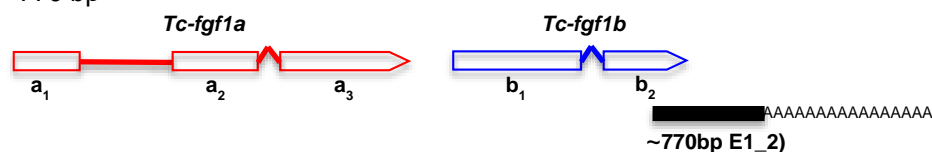
Klon-Name: *Tc-fgf1(b₂)* - 3´RACE-III

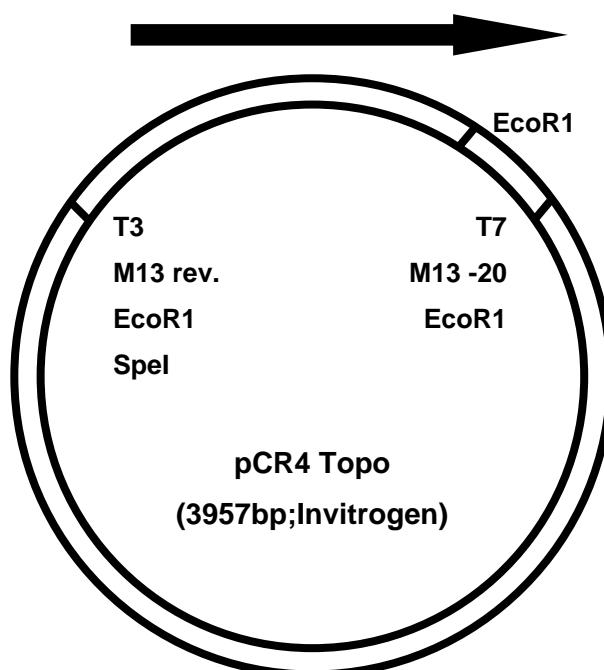**Glean Nr:** TC006603

Insert / -länge: ~ 770 bp

Entstehung: 3´ RACE PCR reaction using Primer#143 & UPM(Clontech)
3´ nested-PCR reaction using Primers:-
NUP(Clontech): 5'–AAGCAGTGGTATCAACGCAGAGT–3' &
NGSP(primer #146): 5´- GAAGAATGGAAAACGGACGCAGTGG -3´ (Romy Weller)

Orientierung: 5´– 3´

Sequenz: mit T3 Primer (AGOWA) (26.07.11)

Mini: 22.07.11 **(Klon E1_2)**   **Midi:** 07.10.2011

Lagerung: -20°C, als pDNA   **back-up**: 20 μl, pDNA (aus Midi)

FGF1(b₂)-3´RACE Clone 143+146_E1-2 (22.07.11; Romy Weller)
GAAGAATGGAAAACGGACGCAGTGGGGCAAAAAATCAGTGAAATTTTTGCCCAACAGA
AATGTATCGGAAGCGGAATTGCAACAGCTAGACTCCAGTTGATGTTTTAAATAATTGAGT
ATTTCTACGTAATAAGTATTAGCAGATGTTTAAGCAAAACCTTGAGCGATAGCTCCAAAAT
TAGATTCGTCTATAATTGTGAGAGGAAGTCGGATTGGCATAAATTTTAACTAGAATTTGAA
TTTCTTGTTTATTGGCGGTTTTACTTTGTAAAATTTTATTGTCACGTCAACGCTGTCCAATT
ATGTTTTTTTTCGAAGGCTAGGAAAAATGCTGGATATTAAAAAAACAAATGCAGTCACACA
AAAGTTAGATTATTTATTTTATTGAAATAACGAAAGTTAGACATAATTCGTCGATTTCTTTA
TGTTTTCTAGTGAAATTTCTTAAGATAAGGAAGTTATTGACTCAGGTACGAGCTGAGTCAT
TGGCTGAAATCACCTATACGCACAAAAGTATTTGTTGTATTTTGTATTTATGTTGGTTTCTA
TCTTTTATTTATGTTAATGTTCTAGTACGAAAGGACCGAATGTTAAAATTATATTTTAGAGT
TTGAATAAAGTTAAAAAAAAAAAAAAAAAAAAAAAAAAAAAAAAAAAAAAAAAAAAAAAAAA
AAAAAAAAAAAAAAAAAAAAAAAAAAAGGGGCCCTCGGGGGGTGAAACCCCCGGTTAAGGG
GGAATTTCGGGGCCCGTAAATTTAATTTCGCCCAAAAGG
Translated Blast results in Frame +1 for 6603
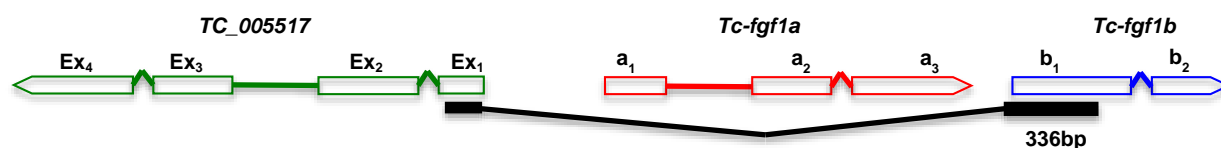Actual size of insert (w/o primers): ~750 bp

Klon-Name: *Tc005517(Ex₁) + Tc-fgf1(b₁) - 5´ RACE*

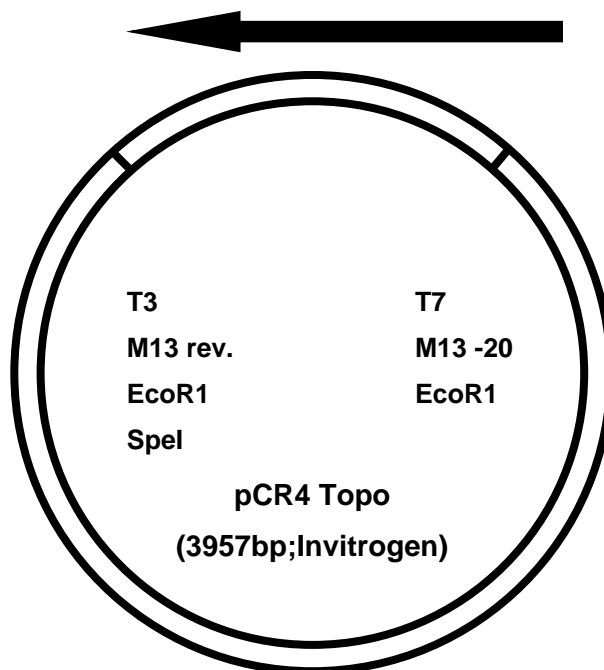**Glean Nr:** TC005517/TC006603

Insert / -länge: 336 bp

Entstehung: 5´ RACE PCR reaction using Primer#18 & UPM(Clontech)
5´ nested-PCR reaction using Primers:-
NUP(Clontech): 5'–AAGCAGTGGTATCAACGCAGAGT–3' &
NGSP(primer #17): 5´- CGCTCCTTGAATCCTGACATGGG -3´ (Rahul Sharma)

Orientierung: 3´– 5´

T3
M13 rev.
EcoR1
SpeI

T7
M13 -20
EcoR1

**pCR4 Topo

(3957bp;Invitrogen)**

Sequenz: mit T3 Primer (AGOWA) (09.06.2010)

Mini: 04.06.10 **(Clone 1_lane 2)**

Midi: 10.03.2011

Lagerung: -20°C, als pDNA

back-up: 20 µl, pDNA (aus Midi)

Tc005517(Ex₁)+FGF1(b₁)-5´RACE Clone1_lane 2–300bp T3 (04.06.10; Rahul Sharma)
CGCTCCTTGAATCCTGACATGGG(primer#17)AAACCTCCCCACTTGAACTAACAACCAG
GACATTGTCTAAATTATCATCCCTTGTGCCCAAAACGTGCCCATCATCTTGTATGGTCAAA
TTAAACCCATTTTCGGACCTGAGTCTCATTACATTCCCATGCCAGCTTGGCTTTTCGTCCA
TTTTCAACTTCATAACAGTGATTAATTGTTAGTTTACGTTAAATTCCGATCATCCCTTATCA
CCTCACAGCATGTCAAACGAAAATAAGTGCGAAAACATGGACAACCAACAGGGAGAAAA
CGCAACGAATTTCCCATGT**ACTCTG CGTTGATACCACTGCTT(NUP)**

Translated Blast results in Frame -1 for 6603
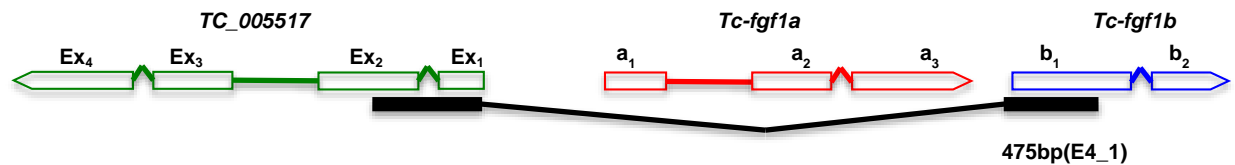Actual size of insert (w/o primers): 290 bp

Klon-Name: *Tc005517(Ex₁-Ex₂) + Tc-fgf1(b₁) - 5´ RACE*
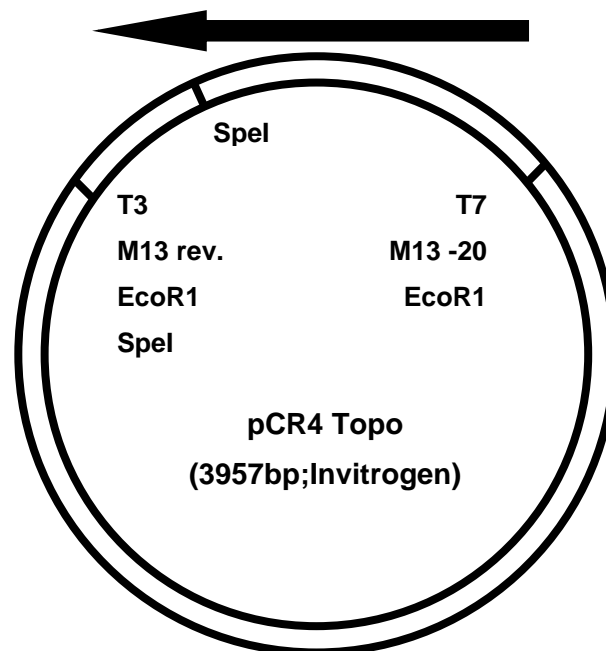
Glean Nr: TC005517/TC006603

Insert / -länge: 475 bp

Entstehung: 5´ RACE PCR reaction using Primer#18 & UPM(Clontech)
5´ nested-PCR reaction using Primers:-
NUP(Clontech): 5'–AAGCAGTGGTATCAACGCAGAGT–3' &
NGSP(primer #17): 5´- CGCTCCTTGAATCCTGACATGGG -3´ (Romy Weller)

Orientierung: 3´– 5

Sequenz: mit T3 Primer (AGOWA) (16.07.11)

Mini: 13.07.11 **(Klon E4_1)**　　　　　　　　　**Midi:** 07.10.2011

Lagerung:　　-20°C, als pDNA　　　　　　　**back-up**: 20 µl, pDNA (aus Midi)

Tc005517(Ex₁₋₂)+FGF1(b₁)-5´RACE Clone E4_1 (13.07.11; Romy Weller)
CGCTCCTTGAATCCTGACATGGG(primer#17)AAATCTCCCCACTTGAACTAACAACCAG
GACATTGTCTAAATTATCATCCCTTGTGCCCAAAACGTGCCCATCATCTTGTATGGTCAAA
TTAAACCCATTTTCGGACCTGAGTCTCATTACATTCCCATGCCAGCTTGGCTTTTCGTCCA
TTTTCAACTTCATAACAGTGATTAATTGTTAGTTTACGTTAAATTCCGATCATCCCTTATCA
CCTCACAGCATGTCAAACGAAAATAAGTGCGAAAACATGGACAACCAACAGGGAGAAAA
CGCAACGAATTTATCAAATTCC**ACTAGT**GGTAGTGCAAAATAGCAGTTTTAGGTACAGTT
TTCACGCGTTTTTTCCAGTGTGTGAAGCTAATACGGGTGTTGCAATAAAAAAACATCGAA
TCTGATGCACTGGACCGTCTTTTGGTGTATCC
CCATGT**ACTCTGCGTTGATACCACTGCTT (nUPM)**
Translated Blast results in Frame -2 for 6603 & for 5517: +2, +1, +3
Actual size of insert (w/o primers): 429 bp

ACTAGT is an additional **SpeI** RE site recognised in the inserted nucleotide fragment.
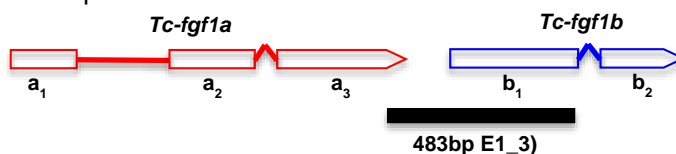
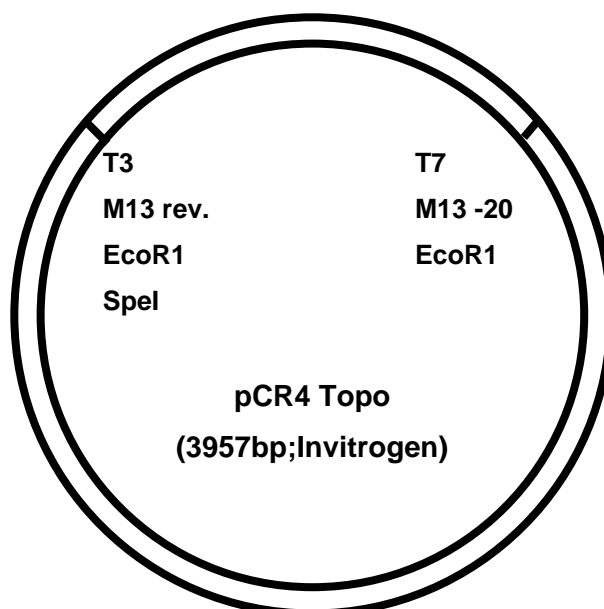**Klon-Name:** *Tc-fgf1(a₃) + Tc-fgf1(b₁)*- 5´RACE

Glean Nr: TC006602/TC006603

Insert / -länge: 483 bp

Entstehung: 5´ RACE PCR reaction using Primer#18 & UPM(Clontech)
5´ nested-PCR reaction using Primers:-
NUP(Clontech): 5'–AAGCAGTGGTATCAACGCAGAGT–3' &
NGSP(primer #16): 5´- CCGCGTACAAATTTCCCGAATCGT -3´ (Romy Weller)

Orientierung: 3´– 5´

Sequenz: mit T3 Primer (AGOWA) (16.07.11)

Mini: 14.07.11 **(Klon E1-3)**   **Midi:** 06.10.2011

Lagerung: -20°C, als pDNA   **back-up**: 20 μl, pDNA (aus Midi)

FGF1(a₃) + FGF1(b₁)-5´RACE Clone 129+14 (06.05.11; Romy Weller)
CCGCGTACAAATTTCCCGAATCGT(primer#16)CAAAACTCAGATATCGTTTACTCTTTGC
TCCTTGAATCCTGACATGGGAAATCTCCCCACTTGAACTAACAACCAGGACATTGTCTAA
ATTATCACCCCTTGTGCCCAAAACGTGCCCATCATCTTGTATGGTCAAATTAAACCCATTT
TCAGACCTGAGTCTCATTACATTCCCATGCCAGCTTGGCTTTTCGTCCATTTTCAACTTCT
AAAATTCACACTTCGATGTAATCAACGTAAACACTGAAATCAGTTCAAGGAAACAATAAAA
AAATGAAACGAAATTACAAATCTGCCAATATTTATTGTTAAAAATGAGTCACGTGTGGAAT
ATTACACAAATGTGAGTAAAAAATATAACAAATGCTAATACTGTTTTCATTGAAAGCGAGA
TCTGCGCGGTAAAAACTTGATCGCCTTTTGGCCGTCCCCATGT**ACTCTGCGTTGATACC
ACTGCTT(NUP)**
Translated Blast results in Frame -3 for 6603
Actual size of insert (w/o primers): 436 bp

Klon-Name: *Tc005517(Ex₁) + Tc-fgf1(a₁) - 3´ RACE*

01.07.2011

Klon Nr. 287

Glean Nr: TC005517/TC006602

Insert / -länge: 1017 bp

TC_005517 | Tc-fgf1a | Tc-fgf1b
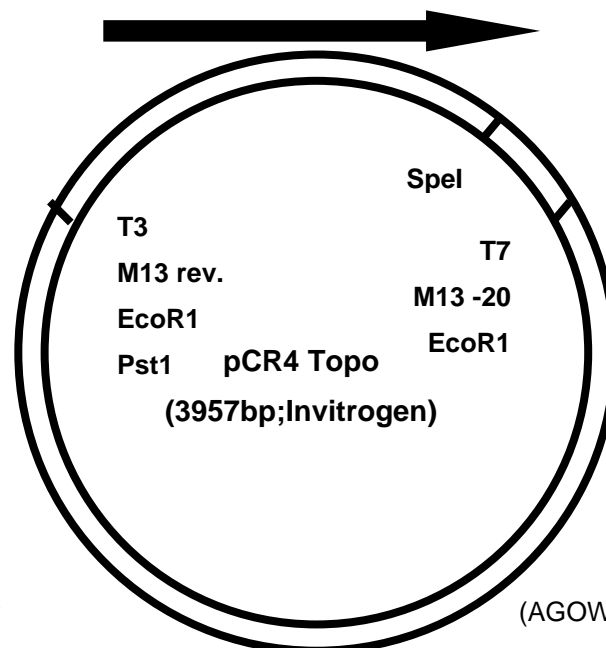
Ex₄ Ex₃ Ex₂ Ex₁   a₁   a₂   a₃   b₁   b₂

1017bp E1ₗₗ_lane5)

Entstehung: 3´ RACE PCR reaction using Primer#129 & UPM(Clontech)
3´ nested-PCR reaction using Primers:-
NUP(Clontech): 5'–AAGCAGTGGTATCAACGCAGAGT–3' &
NGSP(primer #130): 5´- GACATGCTGTGAGGTGATAAGG -3´ (Romy Weller)
Orientierung: 5´– 3´

SpeI

T3
M13 rev.
EcoR1
Pst1

T7
M13 -20
EcoR1

pCR4 Topo
(3957bp;Invitrogen)

Sequenz: mit **T7** Primer   (AGOWA) (20.04.11)

Mini: 14.04.11 (**Klone E1ₗₗ_Lane5**)   **Midi:** 31.05.2011

Lagerung: -20°C, als pDNA   **back-up**: 20 µl, pDNA (aus Midi)

Tc005517(Ex₁)+FGF1(a₁)-3´RACE Clone E1ₗₗ_Lane5 .T7 (01.07.11; Romy Weller)
AAGCAGTGGTATCAACGCAGAGT(NUP)ACTTTTTTTTTTTTTTTTTTTTTTTTTTTTCCTTCATCGATCTC
ATCACTGTCACTCAAACTTTCAACATCGGTACTATCACTGTC**ACTAGT**CCCGTTTTCCATGTTTTTGC
CGATTGTTAATTAAAACCAACAATGGGCACGTTTGTAACAATTCAAAAATCAAGCCGGTGTAAGCAA
AACACCGTAATTTCCGTCAATTATTTCAAACGTGTTTAAAATTCAACTGTTTTCGCGTTCTTACTTCTA
ATTTCTAATTTTCCGCGGTTATAAGTAAAATTTTATTCGGCGGTTACAAAACGATCATAAATCACAAA
TTTTTGATGTTTTACCTTAAATTTTTTGTGCCCAGAATGATGACGGTAGCTTGTTATCAAAACAGGAGC
CGCTGATAACAAAAGTAAATTTATAAATCGATTATAATTTTATTTATTGTCACCAGTATTGCTGGTTGC
CTAAGCTAACACAAAAACTGTTTGTGTGAATATACAGATACCAAATTCTTAAAACCGCACCTACCCAT
AAAAAATAATTCTTTAAATAGTTCAACAACAATTTGAACAGTTAGATTGTTTATAACATTAATTATTGC
ATTAGAGGATCATAGGTTCTTTAGGTATTAAATATTCTTCGGAATGGCTCATGCTCATACACATAATA
ATTAGCACATTTATTAATGCGTTATAACAGACTATAGACGGATTATAGTAAATATTGTCCGCTTTTTTTT
GTAAAAGTAGTGATTGTGTAAGGGGGTGGCGTGCACTATCGTTGCAAGCGCCCCTTTGGCTGGCC
TTGAAGGCCGGCCAATGGCAAGGCGCAAATTGGGTCACGTGCCGAAAGTTTCCACTGCAAATGGC
GGCTAGCAAACATGAGAACATCCACATGGCAGTAAAATCGCAAATCCGCTTAAATGTTCGCAGTAC
TCCTTACCATAACAGGTGATTATTGTTAGTTTACGTTAAATTCGGATCATC**CCTTATCACCTCACAGC
ATGTC(primer#130)**
Translated Blast results in Frame -2 for 6602   Actual size of the insert (w/o primers): 972 bp
ACTAGT RE site is an additional **SpeI** RE site recognised in the inserted nucleotide fragment.

Tc005517(Ex₁)+FGF1(a₁)-3´RACE Clone E1ᵢᵢ_Lane5 .T3 (01.07.11; Romy Weller)
GACATGCTGTGAGGTGATAAGG(primer#130)GATGATCGGAATTTAACGTAAACTAACAATTAATCA
CTGTTATGGTAAGGAGTACTGCGAACATTTAAGCGGATTTTGCGATTTTACTGCCATGTGGATGTTC
TCATGTTTGCTAGCCGCCATTTGCAGTGGAAACTTTCGGCACGTGACCCAATTTGCGCCTTGCCAT
TGGCCGGCCTTCAAGGCCAGCCAAAGGGGCGCTTGCAACGATAGTGCACGCCACCCCTTACACAA
TCACTACTTTTACAAAAAAAGCGGACAATATTTACTATAATCCGTCTATAGTCTGTTATAACGCATTA
ATAAATGTGCTAATTATTATGTGTATGAGCATGAGCCATTCCGAAGAATATCTAATACCTAAAGAACC
TATGATCCTCTAATGCAATAATTAATGTTATAAACAATCTAACTGTTCAAATTGTTGTTGAACTATTTA
AAGAATTATCTTTTATGGGTAGGTGCGGTCTTAAGAATTTGGTATCTGTATATTCACACAAACAGTTT
TTGTGTTAGCTTAGGCAACCAGCAATACTGGTGACAATAAATAAAATTATAATCGATTTATAAATCTA
CTCTTGTTATCAGCGGCTCCTGTCTTGATAACAAGCTACCGTCATCATCCTGGGCACAAAAATTTAA
GGTAAAACATCAAAAATTTGTGATTTATGATCGTCTCGTAACCGCCGAATAAAATTCTACTTATAACC
GCGGAAAATTAGAAATTAGAAGTAAGAACGCGAAAACAGTCGAATTTTAAACACGTCTGAACTAATT
GACGGAAATTACGGTGTTTTGCTTACACCGGCTCGATTTTTGAATTGTTACAAACGTGCCCATTGTT
GGTTTTAATTAACAATCGGCAAAAC<mark>ATGGAAAACGGGACTAGTGACAGTGTAGTACCGATGTTGAAA
GTTTGAGTGACAGTGATGAGATCGATGA</mark>CGAGAGAACAAAAA
TAGAAGT**ACTCTGCGTTGATACCACTGCTT(NUP)**
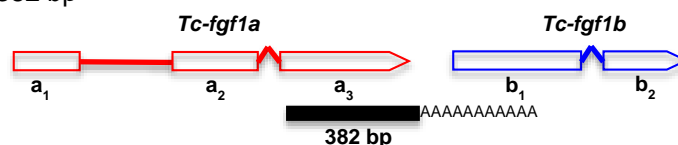
Klon-Name: *Tc-fgf1(a₃)* - 3´RACE-II
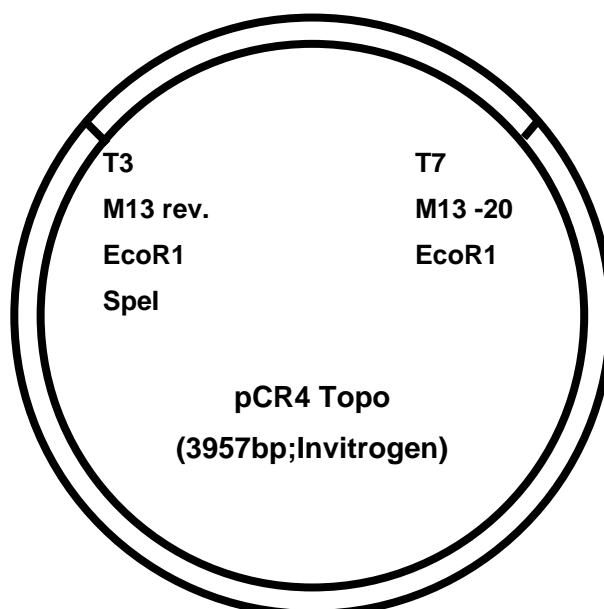
Glean Nr: TC006602

Insert / -länge: 382 bp

Entstehung: 3´ RACE PCR reaction using Primer#129 & UPM(Clontech)
3´ nested-PCR reaction using Primers:-
NUP(Clontech): 5'–AAGCAGTGGTATCAACGCAGAGT–3' &
NGSP(primer #14): 5´- CTACGTCGCCGACCCCAAAG -3´ (Romy Weller)

Orientierung: 5´– 3´

Sequenz: mit T3 Primer (AGOWA) (10.05.11)

Mini: 06.05.11 **(Klon 129 +14)**

Midi: 15.06.11

Lagerung: -20°C, als pDNA

back-up: 20 μl, pDNA (aus Midi)

FGF1(a₃)-3´RACE Clone 129+14 (06.05.11; Romy Weller)
CTACGTCGCCATGGACCCCAAAG(primer#14)GGCGCTTGTACGGGGAGCCAGACATGA
CGGACAATTCTACCATTTTTATCGAGGCGTTTCCAGGCTCTTACAACACCTATCTCTCCCT
AAAGTACGCCCATTTGGGGTGGTACATCGGGATAAAAAAAATCGGGGAAGTTCAAGCGC
GGGCCCAAGACCAAGTACGGCCAAAAGGCGATCAAGTTTTTACCGCGCAGATCTCGCTT
TCAATGAAAACAGTATTAGCATTTGTTATATTTTTTACTCACATTTGTGTAATATTCCACAC
GTGACTCATTTTTAACAATAAATATTGGCAGATTTGAAAAAAAAAAAAAAAAAAAAAAAAAA
AAAAGT**ACTCTGCGTTGATACCACTGCTT(NUP)**

Translated Blast results in Frame +2 for 6602
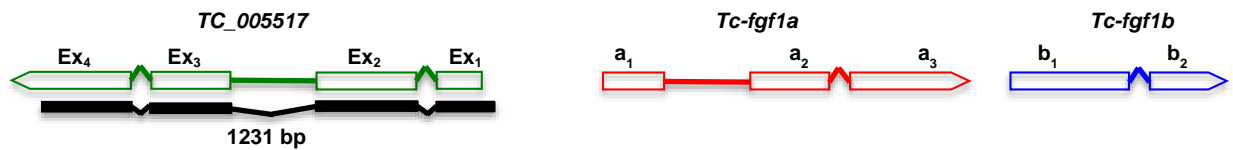Actual size of insert (w/o primers): 335 bp

Klon-Name: *Tc005517(Ex₁-Ex₄) - 5´ RACE*

Glean Nr: TC005517

 Insert / -länge: 1231 bp

TC_005517
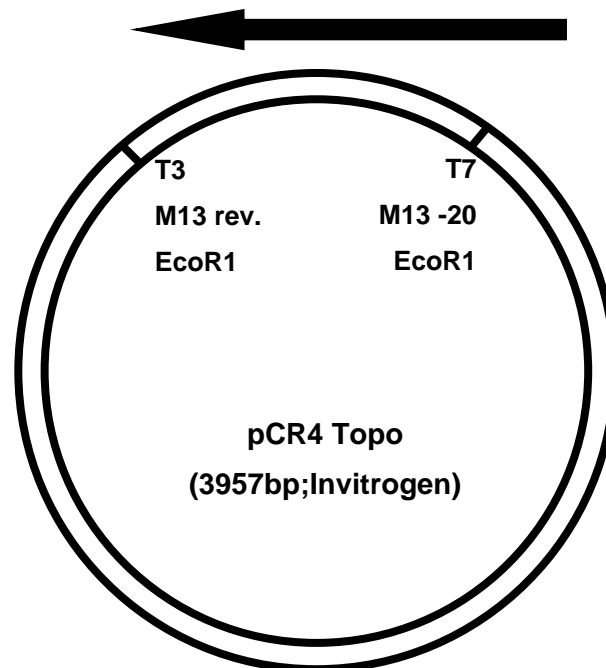
Ex₄ Ex₃ Ex₂ Ex₁

1231 bp

Tc-fgf1a

a₁ a₂ a₃

Tc-fgf1b

b₁ b₂

Entstehung: 5´ RACE PCR reaction using Primer#135 & UPM(Clontech)
5´ nested-PCR reaction using Primers:-
NUP(Clontech): 5'–AAGCAGTGGTATCAACGCAGAGT–3' &
NGSP(primer #128): 5´- CGTACTGGGCGATGGGTTGGTG -3´ (Manuela Lehmann)

Orientierung: 3´– 5´

T3

M13 rev.

EcoR1

T7

M13 -20

EcoR1

**pCR4 Topo
(3957bp;Invitrogen)**

Sequenz: mit T3 Primer (20.04.11); T7 Primer (AGOWA) (27.05.11)

Mini: 14.04.11

Midi: ....

Lagerung: -20°C, als pDNA

back-up: ....

Tc005517(Ex₁₋₄)-5´RACE mit T7 (27.05.11; Manuela Lehmann)*
CGTACTGGGCGATGGGTTGGTG(primer#128)GTAGTGTGCCATGTTGGGTGGCGGCACCGA
TGGGTCGAACATGGGCACAGCCGTGTGGATGTTGGGTGCTTGTGGCCGTTTCGATTTAGCT
TTGTTCAAGCGCGCCTGCTTGTACGAATCCATGTATTTGTTAAATTTCGTATTGAGGATGTTC
TTTCGGTTCATTGTCGTCTCGAATTTTTTGTAATTGTCGCTACTGTGGGTGCGTTTCACGTGA
GGAGCTAGTTTTTTATTACCGTATCGCTGGTAACACTCGTTTTCGTCGTCGGAAAAATCGG
CGAACTCGGGGGGGGACTTCCGTGTCGTCCATCCAGGAAGCGTCACTACCTTTCATTTTGAGCAG
CTGTTGAAGGAAAACGTATTGTGTGTGCTTGCTTGTAGGTGCGGAATAGACTTTTGTTCCAAT
CTCAATTTGTAAATTTTTTATGTCTTCAAGTGAATTGAAACGAATGGCATAGATAGGGGAAGTGA
CTTGGCCTAAAACGTCGAAAACGAAACCTAGAGGTCGCTTGCCGTTGTCTAGGAAGAGGAGCG
TATCCAAGTCGTACGCTGGAGTGTTTGGAAGGGCCGCGATAGTTACTAACTTATCCACAATCCC
GAACACATTTCCCATATGCACAAAACTCTCATTTTCCACGTTAATTTGAAGCGATGACAAGTCCGG
AACCGGGGGCAAATGTTCAATCCCTAGTTCATCACTGACTTTAGGTTGGCTATTCTTAATAGCCCC
CTTATTTTGTGTCGTTGTTTCAATGGGCTGTGAGTCATCGTCATCATCAT

Tc005517(Ex$_{1-4}$)-5´RACE mit T3 (20.04.11; Manuela Lehmann)*
CTGCTTGTACGAATCCATGTATTTGTTAAATTTCGTATTGAGGATGTTCTTTCGGTTCAT
TGTCGTCTCGAATTTTTTGTAATGTCGCTACTGTGGGTGCGTTCACGTGAGAGCTAGTT
TTTATTACCGTATCGCTGGTAACACTCGTTTCGTCGTCGGAAAAATCGGCGAACTCGGG
GGGGACTTCCGTGTCGTCCATCCAGGAAGCGTCACTACCTTTCATTTTGAGCAGCTGTT
GAAGGAAAACGTATTGTGTGTGCTTGCTTGTAGGTGCGGAATAGACTTTTGTTCCAATCT
CAATTTGTAAATTTTTTATGTCTTCAAGTGAATTGAAACGAATGGCATAGATAGGGGAAGT
GACTTGGCCTAAAACGTCGAAAACGAAACCTAGAGGTCGCTTGCCGTTGTCTAGGAAGA
GGAGCGTATCCAAGTCGTACGCTGGAGTGTTTGGAAGGGCCGCGATAGTTACTAACTTA
TCCACAATCCCGAACACATTTCCCATATGCACAAAACTCTCATTTTCCACGTTAATTTGAA
GCGATGACAAGTCCGGAACCGGGGGCAAATGTTCAATCCCTAGTTCATCACTGACTTTA
GGTTGGCTTTTCTTAATAGCCCCCTTATTTTGTGTCGTTGTTTCAATGGGCTGTGAGTCA
TCGTCATCATCATCGTCCCCACTCGTTTCACTGTCCTCCTCATCCTCCGAAGACGAAGAC
GAGGAACTGGACGAGTCCTCGGACCCCTCCTGAGCCCTCCAATTCAGGTTAAGCCTCA
TCATCTCGGAGGAAGAGCTCGAGTCGCTGTCATACACCAAAAGACGGTCCAGTGCATCA
GATTCGATGTTTTTTATTGCAACACCCGTATTAGCTTCACACACACTAGTGGAATTTGATA
AATTCGTTGCGTTTTCTCCCTGTTGGTTGTCCATGTTTTCGCACTTATTTTCGTTTGACGT
GCTGTGAGGTGATAAGGGATGATCGGAATTTAACGTAAACTAACAATTAATCACTGTTAT
GGTAAGGAATACTGCGAACATTTAAGCGGATTTTGCGATTTTACTGCCATGTGCCCCATG
T**ACTCTGCGTTGATACCACTGCTT(NUP)**

Figure S 7: Overview of different *Tc-fgf1a*-RNAi experiments performed using different gene fragments and various concentrations of dsRNA. (Underneath each bar the first number represents the clone number, followed by the concentration of dsRNA injected and "n" represents total number of cuticles analysed. Note, first three bars are based on results obtained from pupal injections, while remaining others from adult injections)
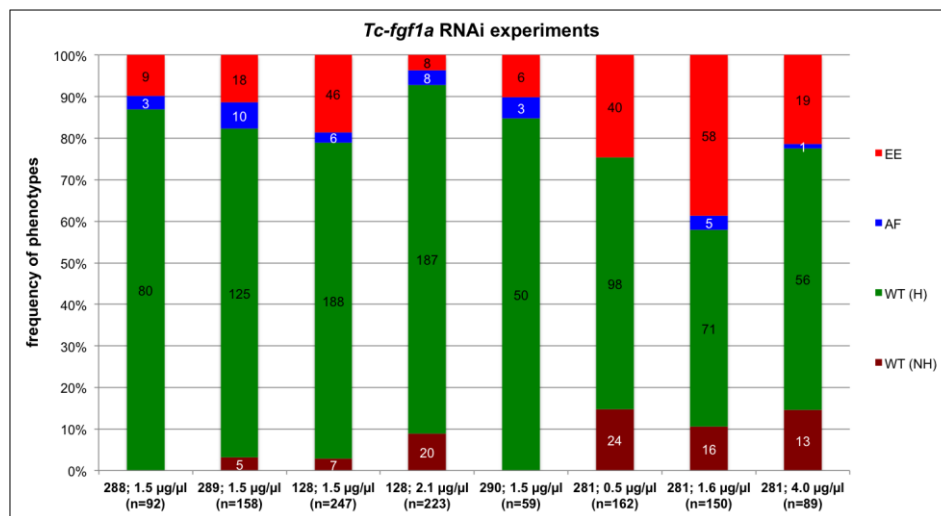

Table S 4: Analysis of affected *Tc-fgf1a* [RNAi] cuticles

	Type 1	Type 2	Type 3	Type 4	Type 5
Exp.9 (128)	1	1	-	1	-
Exp.10 (128)	2	4	2	-	-
Exp.11a (128)	1	-	2	-	-
Exp.17 (281)-I	-	-	-	-	-
Exp.17 (281)-II	1	1	-	1	2
Exp.17 (281)-III	-	1	-	-	-
Exp.21 (288)	-	1	2	-	-
Exp.21 (289)	1	7	2	-	-
Exp.21 (290)	-	2	1	-	-
TOTAL (n = 36)	**6**	**17**	**9**	**2**	**2**

Type 1: Weakly affected cuticles: abnormal shape of antennae and legs and loss of antennal spikes.

Type 2: Intermediate phenotype: fully segmented cuticles with stronger malformation of head appendages, stumpy/shortened legs, dorsal opening and misshaped body.

Type 3: Strong phenotype: posteriorly truncated cuticles with only head and thoracic development.

Type 4: Cuticles with "virtual short abdomen phenotype".

Type 5: Cuticles with "Inside-out phenotype".

Figure S 8: Overview of different *Tc-fgf1b*-RNAi experiments performed using different gene fragments and various concentrations of dsRNA. (Underneath each bar the first number represents the clone number, followed by the concentration of dsRNA injected and "n" represents total number of cuticles analysed. All injections were performed on adult beetles)
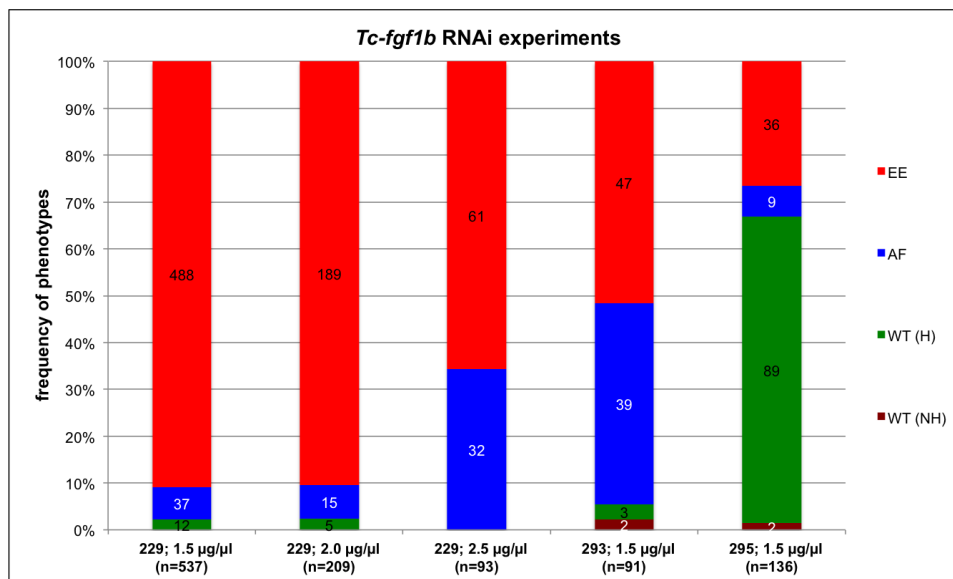

Table S 5: Analysis of affected *Tc-fgf1b* [RNAi] cuticles.

	Class I	Class II	Class III	Class IV	Class V
Exp.10 (229)	3	3	8	8	10
Exp.11a (229)	1	1	3	2	8
Exp.13 (229)	2	4	3	4	4
Exp.15 (229)	1	1	0	0	3
Exp.20a_I (293)	17	8	7	5	2
Exp.20a_II (295)	1	0	3	1	4
Exp.22(I) (229)	0	1	8	1	5
TOTAL (n = 132)	**25**	**18**	**32**	**21**	**36**

Class I: Slightly curved or non-curved cuticles with weakly malformed appendages and dorsal opening.

Class II: Strongly curved (arc-shaped) cuticles with dorsal opening and weakly affected appendages.

Class III: Strongly curved and dorsally open cuticles with deformed body and more strongly affected appendages.

Class IV: Dorsally open cuticle blocks/spheres with attenuated anterior structures (head or thoracic structures).

Class V: Strongly affected cuticle ball with or without appendages.

Table S 6: Analysis of affected *Tc-fgf1a*/*Tc-fgf1b*[RNAi] cuticles.

	Class I	Class II	Class III	Class IV	Class V	Class VI	Class VII
Tc-fgf1a$_3$b$_1$	58	21	19	30	14	13	4
Tc-fgf1a$_3$b$_1$b$_2$	82	12	8	21	8	5	0
Tc-fgf1a$_2$a$_3$ + Tc-fgf1b$_1$b$_2$	3	0	4	8	11	0	0
TOTAL (n = 321)	**143**	**33**	**31**	**59**	**33**	**18**	**4**

Class I: Slightly curved or non-curved cuticles with weakly malformed appendages and dorsal opening.

Class II: Strongly curved (arc-shaped) cuticles with dorsal opening and weakly affected appendages.

Class III: Strongly curved and dorsally open cuticles with deformed body and more strongly affected appendages.

Class IV: Dorsally open cuticle blocks/spheres with attenuated anterior structures (head or thoracic structures).

Class V: Strongly affected cuticle ball with or without appendages.

Class VI: Cuticles with inside-out phenotype.

Class VII: Cuticles with virtual short abdomen phenotype.

Figure S 9: Overview of different *Tc-fgf1a*/*Tc-fgf1b* -RNAi double knockdown experiments performed using different gene fragments. ("n" represents total number of cuticles analysed, all injections were performed on adult beetles)
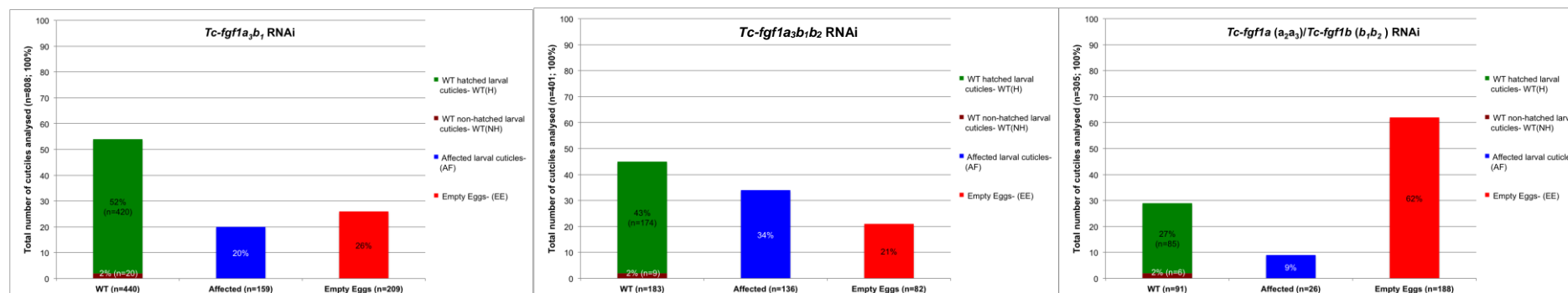
Figure S 10: *Tc-fgf1b* expression in wildtype embryos. (A-F) blastoderm stages; (G-K) extending germbands. All embryos are shown in surface views with anterior to the left. (D, E) embryos in lateral views with dorsal upside; (F) embryo in ventral view. (A-F) During early to late stages of blastoderm maturation, *Tc-fgf1b* expressed ubiquitously in wildtype embryos. (G-K) Later during germ band extensions also, *Tc-fgf1b* continues to expressed ubiquitously.
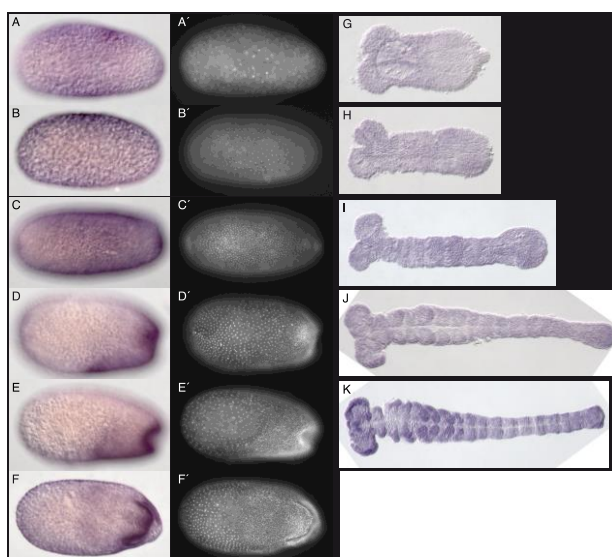

Figure S 11: No early apoptotic cell death in *Tc-fgf1b*[RNAi] embryos. (A-C) positive control embryos; (D-F) wildtype embryos; (G-I) *Tc-fgf1b*[RNAi] embryos (A´-I´) Hoechst counterstained embryos of (A-I) respectively. (A-C) In positive control embryos treated with DNAse-I, the apoptotic signals are detected universally throughout the various developmental stages including early blastoderm (A), late blastoderm (B) and germband extension (C). (D-F) In the wildtype untreated embryos, no such signals of apoptosis were detected at any comparable stage of the development. (G-I) In *Tc-fgf1b*[RNAi] embryos also no symptoms of early apoptotic cell death are detected at any of the comparable stages, as they are indistinguishable from the wildtype embryos.
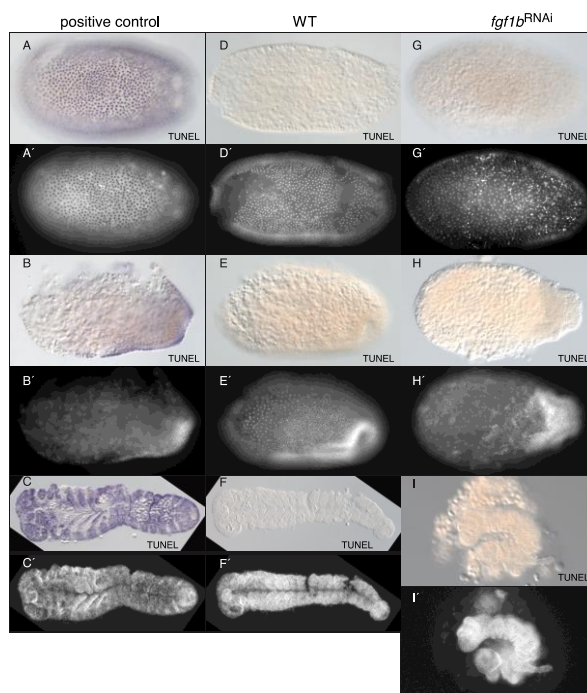
Figure S 12: Overview of different *Tc-fgf18*-RNAi experiments performed using different gene fragments and various concentrations of dsRNA. (Underneath each bar the first number represents the clone number, followed by the concentration of dsRNA injected and "n" represents total number of cuticles analysed. Note, first three bars are based on results obtained from pupal injections, while remaining others from adult injections)

Table S 7: Analysis of affected *Tc-fgf8*[RNAi] cuticles.

	Type I	Type II	Type III	Type IV
Exp.1 (167)	-		-	-
Exp.3 (167)	1		-	-
Exp.4 (167)	3	5	2	1
Exp.6 (167)	3	-	-	-
Exp.9 (125)	-	-	-	-
Exp.10 (167)	1	5	3	2
TOTAL (n = 26)	**8**	**10**	**5**	**3**

Type I: Cuticles with weak phenotype: antennae without spikes, abnormal shape or bifurcated claws of 1 or 2 legs, twisted abdomen and TODs.

Type II: Cuticles with intermediate phenotype: cuticles with complete malformation of the whole body axis.

Type III: Strongly affected cuticle spheres/balls within the egg: difficult to analyze.

Type IV: Others: cuticles with variable phenotypes that cannot be assigned to any of the above category.

Figure S 13: Overview of different *Tc-fgf1r*-RNAi experiments performed using different gene fragments (including an iBeetle fragment) and various concentrations of dsRNA. (Underneath each bar the first number represents the clone number, followed by the concentration of dsRNA injected and "n" represents total number of cuticles analysed. Note, the first bar is based on result obtained from pupal injection, while remaining others from adult injections)

Table S 8: Analysis of affected *Tc-fgfr* RNAi cuticles

	Class I	Class II	Class III	Class IV
Exp.2 (180)	-	1	1	1
Exp.8 (180)	3	9	4	1
Exp.11a (180)	1	-	-	-
Exp.22 (II) (iB_03821)	1	3	4	4
TOTAL (n = 33)	**5**	**13**	**9**	**6**

Class I: Mildly affected cuticles with visible phenotypes like loss of antennal spike(s), misshaped body, weakly malformed legs, bifurcated claws and tracheal opening differences (TOD).

Class II: Affected cuticles with weak to severe reduction reduction/truncation of abdominal segments and dorsal opening.

Class III: Strongly affected cuticles with only formation of head and thorax.

Class IV: Severely affected cuticle spheres/cuticle balls with outgrowing appendages, hard to analyze.

Figure S 14: Overview of different *Tc-dof*-RNAi experiments performed using various concentrations of dsRNA. (Underneath each bar the first number represents the clone number, followed by the concentration of dsRNA injected and "n" represents total number of cuticles analysed. Note, first three bars are based on results obtained from pupal injection, while remaining others from adult injections)
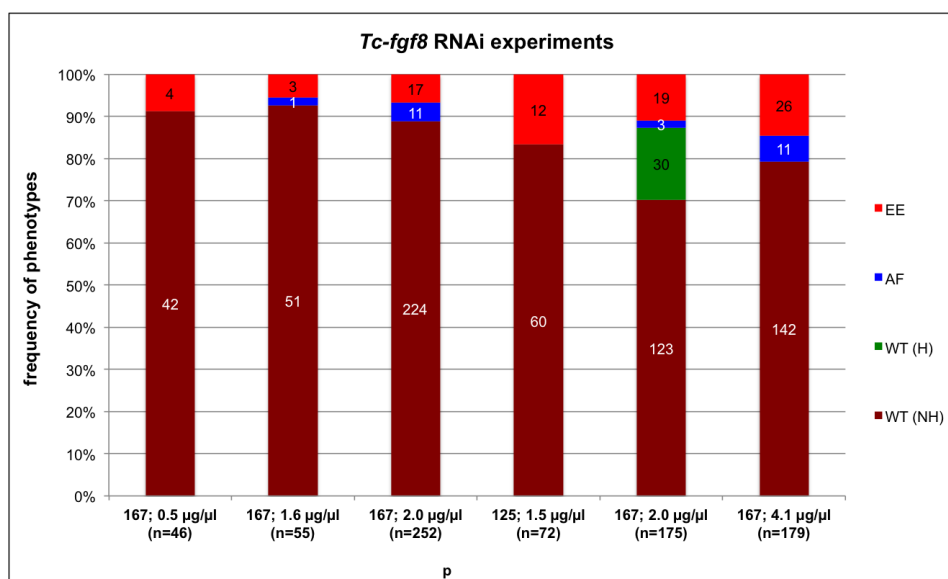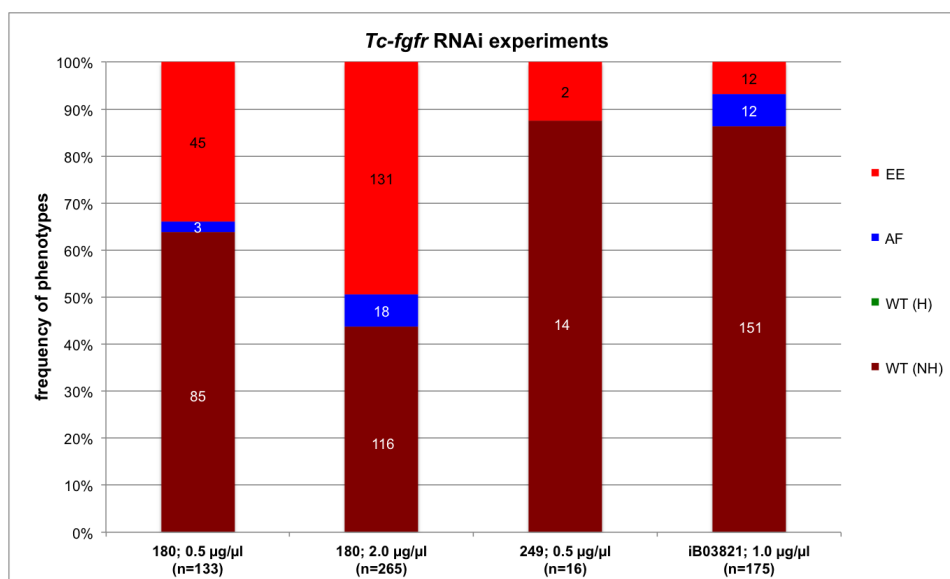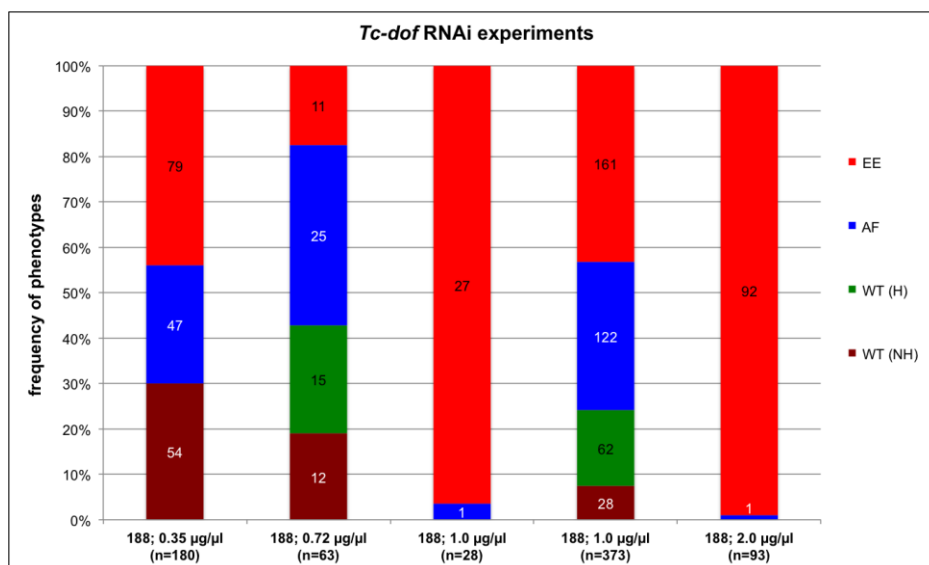
Table S 9: Analysis of affected *Tc-dof* [RNAi] cuticles.

	Class A	Class B	Class C	Class D	Class E	Class F	Class G	Class H	Class I	Sum
Exp.1 (188)	16	6	3	5	6	7	2	1	1	47
Exp.3 (188)	5	0	3	9	1	3	3	1	0	25
Exp.4 (188)	0	0	0	0	1	0	0	0	0	1
Exp.5 (188)	11	3	2	12	1	6	7	2	1	45
Exp.6 (188)	10	8	4	14	4	4	10	2	1	57
Exp.7 (188)	6	1	1	1	0	0	0	1	0	10
Exp.20a-(I)(188)	1	0	0	1	2	1	5	0	0	10
Exp.20a-(II) (188)	0	0	0	0	0	1	0	0	0	1
Total	**49**	**18**	**13**	**42**	**15**	**22**	**27**	**7**	**3**	**196**

Class A: Cuticles with weak abdominal patterning defects (merging of 2 or more abdominal segments into 1) along with TODs and weakly malformed head, legs and posterior appendages.

Class B: Cuticles with wrongly patterned anterior (partially fused head (H) and thoracic segment (T1)) and posterior region (abdominal patterning defects). Strongly malformed legs or loss of one leg is typical for cuticles of this class.

Class C: Cuticles with only two thoracic segments T2 & T3 along with weak to strongly affected head appendages and wrongly patterned abdomen.

Class D: Cuticles with weak to severe posterior truncations (loss of A7/A8 to complete loss of abdomen or even T2-T3 in most severe cases)

Class E: Most severely affected cuticles with head only structures, an undefined cuticle ball and a gut like structure.

Class F: Short cuticles with "gap phenotype" like features.

Class G: Two cuticle spheres corresponding for head thorax and abdomen, sometimes very poorly developed.

Class H: Cuticles with strong anterior reduction, headless cuticles with even loss of 1-2 thoracic segment.

Class I: Cuticles showing left-right asymmetry.

Acknowledgements

First and foremost, I would like to extend my utmost gratitude and thankfulness to my guru Prof. Dr. Reinhard Schröder for giving me the opportunity to work on this project. I am very grateful for his patience, motivation, enthusiasm, and immense knowledge, which he had shared with me. His everlasting energy and dynamic spirit guided me all the time of research and during writing of this dissertation. In addition, he was always accessible and willing to help his students with their research. I am deeply indebted for all his contributions of time, ideas, and funding to make my Ph.D. experience productive and stimulating. In every sense, none of this work would have been possible without him. Thank you for the experiences that I will carry with me throughout my life.

I am also truly grateful to Dr. Anke Beermann (University of Tübingen, Germany) for her outstanding assistance and continuous support throughout my research. Her excellent knowledge, perception and personal experiences with the project have a great impact on my dissertation. I sincerely thank her for her valuable support, logical inputs and proper guidance to make my goals achievable.

I would like to extend my gratitude for Prof. (Emeritus) Dr. Deiter G. Weiss for being a valuable source of advice about science and research and for his motivating passion for science attitude. It was his passion for microscopy that has introduced me to have a rare look on some of his collection of centaury old slides. Thank you for all those experiences. In addition, I wish to acknowledge my former guide, Dr. B.N. Paul (Senior Principal Scientist, IITR, Lucknow) and my co-guide Dr. Mandakini Pradhan (Addl. Professor, Department of Genetcis, SGPGI, Lcuknow) in India, for providing me their kind assistance and continuous support in my scientific career.

I am also thankful to Prof. Dr. Marek Jindra (Department of Genetics Biology Center ASCR, Czech Republic) and Dr. M. Schoppmeier (University of Erlangen-Nürnberg, Germany) for sending me clones required for my research and their valuable suggestions.

In addition my most sincere thanks go to the former and present technical staff members of my lab, Heidrun Blunk, Antje Hlawa, Hilke Brandt and Kerstin Schwandt, for providing me a wonderful support throughout my tenure. My special thanks goes to Antje for being so caring in my early days in the lab and for sharing her thoughts about life, culture and traditions in Germany.

I am also grateful to the peoples in the Animal Physiology Department in Rostock, Bärbel, Maren, and Anne and off course Brigit. Life would not be so easy in Rostock

without Birgit. She has been a great help for me not only in the lab but also for taking care of my personal requirements. Thanks a lot Birgit, I owe a lot to you!

I thank my dearest lab mates, who have been great to be with everyday. First of all, I would like to thank Romy Prühs for her unconditional support and care for all the people in the lab. It's being wonderful to have a colleague like Romy next to your desk. I also thank all the present and former members of my lab including Anja, Tina, Kristin, Suparna, Janine, Rosi and Felix, Jana, Felix Schmöhl. Susanne, Maria and Manuela. My special thanks to Katharina Beer and Romy Weller for assisting me in completion of the FGF8 and FGF1 projects, respectively.

My time at Rostock was made enjoyable in large part due to many of my friends and buddies that became a part of my life. I am grateful to all friends, Furquan-Sana, Devang-Payal, Amit, Naveen, Saijo , Lijo, Nitesh, Raymond, Jeet-Sunita, Shoubhik-Piyali, Venkat-Kalpana, Bhavani, Prakash, Kishore-Samatha, Sumit and Prasanna, who have spent their precious time for countless parties and playing cricket at our beloved ground. I am highly indebted to Furquan, for introducing me about this position in the lab and for taking care of everything in early days. I also thank Vijay Anna for his helpful suggestion and treating me like his younger brother.

I also acknowledge my lovely friends back home and in other countries who were just a "phone-call away" at any odd hour of time for their concerns, love and understanding that has always given me immense strength.

I owe deepest gratitude to my parents without their basic lessons of life; I would not be the person I am today. I obliged much more than I could ever return to them in my whole life. My entire family means a lot to me. I love you all.

My beloved wife (Jaya) and my little angel (my daughter, Prakhya) procure special place in my acknowledgement. I cannot express my gratitude in words but I am very much grateful to them for providing much needed emotional and moral support. In their company everyday was so cheerful that I never felt ups and down. Dear, thanks a lot for standing next to me and providing me strength to fight against odds in our life.

Rahul Sharma

Curriculum vitae

Personal Details:

Name: Rahul Sharma

Date of Birth: 01.12.1983

Place of Birth: Aligarh, India

Nationality: Indian

Gender: Male

Education:

Oct. 2009 - Present	Doctoral Student, Department of Genetics, Institute for Biological Sciences, University of Rostock, Rostock, Germany
Oct. 2008 – Sep. 2009	Scientific Researcher, Department of Genetics, Institute for Biological Sciences, University of Rostock, Rostock, Germany
Apr. 2008 - Aug. 2008	Project Assistant, Immunobiology lab, Indian Institute of Toxicology Research (IITR), Lucknow, UP, India
Aug. 2006 - Mar. 2008	Junior Research Fellow, Genetics Sanjay Gandhi Post Graduate Institute of Medical Sciences (SGPGIMS), Lucknow, UP, India
Aug. 2004 - Jul. 2006	Master of Science (Biotechnology), Kumaun University, Nainital, India
Jul. 1999 - Jun. 2002	Bachelor of Science (Hons.) - Chemistry, Aligarh Muslim University (AMU), Aligarh, India

List of publications:

1. **Sharma R**., Beermann. A., Schröder R.; 2013. FGF signalling controls anterior extraembryonic and embryonic fate in the beetle *Tribolium*; *Dev. Biol. 381: 121-133*

2. **Sharma R.,** Beermann A., Schröder R.; 2013. The dynamic expression of extraembryonic marker genes in the beetle *Tribolium castaneum* reveals the complexity of serosa and amnion formation in a short germ insect; *Gene Expression Patterns 13: 362–371*

List of symposia contributions/participations:

1. **Sharma, R.**, Beermann, A., Schröder, R. 2013. FGF signalling controls anterior extraembryonic and embryonic fate in the beetle *Tribolium*. The 5th EMBO meeting, Amsterdam. (Poster presentation)

2. **Sharma, R.**, Beermann, A., Schröder, R. 2012. Multiple roles of FGF signalling during the development of beetle *Tribolium castaneum*. EURO EVODEVO (4th Meeting of EED), Lisbon. (Poster presentation)

3. **Sharma, R.** 2012. FGF signalling is crucial for synchronous nuclear division and extraembryonic membrane formation. International *Tribolium* Meeting, Lisbon. (Oral presentation)

4. **Sharma, R.,** Beermann, A., Schröder, R. 2011. FGF signalling is required for maintaining the integrity of extraembryonic membranes during early embryogenesis of the beetle *Tribolium castaneum*. Annual Conference of the German Genetics Society (GfG), Würzburg. (Poster presentation)

5. **Sharma, R.**, Beermann, A., Schröder, R. 2010. FGF signalling is required for Dorsal Closure during embryogenesis of the beetle *Tribolium castaneum*. From Signal to Structure in Embryogenesis and Organogenesis, 3rd International Symposium of SFB 592, GRK 1104 and GRK 1305, Freiburg. (Poster presentation)

6. DZG Workshop on "Next Generation Sequencing and Transcriptomics" April 14 -15 2011 at GZMB der Universtität Göttingen, Göttingen, Germany. (Participation)

7. **Sharma, R.**, Beermann, A., Schröder, R. 2010. Multiple Roles of FGF Signalling during embryogenesis of the beetle *Tribolium castaneum*. EURO EVODEVO (3rd Meeting of EED), Paris. (Poster presentation)

8. **Sharma, R.** 2010. FGF signalling is required for Dorsal Closure during embryogenesis of the beetle *Tribolium*. International *Tribolium* Meeting, Paris. (Oral presentation)

9. **Sharma, R.** 2010. FGF signalling is required for Dorsal Closure in the development of beetle *Tribolium castaneum*. 4th Münster Graduate School Meeting 'Cell Dynamics and Disease', Münster. (Oral presentation)

10. **Sharma, R.** 2009. The Role of FGF Signalling in *Tribolium castaneum* Development. Biennial *Tribolium* regional meeting, Cologne, ***Dev Genes Evol (2009) 219:531–533***. (Oral presentation)

Selbstständigkeitserklärung

Ich versichere hiermit an Eides statt, dass ich die vorliegende Arbeit selbstständig angefertigt und ohne fremde Hilfe verfasst habe, keine außer den von mir angegebenen Hilfsmitteln und Quellen dazu verwendet habe und die den benutzten Werken inhaltlich und wörtlich entnommenen Stellen habe ich als solche kenntlich gemacht.

Rostock, 21.02.2014   Rahul Sharma

Declaration

I hereby declare that the work presented in this thesis entitled, "Analysis of the FGF signalling pathway during embryogenesis of the red flour beetle *Tribolium castaneum*" is entirely original and was carried out by me independently at Department of Genetics, Institute for Biological Sciences, University of Rostock under the supervision of Prof. Dr. Reinhard Schröder. I further declare that this thesis has not formed the basis for the award of any degree or diploma, fellowship or similar title of any University or Institution.

Rostock, 21.02.2014   Rahul Sharma